

**EFFECT OF THE INCORPORATION OF SLAG, FLY ASH AND
LIMESTONE CALCINED CLAY ON THE COMPRESSIVE
STRENGTH, ELASTIC MODULUS AND SHRINKAGE OF
CONCRETE**

A THESIS

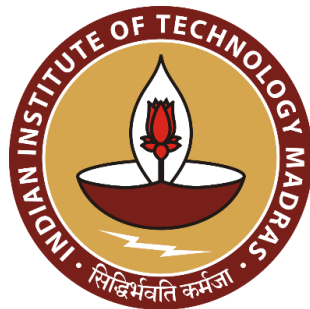
Submitted by

T. SAKTHIVEL

for the award of the degree

of

DOCTOR OF PHILOSOPHY



**DEPARTMENT OF CIVIL ENGINEERING
INDIAN INSTITUTE OF TECHNOLOGY MADRAS
CHENNAI, INDIA
JULY 2019**

தொட்டனைத் தூறும் மணற்கேணி மாந்தர்க்குக்
கற்றனைத் தூறும் அறிவு

-திருக்குறள்

As you delve deeper in sandy soil, you reach the springs below;
The more you learn, the streams of wisdom flow more freely

-Thirukkural

THESIS CERTIFICATE

This is to certify that the thesis titled “**EFFECT OF THE INCORPORATION OF SLAG, FLY ASH AND LIMESTONE CALCINED CLAY ON THE COMPRESSIVE STRENGTH, ELASTIC MODULUS AND SHRINKAGE OF CONCRETE**” submitted by **Mr. T. SAKTHIVEL**, to the Department of Civil Engineering, Indian Institute of Technology Madras, Chennai, for the award of the degree of **DOCTOR OF PHILOSOPHY** is a bonafide record of the research work done by him under our supervision. The content of this thesis, in full or in parts, have not been submitted to any other Institute or University for the award of any degree or diploma.

Dr. Ravindra Gettu
Research Guide
Prof. V. S. Raju Chair Professor
Department of Civil Engineering
Indian Institute of Technology Madras
Chennai - 600 036, India

Dr. Radhakrishna G. Pillai
Research Co-Guide
Associate Professor
Department of Civil Engineering
Indian Institute of Technology Madras
Chennai - 600 036, India

Chennai, India, July 16, 2019

ACKNOWLEDGEMENTS

I would like to dedicate this research work to my teachers, who taught me civil engineering at various levels.

Firstly, I would like to express my sincere gratitude to my guide, Prof. Ravindra Gettu, for his continuous support on my work, for his patience and motivation. His guidance helped me a lot in all the time of my work and writing of this thesis. I consider it as a great opportunity to carry out my research under his guidance and to learn from his expertise. I couldn't have imagined having a better mentor for my research study and for personal life.

I extend my heartfelt thanks to my guide, Dr. Radhakrishna G. Pillai, for his guidance and support during the entire phase of my life as a graduate student. My heartfelt thanks to him for his scholarly inputs and consistent encouragement I received throughout the research work. His commitment and integrity have been an inspiration to me for my career.

I am much thankful to Prof. Manu Santhanam and Dr. Piyush Chaunsali for their valuable comments and suggestions during the weekly concrete materials research scholar meeting.

I extend my gratitude to my doctoral committee members Prof. Devdas Menon for his comments and recommendations at various stages of the work. Also, I thank Prof. M. S. Sivakumar and Prof. S. Nallayarasu for offering comments during the committee meetings.

I am extremely grateful to the head of the department, Prof. K. Ramamurthy, and the former heads, Prof. A. Meher Prasad, and Prof S. R. Gandhi, for providing an excellent laboratory facility in the department and all the administrative support extended for carrying out the research. I would like to thank all the faculty members of the BTCM division for their support during the course of my study. My sincere thanks to Prof. Surendra P. Shah, Prof. Vellore S. Gopalaratnam, Prof. Mark G. Alexander and Prof. Yunus Ballim for their valuable suggestions and feedbacks given to me during their stay at IIT Madras. I am truly pleased to Dr. Sunitha K. Nayar for offering feedback and suggestion for thesis writing. Also, I would like to thank Dr. T. Chellappa for his valuable inputs and comments on language and writing.

My heartfelt gratitude to all the staff in the BT&CM laboratory, especially Ms. Malarrvizhi, Mr. Soundarapandian, Mr. Subrahmanian, Mr. Gaspar, Mr. Krishnan, and Msrs. Krishna, Kanagadri, Chinnaiah and Arun for their support given to me for the completion of laboratory

work and for their help during concrete casting. I thank the departmental workshop facility and central fabrication facility for their help rendered in the fabrication of frames and moulds.

I thank my friends and fellow lab mates, Dr. Jayachandran, Dr. Bahurudeen, Hemalatha, Dr. Dhanya, Srini, Karmugil, Prabha, Sundar, Sujatha, Dr. Vasugi, Dr. Haneefa, Muthu, Dr. Siva, CP Nair, Stefie, Siraj, Aswathy, Sanoop, Sooraj, Reesha, Swathi Manoharan, Dr. Elson, Dr. Praveen, Sriram, Ram, Thirumalai, Yuvaraj, Sachin, Vaisnav and Nithya for the stimulating research discussion and for all the fun we have had in the past years. Also, I thank Swathi, Krithi and Aarthy for their help during the regression analysis and for the plotting the graphs. I would like to extend my thanks to my internship students and Tas for their support.

My deep appreciation goes out to W R Grace & Co India Pvt. Ltd., BASF India Ltd., Alcon Cement Company Pvt. Ltd., JSW, Penna and Ambuja Cements Ltd. for their invaluable contribution in supplying the materials.

My heartfelt thanks to my family for their encouragement and support during my research. I wish to express my thank you to my wife Ms. Kalaivani, and my kids Adhirra and Aaruran for their moral support they gave me for the successful completion. I thank my parents Mr. Thangavel and Ms. Sargunam, and my sister Ms. Manju Mohanraj, niece Ms. Dhanapriya and nephew Mr. Senthilraj who heartened me for my wellbeing. I also thankful to my in-laws Mr. Manoharan and Ms. Mohanambal for their support. Many thanks to Dr. Suganthi, Dr. Karthi and Mr. Parthiban for their support and care. Above all, I owe it all to Lord Kandasamy for granting me health and strength to undertake the research and enable me to its completion.

T. Sakthivel

ABSTRACT

The incorporation of supplementary cementitious materials (SCMs), such as slag and fly ash, in conventional concrete systems yields several benefits such as reduced carbon footprint and longer service life, leading to sustainable construction. Considering the economic and technical advantages, as well the lowering of the environmental impact, these materials are extensively used in many construction projects. At present, the strength, elastic modulus and shrinkage of SCM based concretes used in India are based on values suggested by the international codes or limited studies with locally available SCMs. Hence, there is a need for more extensive testing and evaluation of concrete with SCMs (say, slag and fly ash).

This work provides a comprehensive experimental study on the influence of slag and fly ash on the short- and long-term compressive strength, elastic modulus and the evolution of shrinkage response of concrete. A new Limestone Calcined Clay Cement (LC3), with about 50% clinker, 30% calcined kaolinitic clay and 15% limestone, has also been assessed. Further, the applicability of popular shrinkage prediction models was studied for the blended cement concrete. Consequently, in order to achieve the objectives of the current research work, sixty-three concrete mixes were made with different water-binder ratios and binder contents with varying dosages of slag and fly ash. The concrete mixes were designed such that the compressive strengths were in the range of 25 to 65 MPa. The research programme was performed in four phases. In Phase-1, the characterization of raw materials, preliminary casting and testing of concrete were carried out. In Phase-2 and Phase-3, short and long-term laboratory tests were performed on concrete specimens. The total and autogenous shrinkage strains, after 28 days of curing, were measured up to 1000 days of exposure. In Phase-4, various shrinkage prediction models available in the literature were evaluated.

The findings from the present study show that early age (say ≤ 7 days) compressive strength of blended concrete was normally less than that of OPC concrete. However, extended curing resulted in a substantial increase in the compressive strength over and above that of conventional OPC concrete. The slag-blended concrete develops compressive strength at a higher rate than fly ash blended concrete. From the current work, it can be concluded that ternary blended concrete experienced extended gain of compressive strength. Concretes with LC3 are shown to exhibit equivalent or better compressive strength in comparison with OPC and fly ash blended systems. The relationship between the compressive strength and elastic modulus is seen to be essentially unaffected by the presence of slag and fly ash. Hence, the

existing prediction equations for conventional concretes can be used for blended cement concrete. From, the study, it was observed that IS 456 and *fib* Model Code 2010 are less conservative than the ACI 209 and ACI 318 prediction models. Also, it has been confirmed that the ratio of cube to cylinder compressive strength can be taken as 1.21, for the specimen sizes and concretes considered here.

The results obtained from this study give a better understanding on how slag and fly ash affect the shrinkage response of concrete. It is seen that slag and fly ash, as partial substitutes of OPC, do not have a significant effect on the shrinkage of concrete. The two types of fly ash, however, yielded a marginal difference in the shrinkage evolution. Ternary blended concrete exhibited marked differences of about 100 microstrain in shrinkage compared to binary systems.

The measured shrinkage strains were compared with five different models to assess the adequacy of the shrinkage predictions. The models considered were ACI 209, RILEM B4 and B4s, *fib* Model Code 2010 and IS 1343. Most models yield conservative predictions, except the *fib* Model Code 2010. Also, strength-based models, such as IS 1343 and B4s, gave reasonably good predictions even though they do not explicitly account for the composition. With the aim of more appropriate long-term predictions of the later age shrinkage, the parameters of the B4 and B4s models were adjusted using the early age experimental data.

This work provides an extensive database of the mechanical performance of SCM blended concrete in the Indian context, which can significantly benefit practicing engineers and researchers. In general, it is seen that the use of SCMs does not negatively affect strength development, elastic modulus and shrinkage, considering the same binder content and water-binder ratio.

Keywords: Supplementary cementitious materials (SCMs), Slag, Fly ash, Limestone Calcined Clay (LC3), Compressive strength, Elastic modulus, Shrinkage, Prediction models.

TABLE OF CONTENTS

THESIS CERTIFICATE	v
ACKNOWLEDGEMENTS	vii
ABSTRACT	ix
TABLE OF CONTENTS	xi
LIST OF TABLES	xv
LIST OF FIGURES	xvii
LIST OF ABBREVIATIONS	xxv
1. INTRODUCTION.....	1
1.1 BACKGROUND	1
1.2 OBJECTIVES OF THE PRESENT STUDY	2
1.3 SCOPE.....	3
1.4 STRUCTURE OF THE THESIS.....	4
2. LITERATURE REVIEW.....	7
2.1 GENERAL.....	7
2.2 EFFECT OF SUPPLEMENTARY CEMENTITIOUS MATERIALS ON COMPRESSIVE STRENGTH AND ELASTIC MODULUS	7
2.2.1 Effect of slag and fly ash on the compressive strength development of concrete.....	8
2.2.2 Effect of slag and fly ash on the elastic modulus of concrete	9
2.2.3 Influence of LC3 on compressive strength development and the elastic modulus of concrete	9
2.3 EFFECT OF SUPPLEMENTARY CEMENTITIOUS MATERIALS ON THE SHRINKAGE OF CONCRETE	10
2.3.1 Effect of slag and fly ash on drying shrinkage of concrete	12
2.3.2 Effect of slag and fly ash on autogenous shrinkage of concrete	14
2.4 MODELS FOR PREDICTING THE SHRINKAGE OF CONCRETE	14
2.4.1 ACI 209, 2008 Model.....	15
2.4.2 B4, 2014 Model.....	17
2.4.3 B4s, 2014 Model	23
2.4.4 <i>fib</i> Model Code 2010.....	24
2.4.5 IS 1343, 2012	26
2.5 SUMMARY AND RESEARCH SIGNIFICANCE	28
3. MATERIALS AND EXPERIMENTAL PROGRAMME.....	29
3.1 INTRODUCTION	29

3.2	CONCRETE-MAKING MATERIALS.....	31
3.2.1	Binders.....	31
3.2.2	Aggregates.....	32
3.2.3	Superplasticizers.....	33
3.3	CONCRETE MIX DESIGN.....	34
3.3.1	Mix proportions.....	34
3.3.2	Mixing procedure, casting, curing and storing of specimens.....	37
3.4	EXPERIMENTAL PROGRAMME.....	39
3.4.1	Tests on fresh concrete.....	39
3.4.2	Tests on hardened concrete.....	41
3.5	SUMMARY.....	47
4.	RESULTS AND DISCUSSION – COMPRESSIVE STRENGTH AND ELASTIC MODULUS OF CONCRETE.....	49
4.1	INTRODUCTION.....	49
4.2	COMPRESSIVE STRENGTH.....	49
4.2.1	Effect of cement type on compressive strength development.....	51
4.2.2	Effects of slag and fly ash on compressive strength development.....	56
4.2.3	Effects of replacement level on compressive strength development.....	63
4.2.4	Effects of ternary blends on compressive strength development.....	65
4.2.5	Effects of LC3 on compressive strength development.....	67
4.2.6	Effect of specimen size and shape on compressive strength.....	68
4.2.7	Prediction of Compressive Strength Development.....	69
4.3	ELASTIC MODULUS RESULTS.....	72
4.3.1	Effect of fly ash and slag on the elastic modulus of concrete with CmP cement...73	73
4.3.2	Relations between compressive strength and elastic modulus.....	73
4.4	SUMMARY.....	75
5.	RESULTS AND DISCUSSIONS – TOTAL AND AUTOGENOUS SHRINKAGE OF CONCRETE.....	77
5.1	INTRODUCTION.....	77
5.2	SHRINKAGE MEASUREMENTS IN SLAG AND FLY ASH BLENDED CONCRETE	77
5.2.1	Effect of specimen size on shrinkage of concrete.....	103
5.3	RELATION OF MASS LOSS AND SHRINKAGE STRAIN OF CONCRETE.....	104
5.4	INCREASE IN AUTOGENOUS SHRINKAGE OF CONCRETE.....	106
5.5	SUMMARY.....	109
6.	APPLICATION OF SHRINKAGE PREDICTION MODELS.....	111

6.1 INTRODUCTION	111
6.2 STRENGTH-BASED SHRINKAGE PREDICTION MODELS.....	113
6.2.1 IS 1343, 2012	113
6.2.2 <i>fib</i> Model Code 2010.....	116
6.2.3 RILEM B4s, 2014	120
6.3 COMPOSITION-BASED SHRINKAGE PREDICTION MODELS	124
6.3.1 ACI 209, 2008	124
6.3.2 RILEM B4, 2014.....	128
6.4 ADJUSTMENT OF MODEL PARAMETERS FOR BETTER PREDICTION.....	131
6.4.1 B4s-R.....	131
6.4.2 Effect of aggregate type in the B4 prediction model.....	144
6.4.3 Effect of binder composition on the B4 standard prediction model.....	147
7. CONCLUSIONS AND SCOPE FOR FUTURE WORK	153
7.1 GENERAL CONCLUSIONS.....	153
7.2 SPECIFIC CONCLUSIONS	154
7.2.1 Effect of slag and fly ash on compressive strength development and elastic modulus of concrete	154
7.2.2 Effect of slag and fly ash on shrinkage response of concrete	155
7.2.3 Application of shrinkage prediction models for blended cement concrete	155
7.3 RECOMMENDATIONS FOR FUTURE WORK	156
8. REFERENCES.....	157
APPENDICES (https://www.dropbox.com/s/cdvlbpxyls2kkcy/appendices.pdf?dl=0)	A-1
APPENDIX A - EVOLUTION OF CUBE COMPRESSIVE STRENGTH.....	A-1
APPENDIX B1 - MEASURED SHRINKAGE STRAINS OF CONCRETE ON CYLINDRICAL SPECIMENS.....	A-9
APPENDIX B2 - MEASURED SHRINKAGE STRAINS OF CONCRETE ON PRISMATIC SPECIMENS.....	A-203
APPENDIX C1 - MASS LOSS IN CYLINDRICAL SPECIMENS.....	A-275
APPENDIX C2 – MASS LOSS IN PRISM SPECIMENS.....	A-299
APPENDIX D1 - COMPARISON OF SHRINKAGE OBTAINED EXPERIMENTALLY WITH IS 1343 PREDICTION.....	A-323
APPENDIX D2 - COMPARISON OF SHRINKAGE OBTAINED EXPERIMENTALLY WITH <i>fib</i> MC 2010 PREDICTION.....	A-340
APPENDIX D3 - COMPARISON OF SHRINKAGE OBTAINED EXPERIMENTALLY WITH B4s PREDICTION	A-357
APPENDIX D4 - COMPARISON OF SHRINKAGE OBTAINED EXPERIMENTALLY WITH ACI 209 PREDICTION	A-374

APPENDIX D5 - COMPARISON OF SHRINKAGE OBTAINED EXPERIMENTALLY WITH B4 PREDICTION	A-391
APPENDIX D6 - COMPARISON OF SHRINKAGE OBTAINED EXPERIMENTALLY WITH B4S AND B4S-R PREDICTION	A-408
APPENDIX D7 - COMPARISON OF SHRINKAGE OBTAINED EXPERIMENTALLY WITH B4 PREDICTION BY CONSIDERING AGGREGATE AS UNKNOWN	A-429
APPENDIX D8 - COMPARISON OF SHRINKAGE OBTAINED EXPERIMENTALLY WITH B4 PREDICTION BY CONSIDERING THE EFFECT OF BINDER COMPOSITON AND AGGREGATE AS GRANITE	A-446
APPENDIX E - STEP BY STEP PROCEDURE FOR SHRINKAGE PREDICTION MODELS	A-463
LIST OF PUBLICATIONS BASED ON THIS THESIS	169
DOCTORAL COMMITTEE.....	171
CURRICULUM VITAE.....	173

LIST OF TABLES

Table 2.1 Shrinkage parameters depending on cement type for B4	20
Table 2.2. Aggregate dependent parameter scaling factors for shrinkage for B4.....	21
Table 2.3. Autogenous shrinkage parameters depending on cement type for B4.....	21
Table 2.4 Admixture dependent parameter scaling factors for shrinkage for B4	22
Table 2.5 Shrinkage parameters depending on cement type for B4s.....	24
Table 2.6 Autogenous shrinkage parameters for B4s for regular cement (R), rapid hardening cement (RS) and slow hardening cement (SL).....	24
Table 2.7 Co-efficient used for basic and drying shrinkage of concrete	25
Table 2.8 Unrestrained autogenous shrinkage ($\epsilon_{ca} \times 10^6$).....	26
Table 2.9 Unrestrained drying shrinkage values ($\epsilon_{cd} \times 10^6$).....	27
Table 2.10 Co-efficient depending on the notional size	27
Table 3.1 Details of specimens for category CmP and CmA concrete.....	30
Table 3.1 Physical properties of binders and Supplementary Cementitious Materials (SCMs)	32
Table 3.2 Chemical composition of binders	32
Table 3.3 Physical properties of aggregates	33
Table 3.4 Properties of superplasticizers (as given by from the suppliers)	34
Table 3.5 Concrete mix proportions	35
Table 3.7 Codes and standards followed for the testing of fresh concrete	39
Table 3.8 Fresh concrete properties	40
Table 3.9 Codes and standards followed for the testing of hardened concrete properties.....	41
Table 4.1 Cube compressive strength of concrete (MPa); average and standard deviation	50
Table 4.2 Elastic modulus values at 28 days.	72
Table 5.1 Comparison of compressive strength versus total shrinkage of concrete.....	102
Table 6.1 Some input values for shrinkage prediction calculation	111
Table 6.2 Parameters considered by the shrinkage prediction model.....	112
Table 6.3 Error in the prediction of total shrinkage by IS 1343 prediction model.....	115
Table 6.4. Error in the prediction of total shrinkage by <i>fib</i> MC 2010 prediction model.	119
Table 6.5 Error in the prediction of total shrinkage by B4s prediction model.	122
Table 6.6 Error in the prediction of total shrinkage by ACI 209 prediction model.....	126
Table 6.7 Error in the prediction of total shrinkage by B4 prediction model.....	130
Table 6.8 Regression of B4s standard prediction model for one, two and three years.....	133

Table 6.9 Error in the prediction of total shrinkage by B4s prediction model regressed for one year.	136
Table 6.10 Error in the prediction of total shrinkage by B4s prediction model regressed for two years.	139
Table 6.11 Error in the prediction of total shrinkage by B4s prediction model regressed for three years.	142
Table 6.12. Error in the prediction of total shrinkage by B4 prediction model by considering aggregate as unknown.	146

LIST OF FIGURES

Figure 1.1 key phases involved in the research work	4
Figure 2.1 Evolution of shrinkage response in concrete (<i>plotted based on Neville, 2006</i>)	12
Figure 3.1 Particle size distribution of aggregates used in the study	33
Figure 3.2 Nomenclature for the concrete mixes	35
Figure 3.3 Histories of temperature at two locations in the laboratory, denoted as (a) and (b), and (c) the relative humidity	38
Figure 3.4(a) Axial displacement transducers	42
Figure 3.4(b) Elastic modulus test setup in testing machine with typical loading history and stress-strain curve	45
Figure 3.5 DEMEC strain gauge used for the work.....	44
Figure 3.6 Prepared concrete specimens for measuring shrinkage strain	45
Figure 3.7 Studs fixed at the specimen ends for measuring shrinkage	46
Figure 3.8 Length comparator frame with digital dial gauge in accordance with ASTM C157 (a) with length comparator (b) with standard prismatic specimen	47
Figure 4.1 Effect of cement type on compressive strength development of concrete (a) CmP, CmA and LC3 with $w/c = 0.50$, (b) CmP and CmA with $w/c = 0.65$	52
Figure 4.2 Effects of water-cement ratio on evolution of compressive strength (a) $w/c=0.50$ and 0.60 with CmP.....	54
Figure 4.3 Effect of SCM on the evolution of compressive strength of concrete with CmP (a) $w/b = 0.50$ and (b) $w/b = 0.60$	57
Figure 4.4 Effect of SCM on the evolution of compressive strength of concrete with CmA (a) $w/b = 0.50$ and (b) $w/b = 0.60$	58
Figure 4.5 Effect of binary blends of slag and fly ash on compressive strength development with CmP (a) $w/b = 0.65$, (b) $w/b = 0.55$	59
Figure 4.6 Effect of binary blends of slag and fly ash on compressive strength development with CmA (a) $w/b = 0.65$, (b) $w/b = 0.55$	60
Figure 4.7 Effect of fly ash type on compressive strength development with CmP.....	61
Figure 4.8 Effect of fly ash type on compressive strength development with CmA.....	62
Figure 4.9 Effect of replacement level on the evolution of compressive strength of CmP blended with (a) SgB and (b) FaF	64

Figure 4.10 Effect of replacement level on the evolution of compressive strength of CmA blended with (a) SgB and (b) FaF	65
Figure 4.11 Ternary effect on the evolution of compressive strength of (a) CmP and (b) CmA cement concrete.....	66
Figure 4.12 Effect of fly ash on evolution of compressive strength of concrete with CmP and LC3 binder	67
Figure 4.13 Cube-cylinder strength ratio from this study	68
Figure 4.14 Comparison of $f_c'(t)/f_c'(28)$ data for (a) OPC, (b) SgA, concretes with the ACI prediction model and 95% confidence interval	70
Figure 4.15 Effect of replacement level of slag and fly ash on elastic modulus of concrete ..	73
Figure 4.16 Relation between the elastic modulus and compressive strength of concrete	75
Figure 5.1 Measured shrinkage strain on each side of CmP-NoSCM-0.65-280 cylinders.....	79
Figure 5.2 Measured shrinkage strain on CmP-NoSCM-0.65-280 cylinders (unsealed)	79
Figure 5.3 Measured shrinkage strain on each side of CmP-NoSCM-0.65-280 cylinders (sealed).....	80
Figure 5.4 Measured shrinkage strain on CmP-NoSCM-0.65-280 cylinders (sealed)	80
Figure 5.5 Measured shrinkage strain of CmP-NoSCM-0.65-280 prisms (unsealed).....	81
Figure 5.6 Measured shrinkage strain of CmP-NoSCM-0.65-280 prisms (sealed).....	81
Figure 5.7 Measured mass loss in CmP-NoSCM-0.65-280 cylinders (unsealed)	81
Figure 5.8 Measured mass loss in CmP-NoSCM-0.65-280 prisms (unsealed)	81
Figure 5.9 Effect of cement type on the shrinkage strain of concrete with w/b = 0.50 and total binder content = 310 kg/m ³ : (a) normal scale (b) log scale.....	82
Figure 5.10 Effect of cement type on the shrinkage strain of concrete with w/b = 0.55 and total binder content = 340 kg/m ³ : in (a) normal and (b) log scales.....	83
Figure 5.11 Effect of cement type on the shrinkage strain of concrete with w/b = 0.60 and total binder content = 310 kg/m ³ : in (a) normal and (b) log scales.....	84
Figure 5.12 Effect of cement type on the shrinkage strain of concrete with w/b = 0.45 and total binder content = 360 kg/m ³ : in (a) normal and (b) log scales.....	85
Figure 5.13 Effect of water to binder ratio on the shrinkage strain of binary blended concrete with w/b= 0.50 and total binder content = 310 kg/m ³ of CmP mix: in (a) normal and (b) log scales.....	86
Figure 5.14 Effect of water binder ratio on shrinkage strain of binary blended concrete with w/b= 0.60 and total binder = 310 kg/m ³ content of CmP mix: in (a) normal and (b) log scales	87

Figure 5.15 Effect of water binder ratio on the shrinkage strain of binary blended concrete with w/b= 0.50 and total binder 310 kg/m ³ content of CmA mix: in (a) normal and (b) log scales.....	88
Figure 5.16 Effect of water binder ratio on the shrinkage strain of binary blended concrete with w/b= 0.60 and total binder 310 kg/m ³ content of CmA mix: in (a) normal and (b) log scales.....	89
Figure 5.17 Effect of slag and fly ash on the shrinkage strain of binary blended concrete with w/b= 0.65 and total binder 280 kg/m ³ content of CmP mix: in (a) normal and (b) log scales.....	90
Figure 5.18 Effect of slag and fly ash on the shrinkage strain of binary blended concrete with w/b= 0.55 and total binder 340 kg/m ³ content of CmP mix: in (a) normal and (b) log scales.....	91
Figure 5.19 Effect of slag and fly ash on the shrinkage strain of binary blended concrete with w/b= 0.55 and total binder 340 kg/m ³ content of CmA mix: in (a) normal and (b) log scales.....	92
Figure 5.20 Effect of replacement level of slag on the shrinkage strain of binary blended concrete of CmP mix: in (a) normal and (b) log scales.....	94
Figure 5.21 Effect of replacement level of fly ash on shrinkage strain of binary blended concrete of CmP mix: in (a) normal and (b) log scales.....	95
Figure 5.22 Effect of fly ash type on the shrinkage strain of CmP mix containing 15% fly ash with w/b 0.55 and binder content of 340 kg/m ³ : in (a) normal and (b) log scales...	96
Figure 5.23 Effect of fly ash type on the shrinkage strain of CmP mix containing 15% fly ash with w/b 0.50 and binder content of 310 kg/m ³ : in (a) normal and (b) log scales...	96
Figure 5.24 Effect of fly ash type on the shrinkage strain of CmP mix containing 15% fly ash with w/b 0.60 and binder content of 310 kg/m ³ : in (a) normal and (b) log scales...	96
Figure 5.25 Effect of slag and fly ash on shrinkage strain of ternary blended concrete of CmP mix: in (a) normal and (b) log scales.....	97
Figure 5.26 Effect of fly ash on the shrinkage strain of concrete in comparison with CmP and LC3 binder on M30 grade of concrete: in (a) normal and (b) log scales.....	98
Figure 5.27 Effect of fly ash on the shrinkage strain of concrete in comparison with CmP and LC3 binder on M50 grade of concrete: in (a) normal and (b) log scales.....	99
Figure 5.28 Effect of fly ash on the shrinkage strain of concrete in comparison with CmP and LC3 binder for w/b= 0.45: in (a) normal and (b) log scales.....	100

Figure 5.29 Comparison of strength versus total shrinkage of concretes made with CmP cement	101
Figure 5.30 Comparison of strength versus total shrinkage of concretes made with CmA cement	101
Figure 5.31 Comparison of strength versus total shrinkage of concretes made with LC3 cement	102
Figure 5.32 Effect of specimen size on shrinkage strain of concrete	104
Figure 5.33 Mass loss of concrete on unsealed concrete (a) cylindrical specimen (b) prismatic specimen.....	105
Figure 5.34 Mass loss of concrete on sealed concrete (a) cylindrical specimen (b) prismatic specimen.....	105
Figure 5.35 Measured autogenous shrinkage of concrete on cylindrical specimens.....	107
Figure 5.36 Measured autogenous shrinkage of concrete on prismatic specimens	109
Figure 6.1 Comparison of experimental results and IS 1343 prediction for CmA-NoSCM- 0.55-340 concrete (unsealed), in (a) normal and (b) log scales	113
Figure 6.2 Comparison of experimental results and IS 1343 prediction for CmA-15SgA-0.55- 340 concrete (unsealed), in (a) normal and (b) log scales.....	114
Figure 6.3 Comparison of experimental results and IS 1343 prediction for CmA-15SgB-0.55- 340 concrete (unsealed), in (a) normal and (b) log scales.....	114
Figure 6.4 Comparison of experimental results and IS 1343 prediction for CmA-15FaF-0.55- 340 concrete (unsealed), in (a) normal and (b) log scales.....	114
Figure 6.5 Comparison of experimental results and IS 1343 prediction for CmA-15FaC-0.55- 340 concrete (unsealed), in (a) normal and (b) log scales.....	115
Figure 6.6 Comparison of experimental results and <i>fib</i> MC 2010 prediction for CmA- NoSCM-0.55-340 concrete, (a) normal scale, and(b) log scale	117
Figure 6.7 Comparison of experimental results and <i>fib</i> MC 2010 prediction for CmA-15SgA- 0.55-340 concrete (unsealed), in (a) normal and (b) log scales	117
Figure 6.8 Comparison of experimental results and <i>fib</i> MC 2010 prediction for CmA-15SgB- 0.55-340 concrete (unsealed), in (a) normal and (b) log scales	118
Figure 6.9 Comparison of experimental results and <i>fib</i> MC 2010 prediction for CmA-15FaF- 0.55-340 concrete (unsealed), in (a) normal and (b) log scales	118
Figure 6.10 Comparison of experimental results and <i>fib</i> MC 2010 prediction for CmA- 15FaC-0.55-340 concrete (unsealed), in (a) normal and (b) log scales	118

Figure 6.11 Comparison of experimental results and B4s prediction for CmA-NoSCM-0.55-340 concrete (unsealed), in (a) normal and (b) log scales	121
Figure 6.12 Comparison of experimental results and B4s prediction for CmA-15SgA-0.55-340 concrete (unsealed), in (a) normal and (b) log scales	121
Figure 6.13 Comparison of experimental results and B4s prediction for CmA-15SgB-0.55-340 concrete (unsealed), in (a) normal and (b) log scales	121
Figure 6.14 Comparison of experimental results and B4s prediction for CmA-15FaF-0.55-340concrete (unsealed), in (a) normal and (b) log scales	122
Figure 6.15 Comparison of experimental results and B4s prediction for CmA-15FaC-0.55-340 concrete (unsealed), in (a) normal and (b) log scales	122
Figure 6.16 Comparison of experimental results and ACI 209 prediction for CmA-NoSCM-0.55-340 concrete (unsealed), in (a) normal and (b) log scales	124
Figure 6.17 Comparison of experimental results and ACI 209 prediction for CmA-15SgA-0.55-340 concrete (unsealed), in (a) normal and (b) log scales	125
Figure 6.18 Comparison of experimental results and ACI 209 prediction for CmA-15SgB-0.55-340 concrete (unsealed), in (a) normal and (b) log scales	125
Figure 6.19 Comparison of experimental results and ACI 209 prediction for CmA-NoSCM-0.55-340 concrete (unsealed), in (a) normal and (b) log scales	125
Figure 6.20 Comparison of experimental results and ACI 209 prediction for CmA-NoSCM-0.55-340 concrete (unsealed), in (a) normal and (b) log scales	126
Figure 6.21 Comparison of experimental results and B4 prediction for CmA-NoSCM-0.55-340 concrete (unsealed), in (a) normal and (b) log scales	128
Figure 6.22 Comparison of experimental results and B4 prediction for CmA-15SgA-0.55-340 concrete (unsealed), in (a) normal and (b) log scales	128
Figure 6.23 Comparison of experimental results and B4 prediction for CmA-15SgB-0.55-340 concrete (unsealed), in (a) normal and (b) log scales	129
Figure 6.24 Comparison of experimental results and B4 prediction for CmA-15FaF-0.55-340 concrete (unsealed), in (a) normal and (b) log scales	129
Figure 6.25 Comparison of experimental results and B4 prediction for CmA-15FaC-0.55-340 concrete (unsealed), in (a) normal and (b) log scales	129
Figure 6.26 Comparison of experimental results and B4s prediction regressed for one year for CmA-NoSCM-0.55-340 concrete (unsealed), in (a) normal and (b) log scales .	135
Figure 6.27 Comparison of experimental results and B4s prediction regressed for one year for CmA-15SgA-0.55-340 concrete (unsealed), in (a) normal and (b) log scales....	135

Figure 6.28 Comparison of experimental results and B4s prediction regressed for one year for CmA-15SgB-0.55-340 concrete (unsealed), in (a) normal and (b) log scales	135
Figure 6.29 Comparison of experimental results and B4s prediction regressed for one year for CmA-15FaF-0.55-340 concrete (unsealed), in (a) normal and (b) log scales.....	136
Figure 6.30 Comparison of experimental results and B4s prediction regressed for one year for CmA-15FaC-0.55-340 concrete (unsealed), in (a) normal and (b) log scales	136
Figure 6.31 Comparison of experimental results and B4s prediction regressed for two years for CmA-NoSCM-0.55-340 concrete (unsealed), in (a) normal and (b) log scales	138
Figure 6.32 Comparison of experimental results and B4s prediction regressed for two years for CmA-15SgA-0.55-340 concrete (unsealed), in (a) normal and (b) log scales	138
Figure 6.33 Comparison of experimental results and B4s prediction regressed for two years for CmA-15SgB-0.55-340 concrete (unsealed), in (a) normal and (b) log scales	138
Figure 6.34 Comparison of experimental results and B4s prediction regressed for two years for CmA-15FaF-0.55-340 concrete (unsealed), in (a) normal and (b) log scales	139
Figure 6.35 Comparison of experimental results and B4s prediction regressed for two years for CmA-15FaC-0.55-340 concrete (unsealed), in (a) normal and (b) log scales	139
Figure 6.36 Comparison of experimental results and B4s prediction regressed for three years for CmA-NoSCM-0.55-340 concrete (unsealed), in (a) normal and (b) log scales	141
Figure 6.37 Comparison of experimental results and B4s prediction regressed for three years for CmA-15SgA-0.55-340 concrete (unsealed), in (a) normal and (b) log scales	141
Figure 6.38 Comparison of experimental results and B4s prediction regressed for three years for CmA-15SgB-0.55-340 concrete (unsealed), in (a) normal and (b) log scales	141
Figure 6.39 Comparison of experimental results and B4s prediction regressed for three years for CmA-15FaF-0.55-340 concrete (unsealed), in (a) normal and (b) log scales	142

Figure 6.40 Comparison of experimental results and B4s prediction regressed for three years for CmA-15FaC-0.55-340 concrete (unsealed), in (a) normal and (b) log scales	142
Figure 6.41 Comparison of experimental results and B4 prediction by considering aggregate as unknown for CmA-NoSCM-0.55-340 concrete (unsealed), in (a) normal and (b) log scales	144
Figure 6.42 Comparison of experimental results and B4 prediction by considering aggregate as unknown for CmA-15SgA-0.55-340 concrete (unsealed), in (a) normal and (b) log scales	144
Figure 6.43 Comparison of experimental results and B4 prediction by considering aggregate as unknown for CmA-15SgB-0.55-340 concrete (unsealed), in (a) normal and (b) log scales	145
Figure 6.44 Comparison of experimental results and B4 prediction by considering aggregate as unknown for CmA-15FaF-0.55-340 concrete (unsealed), in (a) normal and (b) log scales	145
Figure 6.45 Comparison of experimental results and B4 prediction by considering aggregate as unknown for CmA-15FaC-0.55-340 concrete (unsealed), in (a) normal and (b) log scales	145
Figure 6.46 Comparison of experimental results and B4 prediction by considering the effect of binder composition and aggregate as granite for CmA-NoSCM-0.55-340 concrete (unsealed), in (a) normal and (b) log scales	148
Figure 6.47 Comparison of experimental results and B4 prediction by considering the effect of binder composition and aggregate as granite for CmA-15SgA-0.55-340 concrete (unsealed), in (a) normal and (b) log scales	148
Figure 6.48 Comparison of experimental results and B4 prediction by considering the effect of binder composition and aggregate as granite for CmA-15SgB-0.55-340 concrete (unsealed), in (a) normal and (b) log scales	148
Figure 6.49 Comparison of experimental results and B4 prediction by considering the effect of binder composition and aggregate as granite for CmA-15FaF-0.55-340 concrete (unsealed), in (a) normal and (b) log scales	149
Figure 6.50 Comparison of experimental results and B4 prediction by considering the effect of binder composition and aggregate as granite for CmA-15FaC-0.55-340 concrete (unsealed), in (a) normal and (b) log scales	149

LIST OF ABBREVIATIONS

SCMs	:	Supplementary cementitious materials
OPC	:	Ordinary portland cement
CmP	:	Cement P
CmA	:	Cement A
LC3	:	Limestone calcined clay cement
SgA	:	Slag A
SgB	:	Slag B
FaF	:	Class F Fly ash
FaC	:	Class C Fly ash
w/c		Water to cement ratio
w/b	:	Water to binder ratio
SP	:	Superplasticizers
SSD	:	Saturated surface dry
SNF	:	Sulphonated naphthalene formaldehyde
PCE	:	Polycarboxylate ether
DEMEC	:	Demountable mechanical
CI	:	Confidence interval
CoV	:	Coefficient of variation
Sd	:	Standard deviation

1. INTRODUCTION

1.1 BACKGROUND

The most significant and common parameters used to quantify the quality of concrete are its strength, durability, shrinkage and creep response. A good concrete should satisfy the purpose for which it has been designed and also, it should be serviceable throughout its design life. The behaviour of concrete can be evaluated based on its short-term and long-term performance. Short-term performance includes the strength of the concrete in compression, tension, flexure and bonding, and its elastic modulus. On the other hand, the long-term performance of concrete includes durability, shrinkage, creep and fatigue response. Performance of concrete is influenced by several factors such as type and composition of cementitious materials, water-binder ratio, binder content, volume of aggregate in the mix, ambient temperature and relative humidity, geometry of the member.

Realistic estimations of shrinkage and creep of concrete are important for long-term performance and serviceability of concrete structures (Vandewalle, 2000). For the design of complex concrete structures, like long-span prestressed bridges and nuclear containment cooling vessels, it is important to use an appropriate prediction model to analyse their time-dependent behaviour. Shrinkage can cause an increase in deflection, and redistribution of stresses in reinforced concrete structures. In addition to this, shrinkage causes loss of prestress in prestressed concrete structures. The main factor of loss is due to elastic shortening, shrinkage and creep of concrete. Subsequently, the design capacity of the concrete member could be reduced or the structure could even suffer premature failure. Also, cracking due to restraining of the volumetric shrinkage strain facilitates corrosion in reinforced/prestressed concrete structures. In the case of pre-stressed concrete elements, the shrinkage induced strain also contributes to the loss of pre-stress.

Supplementary cementitious materials (SCMs) like fly ash, slag, silica fume, metakaolin etc. are used widely as modern construction materials in new infrastructure projects and repair and rehabilitation of existing structures, as they are found to improve the service life of concrete structures (Huo et al. 2001). In spite of tremendous applications of SCMs, the durability and the long-term performance of these blended cementitious materials is far from being completely understood, and their modelling remains critical as the properties vary largely from the conventional ordinary portland cement (OPC) concretes. Amongst the durability

parameters, shrinkage response of concrete is considered to have an important role in determining the long-term serviceability of the structure. Also, the values of elastic modulus and the ultimate shrinkage strain of concrete used in concrete design are often based on the values provided in international codes or based on the limited literature available for the materials used in Indian concretes. Since very limited work on shrinkage response has been carried out on Indian concrete, the information of the shrinkage characteristics of SCMs blended concrete is still limited. Hence, the findings from the present research work will provide more details to the existing data on the short and long-term mechanical performance of blended concrete using slag and fly ash. Further, a new limestone calcined clay cement (LC3) is studied here so that more extensive use in structural applications could be encouraged.

1.2 OBJECTIVES OF THE PRESENT STUDY

The main aim of the thesis is to provide some answers to the key research questions of determining whether SCMs used typically in India change the strength evolution and shrinkage response of concrete significantly and whether existing models can be used for predicting the long-term response reasonably. The specific objectives are:

1. To study the effect of slag, fly ash and limestone calcined clay on the compressive strength development and elastic modulus of concrete.
2. To study the influence of the incorporation of slag, fly ash and limestone calcined clay on the total and autogenous shrinkage response of concrete.
3. To assess the applicability of existing shrinkage prediction models for blended cement concrete and to calibrate the model parameters for better prediction.

The objectives of the study lead to the research approach outlined below:

- Laboratory testing for mechanical performance of concrete blended with slag and fly ash are conducted in accordance with ASTM, IS standards and RILEM recommendations.
- Compression tests at the ages of 2, 7, 28, 90 and 365 days are done, along with tests for the static elastic modulus of concrete at 28 days. The shrinkage evolution of concretes

was monitored from 28 days to about 1000 days on sealed and unsealed prisms and cylinders.

- Application of existing shrinkage prediction models and improvement of the predictions through adjustments of the parameters, where possible.

1.3 SCOPE

The present research work discusses the behaviour of fly ash and slag blended cement, and LC3 concrete in terms of compressive strength development, elastic modulus and shrinkage response in normal strength concrete with 28-day mean cube compressive strengths ranging between 20 and 55 MPa. Materials in this study were restricted to two brands of 53 Grade OPC and LC3, two slags (from two different sources in India) and two fly ashes (Class F and Class C). The parameters varied in the study are water-binder ratio, total binder content, and type and dosage of slag and fly ash; the type and volume fraction of aggregate has been kept constant. All the specimens were moist-cured. Total and autogenous shrinkage responses of concrete were monitored on standard cylindrical and prismatic specimens after the curing period of 28 days. However, the autogenous shrinkage until 28 days was not included in the measurements. The shrinkage prediction models assessed in this study are restricted to ACI 209R-95 2008, RILEM B4:2014 and B4s:2014, *fib* MC 2010 and IS 1343:2012.

1.4 STRUCTURE OF THE THESIS

The key phases and the steps involved in achieving the objective are described in Figure 1.1.

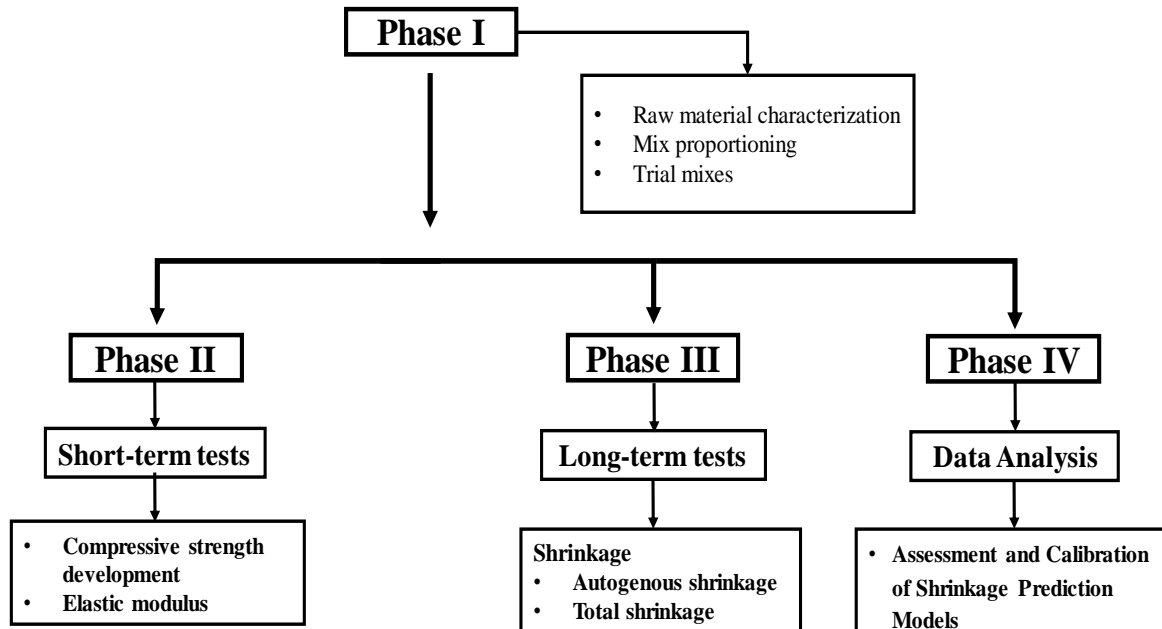


Figure 1.1 Key phases involved in the research work

The thesis is structured as seven chapters including this chapter.

Chapter 2 provides the detailed literature review related to the present study. The influence of SCMs on the strength development and elastic modulus has been presented in the first section. The second section briefly reviews previous studies on the influence of slag and fly ash on the shrinkage response of concrete. The chapter also provides a detailed description of shrinkage prediction models.

Chapter 3 presents the experimental programme, including the information on material characterisation, mix proportion and the composition of concrete. A detailed description of the experimental setup and the procedures used for various tests are also included in this chapter.

Chapter 4 has a detailed discussion of results on the influence of fly ash and slag on compressive strength development and the static elastic modulus of concrete. The evolution of compressive strength with time is presented, followed by a discussion on the influence on the SCM type and its dosage on the strength development and the variations in the results. A

comparison of strength evolution with ACI 209 prediction is done. Also, a comparison of the strength to elastic modulus relation with the standard equation is made.

Chapter 5 deals with the shrinkage response of fly ash and slag blended concrete in comparison with conventional OPC concrete. This chapter discusses the total shrinkage response of concrete followed by the influence of geometry on the shrinkage of concrete. Discussions of the autogenous shrinkage and mass loss also presented in this chapter.

Chapter 6 examines the application and adjustment of various shrinkage prediction models.

Chapter 7 presents a summary of the conclusions drawn from this work and also lists the recommendations for future study.

Three appendices are presented, which provide the data obtained from the tests. Appendix A consists of the compressive strength development plots. Appendices B1 and B2 have the results of shrinkage (total and autogenous) response of concrete on cylindrical and prismatic specimens, respectively. Appendices C1 and C2 consist of data on mass loss in cylindrical and prismatic specimens. Appendices D1 to D8 provide the comparison of the shrinkage prediction models with the experimental results. Appendix E reports the step-by-step procedure for the shrinkage calculation using different prediction models.

2. LITERATURE REVIEW

2.1 GENERAL

In recent times, the demand for supplementary cementitious materials (SCMs) has shown substantial increase in infrastructure and housing projects. It has also been established that these materials provide significant durability and long-term advantages over the conventional ordinary portland cement (OPC) concrete systems (Mokhtarzadeh and French, 2000). Hence, information of the materials on the mechanical performance, the progress and state-of the-art on the subject must be well understood before use in tropical countries like India. The objective of this chapter is to discuss the significance of slag and fly ash on short and long-term mechanical characteristics, such as compressive strength development, elastic modulus and shrinkage response of concrete in comparison with the OPC concrete systems. Also, a detailed description of existing shrinkage prediction models is provided in this chapter. Note that the literature review is limited to the examination of previous work on the effect of SCMs on strength evolution and shrinkage.

2.2 EFFECT OF SUPPLEMENTARY CEMENTITIOUS MATERIALS ON COMPRESSIVE STRENGTH AND ELASTIC MODULUS

Compressive strength of concrete is an important parameter for the design of concrete members, as it gives overall information about the quality of the concrete and has a direct relation with the microstructure of the hydrated cement paste. In addition to this, compressive strength of concrete is a vital factor for structural design and is quantified for compliance purposes. Over the past decade, development in new concrete such as high performance and high strength concrete have become practicable.

The elastic modulus of concrete is also a significant property in the mechanical performance of concrete since it not only controls the deformation but also decreases the stress transfer to the nearby concrete members, which can lead to a premature failure. In the place of pre-stressed concrete construction, elastic shortening is responsible for triggering losses in prestress, and could decrease load carrying capacity and even lead to unpredicted failure of the segments. Hence, information on the elastic modulus of concrete is important in order to control deformation and to provide effective serviceability of the structure (Nassif et al., 2005).

2.2.1 Effect of slag and fly ash on the compressive strength development of concrete

SCMs such as fly ash, ground granulated blast furnace slag (GGBS), silica fume and metakaolin are used widely as in binary blends in high-performance concrete as they enhance the short and long-term performance of concrete (Oner et al., 2005; Yang et al., 2007). Selection of these materials needs more consideration due to their different properties in early age and in long-term, i.e. initial reaction of fly ash, slag and silica fume are slower than the OPC, which retards the early age strength development and hence requires a longer curing period to attain a similar strength as that of OPC concrete. The performance is related to that of the pozzolanic reaction of fly ash and that the hydration of slag yields more refined pore structure. Also, in the long-term it improves the service life of the cement-based materials (Thomas et al., 2008; Ortega et al., 2014). On the other hand, adding a large amount of a single type of SCM could result in the delay of initial setting and low early age mechanical characteristics. In such cases, ternary blends can be used to balance the fresh and hardened properties of concrete (Khan et al., 2000; Bleszynski, et al., 2002; Schlorholtz, 2004).

The initial rate of hydration of slag is primarily dependent on the presence of the lime content. Mostafa et al. (2001) confirm a drastic decrease of free lime that occurs during the early age of hydration in slag. Unlike fly ash, the reactivity of slag mainly depends on temperature (Miura and Iwaki, 2000). In other words, slag cement reacts slowly at lower temperatures (Sivasundaram and Malhotra, 1992). Studies of Hamling and Kriner (1992) and Lim and Wee (2000) report that as the fineness of slag increased from 400 m²/kg to 600 m²/kg, the 28-day compressive strength increased considerably. Furthermore, the source of the slag was not significant for the performance of slag blended concrete (Wainwright and Rey, 2000). The early age strength development of slag-blended concrete was less than in the OPC concrete. Moreover, a substantial increase in the compressive strength was observed for a replacement between 40% and 60% than OPC concrete (Khatib and Hibbert, 2005; Atis and Bilim, 2007; Oner and Akyuz, 2007). However, a significant decrease in the strength was observed for a high replacement of cement by slag (80%). This could be due to the presence of unreacted slag acting as a filler material rather than it contributing to strength development. Studies of Hui-Shen et al. (2009) report that replacement level of 15%-30% was considered as an optimal dosage to get an equivalent strength of OPC concrete at 28 days.

In general, the combined use of different SCMs in concrete could reduce the efficiency of the cementitious systems. In other words, the compatibility between the binders is an issue which is to be considered in the proportioning of the concrete mixture. For instance, the reaction of Class F fly ash requires a high alkalinity of pore water than with slag or silica fume in the mix (Fraay et al., 1989 and Neville, 2006). Since the combination of SCMs having low surface area and the reactivity do not contribute to the early age strength development, Mehta and Gjørv (1994) have recommended to use a mixture of highly and normally reactive materials such as silica fume and fly ash to enhance the compressive strength development at early age (Mehta and Gjørv, 1982; Ozyildirim and Halstead, 1994; Khatri et al., 1995). Studies of Li and Zhao (2003), Tan and Pu (1998), Wu et al. (2003), Mehta and Gjørv (1982) and Ozyildirim and Halstead (1994) report that a ternary blend of slag and fly ash with OPC had excellent short and long-term compressive strength, and it improves the microstructure and the hydration rate compared to binary blends.

2.2.2 Effect of slag and fly ash on the elastic modulus of concrete

Generally, the effect of SCMs on the elastic modulus is similar to that of compressive strength. Therefore, the elastic modulus of SCM concrete is generally lower at early ages and marginally higher at prolonged curing time in comparison with the conventional OPC concrete system. Studies of Ghosh and Timusk (1981), Mehta (1983), Rezansoff and Stott (1990), Swamy and Bouikni (1990), Brooks (1992), Tikalsky and Carrasquillo (1992), ACI 233R-95 (2000), Jin and Li (2003), Newman and Choo (2003) and Johari et al. (2011) observed marginal differences in the elastic modulus of slag and fly ash blended concrete in comparison with conventional OPC concrete. Naik et al. (1998), Lane (1982), and Yildirim (2011) concluded that the early age elastic modulus of Class C fly ash was superior to that of Class F fly ash but on prolonged curing, Class F fly ash yielded an increase in the elastic modulus of concrete. This could be due to the increase in pozzolanic reactivity of fly ash with time. However, ACI 232.2R-96 (2002) and Kuder et al. (2012) report that high volume of slag or fly ash concrete had higher elastic modulus due to the densifying effect of unhydrated cementitious particles acting as fine aggregate.

2.2.3 Influence of LC3 on compressive strength development and the elastic modulus of concrete

Limestone Calcined Clay Cement (LC3) is a ternary blend of limestone, calcined clay (kaolinite) and gypsum with low clinker of 40 to 50%. The production can be done by either

blending or intergrinding the materials. Typically, clay containing 50 to 60% of kaolinite, can be calcined at around 700-800°C to remove the impurities and chemically attached hydroxyl group and thus making it as reactive, amorphous and pozzolanic. The ratio of calcined clay to limestone is typically fixed in the range of 2 to achieve a similar strength of OPC concrete (Scrivener et al., 2014). Githachuri and Alexander (2013) concluded that portland limestone cement shows similar long-term performance in the concrete system. Being more pozzolanic in nature, the calcined clay improves the microstructure and enhances the pore structure at early ages (Tironi et al., 2013). Examining the beneficial effects of limestone and calcined clay, the studies by Antoni et al. (2012) report that the incorporation of limestone and calcined clay as a blend produces similar mechanical properties as that of conventional OPC concrete mix.

2.3 EFFECT OF SUPPLEMENTARY CEMENTITIOUS MATERIALS ON THE SHRINKAGE OF CONCRETE

Volume changes in concrete would be more if it is free to deform; usually the structures are restrained by their foundation, by neighbouring concrete members subjected to different conditions of loading, orientation and reinforcement. Shrinkage is a time-dependent volumetric deformation of concrete related to loss of moisture that occurs at different ages of drying. It is predominantly related to the loss of water in the cement matrix. Shrinkage is categorized as plastic, autogenous, thermal, drying and carbonation shrinkage.

- **Plastic shrinkage** is due to loss of water from the concrete to the surrounding atmosphere through evaporation in the plastic state.
- **Autogenous shrinkage** (chemical shrinkage + self-desiccation) is caused by loss of internal water from the capillary pores after initial setting of concrete due to cement hydration. This may sometimes be called basic shrinkage, especially if the early autogenous shrinkage is not considered.
- **Thermal shrinkage** in concrete is due to the temperature drop after final setting.
- **Drying shrinkage** is due to loss of water from the concrete to the surrounding atmosphere through diffusion.
- **Carbonation shrinkage** is caused by reaction of atmospheric carbon dioxide (CO₂) with the hydrated cement product (CH).

The current study focuses on the shrinkage of hardened concrete caused by loss of moisture both internally and externally. The following section reviews the time-dependent volumetric strain due to autogenous and drying response of concrete.

Drying Shrinkage

Drying shrinkage in concrete is caused by the diffusion of water to the surrounding atmosphere. It refers to loss of capillary water by evaporation resulting in volume reduction. The volume change in concrete due to drying is not equal to volume of water removed (Mehta and Monteiro, 2006). This is because of the fact that the loss of free water from the larger capillary pores does not affect the volume change. However, water held by capillary tension in small pores may cause high shrinkage in concrete. It is only possible that drying shrinkage is connected to the removal of interlayer water. Depending on the size of the capillary pores and the relative humidity, the drying progresses more or less rapidly through the concrete. In a SCM blended concrete, drying shrinkage is low since the capillary pores are very fine and are not well connected by hydrated products.

Autogenous shrinkage

Autogenous shrinkage in concrete is an early deformation caused by loss of water from the capillary pores due to hydration, without any loss of water to the atmosphere. The mechanism and magnitude depend only on the mix proportion of the concrete and not on the external factors such as environmental condition. The magnitude of autogenous shrinkage is different for normal and high-performance concrete (Holt, 2001). Autogenous shrinkage is assumed to be negligible for concretes with higher water to cement ratio (say > 0.40). However, for the high-performance concrete with lower water to binder ratio (≤ 0.42) it is of concern since it contains more cementitious content with less water (Holt, 2001; Nishiyama, 2009). Typically, autogenous shrinkage strains for normal strength concrete are about 40×10^{-6} and 100×10^{-6} at one month and five years, respectively. On the other hand, at lower water-binder ratio (0.17) it is reported as a high value of 700×10^{-6} (Tazawa and Miyazawa, 1995).

Figure 2.1 shows the evolution of autogenous and drying shrinkage of concrete in a standard cylindrical specimen. In general, the total shrinkage of a cementitious material is the sum of autogenous and drying shrinkage.

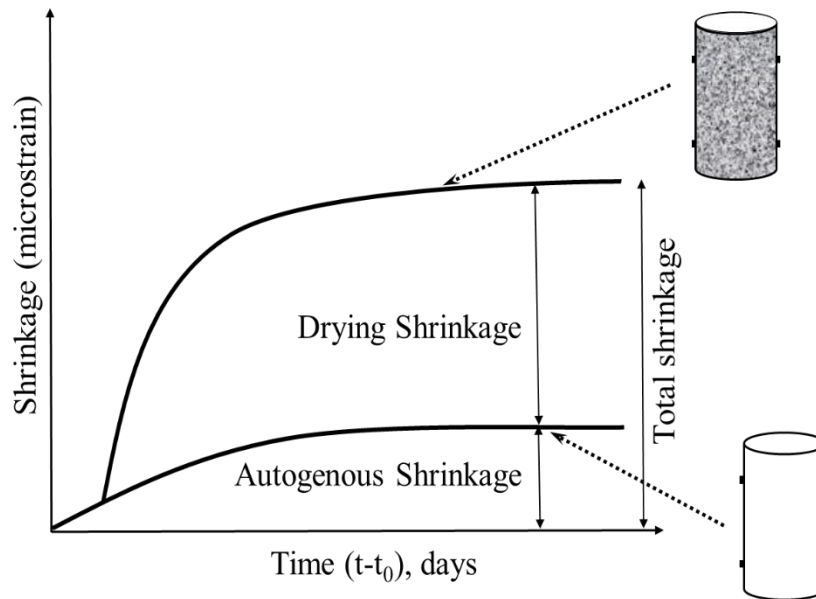


Figure 2.1 Evolution of shrinkage response in concrete (*plotted based on Neville, 2006*)

2.3.1 Effect of slag and fly ash on drying shrinkage of concrete

SCMs with different physical properties and chemical compositions influence the shrinkage response in concrete differently. However, past studies report that the effect of SCMs is highly variable and cannot be generalized on shrinkage response of concrete. Studies of Al-Sugair (1995), Bloom and Bentur (1995) and Wiegink et al. (1996) report that the addition of SCMs increases drying shrinkage. However, studies by others concluded a significant decrease in the shrinkage response of SCM blended concrete (Alsayed, 1998; Jianyong and Yan, 2001). For example, for slag and fly ash concrete with the same binder content, a lower water-binder ratio could produce a lower shrinkage strain. On the other hand, if the binder content is reduced at a constant water-binder ratio, the drying shrinkage tends to increase at early ages and remains constant in the long-term with respect to the portland cement concrete (Brooks and Neville, 1992). This is because slag and fly ash concrete have lower compressive strength at early ages, and subsequently, in the long-term when the compressive strengths of the non-blended and blended concrete are similar, the shrinkage response is similar as well. Previous studies also report that for a similar mix proportion, incorporation of slag tends to have a marginal effect on shrinkage of concrete (Whiting et al., 2000). Likewise, Class F fly ash could reduce drying shrinkage with an increase in the dosage in comparison with the OPC concrete (Gesoğlu et al., 2009). Studies by Deshpande et al. (2007) report that, due to high Ca/Si ratio and low alkali content, Class C fly ash causes more shrinkage than Class F fly ash and OPC mix. Also, high dosages of silica fume could increase the shrinkage response of concrete. In ternary blended

system, Class F and Class C fly ash in combination with silica fume or slag in OPC concrete, could reduce the drying shrinkage further (Guneyisi et al., 2010).

Work of Li and Yao (2001), Lee et al. (2006), and Gesoğlu et al. (2009) concluded that the incorporation of slag in OPC mix could result in lower drying shrinkage because of its lower capillary porosity and its denser microstructure. Thus, the incorporation helps promote the hydration and increases the density of hardened cement paste. This strengthens the pore structure and improves resistance to shrinkage deformation. The findings of Tazawa et al. (1989) and Yuan et al. (2015) are also in agreement with the same. Additionally, it was found that prolonged curing reduces the shrinkage strain in slag blended concrete systems (Wee and Wong, 2002; Deshpande, 2007). Studies of Yuan et al. (2015) report that a decrease in the shrinkage was observed at early ages with an increase in the replacement level of slag. Hooton et al. (2009) stated that replacement levels between 20% and 80% do not affect the shrinkage response of concrete. In the case of high-volume slag blended concrete, Sakai (1992) made the conclusion that for a replacement level of 50-60%, an increase in the shrinkage strain was observed whereas further increase in the replacement (70-80%) resulted in the decrease of shrinkage. Similar behaviour was also reported by Brooks (1992). In contradiction, Wedding et al. (1981); Chen and Chan (1989), and Juenger and Jennings (2001) concluded that an increase in the slag content increases the shrinkage response in concrete. It could be because of the higher paste volume in slag substituted concrete, due to its lower specific gravity and higher proportion of mesopore and pore volume, and high surface area (ACI 233R-95, 2000).

The ACI 232.2R-96 (2002) Recommendation reports that the shrinkage response of fly ash blended concrete increases marginally for a constant water-binder ratio, also the variation remains weak for a replacement level between 20-30%. Previous work from Mehta (1989), ACI 232.2R-96 (2002), and Chindaprasirt et al. (2004) found that the fineness of fly ash is insignificant on the shrinkage response of mortar. This could be due to the reduction of water demand with the presence of fly ash in the system. Ravindrarajah and Tam (1989), observed that an increase in the curing period reduces the shrinkage strain in fly ash blended concrete. This is related with the lower porosity resulting from the slowness of the pozzolanic reaction. Studies of Symons and Fleming (1980), Ghosh and Timusk (1981), Cripwell et al. (1984), Dunstan (1984), Nelson et al. (1992), Tia et al. (2005), Borsoi et al. (2009), and Gesoğlu et al. (2009) conclude that the incorporation of fly ash as a replacement of cement reduces shrinkage compared to that of OPC concrete. The beneficial effect is being more pronounced with an

increase in the replacement level of fly ash (Teorena and Nicolescu, 1982; Atis, 2003; Atis et al., 2004; Rivest et al., 2004; Yang et al., 2007; Khatib, 2008; Davis, 2012). The main mechanism of lower early age drying shrinkage of fly ash blended concrete is due to the filler effect, which decreases the porosity and connectivity between the pores (Papadakis, 2000; Poon et al., 2000; Siddique, 2006; Yang et al., 2007). However, in the long-term, shrinkage might be further reduced compared to that of early age due to the densification of the binder matrix. Such densification is a result of micro-filling, pozzolanic effect and the shape property of fly ash, which prevents the internal moisture evaporation and is different at later ages. In contradiction, Akkaya et al. (2007) report that fly ash and ultra-fine fly ash both increase the shrinkage, and the reason was the decrease of the difference in the connectivity of pore structure, which could make free water escape easily (Akkaya and Konsta, 2004; Atis et al., 2009).

2.3.2 Effect of slag and fly ash on autogenous shrinkage of concrete

The autogenous shrinkage of concrete is a function cement/binder type, which could be more influenced by the hydration of C_4AF and C_3A than that of C_2S and C_3S (Tazawa et al., 1999; Lura et al., 2003). Previous studies of Lim and Wee (2000), Lee et al. (2006), Tazawa (1997), Saric-Coric (2003) point out that autogenous shrinkage of slag blended concrete increases with an increase in the fineness and the replacement level. This is because of the hydration reaction of slag in the long-term, and due to enhancement of pore refinement that leads to increase in capillary tension and contraction stress, which increase the autogenous shrinkage (Omar et al., 2008). Additionally, at higher replacement because of the high paste volume, there is further increase in the autogenous shrinkage. (ACI 233R-95, 2000; Lura et al. 2003). According to Tangtermsirikul (1998) and Naik (2007), the fly ash blended concrete has lower early age autogenous shrinkage because of chemical shrinkage. However, the long-term autogenous shrinkage was found to increase (Naik, 2007; Khayat and Mitchell, 2009). Chindaprasirt et al. (2004) and Termkhajornkit et al. (2005) report that the autogenous shrinkage of fly ash paste increases with the progressing the degree of hydration. Chan et al. (1998) and Lura et al. (2003) conclude that HVFA concrete has further lower autogenous shrinkage.

2.4 MODELS FOR PREDICTING THE SHRINKAGE OF CONCRETE

Over the last century, many models have been developed for predicting shrinkage and creep response in concrete structures, and the main contributors were under the auspices of the American Concrete Institute (ACI), International Union of Laboratories and Experts in

Construction Materials, Systems and Structures (RILEM) and International Federation for Structural Concrete (*fib*). These organisations facilitated the collaboration of various researchers to create the prediction models for shrinkage and creep of concrete. The most significant models for prediction of shrinkage of concrete that are widely accepted are that of ACI: 209R-92, 2008, RILEM B4, 2014 and *fib* Model Code 2010. The input parameters for each prediction model can be divided into intrinsic and extrinsic factors. Intrinsic parameters are the concrete composition, i.e., cement content, type of cement, w/c ratio, aggregate to cement (paste) volume, and properties of aggregate and the standard compressive strength and the elastic modulus of concrete. The extrinsic parameters are relative humidity and temperature, the age at which the drying and the loading (in case of creep) of specimen started, the effective thickness of the cross section (V/S). Both extrinsic and intrinsic factors are considered in the formulation of the prediction models. The detailed description of each prediction model, the factors accounted for in the calculation and the equations are discussed in the following sections. In addition to this, Annex 1 provides the steps for the model calculations.

2.4.1 ACI 209, 2008 Model

The ACI 209, 2008 model uses a hyperbolic function of time multiplied with various correction factors such as curing method, relative humidity, size, slump, type of cement and air content in the mix design. The ACI model prediction is found to correlate well with the experimental measurements for the compressive strength up to 45 MPa (Omar et al., 2008). For 100% RH, the model yields no change in the shrinkage strain, which is inconsistent with the test values. The advantage of the model is its ease of use in calculation. The evolution of shrinkage can be derived from:

$$\varepsilon_{sh}(t, t_c) = \frac{(t - t_c)^\alpha}{f + (t - t_c)^\alpha} \times \varepsilon_{shu} \quad \text{Equation 2.1}$$

where, f and α are constants that depend on the shape and size of the member. The code recommends the average value for f of 35 for 7 days moist curing and 55 for 1-3 days of steam curing, and α as 1 to form flatter hyperbola. The time ratio does not differentiate between drying and autogenous shrinkage. ε_{shu} is the ultimate shrinkage strain and $t - t_c$ is the age of drying. In the absence of laboratory data and for local aggregates with an ambient relative humidity of 40%, the average value for the ultimate shrinkage strain is taken as:

$$\varepsilon_{shu} = 780 \times 10^{-6} \quad \text{Equation 2.2}$$

Other than the standard condition, the model suggests a multiplication factor (γ_{sh}) for the ultimate shrinkage strain.

$$\varepsilon_{shu} = 780 \times \gamma_{sh} 10^{-6} \quad \text{Equation 2.3}$$

$$\gamma_{sh} = \gamma_{sh\ tc} \times \gamma_{sh\ RH} \times \gamma_{sh\ vs} \times \gamma_{sh\ s} \times \gamma_{sh\ \psi} \times \gamma_{sh\ c} \times \gamma_{sh\ \alpha} \quad \text{Equation 2.4}$$

(i) Correction factor for curing ($\gamma_{sh\ tc}$)

For 7 days moist curing and for 1-3 days of steam curing the correction factor ($\gamma_{sh, tc}$) is 1. The correction factor for initial moist curing can also be obtained by linear regression analysis equation shown below.

$$\gamma_{sh\ tc} = 1.202 - 0.2337 \log(t_c)$$

(ii) Correction factor for ambient relative humidity ($\gamma_{sh\ Rh}$)

The correction factor for ambient relative humidity is calculated from the equation below. Further, the code does not predict any swelling of concrete.

$$\begin{aligned} \gamma_{sh\ Rh} &= 1.4 - 1.02h && \text{if } 0.4 \leq h \leq 0.8 \\ \gamma_{sh\ Rh} &= 3.0 - 3.00h && \text{if } 0.8 \leq h \leq 1 \end{aligned}$$

(iii) Correction factor for volume to surface ratio ($\gamma_{sh\ vs}$)

The model allows the capture of size effect of the member in terms of the volume-surface ratio for members with ratio and average thickness other than 38 mm and 150 mm, respectively. Average thickness (d) is defined as four times the volume-surface area ($4V/S$).

$$\gamma_{sh\ vs} = 1.2e^{[-0.00472(v/s)]}$$

Alternatively, it also allows the use of the average-thickness method to account for the effect of member size. The correction factor by this method is higher as compared to volume-surface method.

$$\gamma_{sh d} = 1.2 - 0.0015d$$

$$\gamma_{sh d} = 1.2 - 0.0060(V/S)$$

For $(t - t_c) > 1$;

$$\gamma_{sh d} = 1.17 - 0.00110d$$

$$\gamma_{sh d} = 1.17 - 0.00456(V/S)$$

For both the methods, γ_{sh} should not be taken less than 0.2. Also, the model proposes the values of $\gamma_{sh} \varepsilon_{shu} \geq 100 \times 10^{-6}$ mm/mm, if the concrete is under seasonal wetting and drying cycles and $\gamma_{sh} \varepsilon_{shu} \geq 150 \times 10^{-6}$ mm/mm, if it is under sustained drying.

(iv) Correction for slump ($\gamma_{sh s}$)

$$\gamma_{sh s} = 0.89 + 0.00161s$$

where, s is the slump of the fresh mixed concrete.

(v) Correction for fine aggregate ($\gamma_{sh \psi}$)

$$\gamma_{sh \psi} = 0.30 + 0.014\psi$$

if $\psi \leq 50 \%$

$$\gamma_{sh \psi} = 0.90 + 0.004\psi$$

if $\psi > 50 \%$

where, ψ is the ratio of fine aggregate by weight expressed in percent.

(vi) Correction for cement content ($\gamma_{sh c}$)

$$\gamma_{sh c} = 0.75 + 0.00061c$$

where, c is the cement content in the mix expressed in kg/m³.

(vii) Correction for air content ($\gamma_{sh \alpha}$)

$$\gamma_{sh \alpha} = 0.95 + 0.008\alpha$$

where α is the air content of fresh concrete mix in percent

2.4.2 B4, 2014 Model

The improved B4 model (RILEM TC 242) allows for the enhancement of multi-decade prediction, separates autogenous and drying shrinkage, and introduces a new formula and parameters in consideration with the effects of admixtures and aggregate type. The range of

applicability of B4 are much broader than the previous model B3. The range of various terms for B4 model that have been calibrated typically for practice are (i) $0.22 \leq w/c \leq 0.87$ (ii) $1.0 \leq a/c \leq 13.2$ (iii) $15 \text{ MPa} \leq f_c \leq 70 \text{ MPa}$ (iv) $200 \text{ kg/m}^3 \leq c \leq 1500 \text{ kg/m}^3$ (v) $25 \text{ }^\circ\text{C} \leq T \leq 75$ (vi) $20 \text{ }^\circ\text{C} \leq T_{\text{cur}} \leq 30 \text{ }^\circ\text{C}$, (vii) $12 \leq V/S \leq 120$. Since this has been made a possible calibration with multi-decade bridge data along with wide range of concrete strength with possible compositions. Equivalent time curve for creep and shrinkage was introduced in the model to allow to capture the effect of temperature on shrinkage and creep data and the aging rate. On account of theoretical reasons, all these effects are made as accelerations or decelerations that were governed by the activation energies (U). Thus, results in a horizontal shift in the logarithmic scale. The temperature effect on the curing and aging process is described as:

$$\tilde{t}_0 = t_0 \beta_{Th}$$

$$\beta_{Th} = \exp \left[\frac{U_h}{R} \left(\frac{1}{293} - \frac{1}{T_{\text{cur}} + 273} \right) \right] \quad \text{Equation 2.5}$$

For any constant temperature, $T_{\text{cur}} \in 22 \text{ }^\circ\text{C}, 30 \text{ }^\circ\text{C}$

$$\tilde{t} = (t - t_0) \beta_{Ts}$$

$$\beta_{Ts} = \exp \left[\frac{U_s}{R} \left(\frac{1}{293} - \frac{1}{T + 273} \right) \right] \quad \text{Equation 2.6}$$

$$\hat{t}' = t' \beta_{Th} \text{ and } \hat{t} = \hat{t}' + (t - t') \beta_{Th} \quad \text{Equation 2.7}$$

where, U_h and U_s are the activation energies for hydration and shrinkage. In the absence of test data U_h/R and U_s/R can be taken as 4000 K. In the Equations 5 and 6, T_{cur} and T refers to average curing and environmental temperature respectively. When the temperature is $20 \text{ }^\circ\text{C}$ the equivalent times reduces to actual time and duration (i.e).

$$\tilde{t}_0 = t_0; \tilde{t} = t - t_0 \text{ and } \hat{t}' = t'; \hat{t} = t \quad \text{Equation 2.8}$$

For high water-binder ratio, autogenous shrinkage is normally neglected. Though, for modern high-performance concrete with lower water-binder ratio, chemical and mineral additives exhibit substantial autogenous shrinkage. Hence, the model separates the total shrinkage ($\epsilon_{\text{sh, total}}$) into autogenous (ϵ_{au}) and drying shrinkage (ϵ_{sh}) strains:

$$\epsilon_{\text{sh, total}}(\tilde{t}, \tilde{t}_0) = \epsilon_{\text{sh}}(\tilde{t}, \tilde{t}_0) + \epsilon_{\text{au}}(\tilde{t}, \tilde{t}_0) \quad \text{Equation 2.9}$$

Drying Shrinkage

$$\epsilon_{sh}(\tilde{t}, \tilde{t}_0) = \epsilon_{sh\infty}(\tilde{t}_0) k_h S(\tilde{t}) \quad \text{Equation 2.10}$$

(i) Time curve:

$$S(\tilde{t}) = \tanh \sqrt{\frac{\tilde{t}}{\tau_{sh}}} \quad \text{Equation 2.11}$$

(ii) Final drying shrinkage is given as

$$\epsilon_0 = \epsilon_{cem} \left(\frac{a}{c} \right)^{p_{ea}} \left(\frac{W}{c} \right)^{p_{ew}} \left(\frac{6.5 c}{\rho} \right)^{p_{ec}} \quad \text{Equation 2.12}$$

Shrinkage correction for the effect of aging on elastic stiffness is given as:

$$\epsilon_{sh\infty}(\tilde{t}_0) = -\epsilon_0 k_{\epsilon a} \frac{E(7\beta_{Th} + 600\beta_{Ts})}{E(\tilde{t}_0 + \tau_{sh}\beta_{Ts})} \quad \text{Equation 2.13}$$

The evolution of elastic modulus according to ACI is modified to recover the 28-day value which is given by;

$$E(t) = E_{28} \sqrt{\frac{t}{4 \text{ days} + \left(\frac{6}{7}\right) t}} \quad \text{Equation 2.14}$$

$$E(7\beta_{Th} + 600\beta_{Ts}) = E_{28} \sqrt{\frac{7\beta_{Th} + 600\beta_{Ts}}{4 \text{ days} + 0.85(7\beta_{Th} + 600\beta_{Ts})}} \quad \text{Equation 2.15}$$

$$E(\tilde{t}_0 + \tau_{sh}\beta_{Ts}) = E_{28} \sqrt{\frac{\tilde{t}_0 + \tau_{sh}\beta_{Ts}}{4 \text{ days} + 0.85(\tilde{t}_0 + \tau_{sh}\beta_{Ts})}} \quad \text{Equation 2.16}$$

(iii) Half time drying shrinkage

$$\tau_{sh} = \tau_0 k_{\tau a} \left(k_s \frac{D}{1 \text{ mm}} \right)^2 \quad \text{Equation 2.17}$$

Half time drying shrinkage τ_{sh} characterizes the drying rate and it depends on the effective thickness of the member, where $D = 2V/S$

$$k_s = \begin{array}{l} 1.00 \text{ infinite slab} \\ 1.15 \text{ infinite cylinder} \\ 1.25 \text{ infinite prism} \\ 1.30 \text{ sphere} \\ 1.55 \text{ cube} \end{array}$$

$$\tau_0 = \tau_{cem} \left(\frac{a}{c} \right)^{p_{\tau a}} \left(\frac{W}{0.38c} \right)^{p_{\tau w}} \left(\frac{6.5c}{\rho} \right)^{p_{\tau c}} \quad \text{Equation 2.18}$$

Parameters ϵ_{cem} , τ_{cem} , and the exponential components p_{ea} , p_{ew} , p_{ec} , $p_{\tau a}$, $p_{\tau w}$, and $p_{\tau c}$ are the constants that depend on the type of cement, as given Table 2.1. k_{ea} and $k_{\tau a}$ are dimensionless factors that depend on the aggregate type according to Table 2.2. The information about the aggregates are unknown, the k_{ea} and $k_{\tau a}$ can be taken as 1.

(iv) Humidity dependence

$$k_h = \begin{cases} 1 - h^3 & h \leq 0.98 \\ 12.94(1 - h) - 0.2 & 0.98 \leq h \leq 1 \end{cases} \quad \text{Equation 2.19}$$

Table 2.1 Shrinkage parameters depending on cement type for B4

Parameter	Normal cement (R)	Rapid hardening cement (RS)	Slow hardening cement (SL)
τ_{cem} (days)	0.016	0.08	0.01
$p_{\tau a}$	-0.33	-0.33	-0.33
$p_{\tau w}$	-0.06	-2.40	3.55
$p_{\tau c}$	-0.10	-2.70	3.80
ϵ_{cem}	360×10^{-6}	860×10^{-6}	410×10^{-6}
p_{ea}	-0.80	-0.80	-0.80
p_{ew}	1.10	-0.27	1.00
p_{ec}	0.11	0.11	0.11

Table 2.2. Aggregate dependent parameter scaling factors for shrinkage for B4

Aggregate Type	$k_{\tau a}$	$k_{\epsilon a}$
Diabase	0.06	0.76
Quartzite	0.59	0.71
Limestone	1.80	0.95
Sandstone	2.30	1.60
Granite	4.00	1.05
Quartz Diorite	15.00	2.20

Autogenous Shrinkage

It is necessary to estimate the magnitude and evolution of the autogenous shrinkage which give a strong contribution to the total shrinkage strain when a low water to binder is involved. Although this empirical formula does not include the volume change of fresh concrete within the first few hours before the initial set of concrete. The development of autogenous shrinkage is calculated from:

$$\epsilon_{au}(\tilde{t}, \tilde{t}_0) = \epsilon_{au\infty} \left[1 + \left(\frac{\tau_{au}}{\tilde{t} + \tilde{t}_0} \right)^\alpha \right]^{r_t} \quad \text{Equation 2.20}$$

$$\alpha = r_\alpha \left(\frac{w/c}{0.38} \right)$$

(i) Final autogenous shrinkage

$$\epsilon_{au\infty} = -\epsilon_{au,cem} \left(\frac{a/c}{6} \right)^{r_{\epsilon a}} \left(\frac{w/c}{0.38} \right)^{r_{\epsilon w}} \quad \text{Equation 2.21}$$

(ii) Half time autogenous shrinkage:

$$\tau_{au} = \tau_{au,cem} \left(\frac{w/c}{0.38} \right)^{r_{\tau w}} \quad \text{Equation 2.22}$$

The parameters $\epsilon_{au,cem}$, $\tau_{au,cem}$, r_α and the exponential components $r_{\epsilon a}$, $r_{\epsilon w}$, $r_{\tau w}$, r_t are taken from Table 2.3 based on the type of cement considered.

Table 2.3. Autogenous shrinkage parameters depending on cement type for B4

Parameter	Normal cement (R)	Rapid hardening cement (RS)	Slow hardening cement (SL)
$\tau_{au,cem}$ (days)	1.00	41.00	1.00
$r_{\tau w}$	3.00	3.00	3.00
r_t	-4.50	-4.50	-4.50
r_α	1.00	1.40	1.00
$\epsilon_{au,cem}$	210×10^{-6}	-84×10^{-6}	0
$r_{\epsilon a}$	-0.75	-0.75	-0.75
$r_{\epsilon w}$	-3.50	-3.50	-3.50

Parameters for admixtures and aggregates

For high strength/performance concrete, the model accounts for the effects of admixture and their interaction is taken care of by admixture dependent parameter scaling factors that are given in Table 2.4. The scaling factors are to be multiplied to specific cement-type dependent parameters.

Table 2.4 Admixture dependent parameter scaling factors for shrinkage for B4

Admixture class (% of c)	$\times \tau_{cem}$	$\times \epsilon_{au,cem}$	$\times r_{ew}$	$\times r_a$
Re (≤ 0.5), Fly (≤ 15)	6.00	0.58	0.50	2.60
Re ($> 0.5, \leq 0.6$), Fly (≤ 15)	2.00	0.43	0.59	3.10
Re ($> 0.5, \leq 0.6$), Fly ($> 15, \leq 30$)	2.10	0.72	0.88	3.40
Re ($> 0.5, \leq 0.6$), Fly (> 30)	2.80	0.87	1.60	5.00
Re (> 0.6), Fly (≤ 15)	2.00	0.26	0.22	0.95
Re (> 0.6), Fly ($> 15, \leq 30$)	2.10	1.10	1.10	3.30
Re (> 0.6), Fly (> 30)	2.10	1.10	0.97	4.00
Fly (≤ 15), Super (≤ 5)	0.32	0.71	0.55	1.71
Fly (≤ 15), Super (> 5)	0.32	0.55	0.92	2.30
Fly ($> 15, \leq 30$), Super (≤ 5)	0.50	0.90	0.82	1.25
Fly ($> 15, \leq 30$), Super (> 5)	0.50	0.80	0.80	2.81
Fly (> 30), Super (≤ 5)	0.63	1.38	0.00	1.20
Fly (> 30), Super (> 5)	0.63	0.95	0.76	3.11
Super (≤ 5), Silica (≤ 8)	6.00	2.80	0.29	0.21
Super (≤ 5), Silica (≥ 8)	3.00	0.96	0.26	0.71
Super (≥ 5), Silica (≤ 8)	8.00	1.95	0.00	1.00
Silica (≤ 8)	1.90	0.47	0.00	1.20
Silica ($> 8, \leq 18$)	2.60	0.82	0.00	1.20
Silica (> 18)	1.00	1.50	5.00	1.00
AEA (≤ 0.05)	2.30	1.10	0.28	0.35
AEA (> 0.05)	0.44	4.28	0.00	0.36
WR (≤ 2)	0.50	0.38	0.00	1.90
WR ($> 2, \leq 3$)	6.00	0.45	1.51	0.30
WR (> 3)	2.40	0.40	0.68	1.40

Note: Re - retarder, Fly - fly ash, Super - superplasticizer, Silica - silica fume, AEA - air entraining agent, WR - water reducer.

2.4.3 B4s, 2014 Model

B4s model is a strength-based simplified version of the model B4. It uses the mean cylinder compressive strength (\bar{f}_c) of concrete to estimate the shrinkage strain. Parametric scaling factors that account for the type of cement used, aggregate type and specimen geometry are employed for the estimation of the shrinkage strain. If the information on the strength of the concrete is unknown, \bar{f}_c can be calculated as: $\bar{f}_c \approx f'_c + 8.3$ MPa or $\bar{f}_c \approx f'_c + 8$ MPa.

The methodology for prediction of shrinkage strains using the B4s model is given as:

(i) Estimate of drying shrinkage

The ultimate drying shrinkage strain is given by:

$$\epsilon_0 = \epsilon_{s, \text{cem}} \left(\frac{\bar{f}_c}{40 \text{ MPa}} \right)^{s_{\epsilon f}} \quad \text{Equation 2.23}$$

where, $\epsilon_{s, \text{cem}}$ and $s_{\epsilon f}$ are shrinkage dependent parameters based on the type of cement as given in Table 2.5.

(ii) Drying Shrinkage halftime

Drying shrinkage halftime can be calculated as:

$$\tau_0 = \tau_{s, \text{cem}} \text{ days} \left(\frac{\bar{f}_c}{40 \text{ MPa}} \right)^{s_{\tau f}} \quad \text{Equation 2.24}$$

The parameters $\tau_{s, \text{cem}}$ and $s_{\tau f}$ can be obtained from Table 2.5.

(iii) Autogenous shrinkage half time

$$\tau_{au} = \tau_{au, \text{cem}} \text{ days} \left(\frac{\bar{f}_c}{40 \text{ MPa}} \right)^{r_{\tau f}} \quad \text{Equation 2.25}$$

Refer Table 2.6 for Autogenous shrinkage parameters $\tau_{au, \text{cem}}$ and $r_{\tau f}$.

(iv) Final autogenous shrinkage

$$\epsilon_{au\infty} = -\epsilon_{au, \text{cem}} \left(\frac{\bar{f}_c}{40 \text{ MPa}} \right)^{r_{\epsilon f}} \quad \text{Equation 2.26}$$

The values of $\epsilon_{au, \text{cem}}$ and $r_{\epsilon f}$ are given in Table 2.6

(v) Autogenous shrinkage

$$\epsilon_{au}(\tilde{t}, \tilde{t}_0) = \epsilon_{au\infty} \left[1 + \left(\frac{\tau_{au}}{\tilde{t} + \tilde{t}_0} \right)^{\alpha_s} \right]^{r_t} \quad \text{Equation 2.27}$$

The values of α_s and r_t are given in Table 2.6

Table 2.5 Shrinkage parameters depending on cement type for B4s

Parameter	Normal cement (R)	Rapid hardening cement (RS)	Slow hardening cement (SL)
$\tau_{s,cm}$	0.027	0.027	0.032
S_{cf}	0.21	1.55	-1.84
$\epsilon_{s,cm}$	590×10^{-6}	830×10^{-6}	640×10^{-6}
S_{cf}	-0.51	-0.84	-0.69

Table 2.6 Autogenous shrinkage parameters for B4s for regular cement (R), rapid hardening cement (RS) and slow hardening cement (SL)

Parameter	Normal cement (R), Rapid hardening cement (RS), Slow hardening cement (SL)
$\tau_{au,cm}$	2.26
r_{cf}	0.27
$\epsilon_{au,cm}$	78.2×10^{-6}
r_{cf}	1.03
α_s	1.73
r_t	-1.73

2.4.4 *fib* Model Code 2010

The *fib* model code 2010 was developed by the International Federation for Structural Concrete (*fib*) in the year 2013. Compared with the previous CEB Models, the current model separates the total shrinkage into basic and drying shrinkage. Also, new functions and correction factors have been incorporated to capture the long-term behaviour of concrete for shrinkage prediction. The model is valid for the structural concrete with a mean compressive strength ranges between 20 MPa and 130 MPa, at a mean temperature ranging from 5°C to 30°C and a relative humidity in the range of 40% to 100%. The total shrinkage $\epsilon_{cs}(t, t_s)$ in concrete can be calculated as:

$$\epsilon_{cs}(t, t_s) = \epsilon_{cbs}(t) \times \epsilon_{c ds}(t, t_s) \quad \text{Equation 2.28}$$

The total shrinkage comprises of basic $\varepsilon_{\text{cbs}}(t)$, and drying shrinkage $\varepsilon_{\text{cds}}(t, t_s)$ of concrete is obtained from:

$$\varepsilon_{\text{cbs}}(t) = \varepsilon_{\text{cb0}}(f_{\text{cm}}) \times \beta_{\text{bs}}(t) \quad \text{Equation 2.29}$$

$$\varepsilon_{\text{cds}}(t, t_s) = \varepsilon_{\text{cds0}}(f_{\text{cm}}) \times \beta_{\text{RH}} \times \beta_{\text{ds}}(t - t_s) \quad \text{Equation 2.30}$$

The basic shrinkage parameter is calculated from basic notional shrinkage coefficient $\varepsilon_{\text{cb0}}(f_{\text{cm}})$ and time function $\beta_{\text{bs}}(t)$;

$$\varepsilon_{\text{cb0}}(f_{\text{cm}}) = -\alpha_{\text{bs}} \left[\frac{0.1 \times f_{\text{cm}}}{6 + 0.1 \times f_{\text{cm}}} \right]^{2.5} \times 10^{-6} \quad \text{Equation 2.31}$$

$$\beta_{\text{bs}}(t) = 1 - e^{(-0.2 \times \sqrt{t})} \quad \text{Equation 2.32}$$

Final drying shrinkage can be calculated by notional drying shrinkage parameter $\varepsilon_{\text{cd0}}(f_{\text{cm}})$, humidity co-efficient β_{RH} and the time development function $\beta_{\text{ds}}(t - t_s)$ as given in equations 33, 34 and 35 respectively.

$$\varepsilon_{\text{cd0}}(f_{\text{cm}}) = [(220 + 110 \times \alpha_{\text{ds1}})] \times e^{(-\alpha_{\text{ds1}} f_{\text{cm}})} \times 10^{-6} \quad \text{Equation 2.33}$$

$$\beta_{\text{RH}} = -1.55 [1 - (RH^3)] \quad \text{Equation 2.34}$$

$$\beta_{\text{ds}}(t - t_s) = \left[\frac{t - t_s}{0.035 \times h^2 + (t - t_s)} \right]^{0.5} \quad \text{Equation 2.35}$$

where, h is the notional size of the member. ($h = \frac{A_c}{u}$), where A_c and u are the cross-sectional area of and perimeter of the member in contact with the atmosphere. Co-efficient α_{bs} , α_{ds1} , α_{ds2} are the shrinkage parameters that depend on the strength class of cement as given in Table 2.7

Table 2.7 Co-efficient used for basic and drying shrinkage of concrete

Strength class of cement	α_{bs}	α_{ds1}	α_{ds2}
32.5 N	800	6	0.013
32.5 R, 42.5 N	700	4	0.012
42.5 R, 52.5 N, 52.5 R	600	6	0.012

2.4.5 IS 1343, 2012

The Indian standard code for prediction of prestressed concrete IS 1343:2012 specifies the procedure for estimating shrinkage in concrete. The total shrinkage strain comprises two components, autogenous shrinkage and drying shrinkage strain.

The total shrinkage strain (\mathcal{E}_{cs}) is given by

$$\mathcal{E}_{cs} = \mathcal{E}_{ca} + \mathcal{E}_{cd} \quad \text{Equation 2.36}$$

where, \mathcal{E}_{cd} = Drying shrinkage strain

\mathcal{E}_{ca} = Autogenous shrinkage strain

\mathcal{E}_{cs} = Total shrinkage strain

In the absence of test data, the values of autogenous shrinkage can be taken from Table 2.8.

Table 2.8 Unrestrained autogenous shrinkage ($\mathcal{E}_{ca} \times 10^6$)

Grade of concrete	Autogenous shrinkage $\mathcal{E}_{ca} \times 10^6$
M30	35
M35	45
M45	65
M50	75
M60	95

Development of autogenous shrinkage with time is calculated as

$$\mathcal{E}_{ca}(t) = \beta_{as}(t) \cdot \mathcal{E}_{ca} \quad \text{Equation 2.37}$$

where,

$$\beta_{as}(t) = 1 - \exp(-0.2\sqrt{t}) \quad \text{Equation 2.38}$$

The final drying shrinkage strain ($\mathcal{E}_{cd,\infty}$) is calculated from

$$\mathcal{E}_{cd,\infty} = k_h \cdot \mathcal{E}_{cd} \quad \text{Equation 2.39}$$

Values of \mathcal{E}_{cd} can be taken from the Table 2.9.

Table 2.9 Unrestrained drying shrinkage values ($\epsilon_{cd} \times 10^6$)

f_{ck} (MPa)	<i>Unrestrained drying shrinkage values ($\epsilon_{cd} \times 10^6$) for concrete with portland cement</i>	
	RH= 50%	RH = 80%
25	535	300
50	420	240
75	330	190

Note - The values for the other designated grades may be obtained by interpolation.

k_h is a coefficient depending on the notional size h_0 and is taken from Table 2.10 for corresponding values of h_0 .

Table 2.10 Co-efficient depending on the notional size

h_0 (mm)	k_h
100	1.0
200	0.85
300	0.75
≥ 500	0.70

Development of drying shrinkage strain is calculated from:

$$\epsilon_{cd}(t) = \beta_{ds}(t, t_s) \cdot k_h \cdot \epsilon_{cd} \quad \text{Equation 2.40}$$

$$\beta_{ds}(t, t_s) = \frac{(t, t_s)}{(t, t_s) + 0.04\sqrt{h^3}} \quad \text{Equation 2.41}$$

where,

t = age of the concrete at the moment considered, (days).

t_s = age of the concrete at the beginning of drying shrinkage, (days).

h_0 = notional size of the cross-section, (mm).

$h_0 = \frac{2A_c}{u}$, A_c is the concrete cross-sectional area and u is the perimeter of that part of the cross-section which is exposed to drying.

2.5 SUMMARY AND RESEARCH SIGNIFICANCE

This chapter discussed the literature related to the influence of SCMs on the mechanical performance of concrete, particularly when slag and fly ash are blended in OPC concrete systems. The discussion in the initial part gave an insight on the importance of the SCMs on the compressive strength development, elastic modulus and shrinkage response of concrete. The studies state that the incorporation of slag and fly ash reduces the early age strength development, which could be compensated by prolonged curing. Also, the elastic modulus depends on the compressive strength and it was observed from the previous work that SCM blended concrete does not influence the elastic modulus of concrete. The chapter also delineated the influence of slag and fly ash on the shrinkage behaviour of concrete. The past works shows that the shrinkage response of SCM blended concrete depend on the type and dosage. Various shrinkage prediction models are also deliberated in detail along with the parameters used for the calculation. From the state-of-the-art discussed in this chapter, it can be concluded that limited work has focussed on the shrinkage response of concrete in the Indian context. Hence, this study aims at the understanding of the shrinkage of fly ash and slag blended concrete with locally available materials.

3. MATERIALS AND EXPERIMENTAL PROGRAMME

3.1 INTRODUCTION

Estimates of shrinkage strain for typical concretes used in India, especially with supplementary cementitious materials (SCMs), are very limited. Particularly, since shrinkage testing has been rarely performed in India, the existing knowledge is rare. This scenario makes it difficult for implementing these short-term and long-term material parameters in structural design in a rational manner. Therefore, there is a need for comprehensive testing and evaluation of the mechanical and long-term performance characteristics of concrete so that appropriate values can be used at the designing stage. Consequent to this need, an elaborate experimental programme is performed to obtain and compare the performance characteristics of concrete with various combinations of binders, SCMs and water/binder contents.

This chapter describes the experimental programme used for the mechanical characterization of various types of concrete used in this work. Relevant properties of the raw materials used for preparing the concrete have been provided, along with a discussion on the various mixes and the mix proportioning. The section on test methodology describes the testing parameters, apparatus used, and the procedures adopted for fresh concrete and hardened concrete characterization, including short term and long-term mechanical properties, such as compressive strength, elastic modulus, and the shrinkage response.

In fact, the experimental study involved the three phases as given below.

Phase I - Mix proportioning and fresh concrete characterization: This phase consisted of selection of materials including types of binders and SCMs, characterization of raw materials, fixing binder contents and corresponding water/binder ratios, mix proportioning, trial mixing of concrete to fix chemical admixture dosage, and final batching and specimen preparation, including fresh concrete testing.

Phase II - Characterization of short-term mechanical properties: The evolution of cube compressive strength, and elastic modulus were determined using appropriate tests.

Phase III - Characterization of long-term mechanical properties: Shrinkage behaviour was studied using cylindrical/prismatic specimens over a period of 1000 days

For each mix belonging to a certain category, the types of specimen cast are listed below:

- **Category CmP**
 - 15 cubes of 100 mm
 - 9 cylindrical specimens of 150 mm diameter and 300 mm height
 - 6 prism specimens of 75 mm × 75 mm × 285 mm
- **Category CmA**
 - 15 cubes of 100 mm
 - 6 cylindrical specimens of 150 mm diameter and 300 mm height
- **Category LC3**
 - 15 cubes of 100 mm
 - 9 cylindrical specimens of 150 mm diameter and 300 mm height
 - 6 prism specimens of size 75 mm × 75 mm × 285 mm

The details of the specimen prepared for each mix are provided in Table 3.1. As there was a limited supply of CmA cement, the study was restricted to a few mixes.

Table 3.1 Details of specimens for categories CmP, CmA and LC3 concrete

Category	w/b	Total binder content (kg/m ³)	100 mm cubes	150 mm diameter and 300 mm height cylinders	75 mm × 75 mm × 285 mm prisms
CmP	0.65	280	15 specimens were tested for each water to binder ratio at 2, 7, 28, 90 and 365 days of curing	3 specimens were tested for elastic modulus and 6 specimens were tested for shrinkage on each water to binder ratio	6 specimens were tested for shrinkage on each water to binder ratio
	0.55	340			
	0.50	310			
	0.60	310			
	0.45	360			
	0.40	360			
CmA	0.50	310	15 specimens were tested for each water to binder ratio at 2, 7, 28, 90 and 365 days of curing	6 specimens were tested for shrinkage on each water to binder ratio	-
	0.55	340			
	0.60	310			

Table 3.1 (continued) Details of specimens for categories CmP, CmA and LC3 concrete

Category	w/b	Total binder content (kg/m ³)	100 mm cubes	150 mm diameter and 300 mm height cylinders	75 mm × 75 mm × 285 mm prisms
LC3	0.50	310	15 specimens were tested for each water to binder ratio at 2, 7, 28, 90 and 365 days of curing	3 specimens were tested for elastic modulus and 6 specimens were tested for shrinkage on each water to binder ratio	6 specimens were tested for shrinkage on each water to binder ratio
	0.45	340			
	0.40	360			

3.2 CONCRETE-MAKING MATERIALS

3.2.1 Binders

53 Grade ordinary portland cement (OPC) of two different brands and limestone calcined clay cement (LC3) were used as primary binders. LC3 is a new type of cement, which is a blend of calcined clay, limestone and clinker content of about 50 %. The ratio of calcined clay to the limestone was in the range of 2 (Scrivener, 2014). SCMs were included as partial replacement in OPC mixes to produce binary and ternary blends of binders. The SCMs used are:

- Ground-granulated blast furnace slag from two sources
- Class F fly ash, and
- Class C fly ash
- Limestone calcined clay (preground with the clinker in LC3)

The physical properties of the binders and SCMs were determined based on appropriate standards, and the results are presented in Table 3.2, along with the nomenclature used (IS 1727-2004, ASTM C204-11). The oxide composition of each material was determined using X-Ray fluorescence spectroscopy, and the results are presented in Table 3.3. From the physical characteristics, it is seen that LC3 binder has higher fineness in comparison to all other binders.

Table 3.2 Physical properties of binders and supplementary cementitious materials (SCMs)

Binders and SCMs	Specific Gravity	Specific surface area (m ² /kg)
Cement brand P (CmP)	3.18	320
Cement brand A (CmA)	3.15	340
LC ³ cement (LC3)	3.01	520
Slag from Source A (SgA)	2.86	360
Slag from Source B (SgB)	2.89	430
Class F fly ash (FaF)	2.49	330
Class C fly ash (FaC)	2.46	390

Table 3.3 Chemical composition of binders

Oxides	% Concentration						
	CmP	CmA	LC3	SgA	SgB	FaF	FaC
Al ₂ O ₃	4.07	4.73	10.82	17.38	21.06	29.95	31.46
CaO	59.61	65.11	41.77	35.61	31.46	1.28	13.76
Fe ₂ O ₃	5.37	3.86	3.66	1.04	1.87	4.32	6.17
K ₂ O	0.27	0.54	0.17	0.58	0.88	1.44	0.12
MgO	0.82	1.20	1.78	8.03	8.57	0.61	2.28
Na ₂ O	0.23	0.50	0.18	0.36	0.36	0.16	0.59
SiO ₂	20.42	19.44	31.03	33.82	32.38	59.32	39.89
SO ₃						0.16	3.19

The oxide compositions of both cements CmP and CmA are comparable, and within the expected range. The two slags are also similar in composition. However, as expected, the calcium oxide content of Class C fly ash is higher than Class F fly ash indicating its cementitious nature.

3.2.2 Aggregates

Crushed granite size fractions of 5-10mm and 10-20 mm were used as coarse aggregates in a proportion of 40:60, and locally available river sand with maximum size of 5 mm was used as fine aggregate, for all concrete mixes. The determination of physical properties was done according to IS 2386-I and III, and the results are given in Table 3.4 and Figure 3.1. The particle size distributions of the fine aggregates are seen to fall within Zone II, according to the classification in IS 383-2007.

Table 3.4 Physical properties of aggregates

Physical property	Coarse aggregate						Fine aggregate		
	5 -10 mm			10 - 20 mm			0 - 5 mm		
	Batch 1	Batch 2	Batch 3	Batch 1	Batch 2	Batch 3	Batch 1	Batch 2	Batch 3
Specific gravity (SSD)	2.76	2.72	2.78	2.77	2.60	2.66	2.53	2.34	2.40
Water absorption (%)	0.43	0.41	0.40	0.41	0.60	0.66	0.74	0.80	0.72

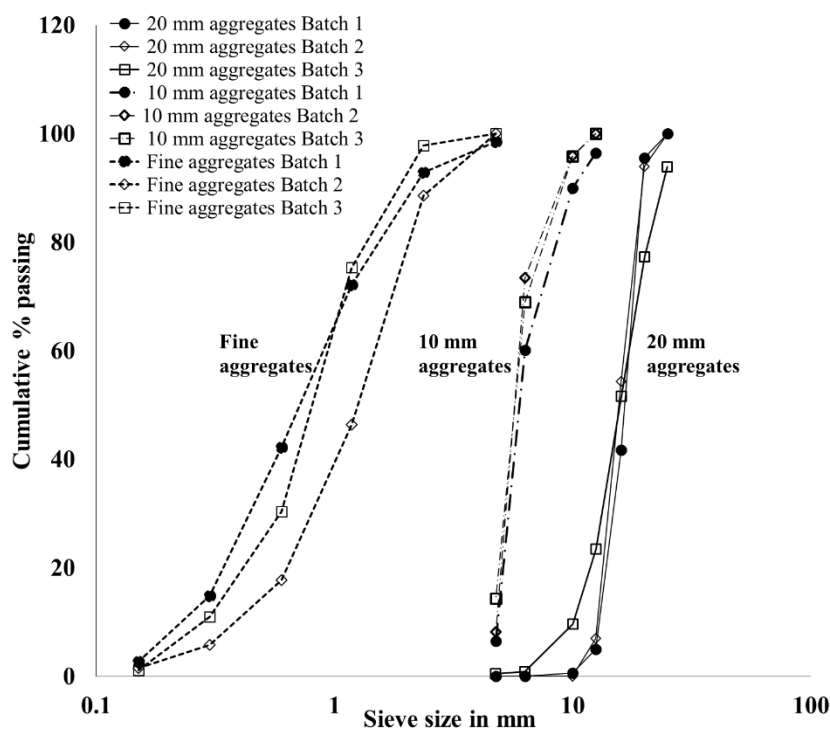


Figure 3.1 Particle size distribution of aggregates used in the study

3.2.3 Superplasticizers

Commercially available sulphonated naphthalene formaldehyde (SNF) and polycarboxylate ether (PCE) superplasticizers were used for the work, and the nomenclature and physical properties are presented in Table 3.5. Following the suggestions of the admixture suppliers, SNF-1 superplasticizer was used for the concrete mixes made with CmP, and SNF-2 was used for mixes with CmA. For the LC3 mixes, PCE based superplasticizer was used since earlier studies done at IIT Madras had shown that SNF based SP could have compatibility issues with LC3 (Nair, 2018).

Table 3.5 Properties of superplasticizers (as given by from the suppliers)

Property	SNF-1 (Daracem 811)	SNF-2 (Daracem 910)	PCE (Master Glenium 8233)
Appearance	Dark brown colour liquid	Dark brown colour liquid	Reddish brown colour liquid
Specific gravity	1.17	1.24	1.08
pH	7 – 8	6.6	6.0
%solid content	44.5	40.9	34.0

3.3 CONCRETE MIX DESIGN

3.3.1 Mix proportions

The concrete mixes for the research work were designed to represent typical grades of concrete used in the construction industry in India. Accordingly, all mixtures were designed to have mean compressive strength ranging between 25 and 60 MPa (i.e., concrete grades ranging between M20-M50). Based on the existing literature on compressive strength development of concretes with binary and ternary blends of the chosen binders, a preliminary estimate of the water content for the different grades of concrete was made. Consequently, the water/binder ratio was varied between 0.35-0.65. The entire casting was done for three categories of concretes as listed in Table 3.1, based on the type of primary binder used (i.e., Cement P – CmP, Cement A – CmA, and LC3 cement). The mix design was done as per IS 10262:2010.

Mixes were prepared with different replacement levels of cement with four SCMs, as listed in Table 3.6. The mix nomenclature style is shown in Figure 3.2. The first three letters indicate the cement type (e.g., ‘CmP’), the next two numbers and three letters represent the level of binder replacement by the lone SCM (in %) and its type in binary blends. For ternary blends, this is followed by the level of binder replacement by the second SCM and its type. For example, a ternary blend with 20% Slag B and 20% Class F fly ash will be denoted as ‘-20SgB-20FaF-’. If there is no SCM in the mix, then, it is denoted as ‘NoSCM’. The two numbers following this indicate the w/b (e.g., ‘-0.55-’). The last three digits indicate the total binder content. For example, CmP- 15gSgA-0.50-310 represents the mix with cement CmP and 15% replacement by Slag A (SgA) for w/b of 0.50 and total binder content of 310 kg/m³. Trial mixes were made to finalise the required SP dosage for a slump of 100 mm ±30 mm, and the SP dosage used is shown in Table 3.6. Note that in the case of CmP-NoSCM-0.50-310, two mixes

were made with slightly different aggregate combinations, as shown in rows 10 and 55 in the table; the second mix with is denoted as CmP-NoSCM-0.50-310x.

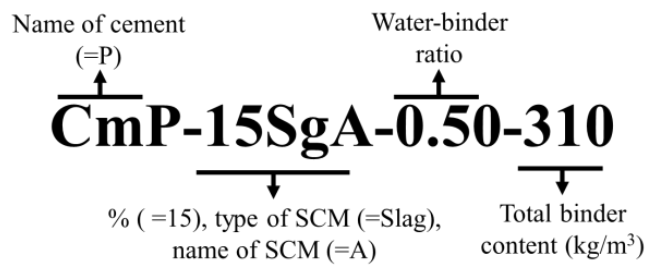


Figure 3.2 Nomenclature for the concrete mixes

Table 3.6 Concrete mix proportions

Sl. No.	Nomenclature	Total binder content (kg/m ³)	Fine aggregate (kg/m ³)		Coarse aggregate (kg/m ³)		Total water content (kg/m ³)	SP, as % weight of binder
			0-5 mm	5-10 mm	10-20 mm			
1	CmP-NoSCM-0.65-280	280	744	477	716	182	0.00	
2	CmP-30SgA-0.65-280						0.00	
3	CmP-30SgB-0.65-280						0.05	
4	CmP-30FaF-0.65-280						0.00	
5	CmP-NoSCM-0.55-340	340	719	461	692	187	0.00	
6	CmP-15SgA-0.55-340						0.00	
7	CmP-15SgB-0.55-340						0.02	
8	CmP-15FaF-0.55-340						0.03	
9	CmP-15FaC-0.55-340						0.55	
10	CmP-NoSCM-0.50-310	310	743	477	715	155	0.02	
11	CmP-15SgA-0.50-310						0.18	
12	CmP-15SgB-0.50-310						0.11	
13	CmP-15FaF-0.50-310						0.00	
14	CmP-15FaC-0.50-310						0.19	
15	CmP-30SgB-0.50-310						0.30	
16	CmP-30FaF-0.50-310						0.10	
17	CmP-30FaC-0.50-310						0.14	
18	CmP-50SgB-0.50-310						0.30	
19	CmP-50FaF-0.50-310						0.30	
20	CmP-20SgB-20FaF-0.50-310						0.55	
21	CmP-20SgB-20FaC-0.50-310						0.55	
22	CmP-20FaF-20FaC-0.50-310	0.36						

Table 3.6 (continued) Concrete mix proportions

Sl. No.	Nomenclature	Total binder content (kg/m ³)	Fine aggregate (kg/m ³)	Coarse aggregate (kg/m ³)		Total water content (kg/m ³)	SP, as % weight of binder
			0-5 mm	5-10 mm	10-20 mm		
23	CmP-NoSCM-0.60-310	310	731	469	704	186	0.36
24	CmP-15SgA-0.60-310						0.00
25	CmP-15SgB-0.60-310						0.05
26	CmP-15FaF-0.60-310						0.36
27	CmP-15FaC-0.60-310						0.36
28	CmA-NoSCM-0.65-280	280	685	529	794	182	0.05
29	CmA-30SgA-0.65-280						0.06
30	CmA-30SgB-0.65-280						0.08
31	CmA-30FaF-0.65-280						0.05
32	CmA-NoSCM-0.55-340	340	662	512	768	187	0.00
33	CmA-15SgA-0.55-340						0.03
34	CmA-15SgB-0.55-340						0.12
35	CmA-15FaF-0.55-340						0.00
36	CmA-15FaC-0.55-340						0.03
37	CmA-NoSCM-0.50-310	310	684	529	793	155	0.40
38	CmA-15SGgA-0.50-310						0.45
39	CmA-15SgB-0.50-310						0.48
40	CmA-15FaF-0.50-310						0.30
41	CmA-15FaC-0.50-310						0.30
42	CmA-30SgB-0.50-310						0.52
43	CmA-30FaF-0.50-310						0.30
44	CmA-30FaC-0.50-310						0.40
45	CmA-50SgB-0.50-310						0.59
46	CmA-50FaF-0.50-310						0.25
47	CmA-20SgB-20FaF-0.50-310						0.12
48	CmA-20SgB-20FaC-0.50-310	0.42					
49	CmA-20-FaF-20FaC-0.50-310	0.30					
50	CmA-NoSCM-0.60-310	310	673	520	781	186	0.05
51	CmA-15SgA-0.60-310						0.05
52	CmA-15SgB-0.60-310						0.04
53	CmA-15FaF-0.60-310						0.10
54	CmA-15FaC-0.60-310						0.15
55	CmP-NoSCM-0.50-310x	310	695	496	744	155	0.02
56	CmP-30FaF-0.45-310		723	491	737	140	0.65
57	LC3- NoSCM-0.50-310		708	491	736	155	1.00
58	CmP-NoSCM-0.40-360	360	703	477	716	144	0.65
59	CmP-30FaF-0.35-410	410	699	475	713	133	0.60
60	LC3-NoSCM-0.40-340	340	704	488	732	136	0.85
61	CmP-NoSCM-0.45-360	360	721	463	694	162	0.10
62	CmP-30FaF-0.45-360		721	463	694	162	0.23
63	LC3-NoSCM-0.45-360		687	476	715	162	0.36

3.3.2 Mixing procedure, casting, curing and storing of specimens

The concrete mixes were prepared in a vertical-axis forced-action pan mixer, with a capacity of 250 litres. Before batching, the moisture content of aggregates was determined and suitable corrections were done for the water content needed for the aggregates to be in (saturated surface dry) SSD conditions. The materials used were weigh-batched and then transferred to the pan mixer that was previously wetted with a cement slurry. The sequence of mixing consisted of dry mixing of coarse and fine aggregate for about 1 minute; 20% of total measured water was added to the aggregates and mixed for 2 minutes, followed by 4 minutes rest to facilitate the saturation of aggregates; subsequently, the binder materials were placed in the pan mixer and mixed for 1 minute; 60% of water was then added and mixed for 1 minute; and finally, the superplasticizer was added to the remaining water and transferred to the concrete and mixed for a minute. Altogether, the mixing was finished in 10 minutes. A slump test was done to assess whether the target slump had been achieved.

The specimens were cast using table vibration for about 15 to 20 seconds. The surface of each specimen was finished and the top was covered with a plastic sheet to keep the moisture evaporation and kept in the casting yard for 24 hours. Subsequently, the specimens were demoulded and shifted to the mist room (RH ~ 85-95%) for curing until the test date. After the curing period, specimens for each test were transferred to a temperature and humidity-controlled room, in which the temperature was maintained at $25\pm 3^{\circ}\text{C}$ and the relative humidity was $65\pm 5\%$. The temperature and humidity were continuously monitored. Figure 3.3 (a) and (b) show sample histories of the temperature at two locations of the laboratory, respectively, and Figure 3.3 (c) shows the humidity level in the laboratory.

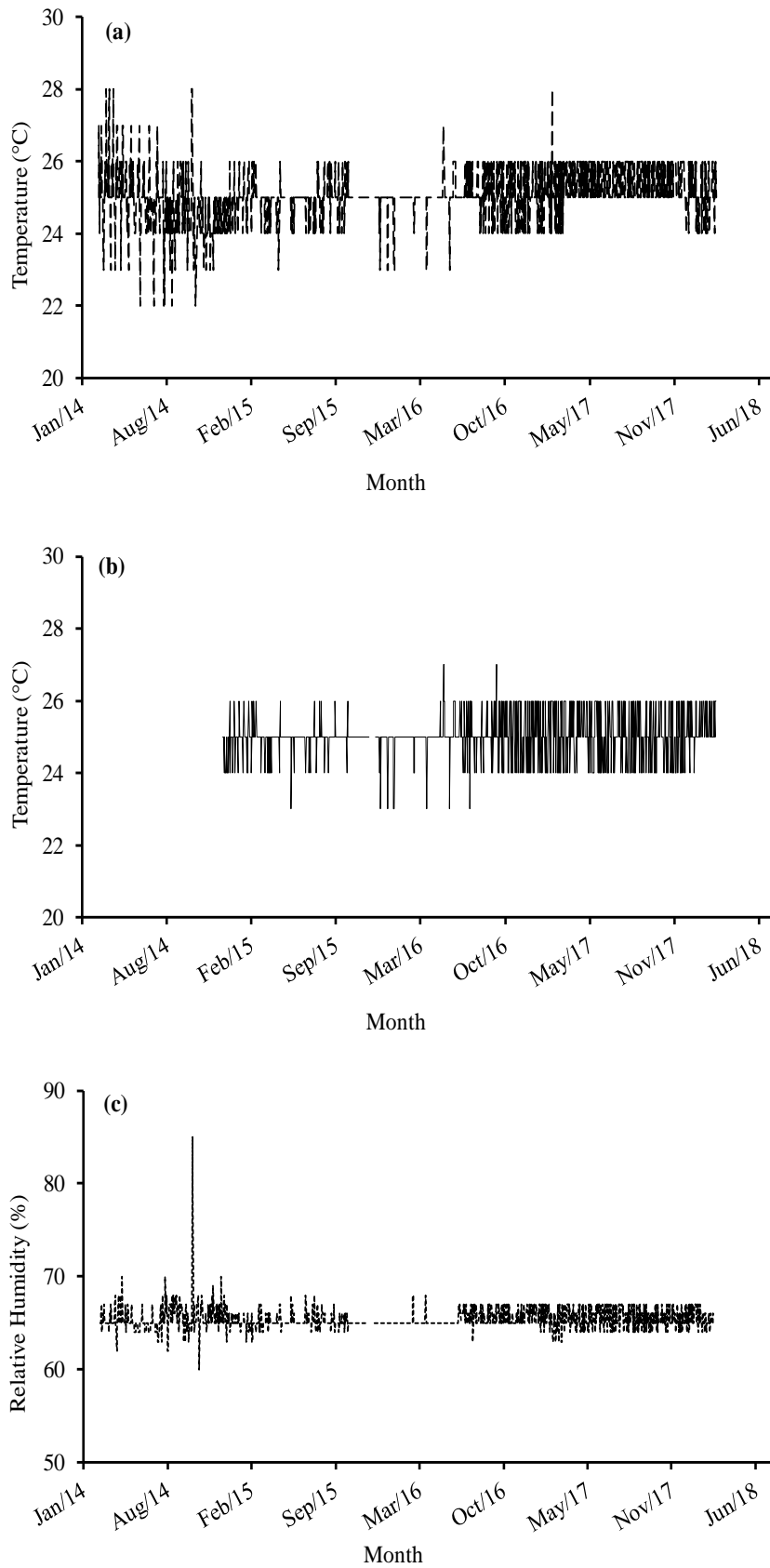


Figure 3.3 Histories of temperature at two locations within the laboratory, denoted as (a) and (b), and (c) the relative humidity

3.4 EXPERIMENTAL PROGRAMME

This section describes the various tests done on the prepared concrete specimens.

3.4.1 Tests on fresh concrete

In order to check the uniformity of the mixes and the workability characteristics, tests on fresh concrete were done conforming to the corresponding codes and standards listed in Table 3.7.

Table 3.7 Codes and standards followed for the testing of fresh concrete

Test	Standard designation
Slump	ASTM C143M-15a-2000
Air content	ASTM C 231-1997
Fresh unit weight	ASTM C138M-16a-2001
Temperature	ASTM C1064M-2012

- *Slump test* - The slump was measured in accordance with ASTM C143M-15 a. The value was used to evaluate the consistency and workability of fresh concrete.
- *Fresh unit weight* - The ASTM C138 standard was followed to determine the unit weight of fresh concrete.
- *Air content* - The air content of freshly mixed concrete was done according to ASTM C231, pressure method type B.
- *Concrete temperature* - The temperature of fresh concrete was obtained in accordance with ASTM C 1064 standard, using a digital thermometer.

The properties of fresh concrete for all mixes are presented in Table 3.8. As seen from the table, the initial slump values for the mixes considered were in the range of 70 and 135 mm, and the slump retained after 30 minutes was between 20 and 100 mm. The measured air content of the mixes was in the range of 1.2 to 2.6 %. The measured fresh concrete unit weight of the concretes made with CmP and CmA is between 2360 and 2440 kg/m³, and between 2290 and 2490 kg/m³, respectively.

Table 3.8 Fresh concrete properties

Sl. No.	Designation	Concrete temperature (°C)	Slump (mm)		Air content (%)	Fresh unit weight (kg/m ³)
			Initial	After 30 minutes		
1	CmP-NoSCM-0.65-280	32	90	50	2.40	2385
2	CmP-30SgA-0.65-280	32	135	90	2.60	2400
3	CmP-30SgB-0.65-280	32	80	40	2.00	2400
4	CmP-30FaF-0.65-280	31	95	30	2.10	2385
5	CmP-NoSCM-0.55-340	30	100	75	2.10	2400
6	CmP-15SgA-0.55-340	32	120	90	2.00	2360
7	CmP-15SgB-0.55-340	30	85	35	1.80	2400
8	CmP-15FaF-0.55-340	30	130	100	1.20	2405
9	CmP-15FaC-0.55-340	29	95	50	1.50	2360
10	CmP-NoSCM-0.50-310	30	100	55	1.80	2370
11	CmP-15SgA-0.50-310	30	95	40	2.10	2400
12	CmP-15SgB-0.50-310	32	130	80	2.50	2370
13	CmP-15FaF-0.50-310	31	100	55	2.40	2405
14	CmP-15FaC-0.50-310	28	95	50	1.80	2370
15	CmP-30SgB-0.50-310	33	80	30	2.10	2390
16	CmP-30FaF-0.50-310	31	100	55	2.10	2390
17	CmP30FaC-0.50-310	29	100	50	2.00	2360
18	CmP-50SgB-0.50-310	31	95	30	2.25	2440
19	CmP-50FaF-0.50-310	30	95	30	1.70	2370
20	CmP-20SgB-20FaF-0.50-310	30	95	50	1.40	2360
21	CmP-20SgB-20FaC-0.50-310	30	85	45	1.30	2365
22	CmP-20FaF-20FaC-0.50-310	30	100	40	1.50	2360
23	CmP-NoSCM-0.60-310	29	85	50	2.00	2360
24	CmP-15SgA-0.60-310	31	100	60	2.20	2390
25	CmP-15SgB-0.60-310	33	120	50	1.90	2385
26	CmP-15FaF-0.60-310	31	110	45	2.00	2400
27	CmP-15FaC-0.60-310	29	80	35	1.80	2360
28	CmA-NoSCM-0.65-280	29	100	45	2.40	2290
29	CmA-30SgA-0.65-280	30	100	40	2.50	2430
30	CmA-30SgB-0.65-280	31	105	40	2.40	2360
31	CmA-30FaF-0.65-280	32	85	40	2.50	2430
32	CmA-NoSCM-0.55-340	30	95	50	2.30	2440
33	CmA-15SgA-0.55-340	32	130	45	2.40	2430
34	CmA-15SgB-0.55-340	29	95	35	2.50	2315
35	CmA-15FaF-0.55-340	30	85	55	2.00	2430
36	CmA-15FaC-0.55-340	32	95	40	1.20	2460
37	CmA-NoSCM-0.50-310	29	80	35	2.50	2490
38	CmA-15SgA-0.50-310	30	80	50	2.00	2425
39	CmA-15SgB-0.50-310	29	110	50	2.20	2360
40	CmA-15FaF-0.50-310	31	90	50	1.80	2450
41	CmA-15FaC-0.50-310	30	90	40	1.40	2430
42	CmA-30SgB-0.50-310	32	110	45	2.00	2460
43	CmA-30FaF-0.50-310	30	110	35	1.50	2430
44	CmA-30FaC-0.50-310	30	125	50	1.30	2430
45	CmA-50SgB-0.50-310	32	120	40	2.00	2430
46	CmA-50FaF-0.50-310	32	100	30	1.80	2460
47	CmA-20SgB-20FaF-0.50-310	32	110	45	1.80	2460

Table 3.8 (continued) Fresh concrete properties

Sl. No.	Designation	Concrete temperature (°C)	Slump (mm)		Air content (%)	Fresh unit weight (kg/m ³)
			Initial	After 30 minutes		
48	CmA-20SgB-20FaC-0.50-310	30	95	55	1.50	2430
49	CmA-20-FaF-20FaC-0.50-310	30	80	50	1.80	2430
50	CmA-NoSCM-0.60-310	30	120	55	1.40	2425
51	CmA-15SgA-0.60-310	29	110	55	2.40	2430
52	CmA-15SgB-0.60-310	27	70	50	2.20	2460
53	CmA-15FaF-0.60-310	30	90	50	2.00	2360
54	CmA-15FaC-0.60-310	30	90	40	1.40	2430
55	CmP-NoSCM-0.50-310x	30	80	50	2.20	2400
56	CmP-30FaA-0.45-310	29	100	50	2.05	2415
57	LC3-NoSCM-0.50-310	32	80	20	2.10	2480
58	CmP-NoSCM-0.40-360	32	90	50	2.40	2385
59	CmP-30FaF-0.35-380	30	120	40	1.90	2400
60	LC3-NoSCM-0.40-340	30	120	30	2.30	2460
61	CmP-NoSCM-0.45-360	29	90	50	2.10	2400
62	CmP-30FaF-0.45-360	30	90	50	2.00	2385
63	LC3-NoSCM-0.45-360	30	120	30	1.90	2410

3.4.2 Tests on hardened concrete

Tests for the hardened concrete properties studied in this work conform to the standards given in Table 3.9.

Table 3.9 Codes and standards followed for the testing of hardened concrete properties

Test	Standard designation
Compressive Strength	IS 516-2004
Elastic modulus	ASTM C 469-2010
Shrinkage	RILEM TC 107-1998; ASTM C157-2008

Compressive strength test

Compressive strength was measured for all the concrete mixes considered in the study. For each concrete mix, three 100 mm cube specimens were tested each at the age of 2, 7, 28, 90 and 365 days. The specimens were tested in a testing system of 3000 kN capacity (Controls make). The loading rate was set at 140 kgf/cm²/min (as per IS 516-2004).

Elastic modulus of concrete test

The testing procedure of ASTM C 469-2010 was adopted to determine the static elastic modulus of concrete. For each concrete, three specimens of 150 mm diameter and 300 mm height were tested at 28 days. Before testing, both the ends of cylinders were sulphur capped/ground to obtain uniform contact surfaces. The tests were conducted in a 3 MN capacity system (Controls make) using the software interface for the E-modulus. Three compressometers as shown in Figure 3.4 (a) were used to measure the strains. The least count of each compressometer is 0.02 micron and it can travel a distance of ± 1.5 mm. The three gauges were placed equidistant around the circumference of the cylinder over a gauge length of 150mm keeping the lock knob in the locked position and secured in place by the help of upper and lower needle points driven onto the specimen using a soft mallet. To secure them, elastic bands were placed around the gauges as shown in Figure 3.4 (b). After setting up the gauges the lock knob is released to allow free movement during the test. The load ramp applied in three cycles, between 5% and 40% of expected ultimate compressive load. A sample loading curve is shown in Figure 3.4 (b). Load vs. time and stress vs. strain were recorded by a computer-based data acquisition system. In addition, the data file in MS Excel format was also obtained and stress vs. strain data for each specimen were plotted separately; a sample curve is shown in Figure 3.4 (b). The slope of the loading portion of the third cycle was used to calculate the elastic modulus of the concrete.



Figure 3.4(a) Axial displacement transducers

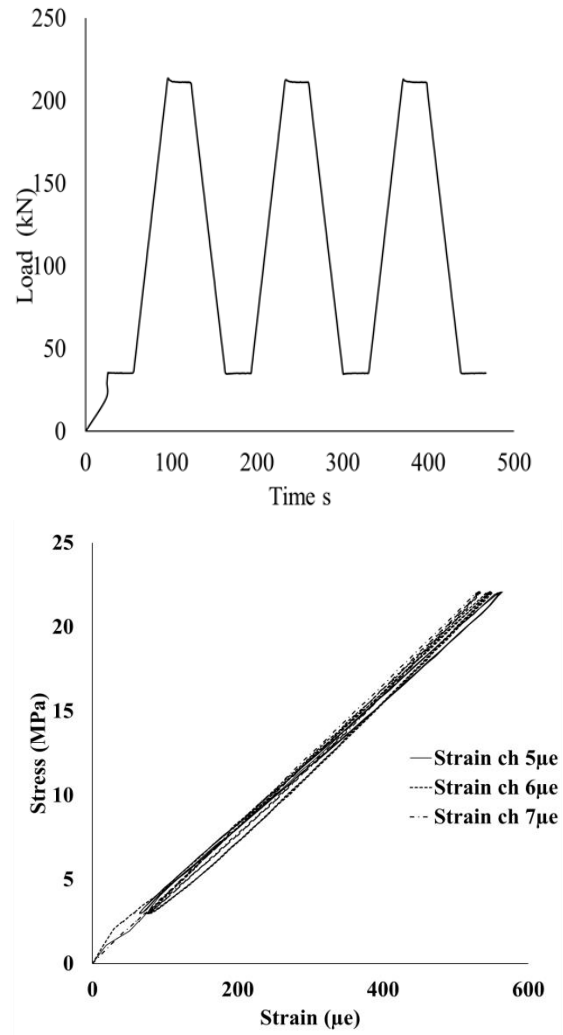


Figure 3.4 (b) Elastic modulus test setup in testing machine with typical loading history and stress-strain curve.

After the test was completed, each specimen was subjected to monotonic compressive loading until failure to determine the compressive strength.

Shrinkage test

As recommended by RILEM TC 107-1998, 150 mm diameter and 300 mm height cylinders, and in accordance with ASTM C-157-2008, 75 × 75 × 285 mm prismatic specimens were used to evaluate the shrinkage response. Both methods were used in order to assess if the results are comparable as either method is often used in practice. After 28 days of curing in a mist room, all the specimens for the shrinkage study were transferred to the testing room ($t_0 = 28$ days). The specimens were kept at 25°C and 65% RH in the testing room.

Shrinkage tests on cylinder specimens

A 150 mm gauge length digital demountable mechanical (DEMEC) strain gauge as shown in Figure 3.5 was used in this study. It consists of a digital dial gauge attached to an invar bar. A fixed conical point is attached at one end of the bar and a moving conical point is mounted on a knife edge pivot on the other side. The pivot movement is measured by the dial gauge. The least count of the dial gauge is 0.001 mm. A reference invar bar is used to calibrate the dial gauge before taking measurement on each day.



Figure 3.5 DEMEC strain gauge used for the work

A setting-out bar made of invar with two conical points at 150 mm gauge length was used to fix the reference disc in position on the cylindrical specimens, as shown in Figure 3.6. Three specimens each were used to measure the total and autogenous shrinkage. Firstly, the surface of the specimen was cleaned with emery paper to remove irregularities so as to ensure that the reference discs were fixed properly and in the same plane. Two vertical lines (as shown in Figure 3.6, and named as Side 1 and Side 2) were drawn diametrically opposite to each other. Reference discs of 9 mm diameter provided with a conical hole of diameter 2 mm at the centre were used. A two-component epoxy-based adhesive was applied and with the help of the invar setting-out bar, the reference disc was glued firmly. The setting-out bar was held in position for a minute to allow the adhesive to harden.

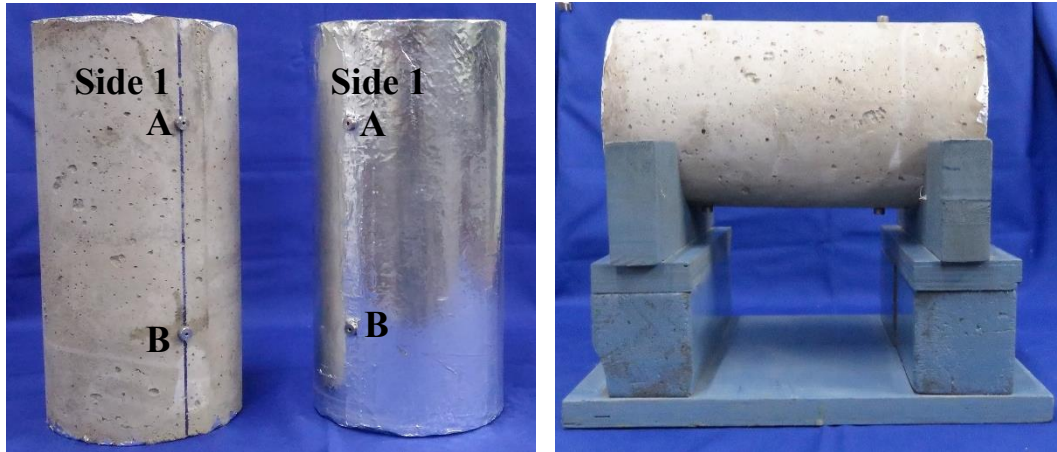


Figure 3.6 Prepared concrete specimens for measuring shrinkage strain

A commercially available aluminium tape, of soft foil backing with high performance transparent acrylic adhesive on one side, was used for wrapping the specimens in this work. The width and thickness of the foil were 120 mm and 0.06 mm, respectively. For measuring total shrinkage, three cylinders were covered with aluminium tape only on the top and bottom faces ensuring that the entire length of the vertical curved faces were exposed. For the specimens used for measuring the autogenous shrinkage response of concrete, aluminium tape was wrapped over the curved face of the cylinder, as well as the top and bottom so that no surface is exposed. Altogether, the preparation of specimens was done within two hours, and the measurement for total and autogenous shrinkage commenced immediately after that.

Two sets of measurements were taken on each side of the specimen by placing the fixed conical point of the DEMEC gauge at position A and the moving pivot at position B (noted as AB), and by placing the fixed point at B and moving pivot at A (BA). Average of AB and BA values were noted for calculating the length change for each side. All the measurements were recorded in mm. Similarly, the measurement for the other side (Side 2) was taken and the shrinkage strain was calculated.

Shrinkage tests on prism specimens

In accordance with ASTM C 157-2008, shrinkage was measured using six $75 \times 75 \times 285$ mm concrete prisms. Metal studs were placed in position at the centre of the two ends of the concrete mould and held there by passing the unthreaded portion through a hole in the end plates of the moulds (see the stud structure in Figure 3.7). The studs were ensured to be at the centre of the side plates in order to set the axis of the specimen and the studs during the testing.

After casting, the process of curing and the specimen preparation after the curing period was the same as that used for cylindrical specimen, for both autogenous and total shrinkage measurements.

A length comparator frame, as shown in Figure 3.8 (fabricated at IIT Madras), was used for determining the change in length of the prism specimens. It is provided with a digital dial gauge of 0.001 mm precision. The dial gauge is rigidly mounted on the frame in a measuring yoke. A reference bar made of invar with a length of 300 mm was used to calibrate the frame. The two ends of the bar are machined as 6 mm diameter spherical ends. Before each measurement, the base, shrinkage studs in the specimen, and the reference invar bar were thoroughly cleaned with acetone or ethanol so as to ensure that there was no dust or sand particles, which may alter the true measurements. In order to ensure that the zero setting of the measuring system is consistent throughout the test period, before each set of reading the reference invar bar was placed in position in the comparator and zero value of the dial gauge was set. After the initial checks, stainless steel balls were placed in the conical groove of the shrinkage studs and the specimen was placed on the length comparator. The dial gauge reading was observed. Two set of readings were measured on each specimen, by placing the mark position upward and after turning it upside down. The average of these was considered for calculating the shrinkage strain of the specimen.

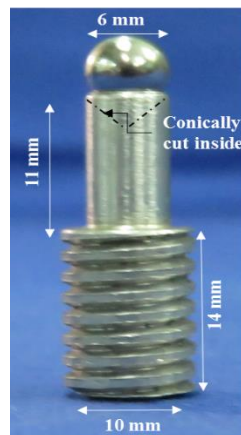


Figure 3.7 Studs fixed at the specimen ends for measuring shrinkage

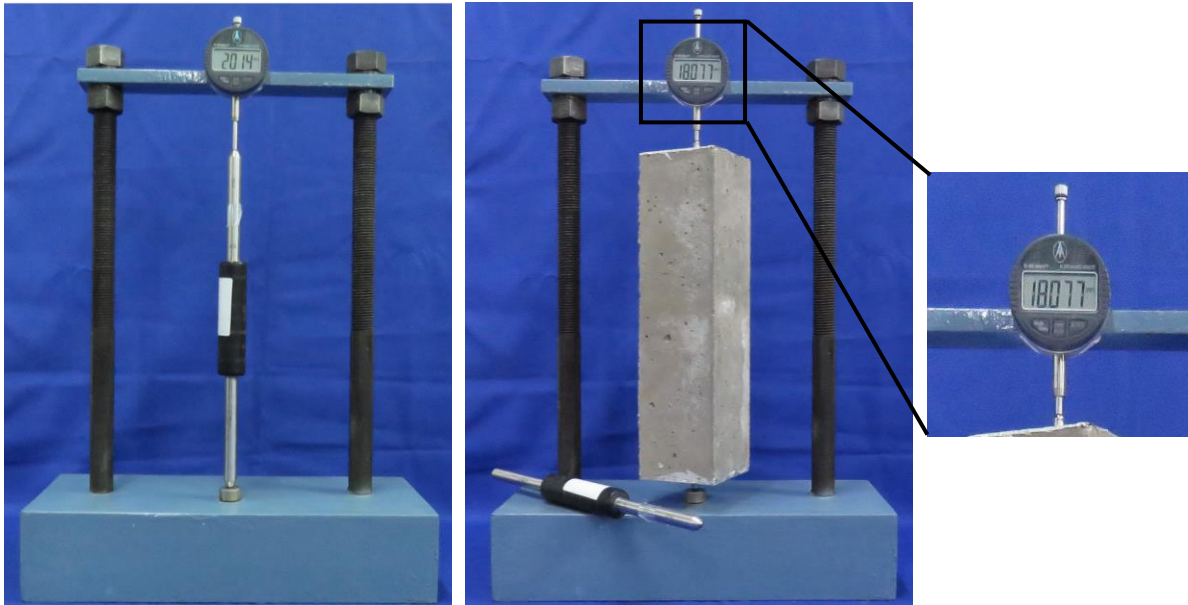


Figure 3.8 Length comparator frame with digital dial gauge in accordance with ASTM C157: (a) with length comparator, and (b) with standard prismatic specimen

Shrinkage measurements for cylinders and prisms were made every day for the first one week. Thereafter, the readings were periodically taken once in two days for two weeks, once in three days for the next two weeks, followed by weekly once for a month. After that, for every fifteen days, measurements were taken for about ten months each and later once in thirty days.

3.5 SUMMARY

This chapter gives the details of the test programme for the mechanical properties and shrinkage response of concrete. The details of various materials used and the concrete mixes have also been discussed. The testing methodologies for the fresh and hardened concrete properties are also discussed.

4. RESULTS AND DISCUSSION – COMPRESSIVE STRENGTH AND ELASTIC MODULUS OF CONCRETE

4.1 INTRODUCTION

Supplementary cementitious materials (SCMs) are used in many concrete mixes to reduce the cement content, and also to enhance the long-term performance and durability of the concrete. Ground granulated blast furnace slag (GGBS) or slag, fly ash, silica fume and metakaolin are often included as SCMs. Utilization of these materials not only reduces the environmental impact but also enhances the properties of concrete in fresh and hardened states. However, considerable differences in the mechanical properties could be observed in SCM blended concrete from a normal conventional concrete system because of the hydration kinetics and the hydrated structures resulting from the varying replacement level of cement by SCMs (Lothenbach et al., 2011; Chowdhury and Basu, 2010). Hence this part of research aims to address the effects of SCMs on the mechanical properties of concrete, mainly the strength development and the elastic modulus of concrete.

This chapter reports on the effect of slag and fly ash on the compressive strength development and the static elastic modulus of concrete. The discussion will essentially focus on the effect of water to binder ratio, the effect of replacement level of slag and fly ash in the concrete system, the influence of fly ash type, and the effect of ternary blends on the evolution of compressive strength. Also, tests were carried out to determine the elastic modulus of concrete at the age of 28 days for different binder systems that were compared with existing standards.

4.2 COMPRESSIVE STRENGTH

Cubes of 100 mm were curing in a mist room until testing at the ages of 2, 7, 28, 90, and 365 days. The average compressive strength was obtained from at least three specimens, and is given along with the standard deviation in Table 4.1. Overall, the scatter is low and within acceptable limits. The individual compressive strength plots with the standard deviation are shown in Figures A-1 to A-16 in Appendix A. The mean compressive strengths of concrete ranged from 20 to 55 MPa at 28 days, and from 32 to 64 MPa at 365 days. The 7-day to 28-day compressive strength ratio for the concretes in this study was in the range of 0.50 to 0.98. This shows that the evolution of the compressive strength within 7 days could be higher than the general recommendation of 0.67 (Neville, 2006).

Table 4.1 Cube compressive strength of concrete (MPa): average (and standard deviation)

Sl. No.	Mix Designation	Age of testing (in days)				
		2	7	28	90	365
1	CmP-NoSCM-0.65-280	9.6 (1.1)	19.6 (1.3)	30.2(0.7)	32.1 (1.2)	33.9 (1.0)
2	CmP-30SgA-0.65-280	11.0 (1.7)	19.0 (2.2)	31.1(0.8)	32.0 (1.5)	34.2 (1.7)
3	CmP-30SgB-0.65-280	13.4 (0.9)	24.9 (1.3)	33.3 (1.5)	38.6 (1.1)	39.2 (0.1)
4	CmP-30FaF-0.65-280	5.9 (0.9)	13.1 (0.7)	22.3 (1.3)	36.3 (1.4)	39.0 (0.0)
5	CmP-NoSCM-0.55-340	28.3 (0.8)	39.7 (1.7)	44.4 (2.2)	46.5 (0.4)	48.0 (1.0)
6	CmP-15SgA-0.55-340	15.3 (0.5)	22.6 (1.0)	40.7 (1.2)	47.2 (1.8)	50.0 (1.9)
7	CmP-15SgB-0.55-340	23.6 (1.2)	33.6 (0.9)	48.1 (1.0)	53.5 (0.8)	55.5 (0.4)
8	CmP-15FaF-0.55-340	12.9 (0.5)	23.3 (1.2)	39.8 (1.4)	50.8 (0.9)	54.8 (1.8)
9	CmP-15FaC-0.55-340	14.7 (1.2)	30.9 (1.5)	43.7 (0.7)	54.1 (1.1)	57.7 (0.4)
10	CmP-NoSCM-0.50-310	32.1 (1.2)	40.2 (1.1)	45.7 (0.5)	48.6 (0.6)	49.3 (1.4)
11	CmP-15SgA-0.50-310	15.6 (0.6)	38.3 (0.7)	52.5 (0.7)	59.5 (1.2)	62.2 (1.9)
12	CmP-15SgB-0.50-310	24.8 (1.9)	38.2 (1.7)	52.6 (1.1)	56.0 (0.4)	58.1 (1.1)
13	CmP-15FaF-0.50-310	18.1 (1.6)	23.8 (1.7)	35.6 (0.7)	57.1 (1.1)	62.9 (0.2)
14	CmP-15FaC-0.50-310	19.5 (0.7)	27.0 (0.1)	42.0 (1.5)	58.8 (1.5)	61.1 (0.1)
15	CmP-30SgB-0.50-310	24.4 (1.9)	39.8 (1.5)	52.2 (0.9)	62.9 (1.4)	63.4 (1.5)
16	CmP-30FaF-0.50-310	11.7 (0.1)	20.4 (1.7)	37.0 (0.9)	50.0 (0.8)	55.3 (0.5)
17	CmP-30FaC-0.50-310	22.4 (1.4)	33.7 (1.5)	47.1 (0.9)	59.0 (1.4)	59.0 (0.8)
18	CmP-50SgB-0.50-310	17.2 (0.8)	25.8 (1.0)	42.1 (1.7)	61.6 (1.5)	62.8 (0.2)
19	CmP-50FaF-0.50-310	4.3 (1.2)	10.8 (0.8)	21.2 (1.0)	43.1 (1.2)	44.0 (0.2)
20	CmP-20SgB-20FaF-0.50-310	17.9 (1.0)	25.0 (0.2)	32.7 (1.3)	50.3 (1.1)	52.3 (1.0)
21	CmP-20SgB-20FaC-0.50-310	19.4 (0.8)	28.1 (1.3)	39.6 (0.7)	53.5 (1.5)	55.0 (0.7)
22	CmP-20FaF-20FaC-0.50-310	12.3 (1.2)	32.3 (1.0)	43.7 (1.7)	50.6 (0.7)	50.5 (0.7)
23	CmP-NoSCM-0.60-310	12.9 (0.8)	20.1 (1.4)	32.4 (1.2)	34.5 (0.8)	37.1 (1.9)
24	CmP-15SgA-0.60-310	13.1 (0.7)	27.9 (1.8)	43.8 (0.8)	45.3 (1.1)	46.1 (0.3)
25	CmP-15SgB-0.60-310	11.9 (1.1)	19.4 (0.9)	32.5 (0.5)	40.2 (1.0)	42.9 (0.5)
26	CmP-15FaF-0.60-310	9.3 (0.6)	23.7 (0.4)	31.3 (0.8)	41.5 (1.2)	44.8 (0.2)
27	CmP-15FaC-0.60-310	16.5 (0.9)	23.5 (0.8)	34.7 (1.1)	42.1 (1.1)	44.3 (1.6)
28	CmA-NoSCM-0.65-280	15.6 (0.9)	24.3 (1.1)	26.3 (0.6)	31.9 (0.8)	34.3 (2.3)
29	CmA-30SgA-0.65-280	15.9 (0.9)	20.8 (0.6)	24.1 (1.5)	31.0 (1.2)	31.7 (1.0)
30	CmA-30SgB-0.65-280	11.4 (0.8)	21.5 (2.0)	26.0 (0.3)	29.3 (1.4)	36.0 (1.9)
31	CmA-30FaF-0.65-280	12.6 (0.5)	15.8 (0.8)	19.5 (0.6)	28.3 (0.5)	32.0 (1.9)
32	CmA-NoSCM-0.55-340	28.1 (1.6)	35.6 (0.9)	43.7 (0.6)	44.4 (2.2)	45.2 (0.9)
33	CmA-15SgA-0.55-340	21.0 (0.8)	29.2 (0.8)	39.5 (1.5)	40.6 (1.4)	40.9 (2.8)
34	CmA-15SgB-0.55-340	29.7 (0.7)	37.1 (0.7)	44.6 (1.4)	46.9 (1.2)	50.4 (0.5)
35	CmA-15FaF-0.55-340	20.3 (0.9)	33.0 (0.9)	40.2 (2.3)	44.4 (0.7)	49.4 (1.1)
36	CmA-15FaC-0.55-340	15.2 (0.2)	23.2 (0.5)	42.5 (2.0)	45.3 (1.0)	45.1 (2.7)
37	CmA-NoSCM-0.50-310	30.7 (0.3)	34.2 (0.9)	43.2 (1.2)	54.4 (0.8)	54.7 (1.5)
38	CmA-15SgA-0.50-310	16.2 (0.5)	24.7 (1.5)	43.8 (0.4)	54.2 (1.7)	56.1 (1.4)
39	CmA-15SgB-0.50-310	27.6 (0.9)	35.6 (0.9)	48.1 (1.8)	49.1 (1.0)	55.0 (1.7)
40	CmA-15FaF-0.50-310	26.2 (1.6)	33.1 (0.6)	46.6 (2.7)	51.1 (2.2)	54.5 (1.9)
41	CmA-15FaC-0.50-310	21.5 (1.4)	23.4 (0.9)	44.0 (1.2)	46.0 (1.8)	45.6 (0.6)
42	CmA-30SgB-0.50-310	26.5 (0.7)	35.6 (1.0)	44.3 (1.1)	52.9 (1.0)	55.8 (0.6)
43	CmA-30FaF-0.50-310	10.8 (0.9)	19.4 (0.9)	35.7 (0.9)	39.1 (1.0)	40.9 (1.9)
44	CmA-30FaC-0.50-310	15.9 (0.9)	25.0 (1.2)	40.3 (1.0)	47.3 (2.5)	46.8 (0.5)
45	CmA-50SgB-0.50-310	30.4 (1.1)	37.0 (0.6)	45.9 (0.5)	57.2 (2.8)	61.3 (1.0)
46	CmA-50FaF-0.50-310	4.8 (0.3)	13.0 (0.0)	25.7 (0.6)	28.4 (1.0)	32.3 (1.9)

Table 4.1 (continued) Cube compressive strength of concrete (MPa): average (and standard deviation)

Sl. No.	Mix Designation	Age of testing (in days)				
		2	7	28	90	365
47	CmA-20SgB-20FaF-0.50-310	21.2 (1.3)	36.6 (1.1)	42.4 (0.9)	50.6 (0.6)	55.1 (0.3)
48	CmA-20SgB-20FaF-0.50-310	21.1 (1.5)	29.6 (1.1)	43.4 (0.7)	44.6 (2.2)	43.9 (1.5)
49	CmA-20SgB-20FaC-0.50-310	14.8 (0.8)	18.4 (1.8)	27.3 (1.4)	40.3 (1.1)	49.3 (1.7)
50	CmA-NoSCM-0.60-310	17.4 (1.1)	25.7 (1.2)	31.4 (1.2)	36.7 (1.5)	42.7 (2.6)
51	CmA-15SgA-0.60-310	16.1 (0.5)	25.4 (1.3)	32.8(2.5)	39.8 (1.1)	43.9 (2.4)
52	CmA-15SgB-0.60-310	16.4 (0.5)	24.0 (1.0)	39.4 (1.2)	42.7 (1.6)	42.7 (0.4)
53	CmA-15FaF-0.60-310	20.9 (0.2)	25.7 (1.4)	35.9 (1.2)	43.1 (0.4)	44.7 (1.6)
54	CmA-15FaC-0.60-310	15.2 (0.2)	20.2 (0.5)	26.6 (1.6)	30.7 (0.1)	35.5 (1.2)
55	CmP-NoSCM-0.50-310x	31.3 (1.5)	41.6 (1.4)	46.3 (0.9)	49.9 (0.8)	50.6 (0.9)
56	CmP-30FaA-0.45-310	17.2 (1.1)	26.9 (0.3)	38.3 (1.0)	46.2 (0.8)	48.7 (2.7)
57	LC3-NoSCM-0.50-310	29.3 (0.9)	41.1 (0.2)	44.9 (0.2)	52.1 (0.7)	53.2 (0.9)
58	CmP-NoSCM-0.40-360	35.5 (1.4)	47.7 (1.5)	54.9 (0.2)	56.6 (0.5)	57.2 (0.6)
59	CmP-30FaF-0.35-380	26.8 (1.1)	47.2 (1.3)	53.4 (1.6)	60.7 (2.0)	62.6 (1.1)
60	LC3-NoSCM-0.40-340	33.9 (0.7)	48.9 (1.7)	55.3 (1.3)	60.6 (2.3)	61.9 (1.8)
61	CmP-NoSCM-0.45-360	21.2 (0.4)	33.7 (1.3)	47.3 (2.3)	48.9 (0.9)	48.9 (0.3)
62	CmP-30FaF-0.45-360	13.4 (0.5)	26.0 (0.9)	42.7 (0.2)	50.5 (1.0)	51.1 (1.6)
63	LC3-NoSCM-0.45-360	23.4 (0.9)	36.7 (1.2)	49.2 (1.6)	54.6 (0.8)	55.4 (0.6)

4.2.1 Effect of cement type on compressive strength development

Indian standards require that the ratio of calcium oxide (CaO) to silicon dioxide (SiO₂) content in ordinary portland cement to be not less than 2, which CmP and CmA satisfy. The CaO/ SiO₂ ratio for CmP, CmA and LC3 was 2.78, 3.34, and 1.34, respectively. The compressive strength results were higher when the sum of CaO+SiO₂ and CaO/SiO₂ was larger. The 28-day mean compressive strength obtained with CmP, CmA and LC3 cements was 45.7, 43.2, and 44.9 MPa, respectively, when the water-binder ratio was 0.50 and total binder content was 310 kg/m³. Though the 28-day strength was comparable, there was a continued gain in the strength of CmA concrete beyond 28 days, which was not observed in the other cements. This could be attributed to the higher CaO/SiO₂ content, which produces more C-S-H at later ages. The same trend was observed in all the mixes produced with the CmA cement. Figure 4.1 (b), (c) and (d) compare the strength development of CmP and CmA concrete for each water to cement ratio. Except for w/c of 0.55, CmA concrete tends to have marginally higher early age strength, though the 28-day strength was comparable. It can be seen from Figure 4.2 that the compressive strength of all the concretes, as anticipated, are higher at lower water to cement ratio.

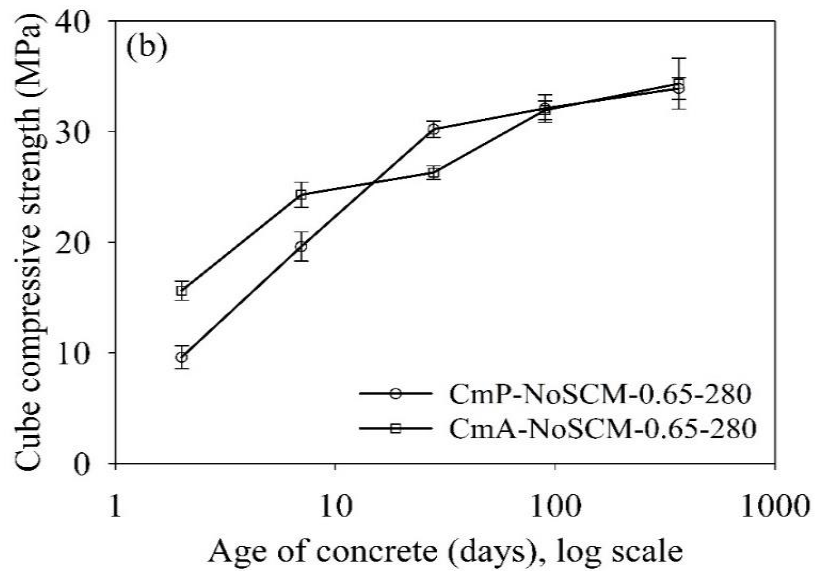
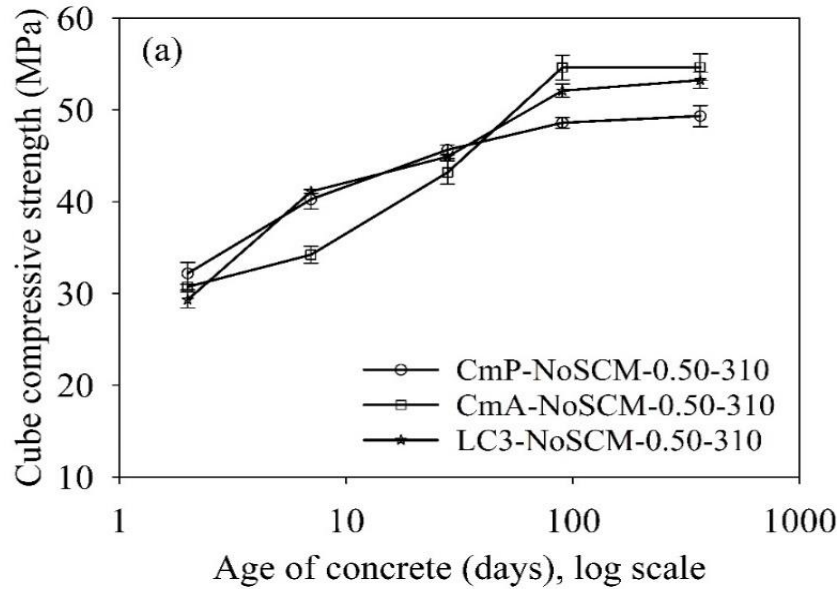


Figure 4.1 Effect of cement type on compressive strength development of concrete:
 (a) CmP, CmA and LC3 with $w/c = 0.50$, (b) CmP and CmA with $w/c = 0.65$.

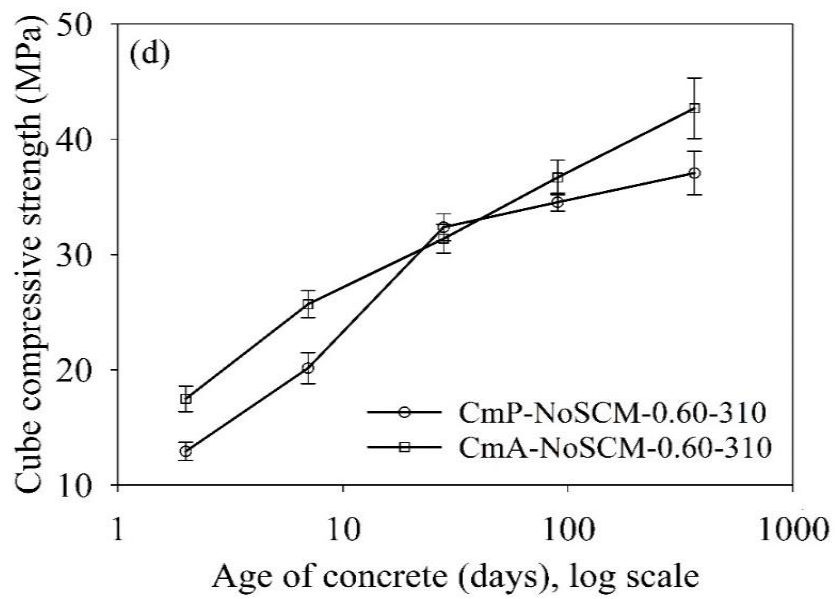
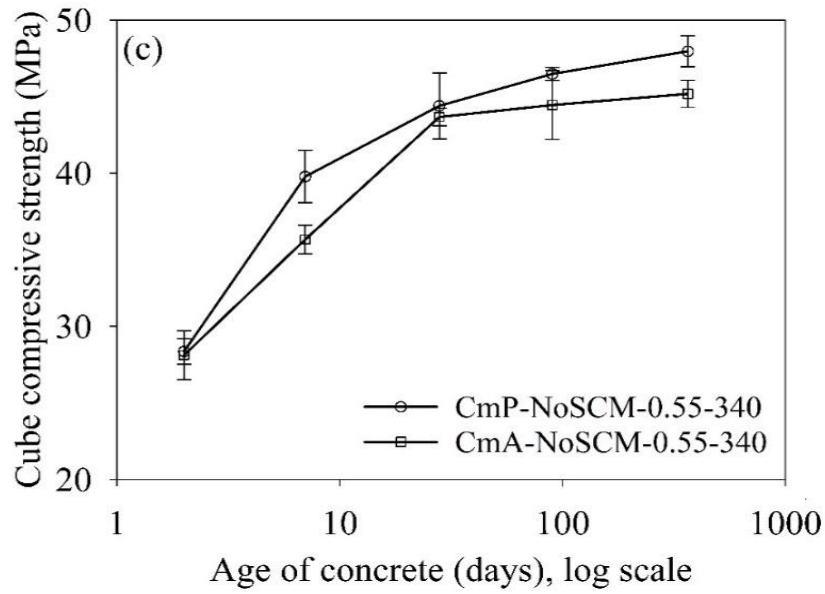


Figure 4.1 Effect of cement type on compressive strength development of concrete:
 (c) CmP and CmA with $w/c = 0.55$, (d) CmP and CmA with $w/c = 0.60$.

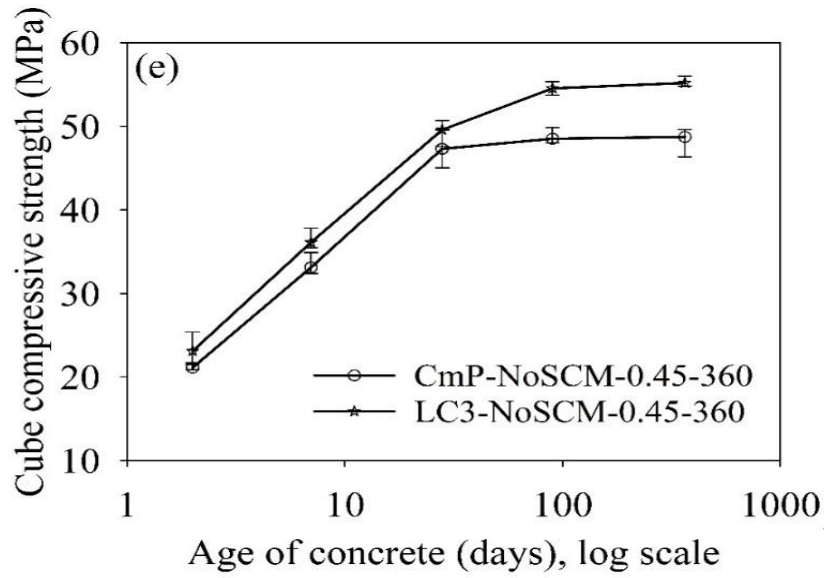


Figure 4.1 Effect of cement type on compressive strength development of concrete:
(e) CmP and LC3 with $w/c = 0.45$

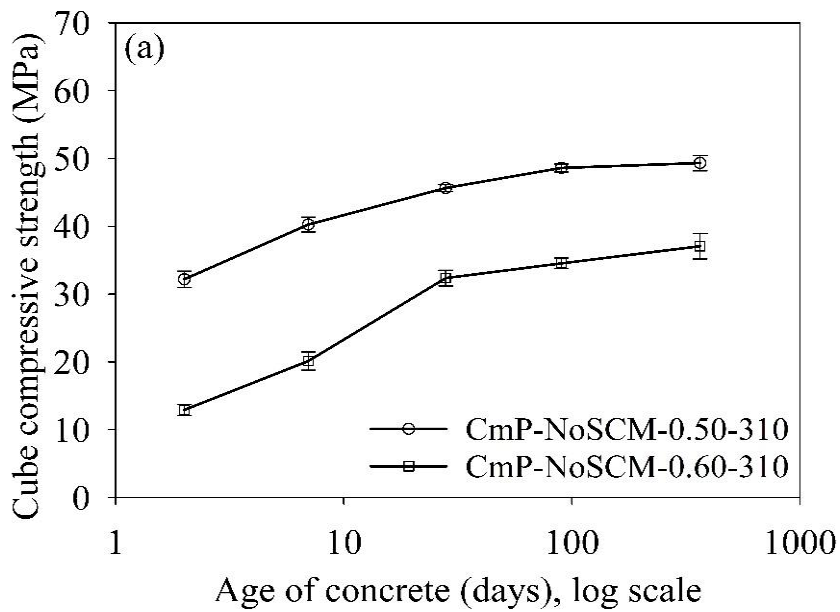


Figure 4.2 Effects of water-cement ratio on the evolution of compressive strength:
(a) $w/c=0.50$ and 0.60 with CmP

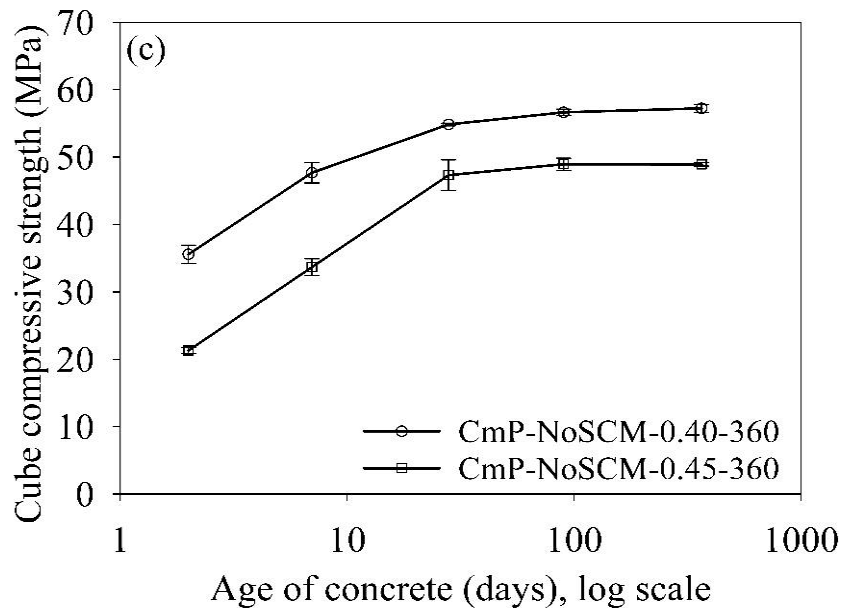
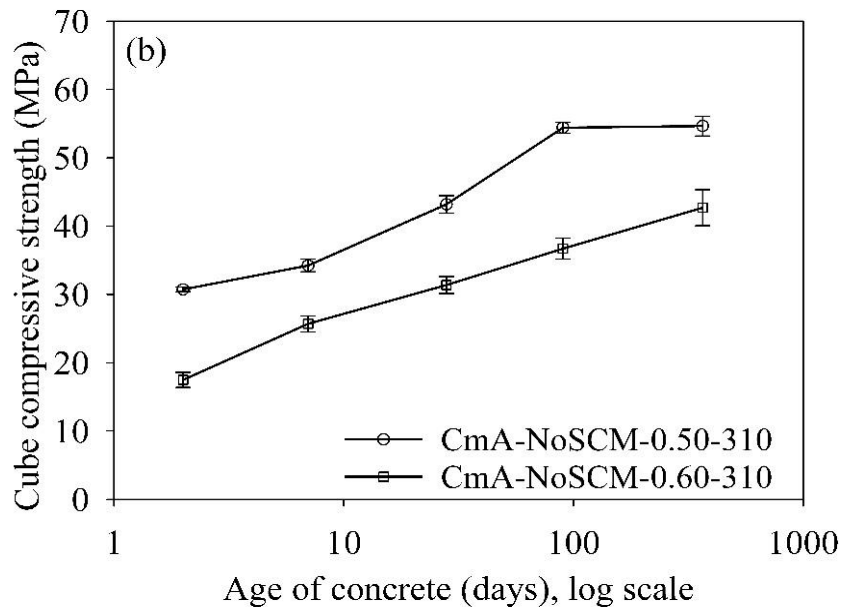


Figure 4.2 Effects of water-cement ratio on evolution of compressive strength:
 (b) w/c=0.50 and 0.60 with CmA and (c) w/c=0.40 and 0.45 with CmP

4.2.2 Effects of slag and fly ash on compressive strength development

Figure 4.3 (a) shows that the 2-day strength of blended cement concrete is lower compared to that of the CmP-NoSCM mix. However, the later strengths are higher in the SgA and SgB mixes, yielding the same as those of CmP concrete at 7 days. In the case of water to binder ratio of 0.60, as seen in Figure 4.3 (b), SgB and FaF mixes exhibit lower strength at early ages though the 28-day strength is comparable with that of the CmP-NoSCM concrete. On the other hand, SgA concrete shows better strength at all ages with the CmP concrete having the least long-term strength.

The compressive strength results of concrete with CmA are presented in Figure 4.4 (a) and Figure 4.4 (b). As seen in the case of CmA mixes, the strength at $w/b = 0.50$ is lower for the blended binders. However, for this cement, the strengths at other ages are similar for all the concretes. As shown in Figure 4.5 (a), at higher water to binder ratio ($w/b = 0.65$) the strength development of the CmP-NoSCM concrete was comparable with SgA blended concrete. As expected, Class F fly ash concrete exhibits lower compressive strength at early ages. However, the long-term strength developed is more pronounced at 90 days and above. CmP-30SgB-0.65-280 concrete exhibits a substantial increase in the strength in comparison with other concretes. It can be seen from Figure 4.6 (a) that there was no significant trend observed in the strength development in comparison with CmP mix. Figure 4.5 (b) and Figure 4.6 (b) depict the strength development of CmP and CmA concrete with w/b of 0.55 and total binder content of 340 kg/m^3 . It is clear from the plots that the early age strength of No-SCM concrete in both the binders is comparatively higher. Nevertheless, there is no significant increase in the strength beyond 28 days. At the same time, in the case of blended concrete, the development of compressive strength is more pronounced beyond 28 days. The results agree with those reported by other researchers (Shariq et al., 2010; Lübeck et al., 2012) that the early strength of slag and fly ash is lower when compared to the strength of non-blended concrete, due to the slow rate of hydration.

Figure 4.7 and Figure 4.8 describe the effect of fly ash type on the evolution of compressive strength, where it can be observed that is a significant increase in the strength of fly ash blended concrete (both FaF and FaC) in the long term. Also, Class C fly ash concrete exhibits higher strength in comparison with that of Class F fly ash, which can be attributed to the higher calcium oxide content of the former (Yildirim et al., 2011; Yurdakul et al., 2014).

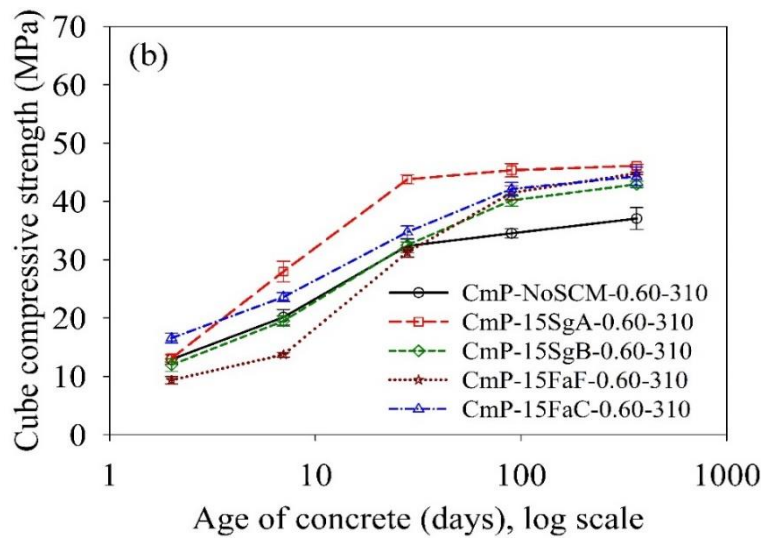
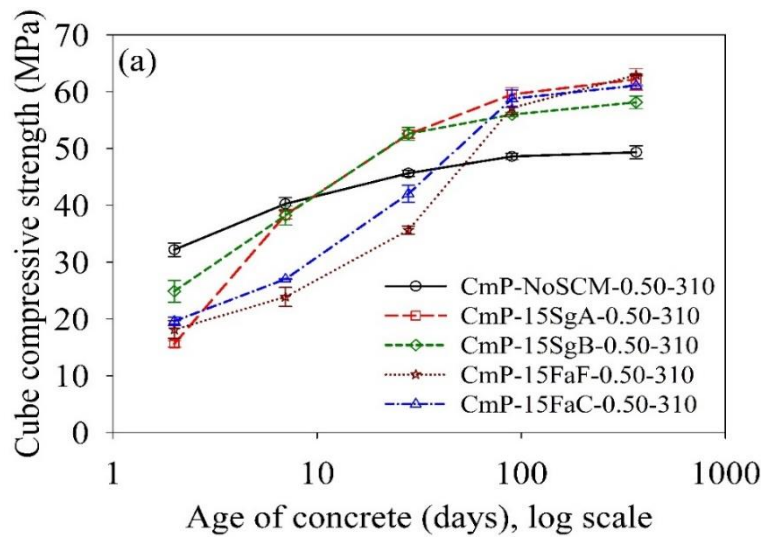


Figure 4.3 Effect of SCM on the evolution of compressive strength of concrete with CmP
 (a) w/b = 0.50 and (b) w/b = 0.60

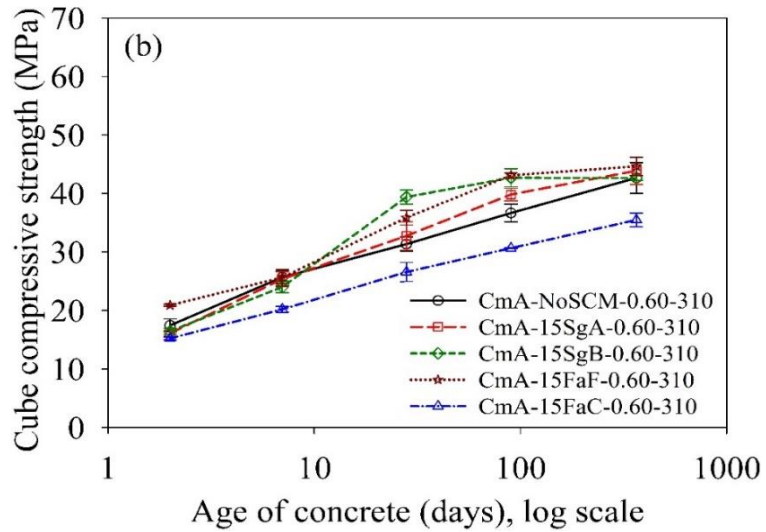
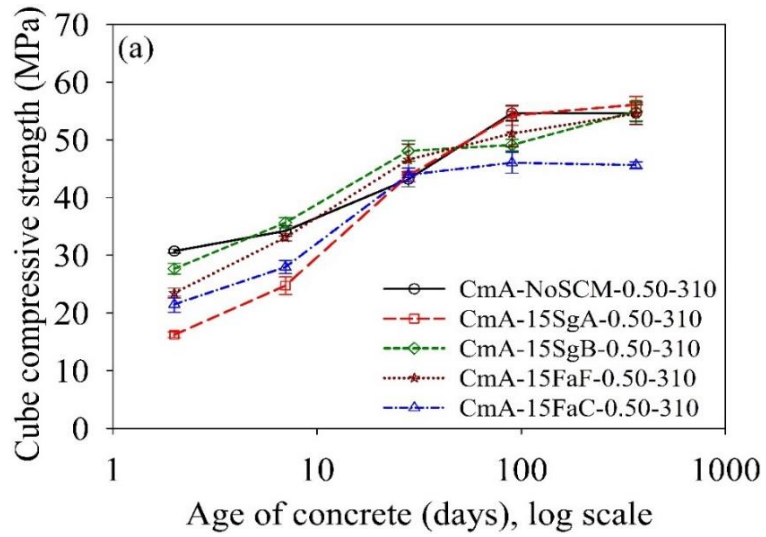


Figure 4.4 Effect of SCM on the evolution of compressive strength of concrete with CmA
 (a) $w/b = 0.50$ and (b) $w/b = 0.60$

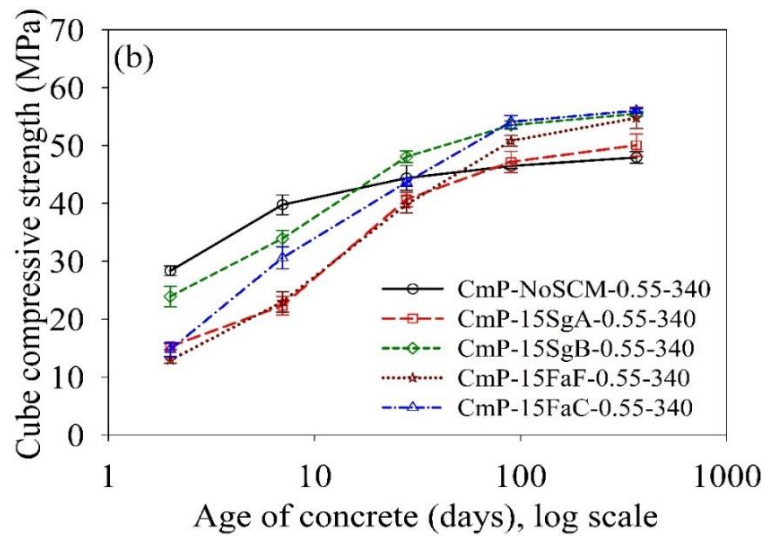
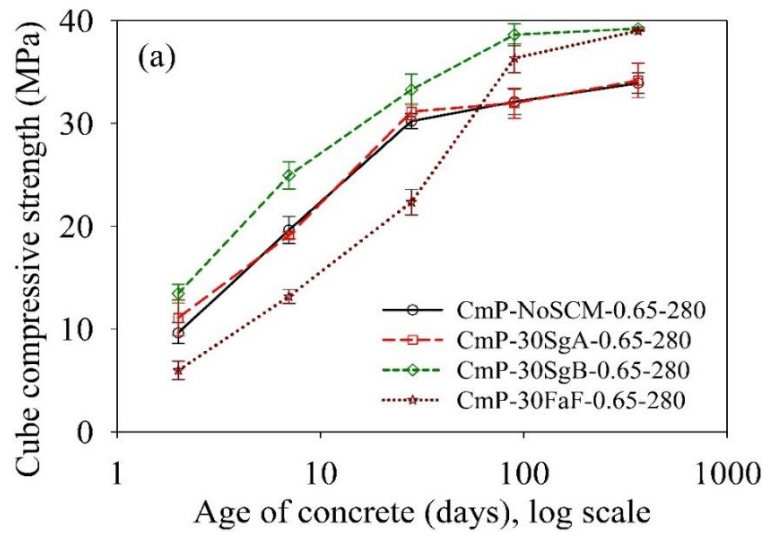


Figure 4.5 Effect of binary blends of slag and fly ash on compressive strength development with CmP (a) w/b =0.65, (b) w/b = 0.55

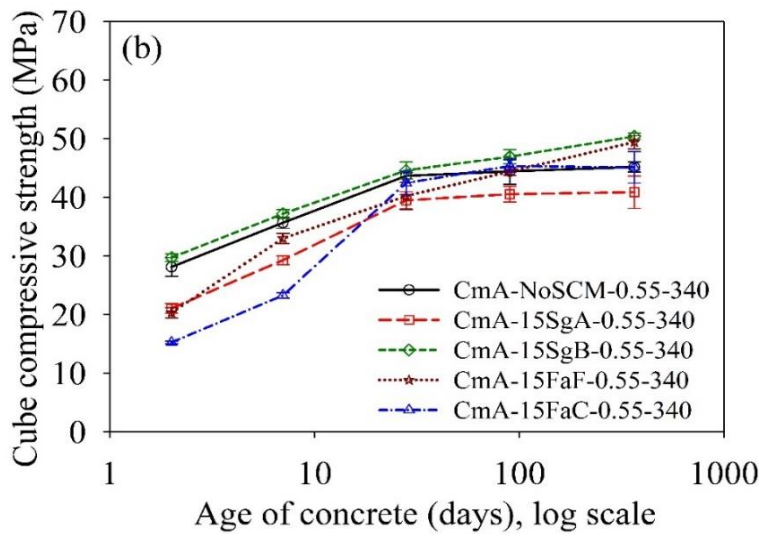
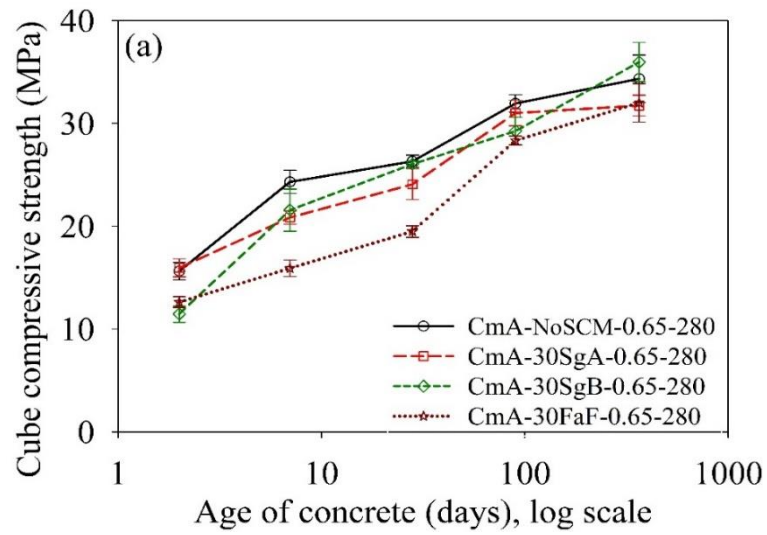


Figure 4.6 Effect of binary blends of slag and fly ash on compressive strength development with CmA (a) $w/b = 0.65$, (b) $w/b = 0.55$

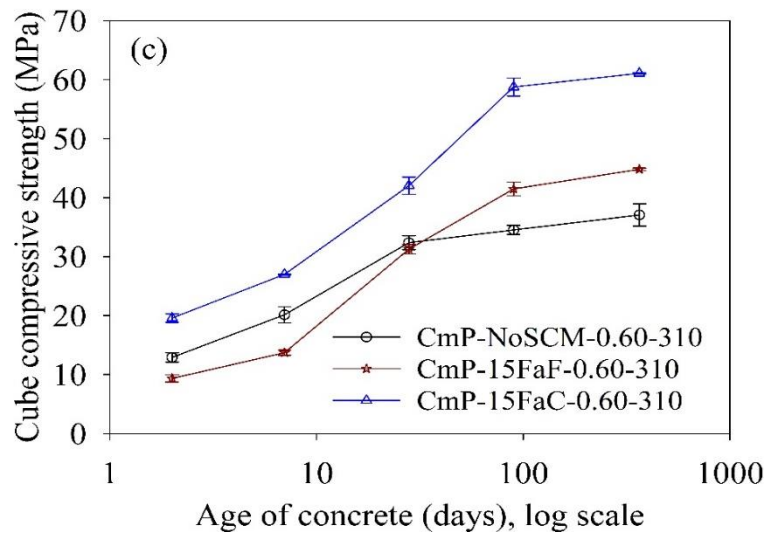
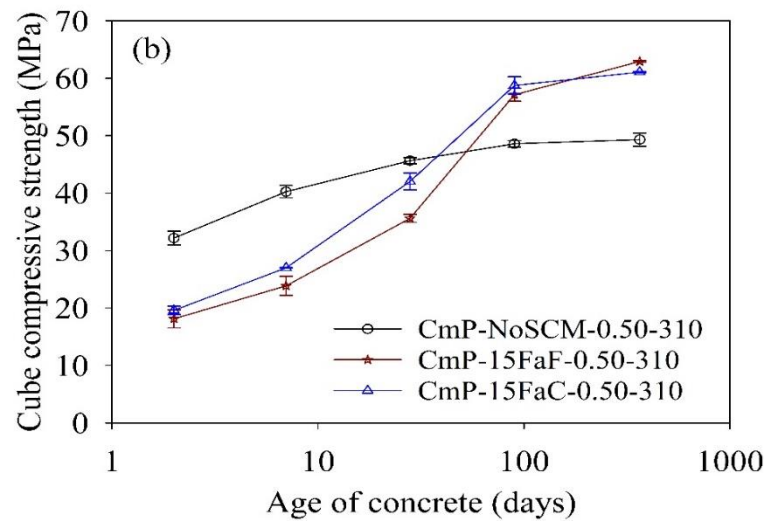
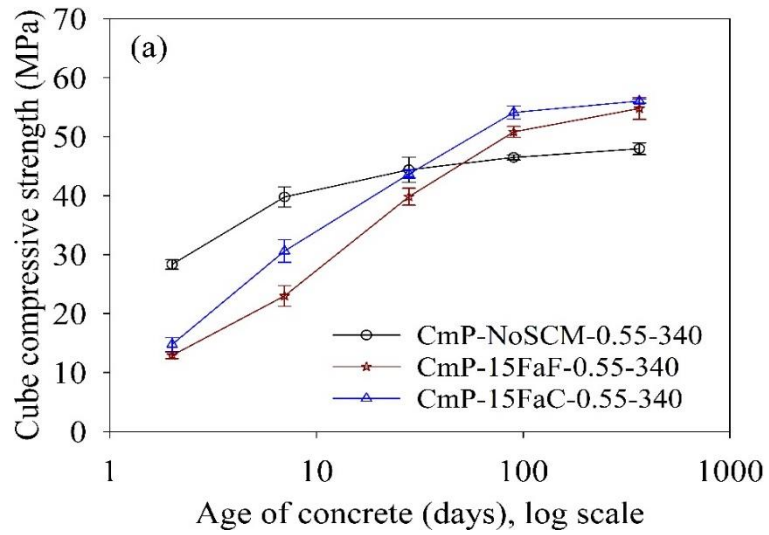


Figure 4.7 Effect of fly ash type on compressive strength development with CmP
 (a) w/b= 0.55, (b) w/b =0.50, and (c) w/b = 0.60

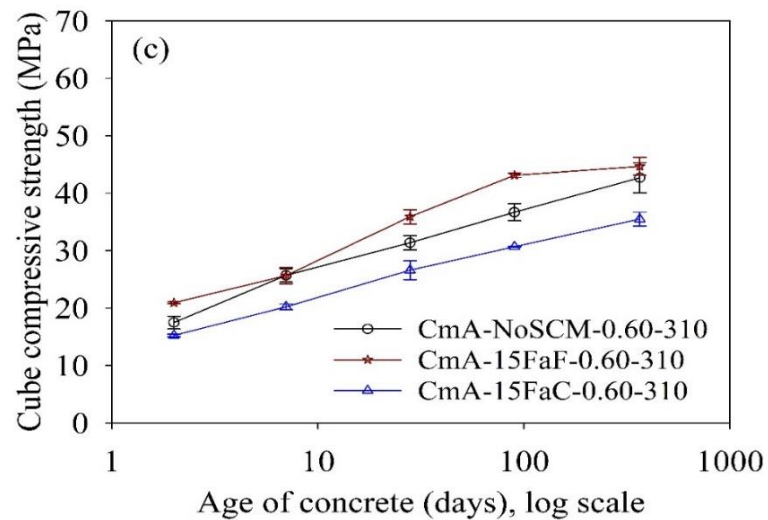
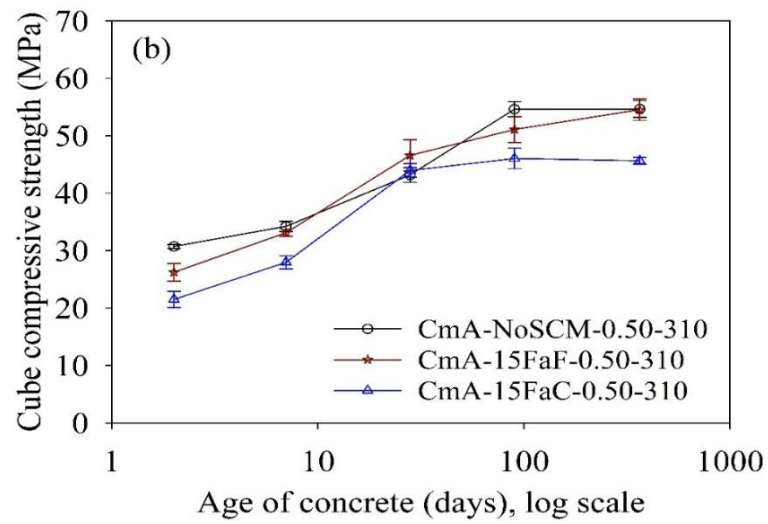
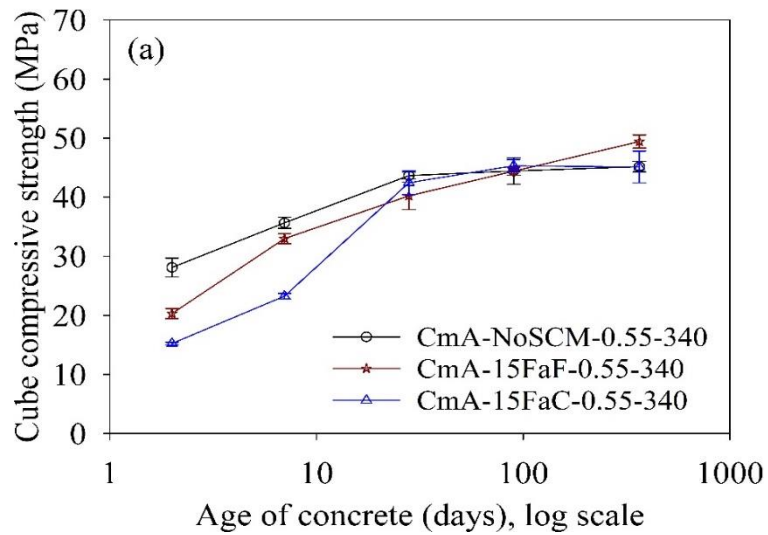


Figure 4.8 Effect of fly ash type on compressive strength development with CmA
 (a) w/b= 0.55, (b) w/b =0.50, and (c) w/b = 0.60

4.2.3 Effects of replacement level on compressive strength development

Figure 4.9 and Figure 4.10 indicate the influence on the development of compressive strength when cement is replaced by an equal mass of slag (SgB) and fly ash (FaF) while maintaining a constant water to binder ratio. It can be seen from Figure 4.9 that as the replacement level increases, the early age strength decreases while the long-term strength development is achieved. Similar results were reported by Hooton (2000) that an increase in the dosage of slag, for a given water-binder ratio and nominal air content, yielded an increase in the compressive strength at 28 days and beyond.

From Figure 4.9 (a) it is clear that there was a marked difference in the strength at 2 days. On the other hand, the 7-day strength was comparable with No-SCM concrete. Thereafter, the strength development was more pronounced. However, as seen from Figure 4.10 (a), the concretes made with CmA binders have similar strength, at all ages of testing.

Figure 4.9 (b) and Figure 4.10 (b) expound the compressive strength of FaF series concrete with CmP and CmA binders, respectively. At early ages, i.e., 2 and 7 days, the FaF blended concrete yields lower compressive strength in comparison with control mix. Subsequently, the long-term compressive strength tends to increase with the prolonged curing time. This may be because of the higher fineness of the Class F fly ash, which enhances the pozzolanic properties and particle packing density (Sata et al., 2007). As in the case of 50% replacement level, the strength developed in concrete with FaF blended cement is noticeably reduced compared with non-blended concrete, as expected (Yang et al., 2007)

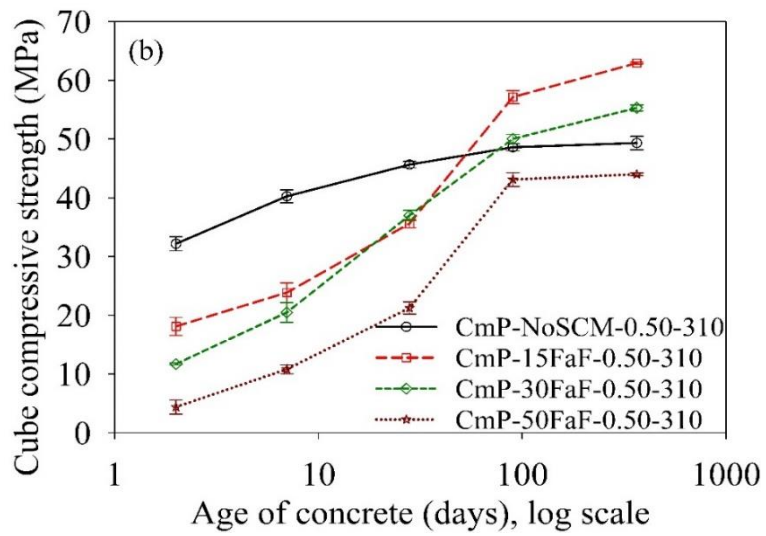
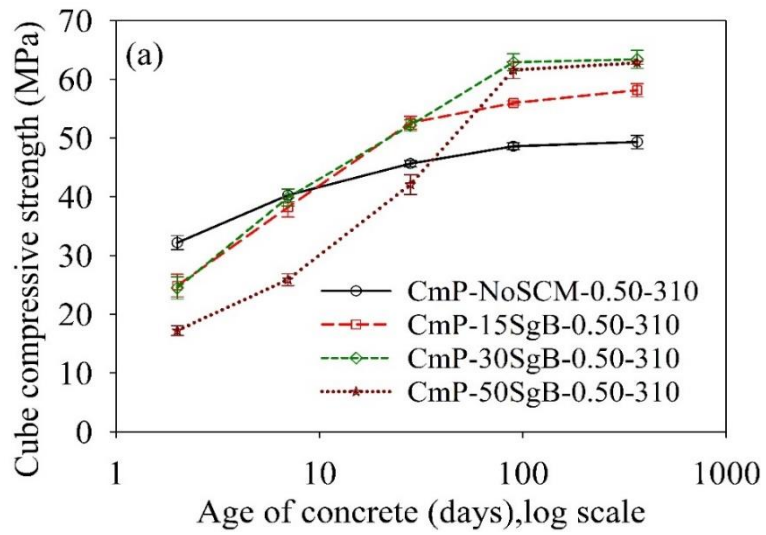


Figure 4.9 Effect of replacement level on the evolution of compressive strength of CmP blended with (a) SgB and (b) FaF

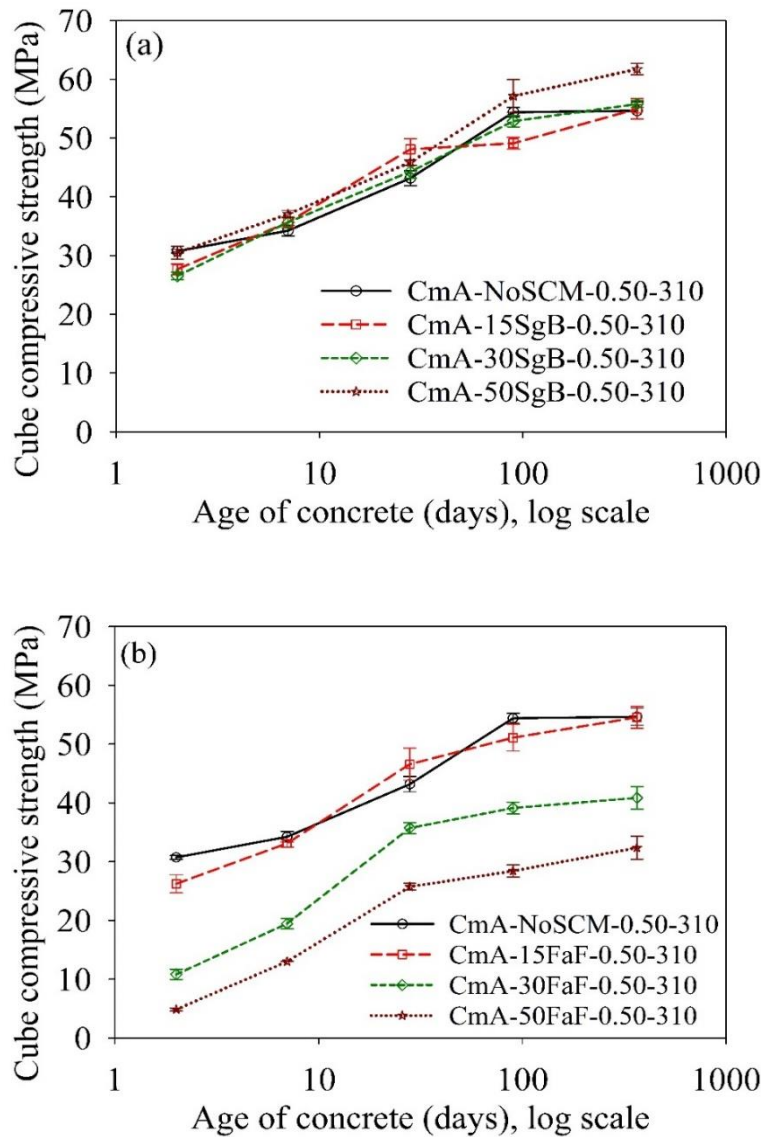


Figure 4.10 Effect of replacement level on the evolution of compressive strength of CmA blended with (a) SgB and (b) FaF

4.2.4 Effects of ternary blends on compressive strength development

As observed in Figure 4.11(a), the strength of ternary blended concrete with CmP cement is lower until 28 days. Correspondingly, SgB-FaC mix shows good enhancement of strength in comparison with other ternary blended system. Similar results were found by Yurdakul et al. (2014). Furthermore, a marginal difference in the strength was observed in the cases of SgB-FaF and SgB-FaC concrete. In the case of FaF-FaC blended concrete, the 2-day strength was less than the other mixes. However, at 7 and 28 days there was substantial increase in the strength and similar strength is attained at 90 and 365 days. Altogether, the ternary blend provides a positive effect on the evolution of compressive strength, with the result being more

pronounced at 90 days and above. In the case of CmP mix concrete (Figure 4.11(b)), ternary blended concrete shows lower strength. However, the No-SCM concrete strength evolution stabilised at 365 days, whereas, for SgB-FaF and FaF-FaC blended concrete systems there is further increase in strength.

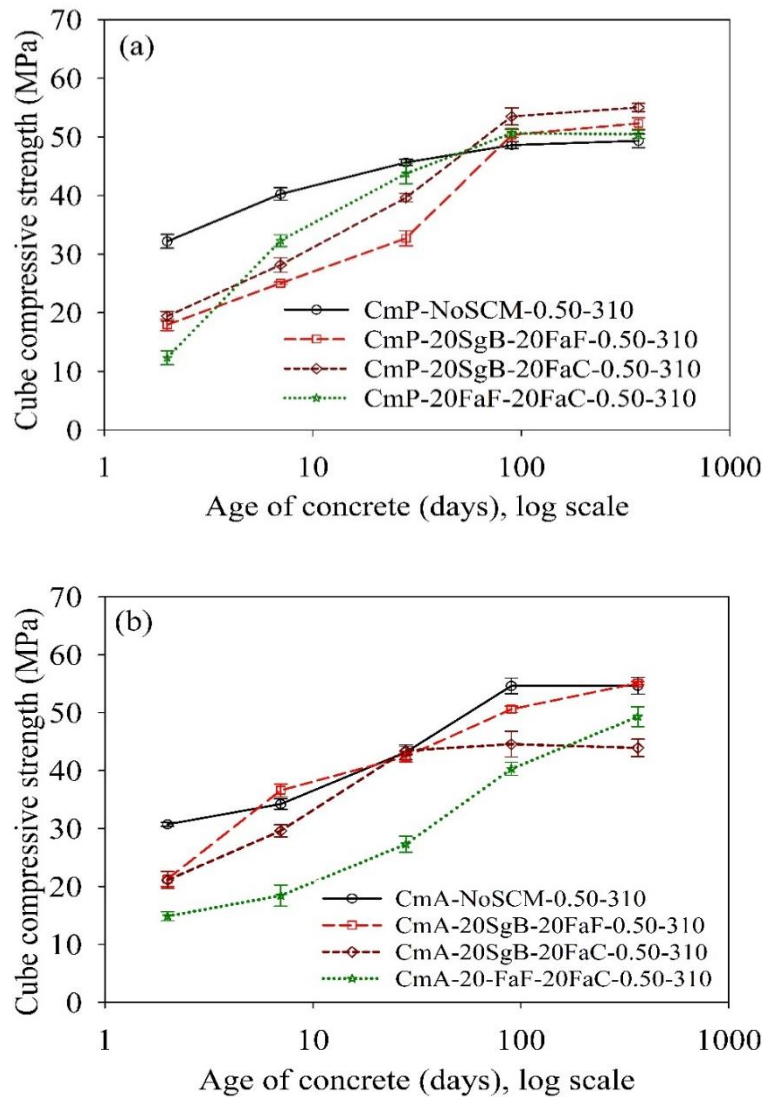


Figure 4.11 Ternary effect on the evolution of compressive strength of (a) CmP and (b) CmA cement concretes

4.2.5 Effects of LC3 on compressive strength development

As noted from Figure 4.12 (a), the evolution of compressive strength in M30 and M50 concrete mixes was comparable for the CmP-NoSCM and LC3-NoSCM mixtures up to 28 days. This is despite the fact that the LC3-NoSCM-0.40-340 had lower binder content to produce the similar target strength, which signifies improved strength potential with LC3 concrete. Nonetheless, for the CmP-30FaF concrete mix, which had lower water content in the mix to attain similar 28 days strength, the early age strength characteristics were found to be lower. There was a negligible increase in the compressive strength at later ages (from 28 day to 365 day) in the CmP-30FaF and LC3-NoSCM mixes as opposed to the CmP-NoSCM system. In addition, the M30 mix of fly ash blend concrete and LC3 binder concrete showed a marginal increase in the compressive strength than M50 concrete. Figure 4.12 (b) shows the compressive strength development of concrete made with constant water to binder ratio and binder content of 0.45 and 360 kg/m³, respectively. The compressive strength of LC3 concrete was found to be higher at all the ages. The results indicate that with similar mixture proportions, the LC3 binder can produce better compressive strength in comparison with No-SCM and 30FaF mix

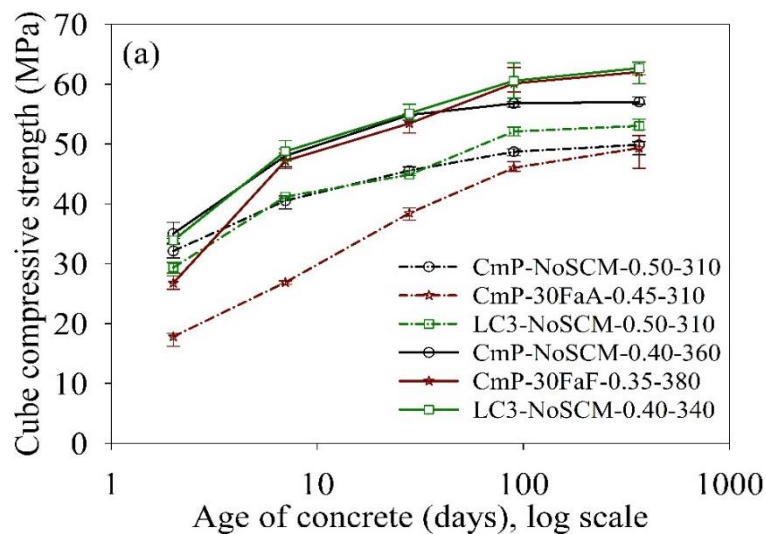


Figure 4.12 (a) Effect of fly ash on evolution of compressive strength of concrete with CmP and LC3 binders

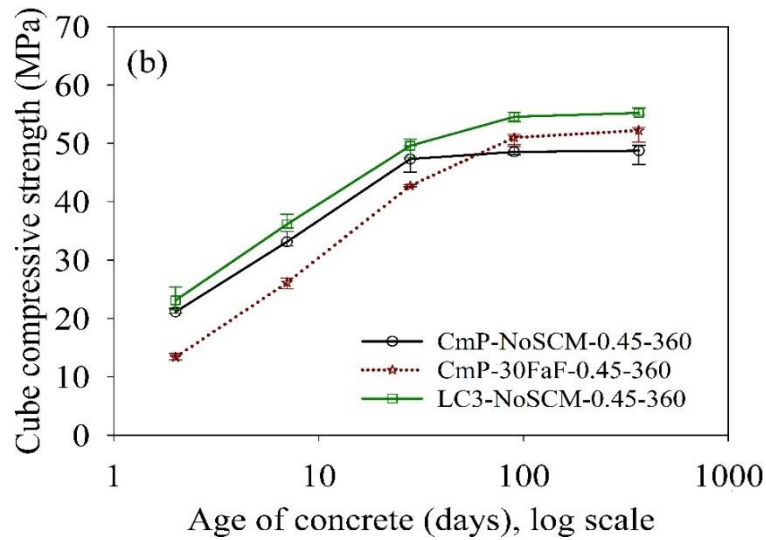


Figure 4.12 (b) Effect of fly ash on evolution of compressive strength of concrete with CmP and LC3 binders, for $w/b=0.45$ and total binder content 360kg/m^3

4.2.6 Effect of specimen size and shape on compressive strength

A general cube to cylinder strength conversion factor of 1.25 is taken for normal strength concrete (Narayanan, 1994). However, the ratio does not remain constant for all strength as the influence of the shape of the specimen decreases with higher concrete strength (Neville, 2006). The variation of cube to cylinder ratio for the concrete with respect to the cylinder compressive strength obtained at 28 days from this work is shown in the Figure 4.13, for the specimen dimensions considered. The average 28-day 100 mm cube to 150 mm diameter cylinder strength ratio obtained is between 1.18 and 1.29, and the value of 1.25 can be considered for practice for these types of specimens.

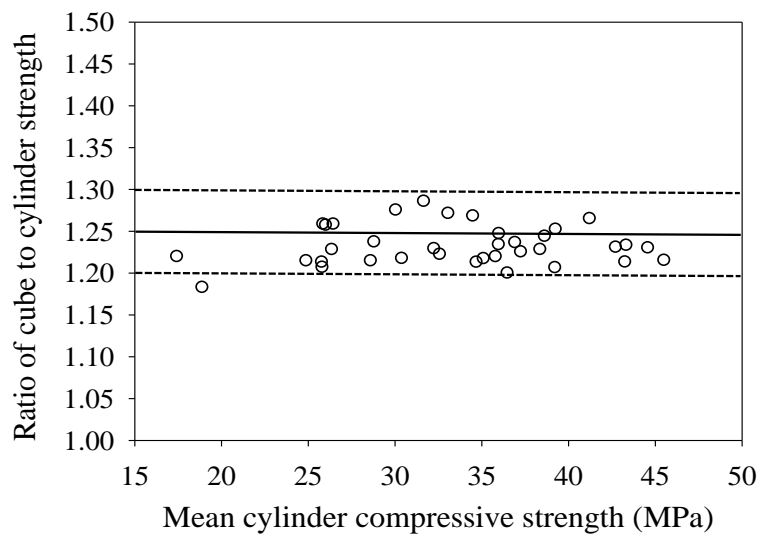


Figure 4.13 Cube-cylinder strength ratio from this study

4.2.7 Prediction of Compressive Strength Development

ACI 209 provides an empirical model to predict the compressive strength as a function of time which is expressed as follows.

$$f'_c(t) = \frac{t}{\alpha + \beta t} f'_c(28) \quad \text{Equation 4.1}$$

where, α and β are constants, $f'_c(28)$ is the mean cylinder compressive strength of concrete at 28 days and $f'_c(t)$ is the compressive strength of concrete at any age t . For 150 mm diameter and 300 mm long cylinders, and for Type I cement and moist curing, ACI 209 suggests the constants α and β to be taken as 4 and 0.85, respectively. Considering the parameters to be valid for all types of specimens and concretes, the ratio of compressive strength of concrete at time t to the mean compressive strength at 28 days can be expressed as follows.

$$\frac{f'_c(t)}{f'_c(28)} = \frac{t}{4 + 0.85 t} \quad \text{Equation 4.2}$$

Figure 4.14 represents the variation of the $\frac{f'_c(t)}{f'_c(28)}$ ratio (denoted as strength ratio, f_{Cratio} , herein) as a function of time, for various concretes. The ratio corresponding to the experimental data is indicated by the markers. The solid curve gives the trend estimated by Equation 4.2, and the dashed lines give the 95% confidence interval (CI), which were calculated by assuming a normal distribution, as follows:

$$CI = f_{Cratio} \pm 1.96 \times \text{CoV}_{\text{experiment}} \times f_{Cratio} \quad \text{Equation 4.3}$$

where, $\text{CoV}_{\text{experiment}}$ is the coefficient of variation of the experimentally observed f_{Cratio} at corresponding age.

As seen in Figure 4.14 (a), the OPC concrete with high w/b, CmP cement, and without any SCMs (CmP-NoSCM-0.65-280 and CmP-NoSCM-0.60-310) follows the trend predicted by ACI 209. The early-age strength of other OPC concrete is relatively higher than those predicted by the ACI equation. Also, almost all the concrete with CmA cement exhibit higher f_{Cratio} than predicted, especially when cured for more than 28 days. This may be because of the higher amount of CaO in this cement than in CmP cement. As shown in Figure 4.14 (b) and Figure

4.14 (c), respectively, all SgB blended concrete had higher strength than expected while the SgA blended concrete followed the predicted trend. This can be attributed to the higher fineness of SgB in comparison with SgA. Figure 4.14 (d) and (e) show the effects of FaF and FaC, respectively, with FaC concretes having higher than the expected strength. However, in FaF concrete, the long-term strength ratios at 90 and 365 days are much higher than other blended concrete. This may be because the Class F fly ash exhibits retarded pozzolanic action (Sata et al. 2007).

It is to be noted that the blended binders can vary significantly in terms of physical and chemical properties, and therefore the trends obtained should be used in calculations only when experimental data are not available and only when the binders are similar to those used here.

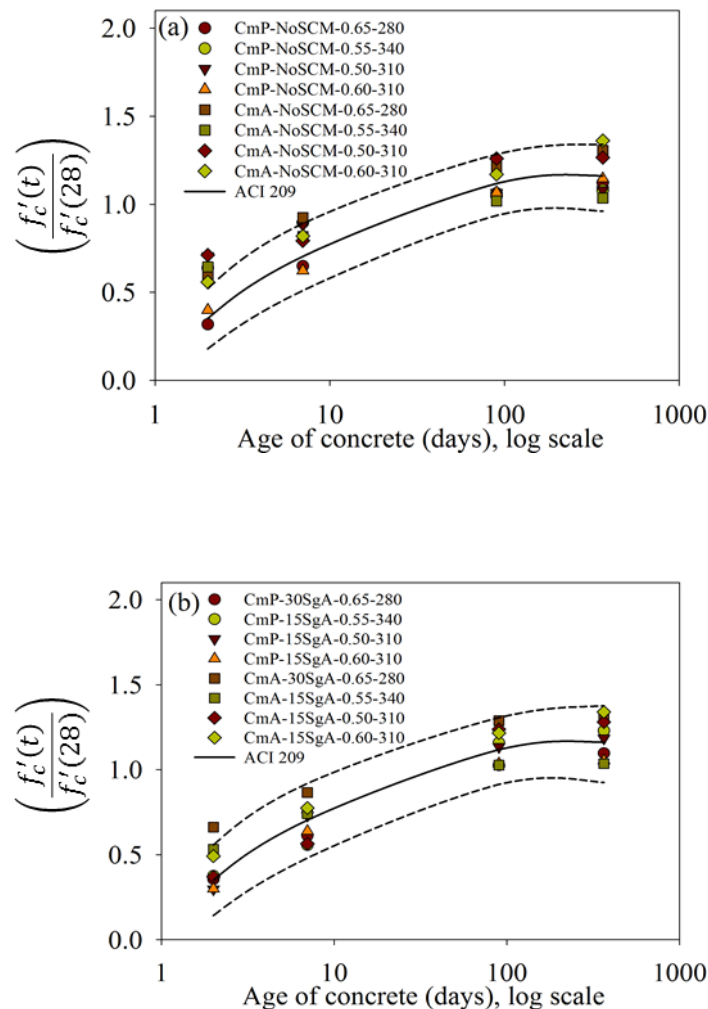


Figure 4.14 Comparison of $\left(\frac{f'_c(t)}{f'_c(28)}\right)$ data for (a) OPC, (b) SgA, concretes with the ACI prediction model and 95% confidence interval

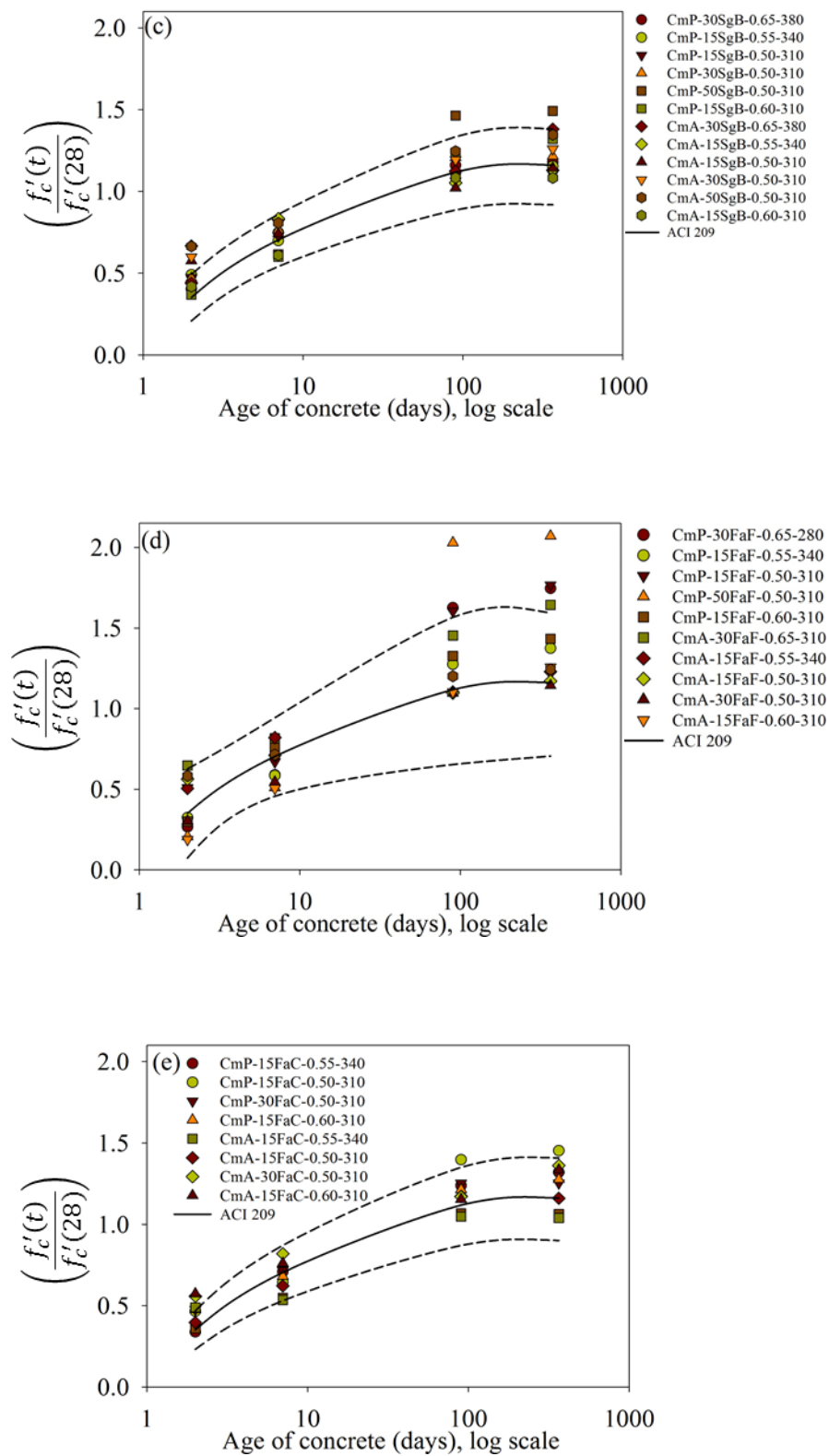


Figure 4.14 Comparison of $\left(\frac{f'_c(t)}{f'_c(28)}\right)$ data for (c) SgB, (d) FaF and (e) FaC concretes with the ACI prediction model and 95% confidence interval

4.3 ELASTIC MODULUS RESULTS

The results of the elastic modulus tests on concrete at 28 days are presented in Table 4.2, as the average of three specimens. The serial numbering in the table corresponds to earlier Tables 3.6, 3.8 and 4.1 for facilitating cross-referencing – note that there is a break in numbering as the elastic modulus was not determined for the concretes with CmA. The values are in the range of 22 to 40 GPa, with standard deviations varying between 0.05 and 2.2 GPa.

Table 4.2 Elastic modulus values at 28 days.

Sl. No.	Mix Designation	Mean elastic moduli (S.D), in GPa
1	CmP-NoSCM-0.65-280	29.7 (1.5)
2	CmP-30SgA-0.65-280	31.4 (0.1)
3	CmP-30SgB-0.65-280	34.4 (1.0)
4	CmP-30FaF-0.65-280	29.3 (0.0)
5	CmP-NoSCM-0.55-340	35.7 (0.4)
6	CmP-15SgA-0.55-340	37.4 (1.2)
7	CmP-15SgB-0.55-340	36.7 (0.5)
8	CmP-15FaF-0.55-340	34.4 (0.1)
9	CmP-15FaC-0.55-340	34.5 (0.9)
10	CmP-NoSCM-0.50-310	33.4 (1.5); 36.1 (1.1)*
11	CmP-15SgA-0.50-310	40.1 (0.7)
12	CmP-15SgB-0.50-310	35.8 (1.3)
13	CmP-15FaF-0.50-310	30.1 (0.7); 31.2 (1.2)*
14	CmP-15FaC-0.50-310	36.7 (2.2)
15	CmP-30SgB-0.50-310	37.5 (0.5)
16	CmP-30FaF-0.50-310	32.8 (1.3); 33.8 (0.8)*
17	CmP-30FaC-0.50-310	35.2 (0.8)
18	CmP-50SgB-0.50-310	36.9 (1.5)
19	CmP-50FaF-0.50-310	22.8 (1.1)
20	CmP-20SgB-20FaF-0.50-310	31.7 (1.7)
21	CmP-20SgB-20FaC-0.50-310	39.3 (0.6)
22	CmP-20FaF-20FaC-0.50-310	34.3 (1.6)
23	CmP-NoSCM-0.60-310	36.6 (0.6)
24	CmP-15SgA-0.60-310	32.8 (1.9)
25	CmP-15SgB-0.60-310	29.3 (1.4)
26	CmP-15FaF-0.60-310	34.3 (0.9)
27	CmP-15FaC-0.60-310	39.9 (0.9)
55	CmP-NoSCM-0.50-310x	35.7 (1.3)
56	CmP-30FaA-0.45-310	27.7 (2.2)
57	LC3-NoSCM-0.50-310	34.7 (1.9)
58	CmP-NoSCM-0.40-360	40.6 (0.9)
59	CmP-30FaF-0.35-380	39.9 (1.0)
60	LC3-NoSCM-0.40-340	38.2 (0.8)
61	CmP-NoSCM-0.45-360	35.8 (0.6)
62	CmP-30FaF-0.45-360	33.6 (1.6)
63	LC3-NoSCM-0.45-360	37.6 (1.3)

* Data from additional sets cast separately for a different test programme

4.3.1 Effect of fly ash and slag on the elastic modulus of concrete with CmP cement

The elastic modulus of FaF blended concrete was lower than the CmP mixes concrete at all replacement levels in this study. The concrete with 30% replacement level had slightly higher values than 15%, and much lower for 50% replacement. The impact of Slag B is seen to be the same as that of compressive strength at any replacement level. Figure 4.15 points out that there was a significant increase in the elastic modulus for concrete with slag replacement between 15% and 30%. Furthermore, 50% replacement with slag and fly ash did not give much higher modulus at 28 days. However, it should be noted that the plots combine data from mixes of different binder contents, water contents and strengths, and therefore should be considered with caution.

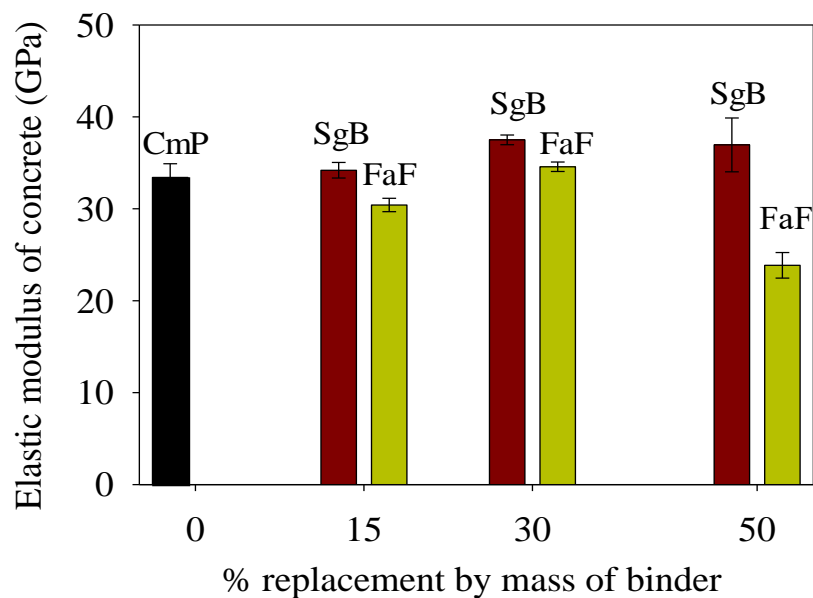


Figure 4.15 Effect of replacement of cement with slag and fly ash on the elastic modulus of concrete with CmP cement

4.3.2 Relations between compressive strength and elastic modulus

A comparison of the measured mean elastic modulus of concrete and the model predictions (say, IS 456:2000; ACI 318:2008; ACI 209:2005; and *fib* Model Code 2010) as functions of the measured cube compressive strength is shown in Figure 4.16. The description and details of the code recommendations are discussed below.

IS 456 estimates the elastic modulus of concrete at 28-days, E_c as follows:

$$E_c = 5000 \sqrt{f_{ck}} \quad \text{Equation 4.4}$$

where, f_{ck} is the characteristic 28-day cube compressive strength (MPa).

The ACI 318 report recommends the following model for E_c .

$$E_c = 4733 \sqrt{f'_c} \quad \text{Equation 4.5}$$

where, f'_c is the specified cylinder compressive strength of concrete (MPa).

However, ACI 209 suggests that the elastic modulus of concrete at any time t (defined as E_{ct}) can be calculated as follows.

$$E_{ct} = g_{ct} [w^3 (f'_c)_t]^{1/2} \quad \text{Equation 4.6}$$

where, g_{ct} is equal to 0.043; w is the unit weight of concrete (kg/m^3); and $(f'_c)_t$ is the cylinder compressive strength at time t (MPa).

The elastic modulus of concrete can be predicted using the *fib* Model Code-2010 as follows.

$$E_{ci} = E_{c0} \times \alpha_E \times \left(\frac{f_{cm}}{10} \right)^{0.3} \quad \text{Equation 4.7}$$

where, E_{ci} is the modulus of elasticity of concrete at 28 days (MPa); f_{cm} is the mean cylinder compressive strength of concrete (MPa); E_{c0} is 21.5×10^3 MPa; and α_E is 1.0 and 1.2 for quartzite and basalt or dense limestone aggregates, respectively.

IS-456 and ACI 318 consider the characteristic compressive strength from cubes (f_{ck}) and cylinders (f'_c), respectively, whereas *fib* MC-2010 and ACI 209 use the mean compressive strength of cylinders in the calculation of elastic modulus. For comparing the predictions, the mean cylinder compressive strength was converted to the mean cube compressive strength by multiplying with 1.21, taken from the average ratio of cube to cylinder mean compressive strength obtained in the tests conducted this study. Also, for IS 456 and ACI 318 the characteristic/desired compressive strength was calculated from $\sigma_{characteristic} = \sigma_{mean} - ks$, where constant “ k ” was taken as 1.65 and the standard deviation “ s ” was taken as 1.12 from the cube compressive strength data in this study. A plot of the mean values and the predictions of elastic

modulus of concrete is given in Figure 4.16. It is clearly seen that the ACI 318 and ACI 209 model predictions are more conservative than the recommendations of IS 456 and *fib* MC 2010.

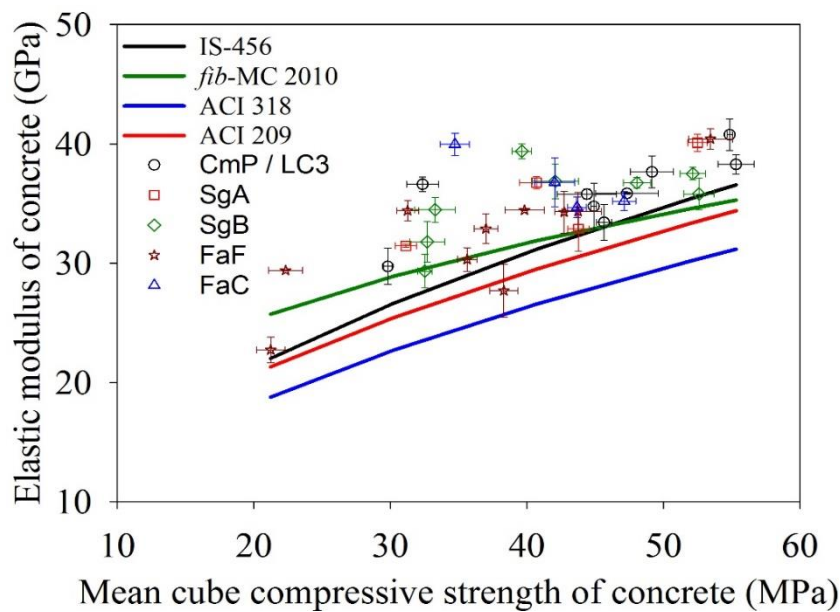


Figure 4.16 Relation between the elastic modulus and compressive strength of concrete

4.4 SUMMARY

This chapter describes the effects of supplementary cementitious materials on compressive strength development and elastic modulus as observed from the tests conducted in this work. The major findings are: (i) water to binder ratio is an important factor that influence the evolution of compressive strength on blended concrete; (ii) fly ash blended concrete systems develop compressive strength at slower rate than the slag blended concrete; (iii) fly ash concrete shows substantial strength gain after 28 days, while the same was not perceived in the slag bended concrete systems; (iv) strength development of Class C fly ash was higher than Class F fly ash concrete; (v) ternary blended concrete shows a prolonged strength gain at all ages of testing; and (vi) early age strength ratio of No-SCM concrete are reasonably higher than the ACI prediction; also, with prolonged curing time, FaF blended concretes yielded considerably higher strengths than other concretes; (vii) the elastic modulus predictions of ACI 209 and ACI 318 are more conservative than those of *fib* MC 2010 and IS 456.

5. RESULTS AND DISCUSSIONS – TOTAL AND AUTOGENOUS SHRINKAGE OF CONCRETE

5.1 INTRODUCTION

Shrinkage in concrete, particularly drying shrinkage, is a major concern for structural design as it directly affects the risk of cracking in concrete elements. Drying shrinkage is the phenomenon that is caused by the loss of moisture from the pores of hardened concrete. The rate of evaporation or drying depends on the temperature, relative humidity, water to cement ratio and the surface area that is exposed to the surrounding atmosphere. Consequently, drying shrinkage occurs when the concrete member is exposed to the atmosphere and is allowed to undergo volume change. It is considered that the shrinkage of normal concrete after the curing stage is predominantly due to drying since the contribution from the autogenous shrinkage is minimal or even negligible (Tia et al., 2005; Holt, 2005).

This chapter presents the measured shrinkage strain data from cylinders and prismatic specimens exposed to controlled laboratory environment. Total and autogenous shrinkage of non-blended cement concrete, and concrete blended with fly ash and slag have been discussed in terms of the effects of: a) different binder composition, b) different water to binder ratios and total binder content, c) supplementary cementitious material and their dosage and d) size of the specimen. Note that though the conventional term "autogenous shrinkage" is used in this work, some researchers prefer to use the term "basic shrinkage" for the shrinkage strains measured on sealed specimens, which could be all the more relevant when the very early age deformations are not accounted for, as in the present work where measurements are initiated only after the 28 day curing period. Additionally, the loss of mass in sealed and unsealed specimens have also been measured to complement the shrinkage data.

5.2 SHRINKAGE MEASUREMENTS IN SLAG AND FLY ASH BLENDED CONCRETE

The testing procedure for the shrinkage measurements was discussed in Section 3.4.2. of Chapter 3. Figure 5.1 through Figure 5.8 presents typical plots of shrinkage and mass loss in the cylinders and prisms under sealed and unsealed conditions. The plots are given for each pair of measurements made on every specimen, as well as the average values. Appendix B1 presents all the plots of measured total and autogenous shrinkage strains on normal and logarithmic scales. Similarly, the shrinkage strains of all prismatic specimens are plotted and

given in Appendix B2, which were obtained from the absolute change in the length of each specimen. Mass losses in the cylinder and prism specimens were measured at the same time interval as the shrinkage measurement, and the details are presented for all specimens in Appendices C1 and C2. The measurements are generally plotted up to more than 1000 days, after exposure or curing up to 28 days (i.e., $t_0 = 28$ days).

As discussed in Chapter 3, the specimens were prepared within two hours after the desired curing period and the measurements were started. However, the time of measurement could not be exactly the same and therefore the measurements made within the first 24 hours are not reported. The plots in the following sections represent the average shrinkage strain from three identical specimens, for total and autogenous shrinkage, both with time in the normal scale and in log scale.

Figure 5.9 through Figure 5.12 show the shrinkage responses of concretes with the OPCs CmP and CmA, along with that with LC3. As seen from Figure 5.1, CmA concrete shows lower shrinkage by about 150 microstrain than the LC3 concrete, and the responses of the CmP and CmA concretes differ marginally by 80 microstrain. Figure 5.10 through Figure 5.12 give the comparisons between the CmP and CmA concretes for water-binder ratio and total binder content of 0.55 and 340 kg/m³; 0.60 and 310 kg/m³; 0.45 and 360 kg/m³, respectively. Overall, there is a small difference in the shrinkage strain among the different types of concrete with CmP and CmA, for the various water to binder ratios and binder contents. A comparison of CmP and LC3 concrete for a constant water- binder ratio and binder content in Figure 5.12, shows that the shrinkage strains of CmP and LC3 concrete are comparable until around 70 days. Afterwards, the rate of evolution of shrinkage was slightly higher in the case of LC3 concrete as compared with CmP.

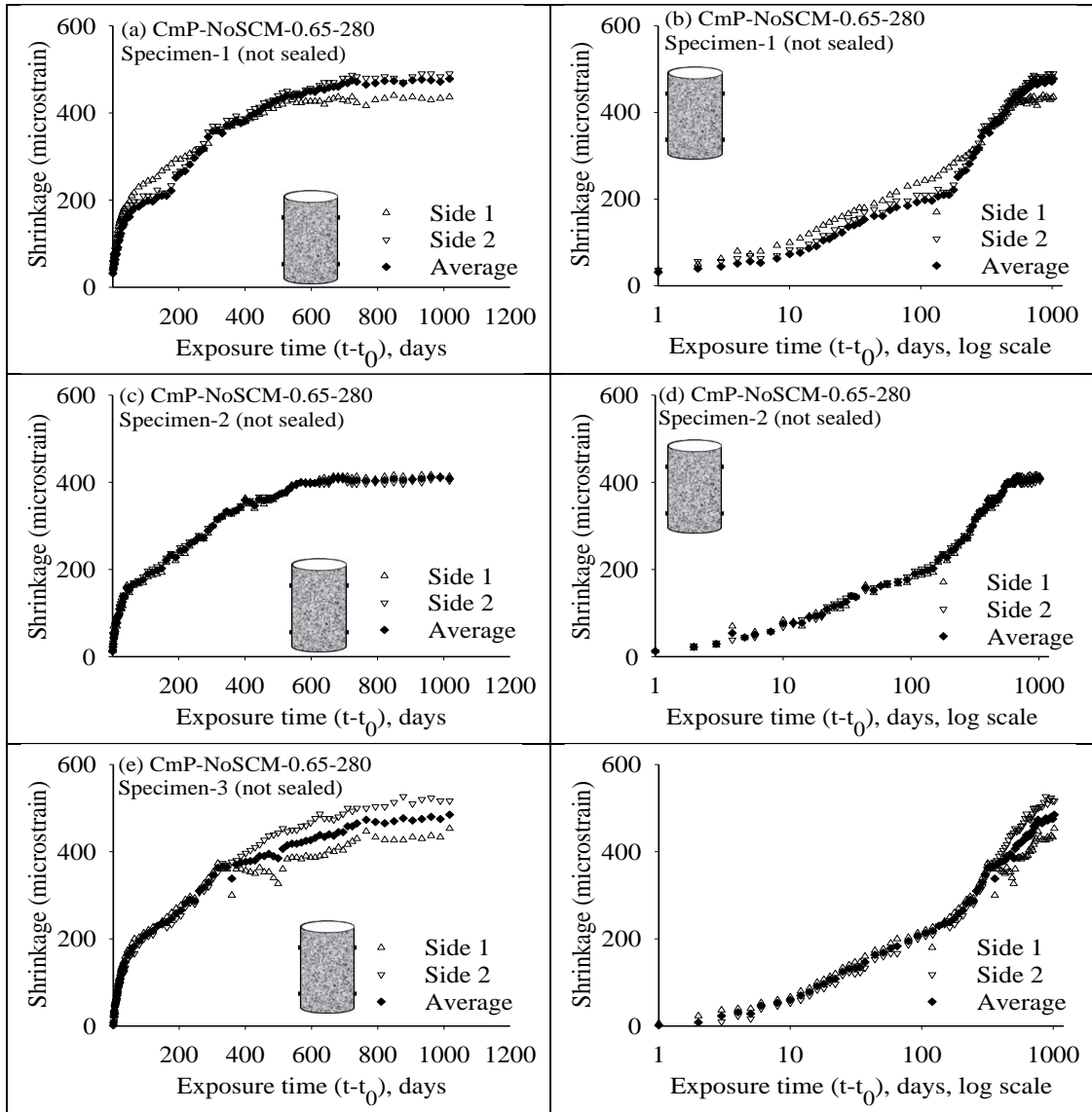


Figure 5.1 Measured total shrinkage strain on unsealed CmP-NoSCM-0.65-280 cylinders

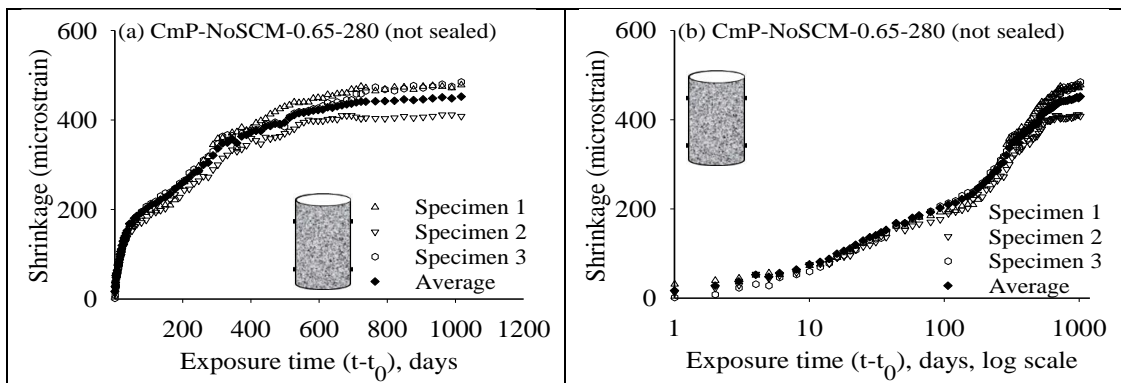


Figure 5.2 Measured total shrinkage strain on unsealed CmP-NoSCM-0.65-280 cylinders

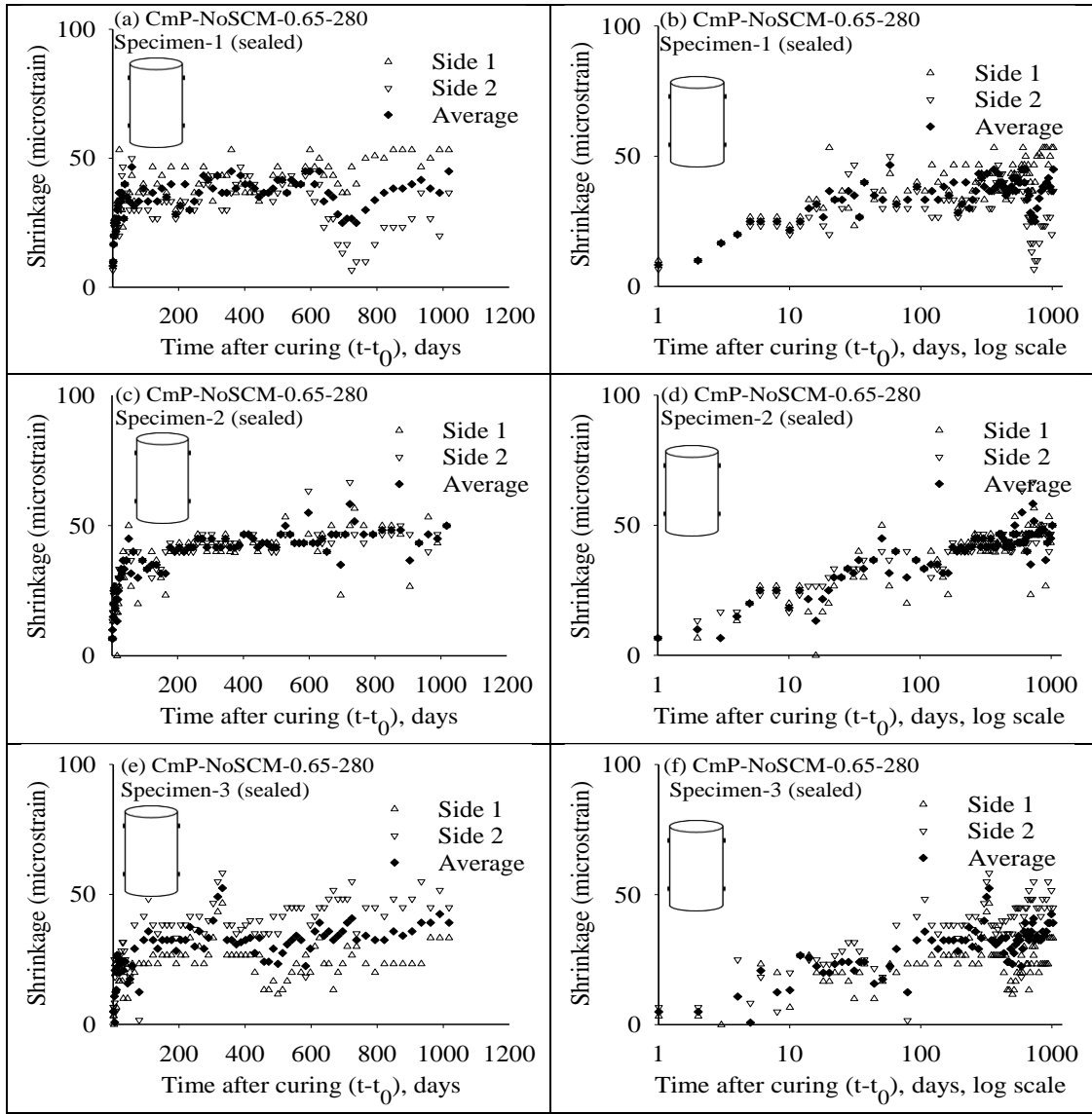


Figure 5.3 Measured autogenous shrinkage strain on sealed CmP-NoSCM-0.65-280 cylinders

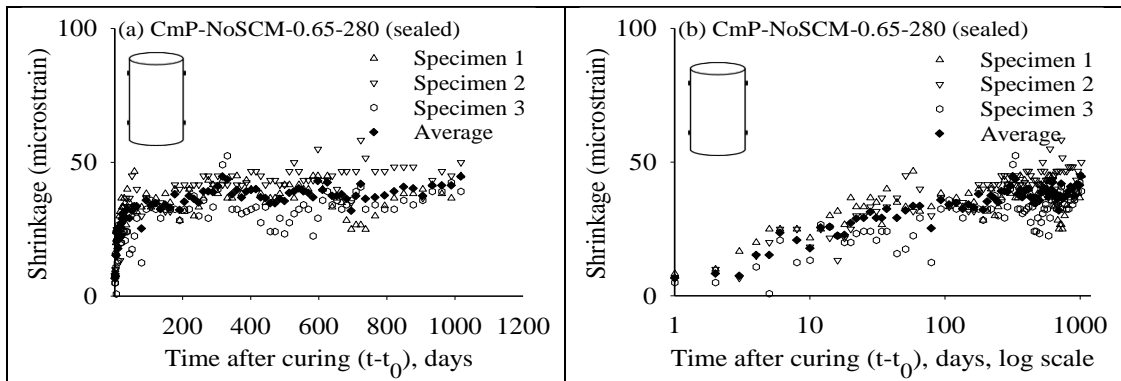


Figure 5.4 Measured autogenous shrinkage strain on sealed CmP-NoSCM-0.65-280 cylinders

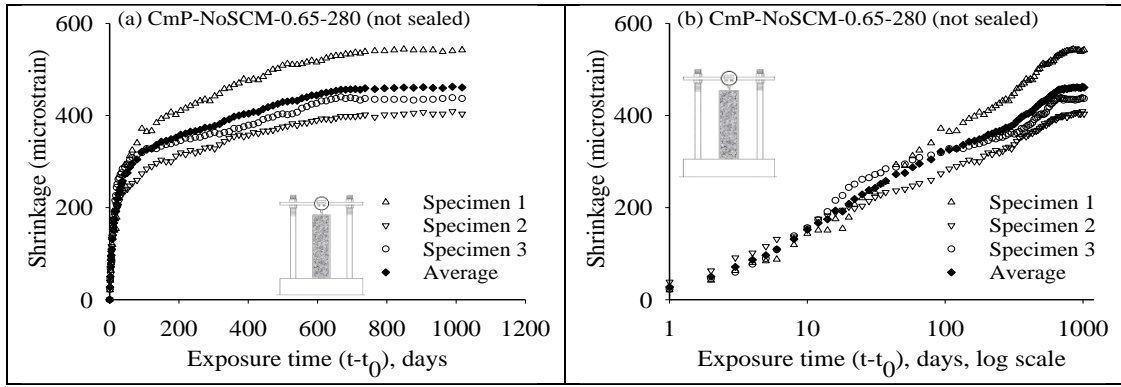


Figure 5.5 Measured total shrinkage strain on unsealed CmP-NoSCM-0.65-280 prisms

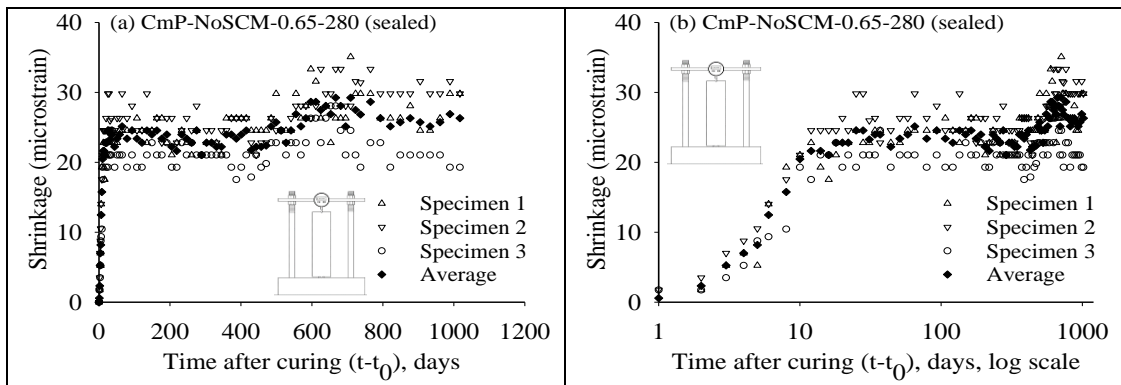


Figure 5.6 Measured autogenous shrinkage strain on sealed CmP-NoSCM-0.65-280 prisms

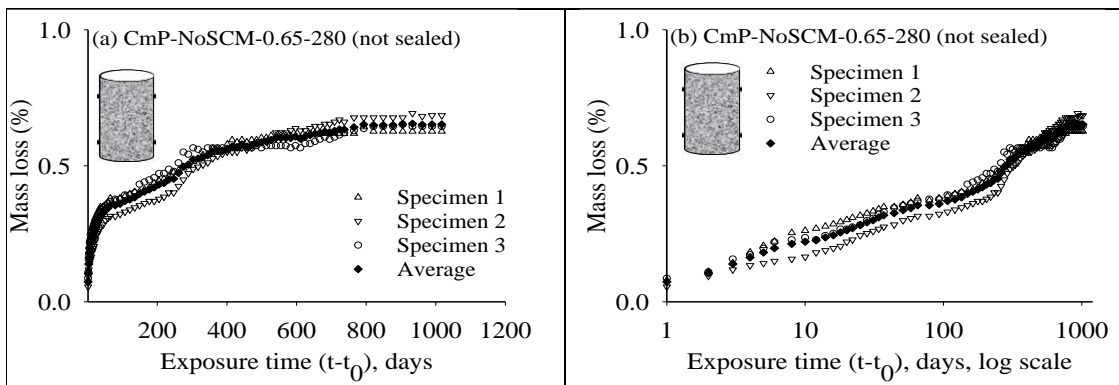


Figure 5.7 Measured mass loss in unsealed CmP-NoSCM-0.65-280 cylinders

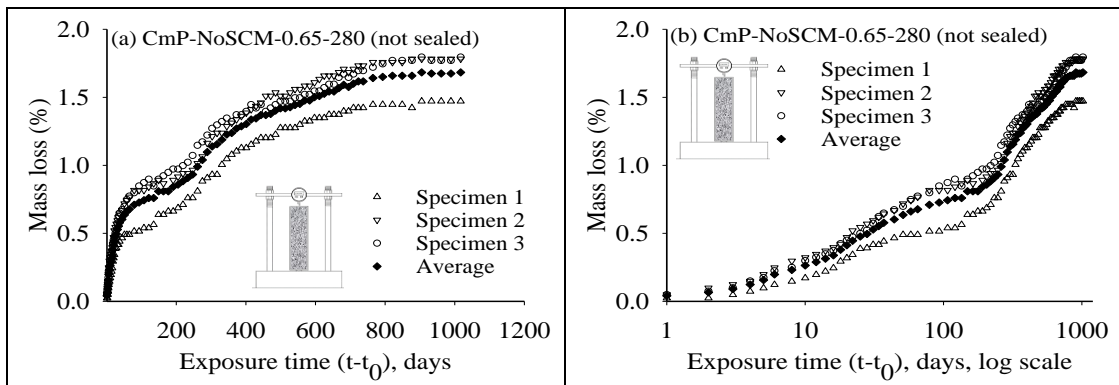


Figure 5.8 Measured mass loss in unsealed CmP-NoSCM-0.65-280 prisms

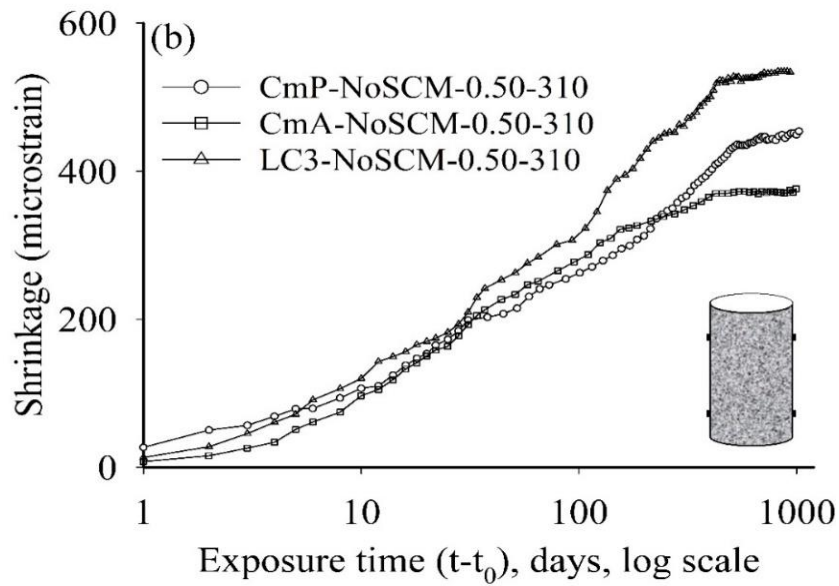
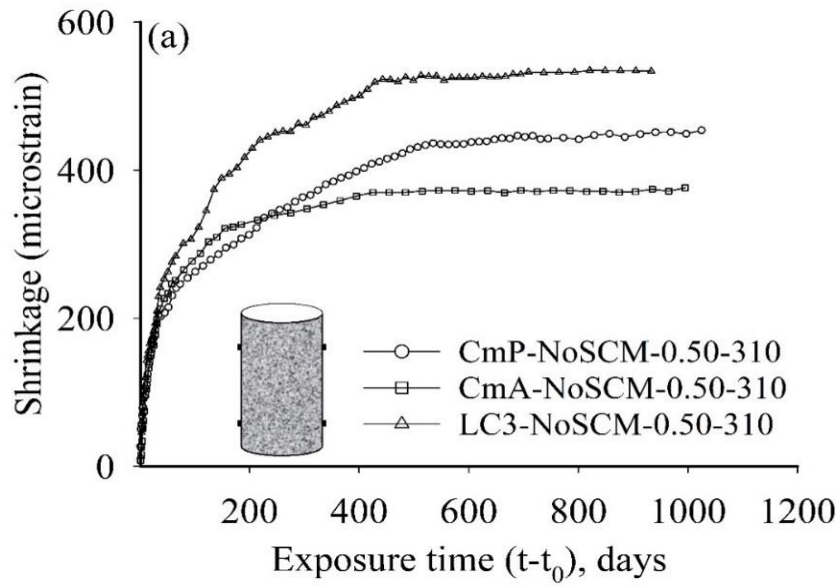


Figure 5.9 Effect of cement type on the total shrinkage strain of concrete with $w/b = 0.50$ and total binder content = 310 kg/m^3 , for CmP, CmA and LC3 cements: in (a) normal and (b) log scales

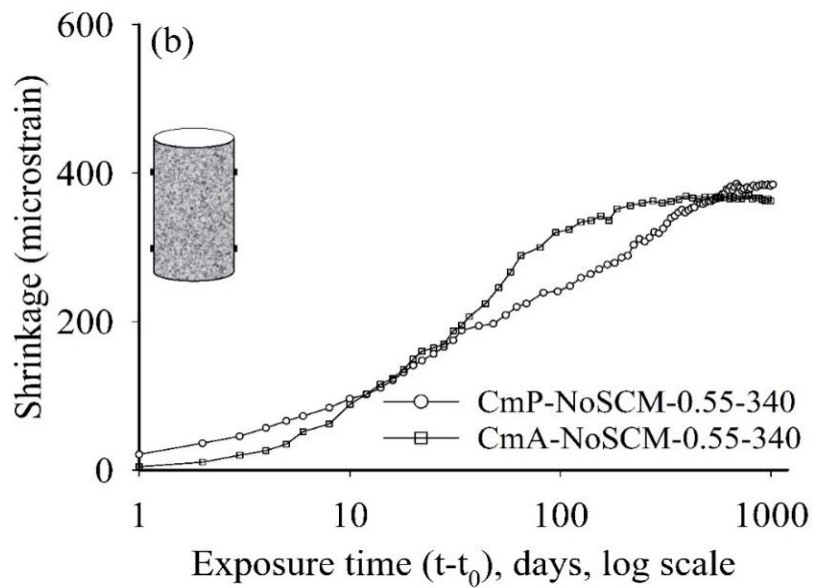
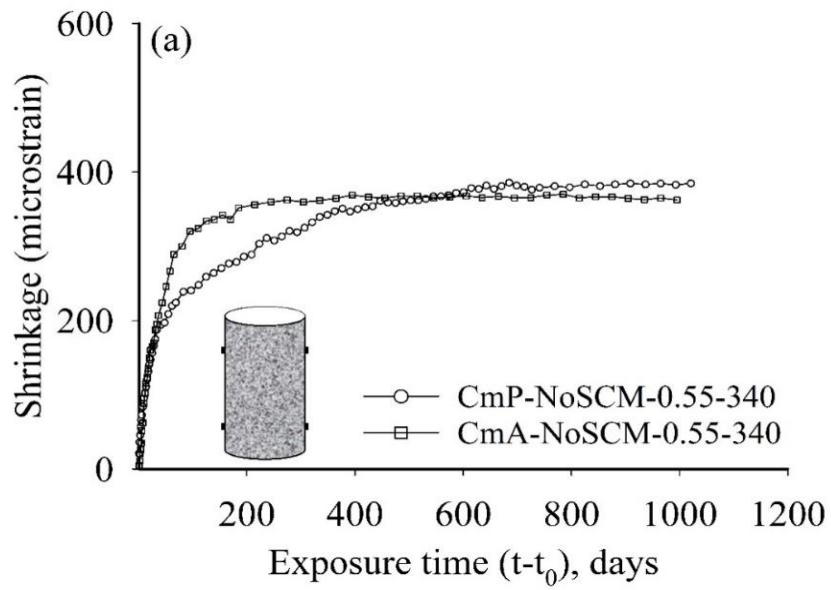


Figure 5.10 Effect of cement type on the total shrinkage strain of concrete with $w/b = 0.55$ and total binder content = 340 kg/m^3 : in (a) normal and (b) log scales

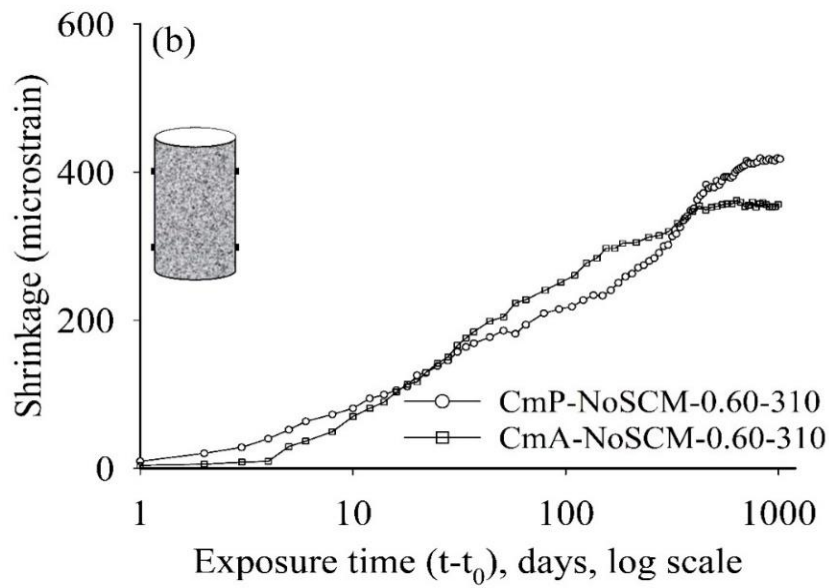
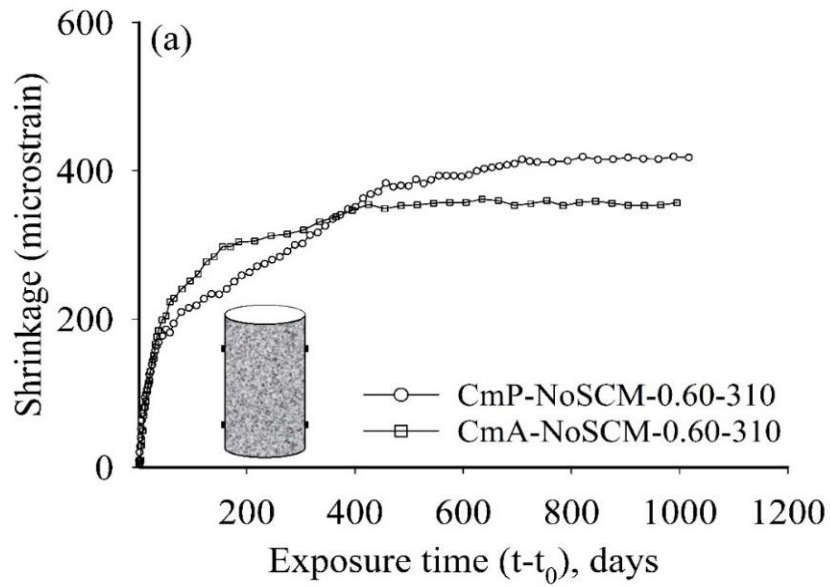


Figure 5.11 Effect of cement type on the total shrinkage strain of concrete with $w/b = 0.60$ and total binder content = 310 kg/m^3 : in (a) normal and (b) log scales

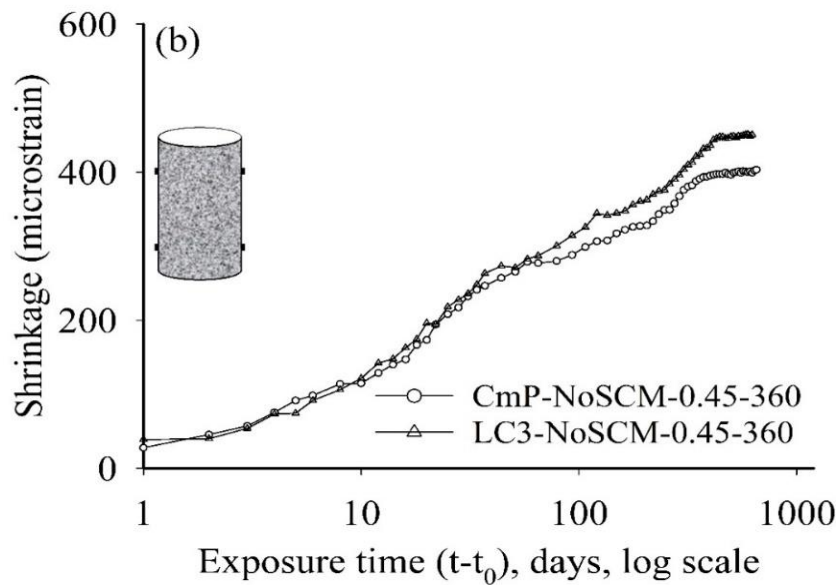
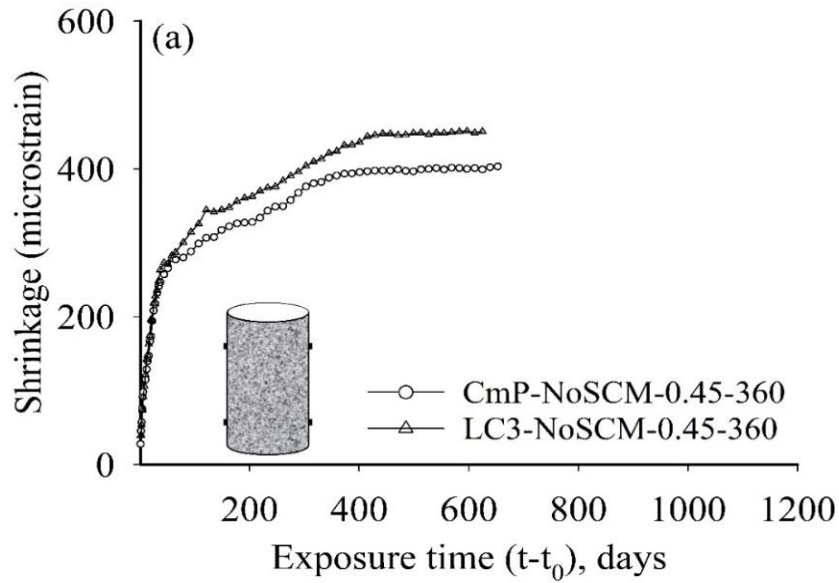


Figure 5.12 Effect of cement type on the total shrinkage strain of concrete with $w/b = 0.45$ and total binder content = 360 kg/m^3 : in (a) normal and (b) log scales

The influence of slag and fly ash on the shrinkage response of blended concrete can be assessed through the results presented in Figure 5.13 through Figure 5.16. The plots indicate that the evolution of shrinkage strain, for the concretes considered here, is practically independent of water-binder ratio even in the case of blended binders. As seen from Figure 5.13, the early age shrinkage response of the different classes of concrete is similar. However, at about 1000 days, the total shrinkage of the No-SCM concrete was comparatively higher than

the blended concrete systems, in most cases. Similarly, FaF and SgA blended concrete shows approximately 10% higher in strains than the Class C fly ash and SgB mixes. Figure 5.17 through Figure 5.19 show that the shrinkage response does not differ significantly among the SCMs, at the dosages considered. This follows the suggestion of Bissonnette et al. (1999) that water-binder ratio does not have a strong effect on drying shrinkage since factors such as total porosity, pore-size distribution and elastic modulus may have opposing influence that can offset the trend.

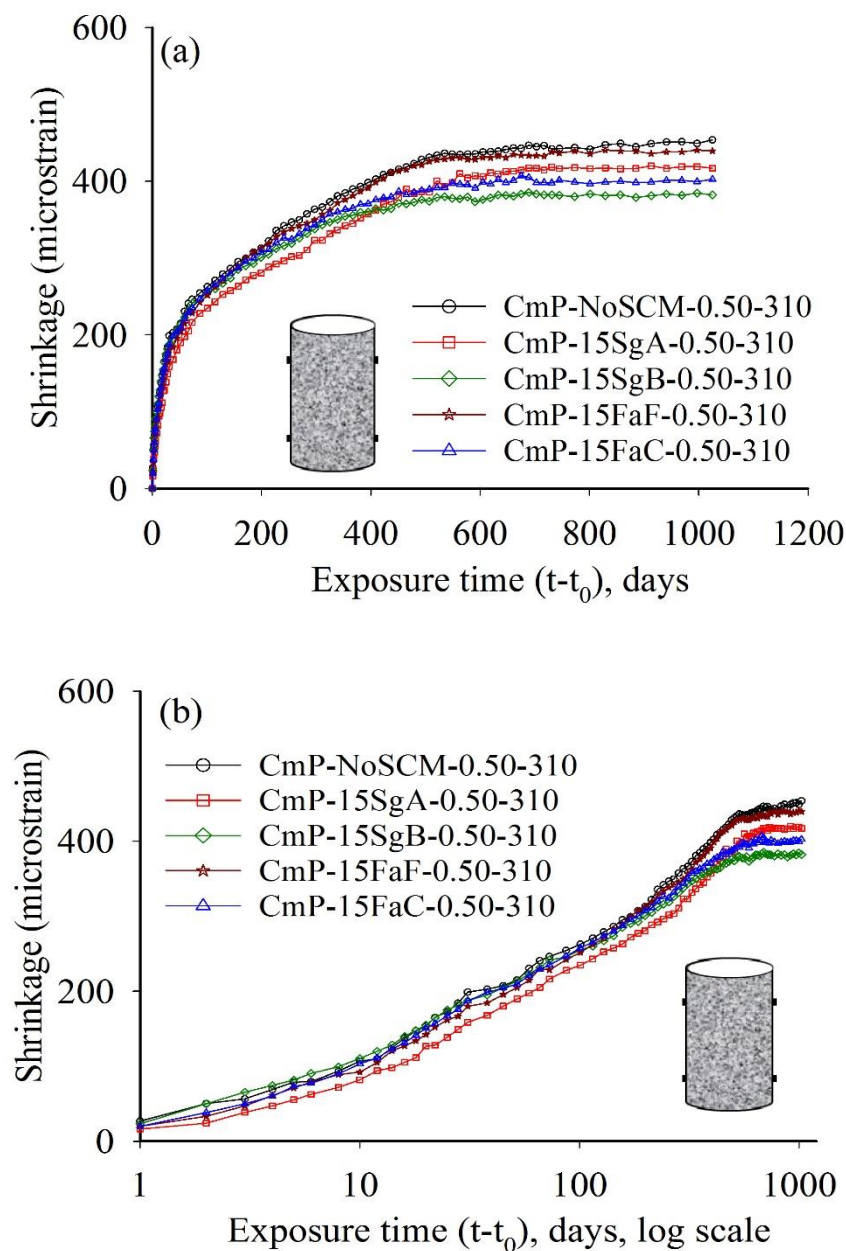


Figure 5.13 Effect of water to binder ratio on the total shrinkage strain of binary blended concrete with $w/b = 0.50$ and total binder content = 310 kg/m^3 of CmP mix: in (a) normal and (b) log scales

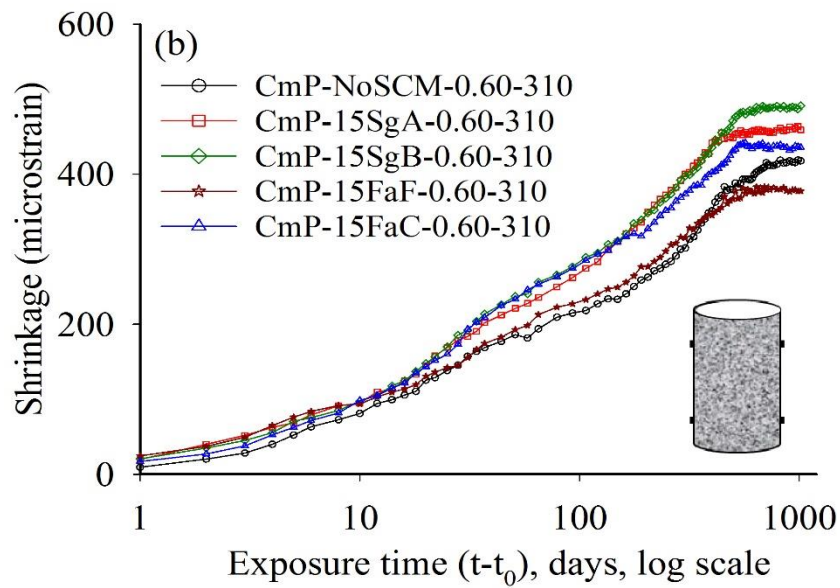
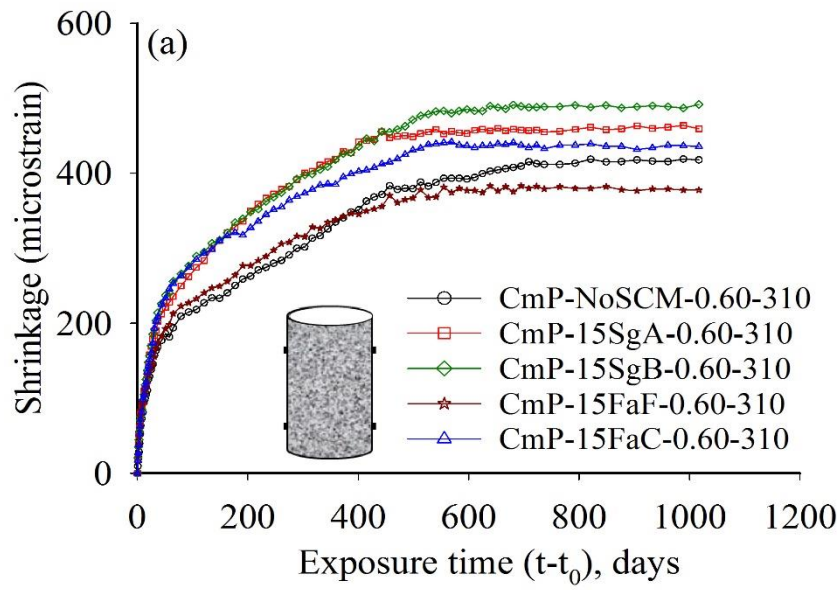


Figure 5.14 Effect of water binder ratio on total shrinkage strain of binary blended concrete with $w/b= 0.60$ and total binder = 310 kg/m^3 content of CmP mix: in (a) normal and (b) log scales

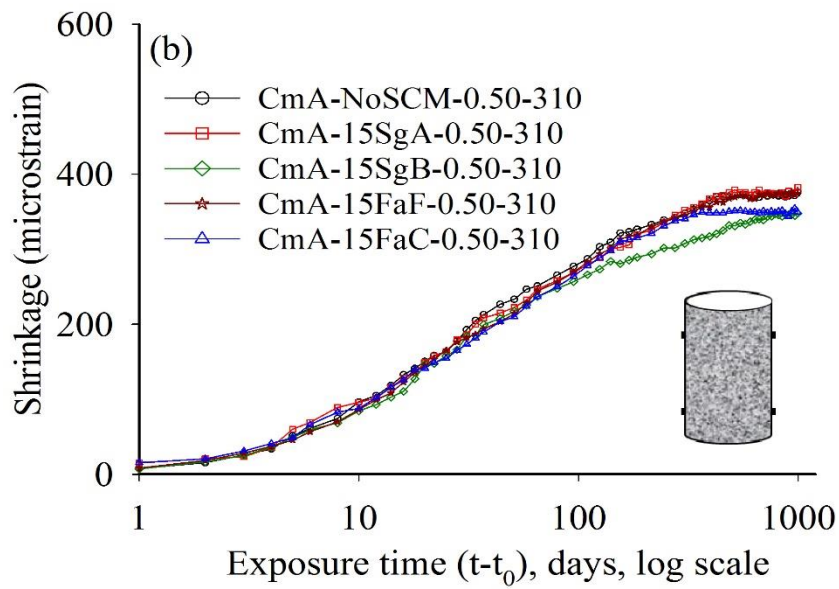
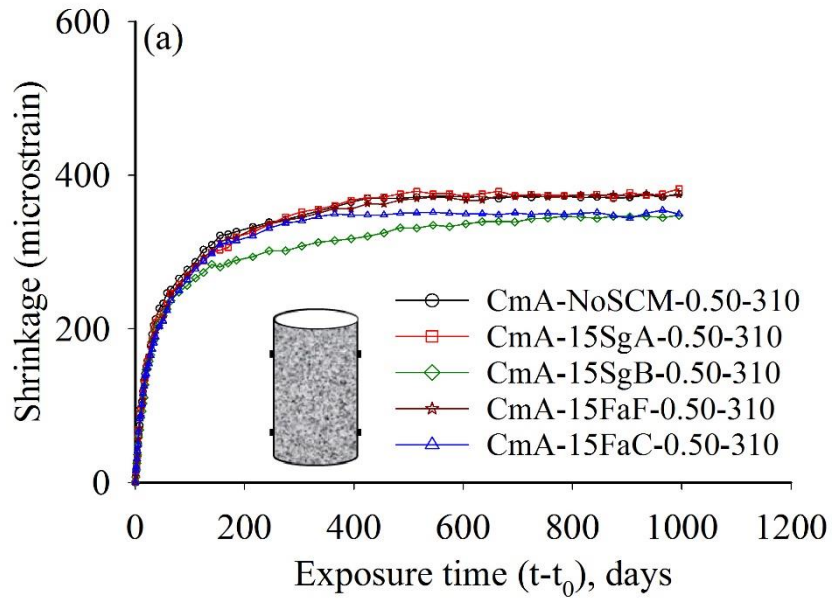


Figure 5.15 Effect of water binder ratio on the total shrinkage strain of binary blended concrete with $w/b = 0.50$ and total binder 310 kg/m^3 content of CmA mix: in (a) normal and (b) log scales

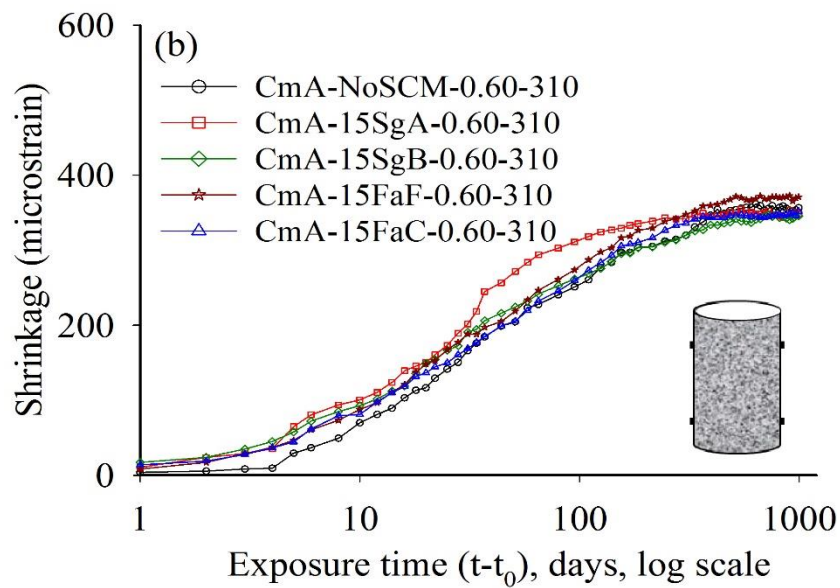
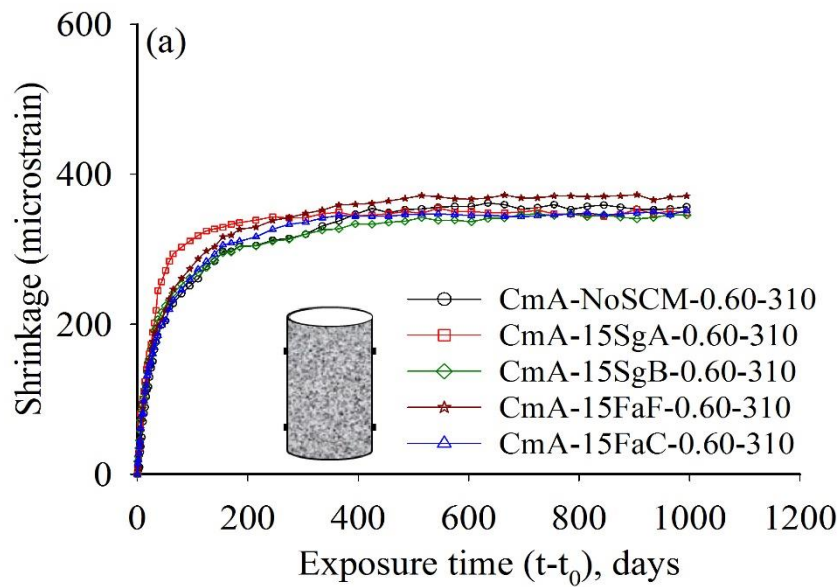


Figure 5.16 Effect of water binder ratio on the total shrinkage strain of binary blended concrete with $w/b=0.60$ and total binder 310 kg/m^3 content of CmA mix: in (a) normal and (b) log scales

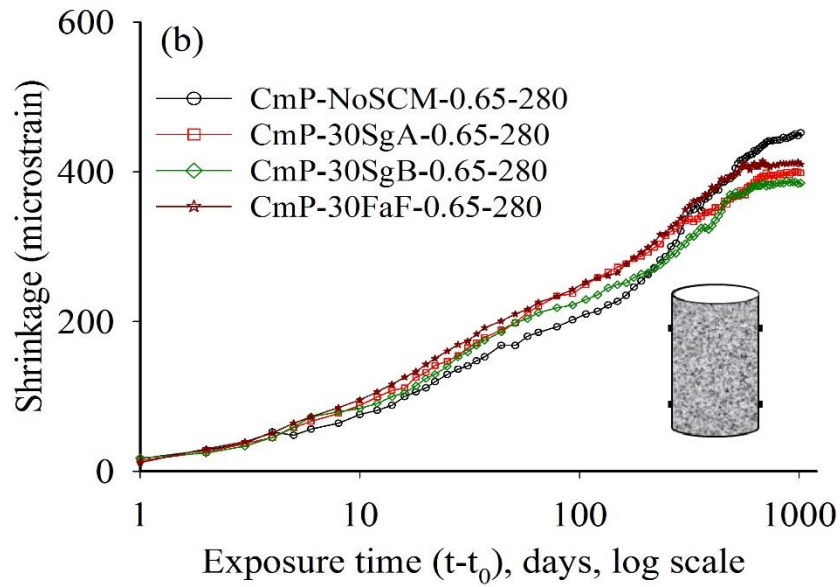
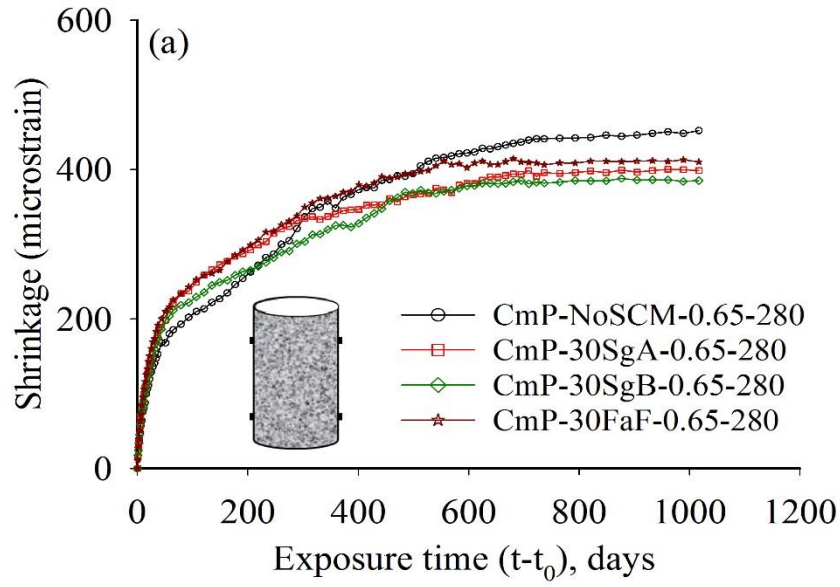


Figure 5.17 Effect of slag and fly ash on the total shrinkage strain of binary blended concrete with $w/b = 0.65$ and total binder 280 kg/m^3 content of CmP mix: in (a) normal and (b) log scales

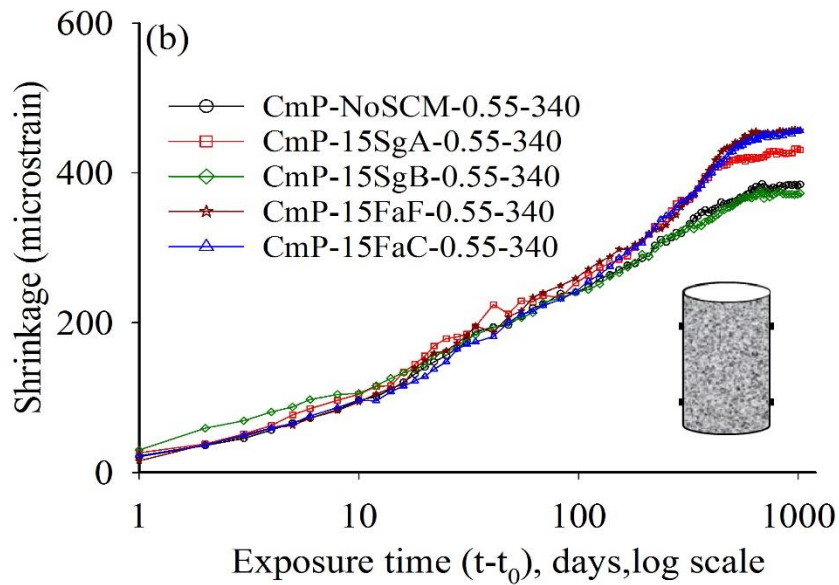
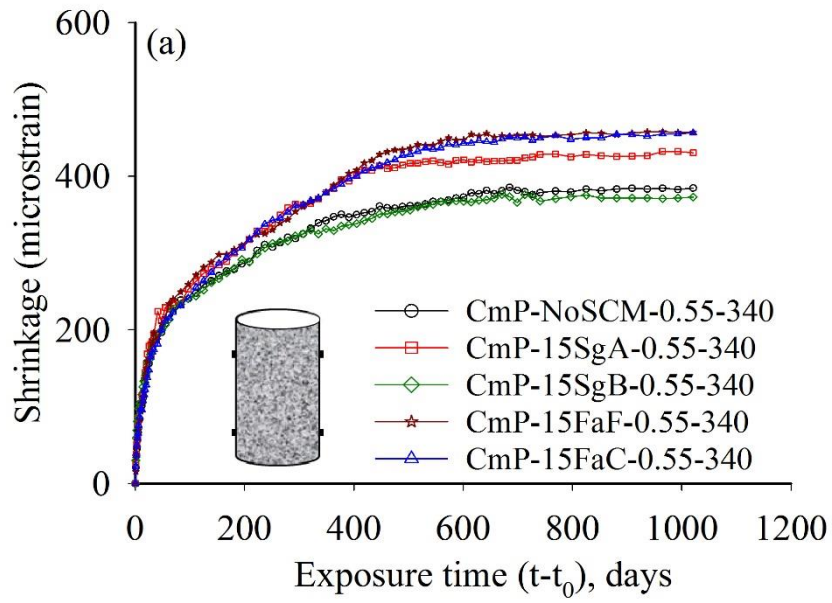


Figure 5.18 Effect of slag and fly ash on the total shrinkage strain of binary blended concrete with $w/b=0.55$ and total binder 340 kg/m^3 content of CmP mix: in (a) normal and (b) log scales

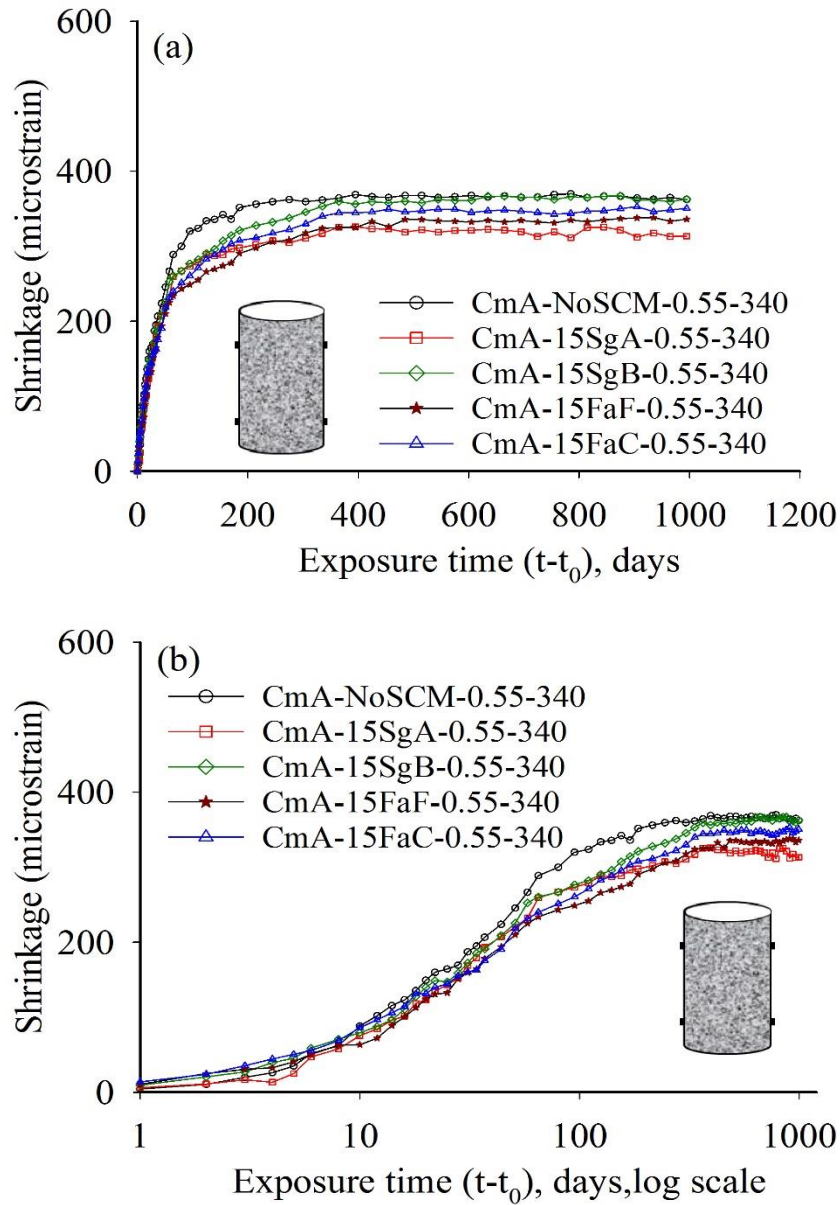


Figure 5.19 Effect of slag and fly ash on the total shrinkage strain of binary blended concrete with w/b= 0.55 and total binder 340 kg/m³ content of CmA mix: in (a) normal and (b) log scales

As illustrated in Figure 5.20 until the exposure of 50 days of drying, SgB concrete system shows comparable shrinkage strains with reference to that of NoSCM concrete. However, there was a marginal difference in strain in the case of 30% replacement of CmP with SgB. Thereafter, the shrinkage response of 30% replacement with SgB concrete exhibited higher shrinkage and attained a comparable strain with NoSCM concrete around 1000 days. However,

in the case of 50% replacement level, there was a considerable decrease of strain. As seen from Figure 5.20, the shrinkage of concrete with SgB dosage of 15% and 50% attains a maximum strain of about 400 days though there was further increase in the strain in No-SCM and 30% SgB concrete. Altogether, the shrinkage strain was reduced by using slag in the binary system compared to the mix made without slag. The influence of the incorporation of fly ash at 15%, 30%, and 50% replacement of CmP on the total shrinkage of concrete is seen in Figure 5.21. Fly ash concrete undergoes lower shrinkage than the control concrete with the same w/b and total binder content. The shrinkage was comparable for fly ash blended concrete and the concrete with control mix concrete until the exposure time of about 200 days. After this age, the rate of shrinkage decreased for the 15% and 50% fly ash blended concrete to reach values of about 50 and 70 microstrain, respectively, more than the NoSCM concrete.

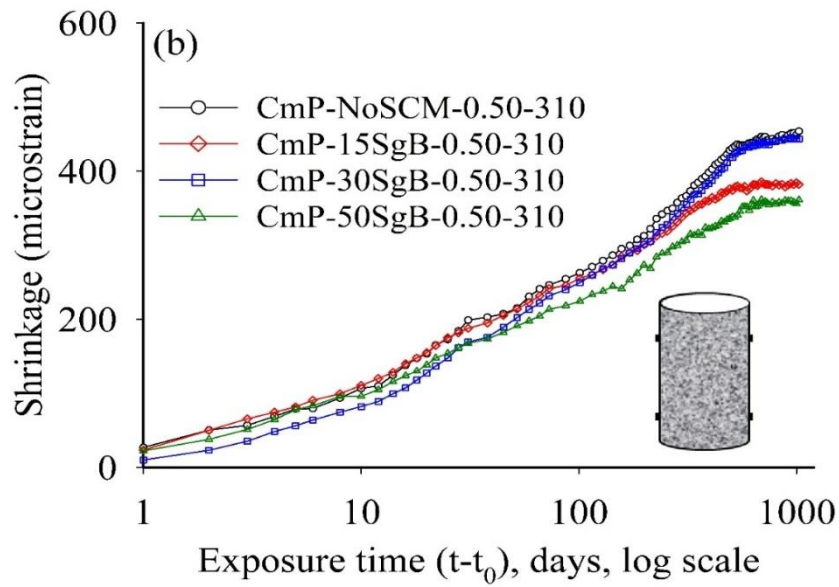
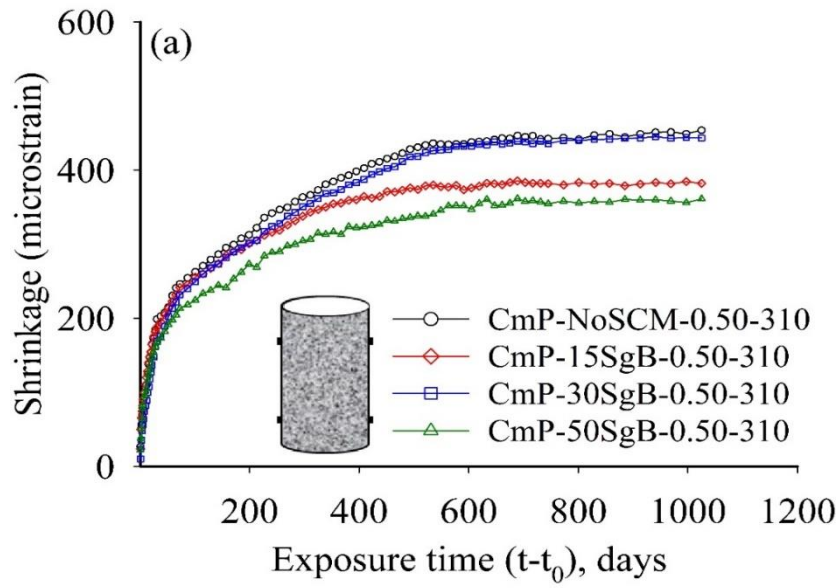


Figure 5.20 Effect of replacement level of slag on the total shrinkage strain of binary blended concrete of CmP mix: in (a) normal and (b) log scales

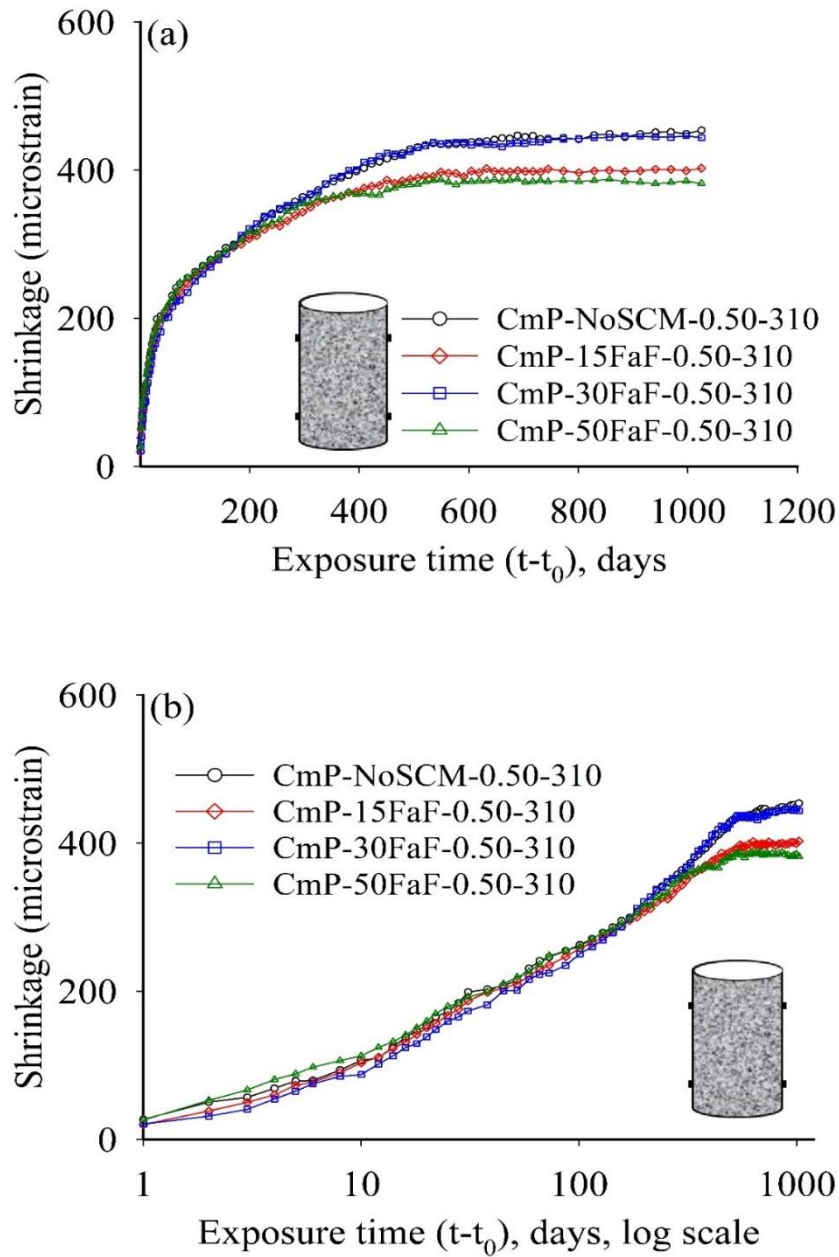


Figure 5.21 Effect of replacement level of fly ash on the total shrinkage strain of binary blended concrete of CmP mix: in (a) normal and (b) log scales

The effect of two types of fly ashes, Class F and Class C, with different CaO content, on the shrinkage were assessed in Figure 5.22 through Figure 5.24. It is noticed that the shrinkage response of concrete containing fly ashes is either higher than or equal to that of the control mix concrete. Similar behaviour has been reported by Sennour and Carrasquillo (1989), Siddique (2004), and Saha and Sarker (2017).

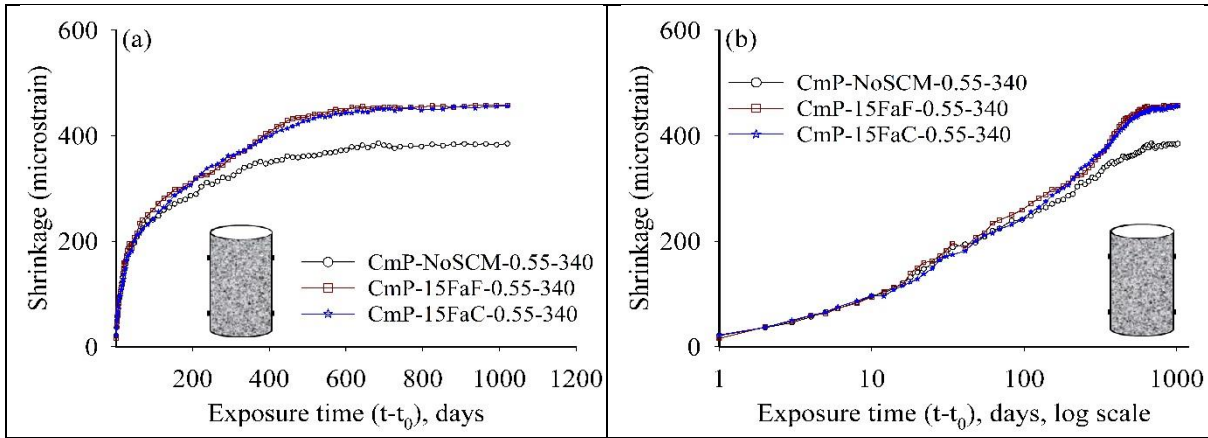


Figure 5.22 Effect of fly ash type on the total shrinkage strain of CmP mix containing 15% fly ash with w/b 0.55 and binder content of 340 kg/m^3 : in (a) normal and (b) log scales

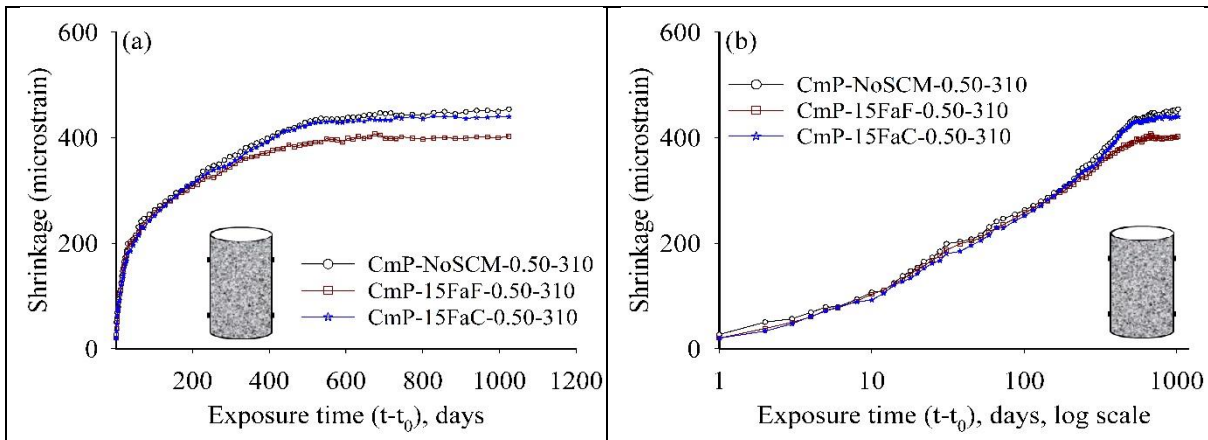


Figure 5.23 Effect of fly ash type on the total shrinkage strain of CmP mix containing 15% fly ash with w/b 0.50 and binder content of 310 kg/m^3 : in (a) normal and (b) log scales

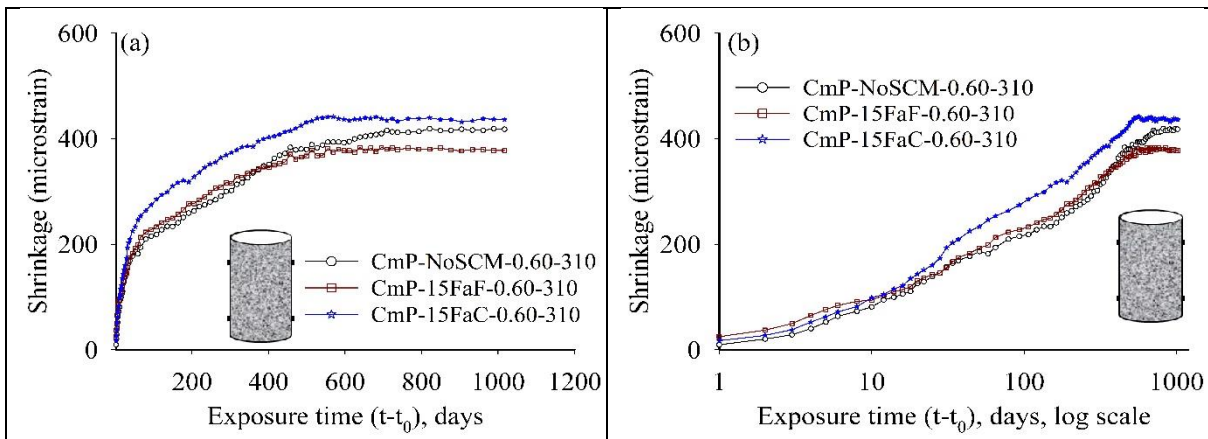


Figure 5.24 Effect of fly ash type on the total shrinkage strain of CmP mix containing 15% fly ash with w/b 0.60 and binder content of 310 kg/m^3 : in (a) normal and (b) log scales

As seen from Figure 5.25, there was substantial decrease in shrinkage in concrete with ternary blended binders in comparison with the control concrete, and also with binary blended binders. Similar conclusions were observed by Gesoğlu et al. (2009) and Guneyisi et al. (2010).

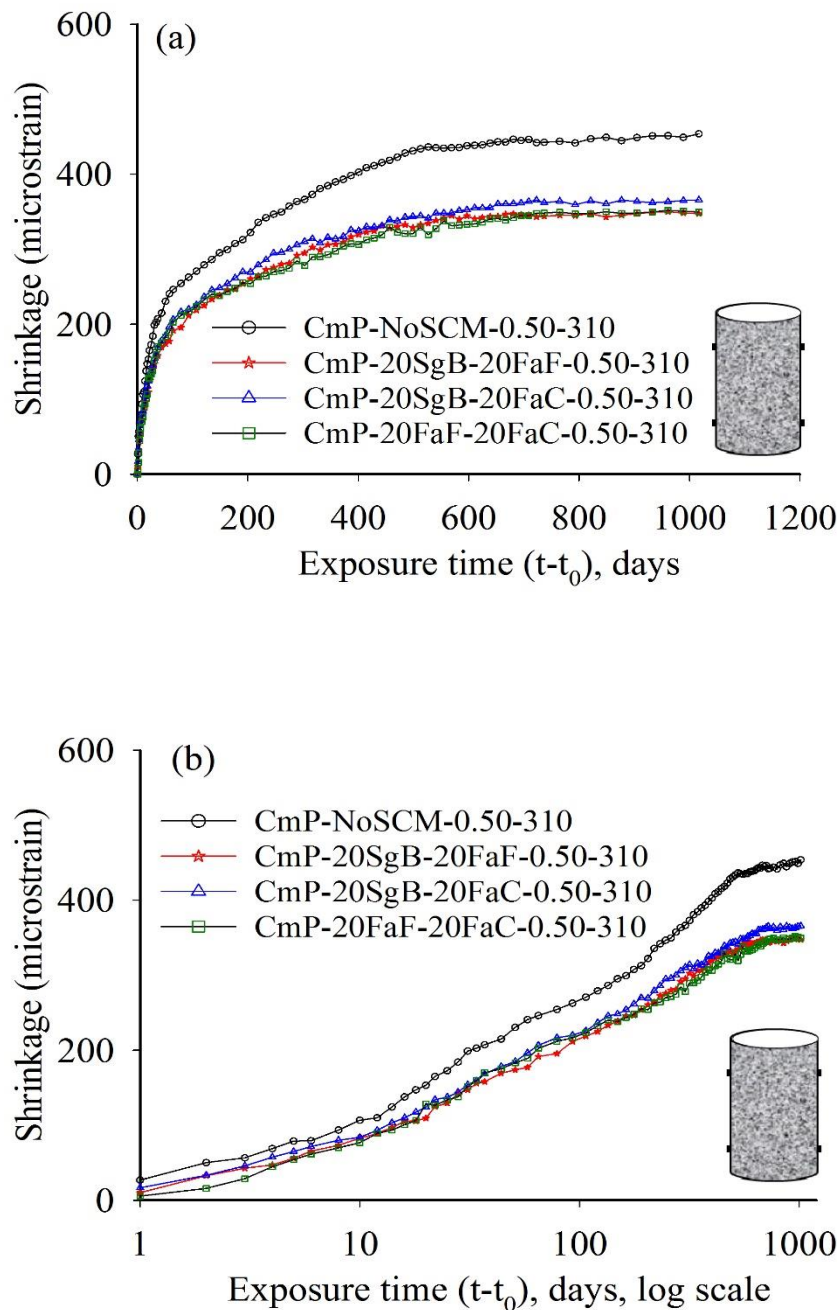


Figure 5.25 Effect of slag and fly ash on the total shrinkage strain of ternary blended concrete of CmP mix: in (a) normal and (b) log scales

As seen from Figure 5.26 and Figure 5.27, M50 grade concrete had comparatively lower shrinkage in comparison with the M30 grade concretes. As seen in Figure 5.28 (with the same binder content and w/b), the shrinkage of the different systems were comparable.

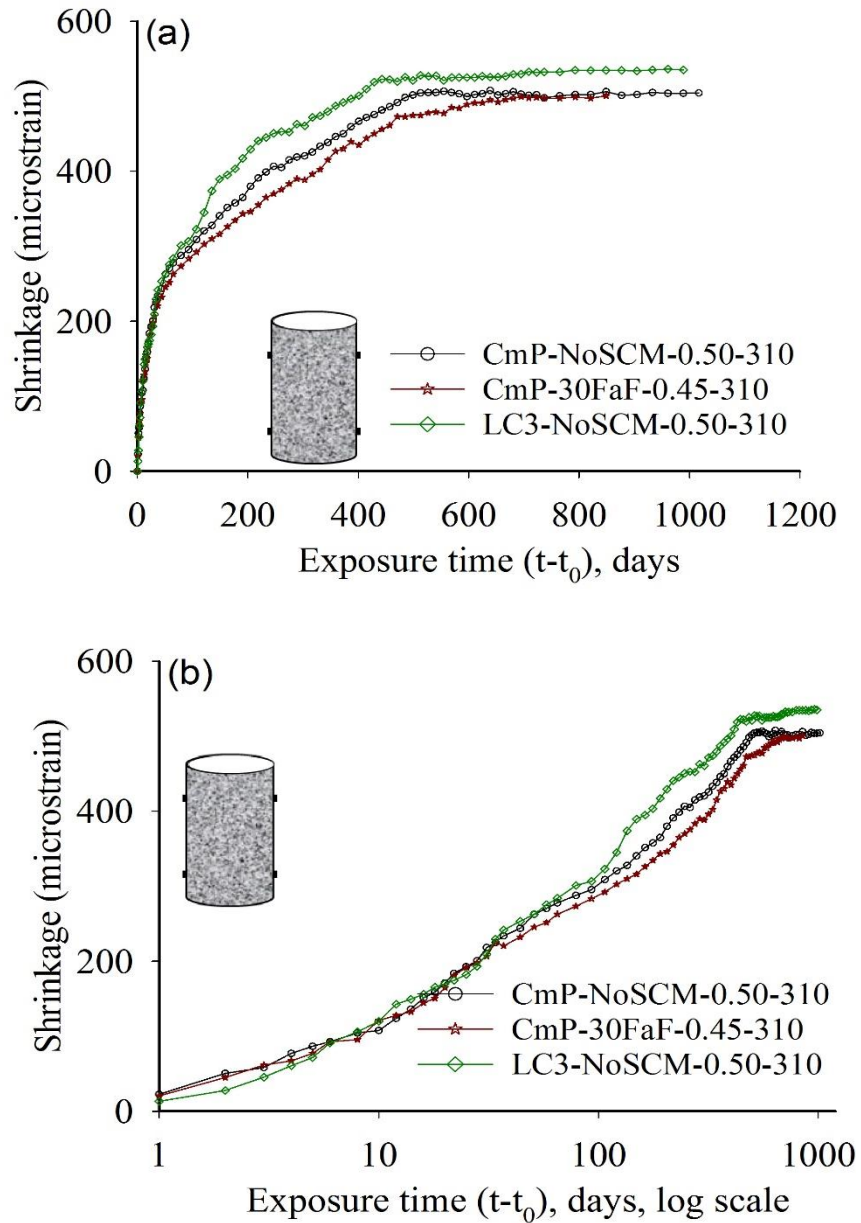


Figure 5.26 Effect of fly ash on the total shrinkage strain of concrete in comparison with CmP and LC3 binder on M30 grade of concrete: in (a) normal and (b) log scales

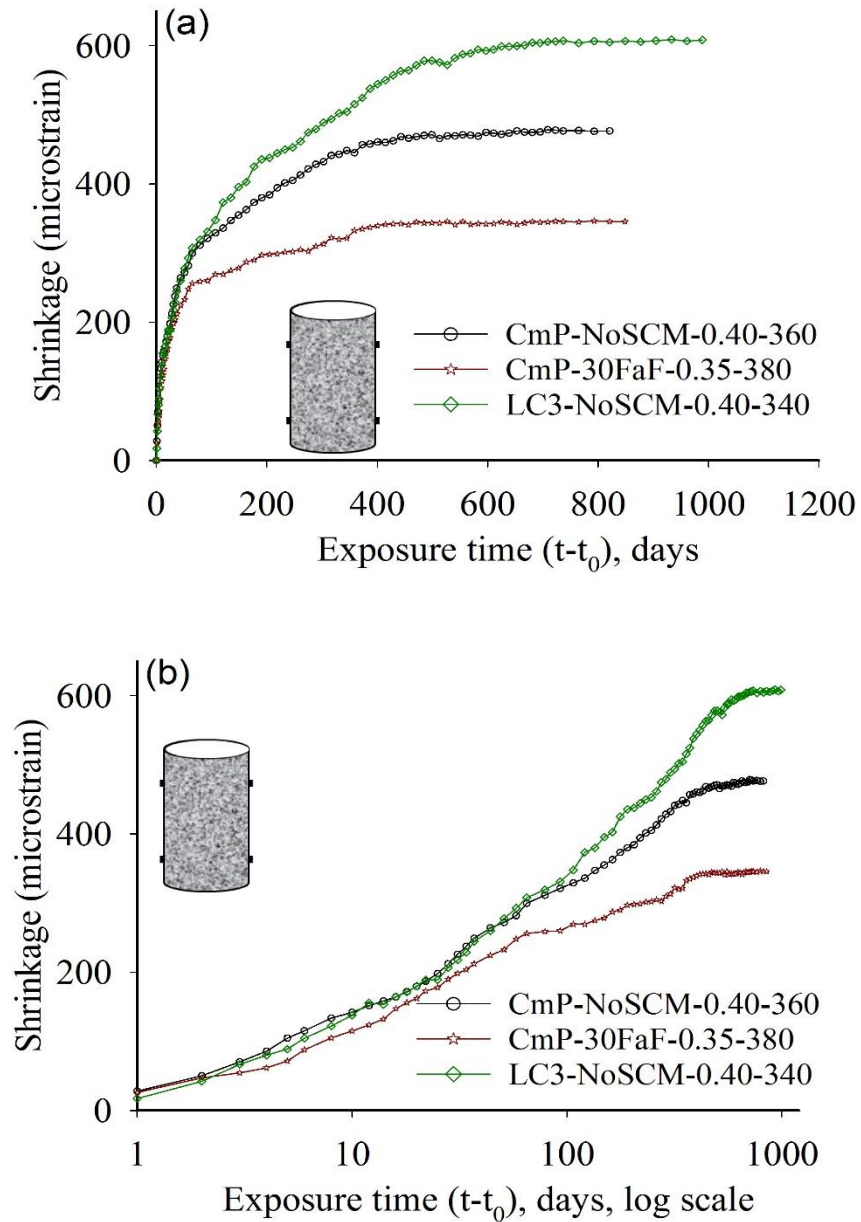


Figure 5.27 Effect of fly ash on the total shrinkage strain of concrete in comparison with CmP and LC3 binder on M50 grade of concrete: in (a) normal and (b) log scales

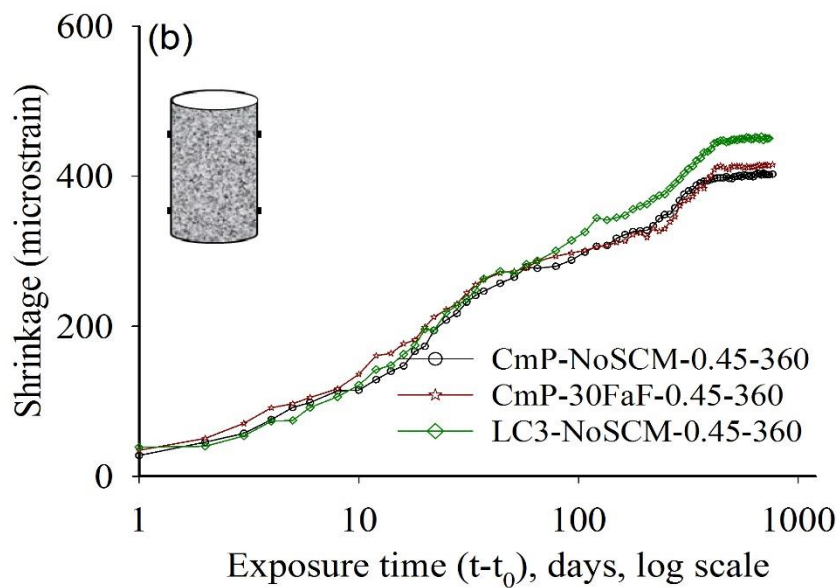
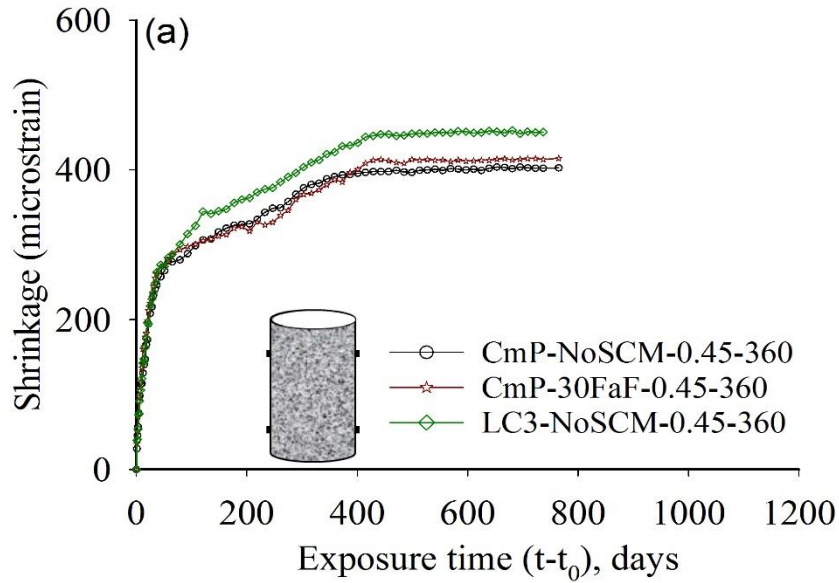


Figure 5.28 Effect of fly ash on the total shrinkage strain of concrete in comparison with CmP and LC3 binder for $w/b= 0.45$: in (a) normal and (b) log scales

Figure 5.29 through Figure 5.31 show the comparison of 28-day compressive strength with the shrinkage strain of concrete made with CmP, CmA and LC3 cements, respectively. As seen from the figures, the total shrinkage strain of concretes at 2 years made with CmP, CmA and LC3 cement was in the range of 350 to 500 microstrain, 300 to 380 microstrain and 450 to 600 microstrain, respectively. From the plots in those groups of concrete, there is not much

difference within the range of concrete considered. However, no clear trend was observed between the strength and the shrinkage strain of blended cement concrete. Table 5.1 provides the data used in the comparison of compressive strength and the shrinkage strain, along with the standard deviations. The data is grouped in terms of the cement used. The serial numbering, however, follows that of Table 3.6, Table 3.8 and Table 4.1 for facilitating cross-referencing.

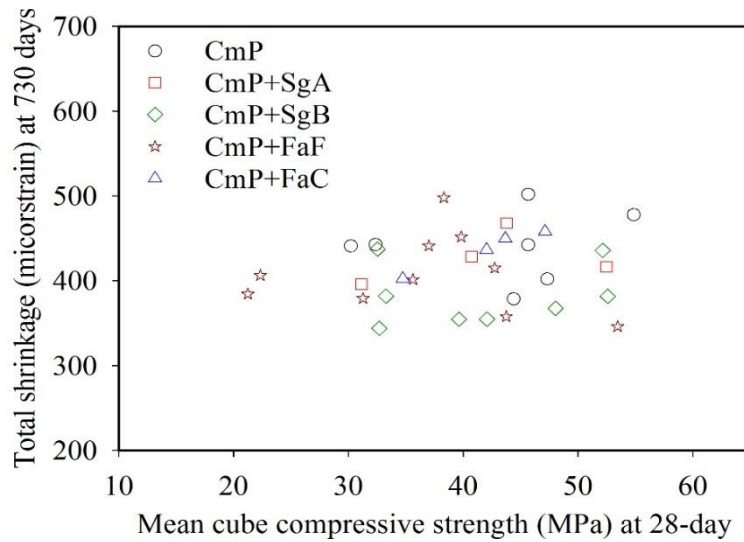


Figure 5.29 Comparison of total shrinkage versus strength of concretes made with CnP cement

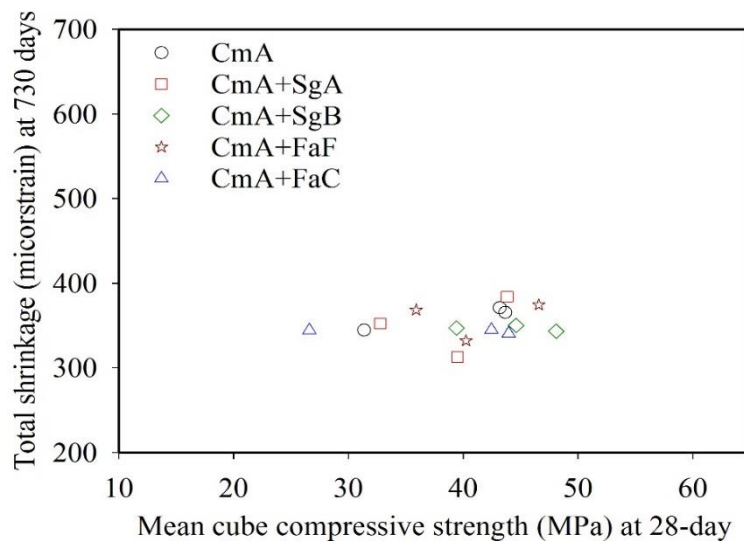


Figure 5.30 Comparison of total shrinkage versus strength of concretes made with CmA cement

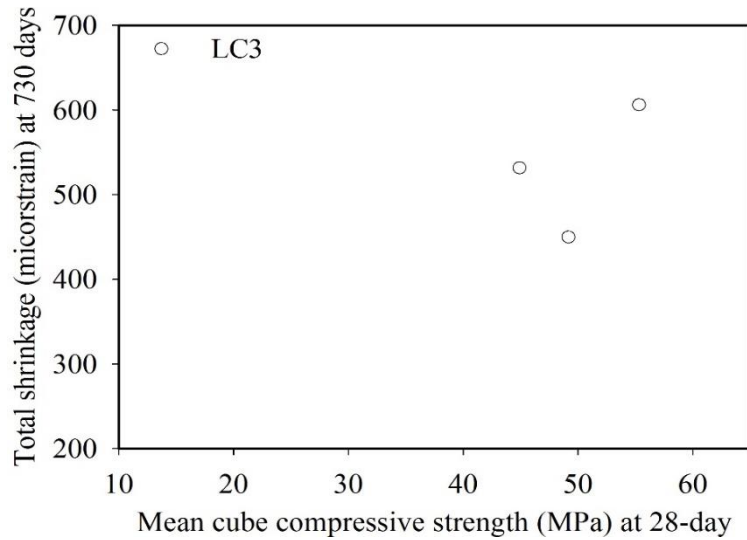


Figure 5.31 Comparison of total shrinkage versus strength of concretes made with LC3 cement

Table 5.1 Comparison of compressive strength and total shrinkage of concrete

Sl. No.	Mix Nomenclature	Total shrinkage at 730 days (microstrain)		Mean cube compressive strength at 28-day (MPa)	
		Average	Std. Dev	Average	Std. Dev
1	CmP-NoSCM-0.65-280	441	32	30.2	0.7
5	CmP-NoSCM-0.55-340	379	38	44.4	2.2
10	CmP-NoSCM-0.50-310	443	13	45.7	0.5
23	CmP-NoSCM-0.60-310	443	35	32.4	1.2
55	CmP-NoSCM-0.50-310x	502	48	46.3	0.8
58	CmP-NoSCM-0.40-360	478	22	54.9	0.2
61	CmP-NoSCM-0.45-360	402	78	47.3	2.3
2	CmP-30SgA-0.65-280	396	38	31.1	0.8
6	CmP-15SgA-0.55-340	428	25	40.7	1.2
11	CmP-15SgA-0.50-310	416	63	52.5	0.7
24	CmP-15SgA-0.60-310	468	34	43.8	0.8
3	CmP-30SgB-0.65-280	382	40	33.3	1.5
7	CmP-15SgB-0.55-340	368	29	48.1	1.0
12	CmP-15SgB-0.50-310	382	38	52.6	1.1
15	CmP-30SgB-0.50-310	436	31	52.2	0.9
18	CmP-50SgB-0.50-310	355	22	42.1	1.7
20	CmP-20SgB-20FaF-0.50-310	344	26	32.7	1.3
21	CmP-20SgB-20FaC-0.50-310	355	12	39.6	0.7
25	CmP-15SgB-0.60-310	437	74	32.5	0.5
4	CmP-30FaF-0.65-280	406	46	22.3	1.3
8	CmP-15FaF-0.55-340	452	30	39.8	1.4
13	CmP-15FaF-0.50-310	402	38	35.6	0.7

Table 5.1 (Continued) Comparison of compressive strength versus total shrinkage of concrete

Sl. No	Mix Nomenclature	Total shrinkage at 730 days (microstrain)		Mean cube compressive strength at 28-day (MPa)	
		Average	Std. Dev	Average	Std. Dev
16	CmP-30FaF-0.50-310	441	14	37.0	0.9
19	CmP-50FaF-0.50-310	384	51	21.2	1.0
22	CmP-20FaF-20FaC-0.50-310	358	47	43.7	1.7
26	CmP-15FaF-0.60-310	379	43	31.3	0.8
56	CmP-30FaF-0.45-310	498	88	38.3	1.0
59	CmP-30FaF-0.35-380	346	31	53.4	1.6
62	CmP-30FaF-0.45-360	415	38	42.7	0.2
9	CmP-15FaC-0.55-340	450	19	43.7	0.7
14	CmP-15FaC-0.50-310	437	20	42.0	1.5
17	CmP-30FaC-0.50-310	458	11	47.1	0.9
27	CmP-15FaC-0.60-310	403	72	34.7	1.1
32	CmA-NoSCM-0.55-340	366	18	43.7	0.6
37	CmA-NoSCM-0.50-310	371	26	43.2	1.3
50	CmA-NoSCM-0.60-310	345	25	31.4	1.2
33	CmA-15SgA-0.55-340	313	41	39.5	1.5
38	CmA-15SgA-0.50-310	384	22	43.8	0.4
51	CmA-15SgA-0.60-310	352	23	32.8	2.4
34	CmA-15SgB-0.55-340	350	28	44.6	1.4
39	CmA-15SgB-0.50-310	343	33	48.1	1.8
52	CmA-15SgB-0.60-310	347	80	39.4	1.2
35	CmA-15FaF-0.55-340	332	49	40.2	2.3
40	CmA-15FaF-0.50-310	374	18	46.6	2.7
53	CmA-15FaF-0.60-310	368	18	35.9	1.2
36	CmA-15FaC-0.55-340	345	56	42.5	2.0
41	CmA-15FaC-0.50-310	341	19	44.0	1.2
54	CmA-15FaC-0.60-310	344	13	27.0	1.6
57	LC3-NoSCM-0.50-310	532	50	44.9	0.2
60	LC3-NoSCM-0.40-340	606	76	55.3	1.3
63	LC3-NoSCM-0.45-360	450	43	49.2	1.6

5.2.1 Effect of specimen size on shrinkage of concrete

Shape and size of the specimen impact the rate of moisture loss and degree of overall restraint provided by the core, which will have a higher moisture content than the surface. Generally, there is lower shrinkage in large specimens due to the fact that only the outer portion is drying and the shrinkage is restrained by the non-shrinking core. The amount and the rate of drying,

and the tendency for the surface zone to crack are therefore affected by the geometry of the specimen. Studies by Almudaiheem and Hansen (1987), and Omar et al. (2008) confirm that the shrinkage strain increases with a decrease in the size of the member. Figure 5.32 shows the comparison between the measured shrinkage strains of cylindrical and prismatic specimens up to 1000 days. It can be seen that the long-term strains in several cases are comparable through there are many cases that show higher strains in the prismatic specimens than in the cylinders, as expected due to the higher surface area to volume ratio. In general, no trend could be identified to relate the shape effect with the binder system. However, many models consider the surface area to volume ratio in the simulation, which could be used to relate the shrinkage strains with the ease of diffusion that depends on the binder characteristics.

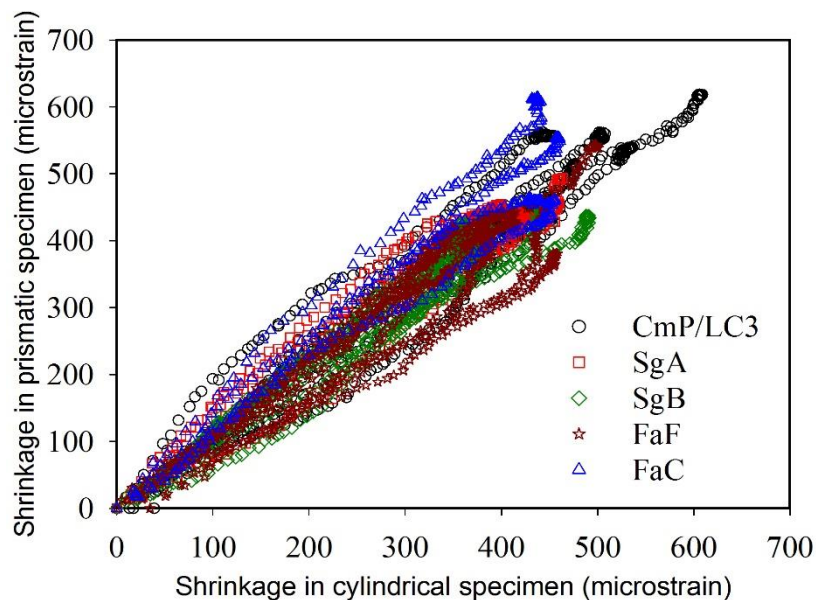


Figure 5.32 Effect of specimen size on shrinkage strains of concrete

5.3 RELATION OF MASS LOSS AND SHRINKAGE STRAIN OF CONCRETE

The results of mass loss due to drying for different concrete mixes are shown in Figure 5.33. It is clear that the concrete mixtures with high water to binder ratio (w/b of 0.65) exhibit higher mass loss. Similar to the drying shrinkage results of concrete, the inclusion of SCMs in the concrete decreases considerably the mass loss for all the water-binder ratios. It seems that the mass loss of SCM concrete also slows down earlier than that of the control mix concrete. Overall, this tendency conforms to the characteristics of SCM blended concrete with lower porosity and fine pores, along with more drying by self-desiccation than by diffusion.

Figure 5.33 presents the mass loss over time for all the specimens. As expected, the plots show that all the mixes suffer higher mass loss at early ages of exposure. It was observed that the initial moisture content had an overall effect on the drying process. At the beginning of the drying period, the specimens are in moist conditions and thus, the supersaturated surface that is exposed to the environment starts drying. As the surface water dries, water diffuses from the core to the surface. Hence the rate of drying is reduced. After about 800 days of drying, it can be seen that there is a stabilization of mass loss in all the concrete systems. Figure 5.34 shows the mass loss in the sealed specimens, which indicates that the sealing system is good but not perfect. This could also explain the significant shrinkage strains recorded on the sealed specimens, especially some of the prisms, even at later ages.

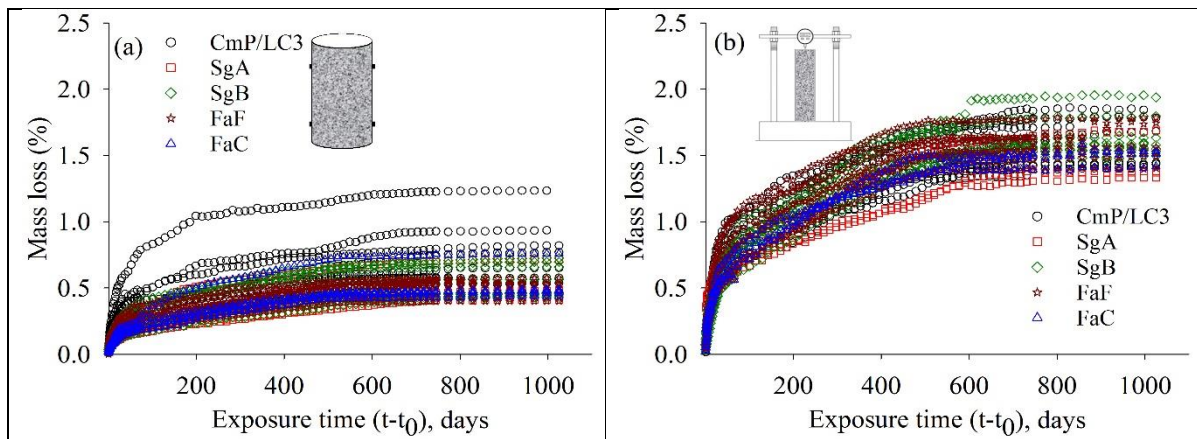


Figure 5.33 Mass loss of concrete in unsealed (a) cylindrical specimens and (b) prismatic specimens

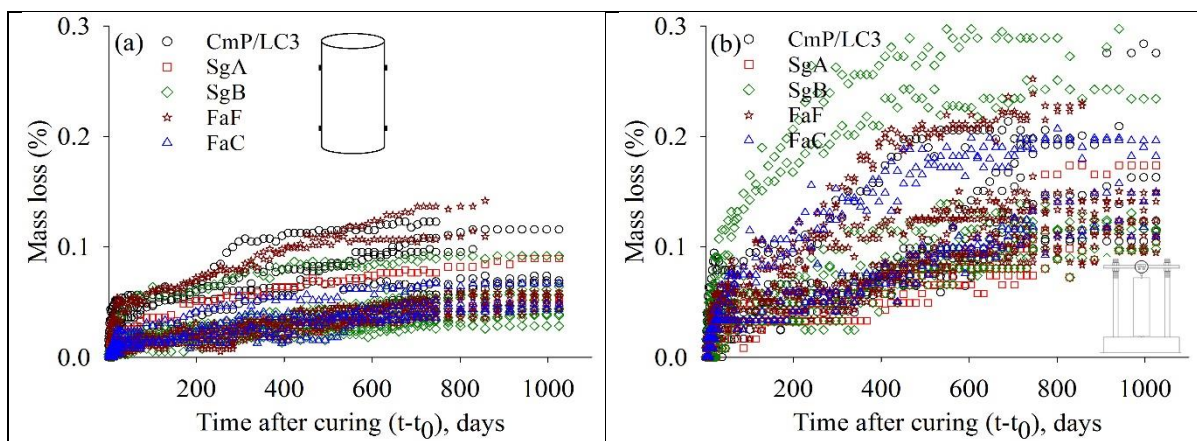
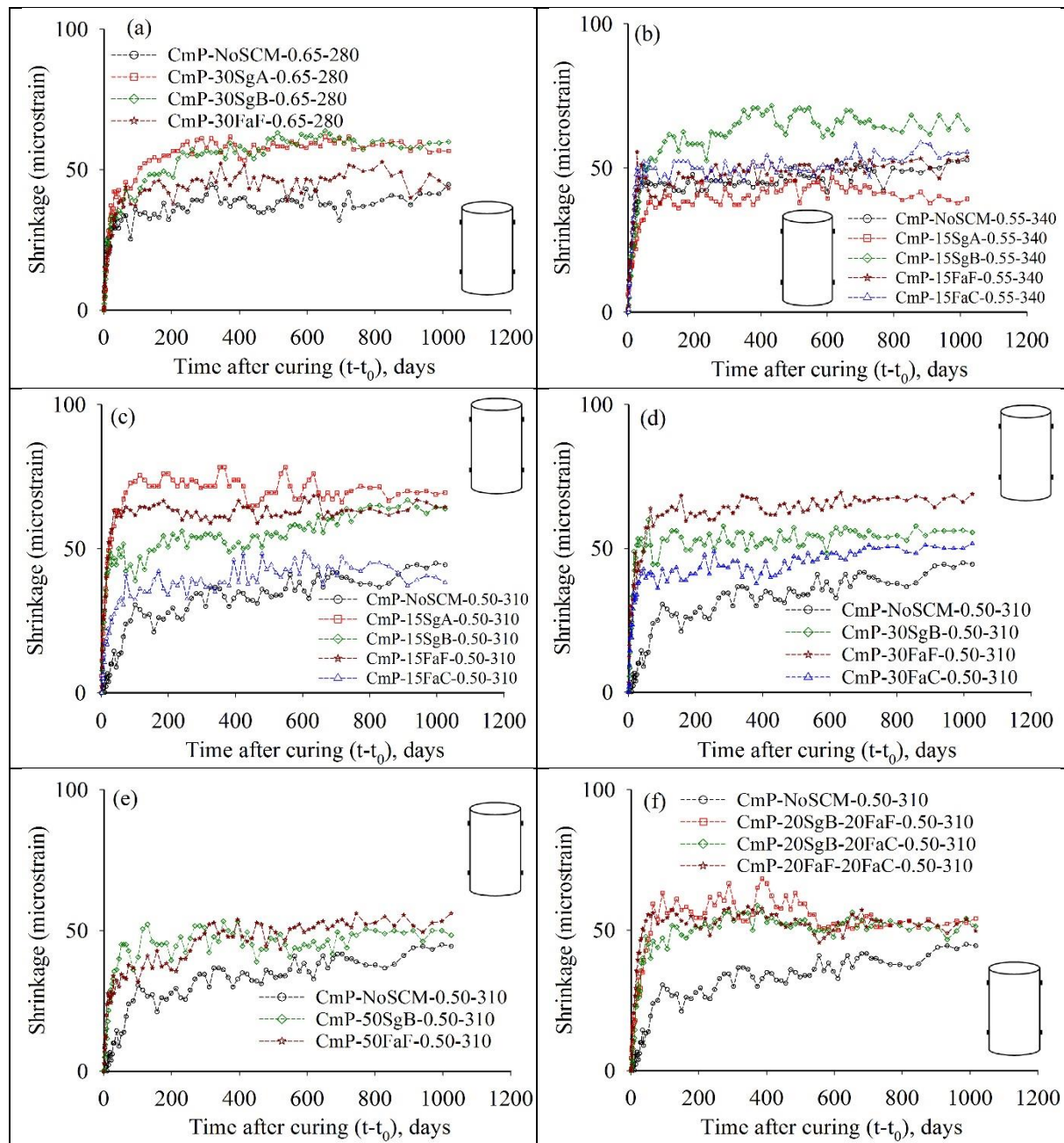


Figure 5.34 Mass loss of concrete in sealed (a) cylindrical specimens and (b) prismatic specimens

5.4 INCREASE IN AUTOGENOUS SHRINKAGE OF CONCRETE

The measurements of autogenous or basic shrinkage of concrete mixes on cylindrical and prismatic specimens are presented in Figure 5.35 and Figure 5.36. It is clear that the autogenous shrinkage increases by about 30 to 60 microstrain after the curing period, in most of the concrete mixes considered.



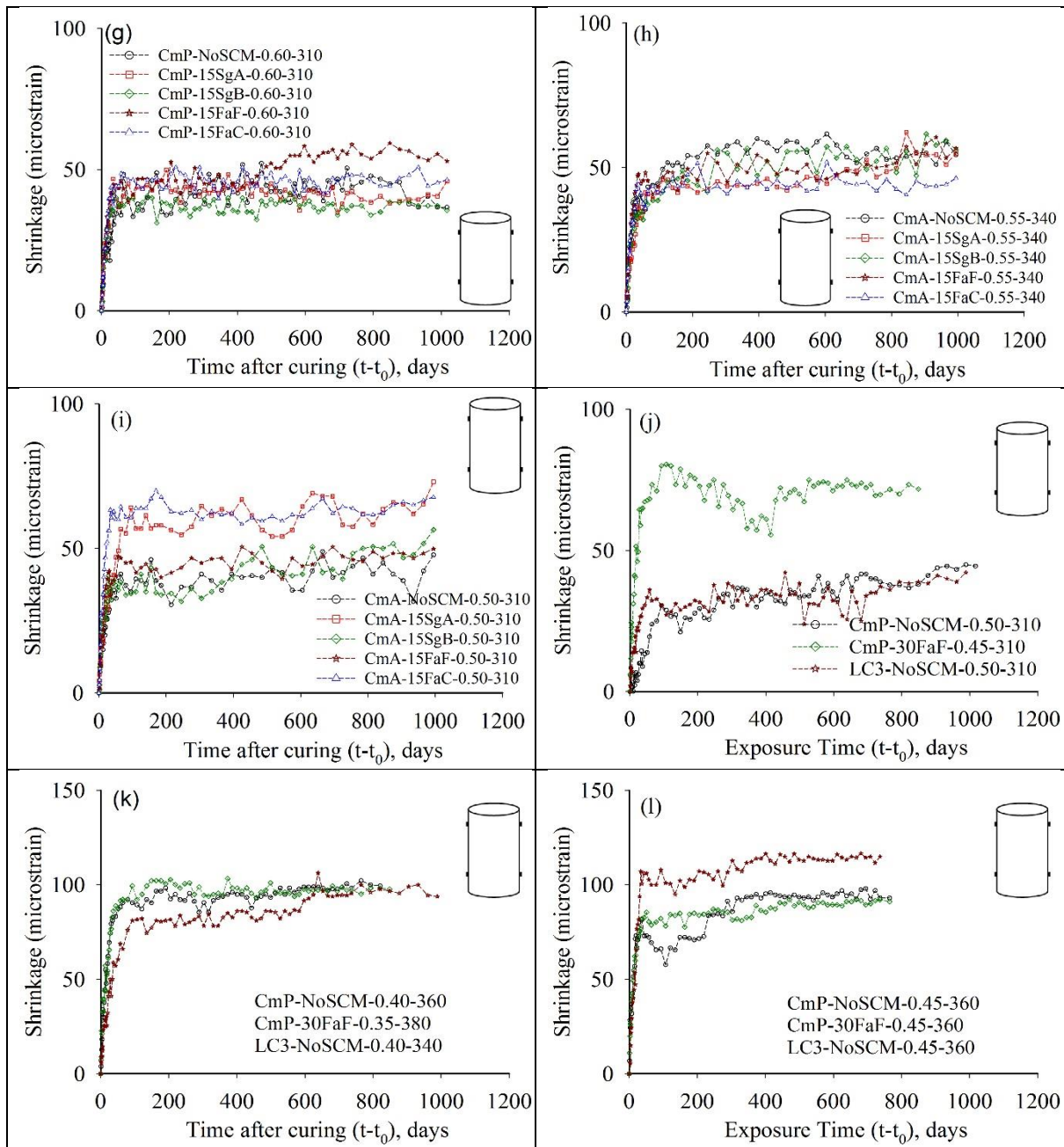
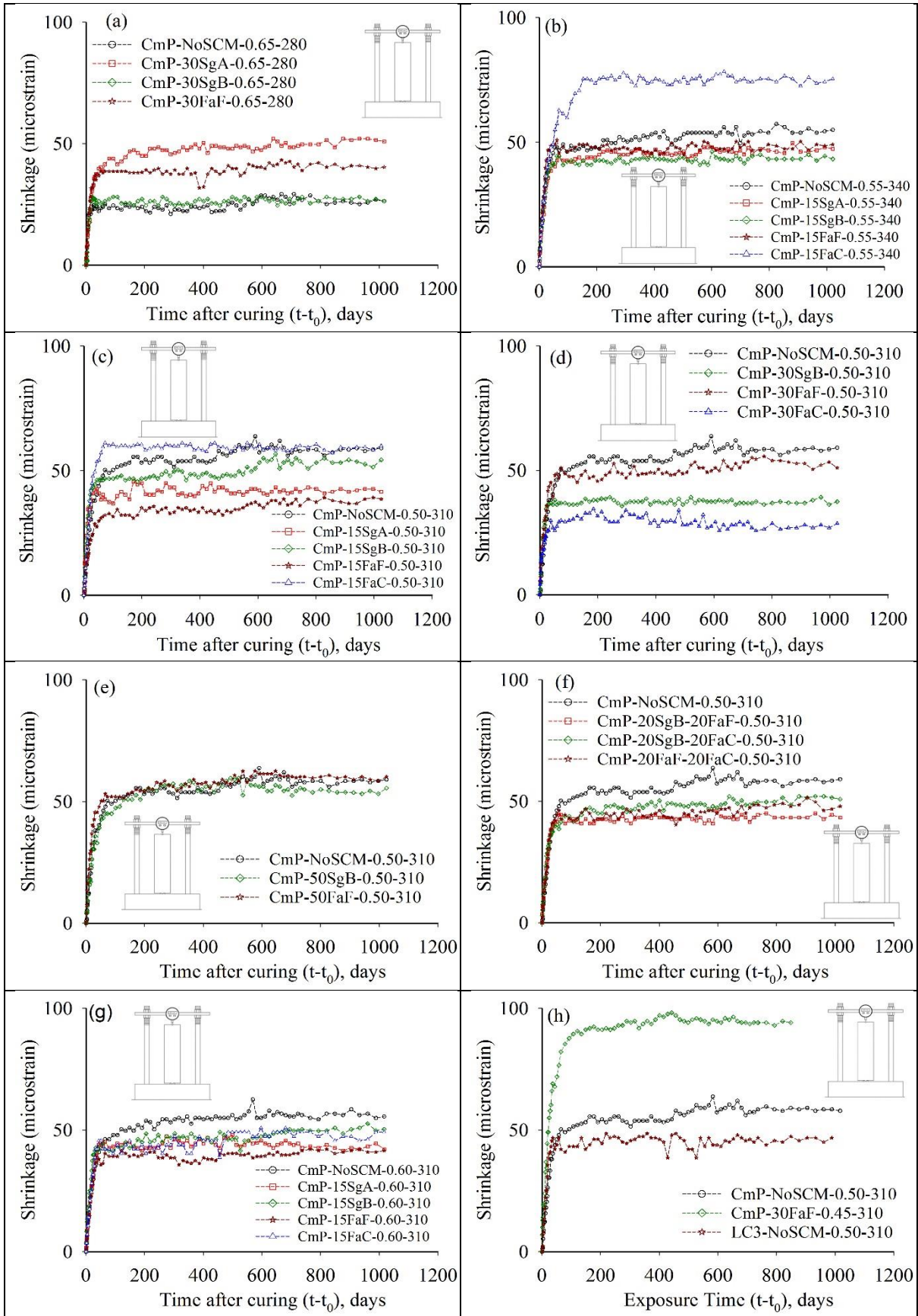


Figure 5.35 Measured autogenous shrinkage of concrete on cylindrical specimens



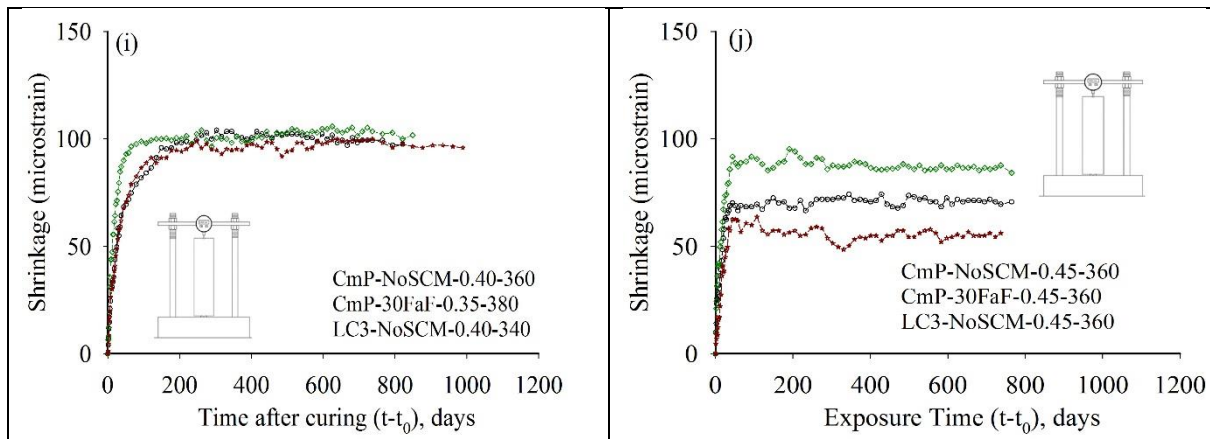


Figure 5.36 Measured autogenous shrinkage of concrete on prismatic specimens

However, some mixes as seen in Figure 5.35 (j, k, and l) and Figure 5.36 (h, i, and j) exhibit higher autogenous shrinkage strains of about 100 microstrain. This could be attributed to the lower water-binder ratio in these particular concrete mixes. The results from the present study confirms the conclusions of earlier work, such as Lura et al. (2003), that the autogenous shrinkage is found to increase with a decrease in the water to binder ratio (≤ 0.40). However, the trends indicate a high initial strain occurring over the first few days of measurement that seems abnormal. This could reflect some moisture loss through the sealing systems used or the loss of mass of the sealing system itself. This would need further assessment for conclusions to be made based on these data sets.

5.5 SUMMARY

The results indicate that, in general, the incorporation of SCMs in concrete does not significantly change the shrinkage response of concrete. Also, Class F and Class C fly ash show almost comparable shrinkage strains. Higher the amount of replacement of cement by fly ash or slag, lower is the shrinkage strain in concrete. Ternary blended concrete systems experience slightly lower shrinkage strains in comparison with the binary blends. The autogenous shrinkage response of normal strength concrete (for w/b above 0.45) is considered to be small in the contribution of the total shrinkage strain of concrete beyond the curing period of 28 days, as expected.

6. APPLICATION OF SHRINKAGE PREDICTION MODELS

6.1 INTRODUCTION

Shrinkage is an important factor that influences the long-term behaviour of concrete. Accordingly, an accurate prediction for the shrinkage is important to ensure a safe and durable design. Most shrinkage prediction models are derived from the statistical analysis of laboratory data pertaining to conventional concrete systems. As a result, the applicability of these prediction models to a blended cement concrete needs to be assessed. Also, there may be a need to modify the existing models based on recent data sets, related to SCM blended concrete.

A detailed description of several models was given in Section 2.4. In order to evaluate the applicability of these models, a comparison of the measured shrinkage results is done with the models of IS 1343, *fib* MC 2010, RILEM B4s, ACI 209 and RILEM B4 in this chapter. Since there were variations in the environmental conditions and the time of measurement during the first day, the comparison is made only from the first day of drying onwards.

Some input values for the calculations are mentioned in Table 6.1, which are common for all types of concrete.

Table 6.1 Input values for shrinkage prediction calculation

Relative humidity	65%
Temperature	25°C
Volume/Surface ratio, v/s	37.5 mm
Surface-volume parameter, h_0	75 mm
Curing period	28 days
Age at exposure	28 days
Cement type	OPC 53 grade cement (taken to be similar to ASTM Type I cement)

Table 6.2 gives the input parameters considered for the prediction using the different shrinkage prediction models.

Table 6.2 Parameters considered by the shrinkage prediction models

Input parameters	Units	ACI 209	B4	B4s	fib MC 2010	IS 1343
Cement content (c)	kg/m ³	✓	✓			
Water to cement ratio (w/c)	-		✓			
Aggregate to cement ratio (a/c)	-		✓			
Cement type	-	✓	✓		✓	✓
Density of concrete	kg/m ³	✓	✓			
Fine aggregate content (ψ)	kg/m ³	✓				
Slump (s)	mm	✓				
Air content (α)	%	✓				
Relative humidity (h, RH)	decimal	✓	✓	✓	✓	✓
Temperature (T)	°C	✓	✓	✓	✓	✓
Volume-surface area (v/s)	mm	✓	✓			
Cross sectional area to perimeter (A_c/u)	mm				✓	✓
Age of concrete (t)	days	✓	✓	✓	✓	✓
Curing time (t_c, t_0 or t_s)	days	✓	✓	✓	✓	✓
Mean cube compressive strength (f_{ck})	MPa					✓
Mean cylinder compressive strength (f_{cm} or \bar{f}_c)	MPa		✓	✓	✓	
Specimen geometry	mm		✓	✓		

✓	Considered for the calculation of shrinkage prediction
	Not considered for the calculation of shrinkage prediction

6.2 STRENGTH-BASED SHRINKAGE PREDICTION MODELS

The shrinkage prediction models that consider compressive strength of concrete as the primary factor affecting the shrinkage are denoted as strength-based prediction models. It has been observed in the previous chapter that there is no trend observed between the long-term shrinkage and the 28-day compressive strength. Nevertheless, the applicability of the IS 1343, *fib* MC 2010, and B4s models that fall under this category are assessed by examining the errors in the estimation.

6.2.1 IS 1343, 2012

The IS 1343 standard considers the characteristic compressive strength (f_{ck}) for the prediction of the shrinkage strain, which is calculated as $\sigma_{characteristic} = \sigma_{mean} - ks$, where σ_{mean} is the mean cube compressive strength, as given in Table 4.1 of Chapter 4, “ k ” is taken as 1.65 and “ s ” is the standard deviation, taken as 1.12 from the measured cube compressive strength data in this study. The code provides the parameters and the co-efficient values only for some grades of concrete, so values for other grades have been calculated by interpolation or extrapolation.

A comparison of the measured shrinkage of concrete with the IS 1343 prediction models is given in Figure 6.1 through Figure 6.5 for the concrete with CmA cement, 340 kg/m³ binder content and w/b = 0.55. It appears that the prediction is good with a slight conservative trend, as expected in an equation meant for design purposes. The predictions for other concretes are given in Appendix D1.

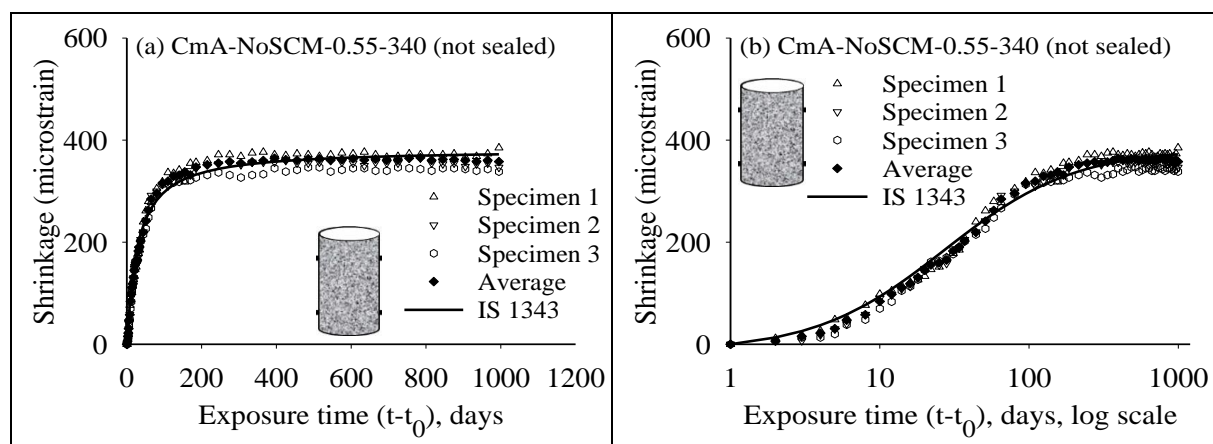


Figure 6.1 Comparison of experimental results and IS 1343 prediction for CmA-NoSCM-0.55-340 concrete (unsealed): in (a) normal and (b) log scales

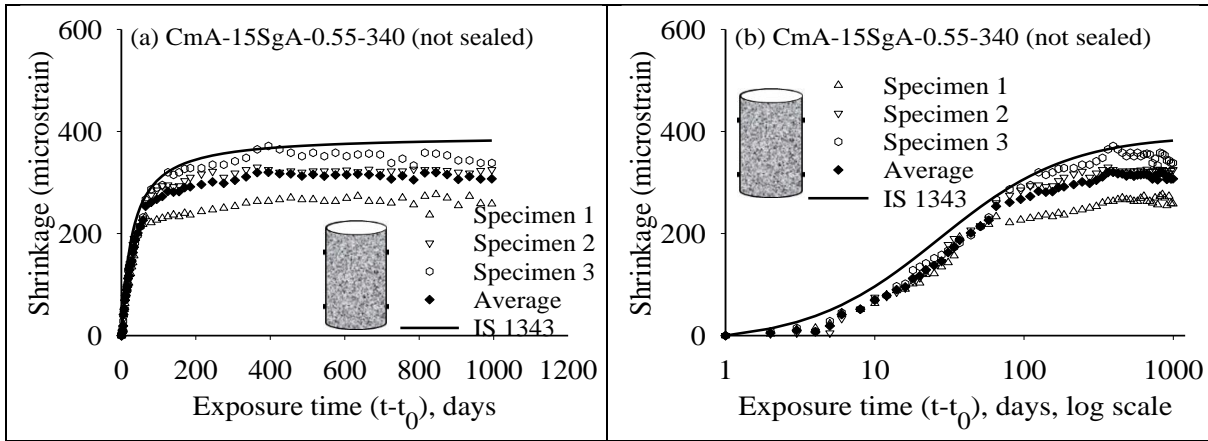


Figure 6.2 Comparison of experimental results and IS 1343 prediction for CmA-15SgA-0.55-340 concrete (unsealed): in (a) normal and (b) log scales

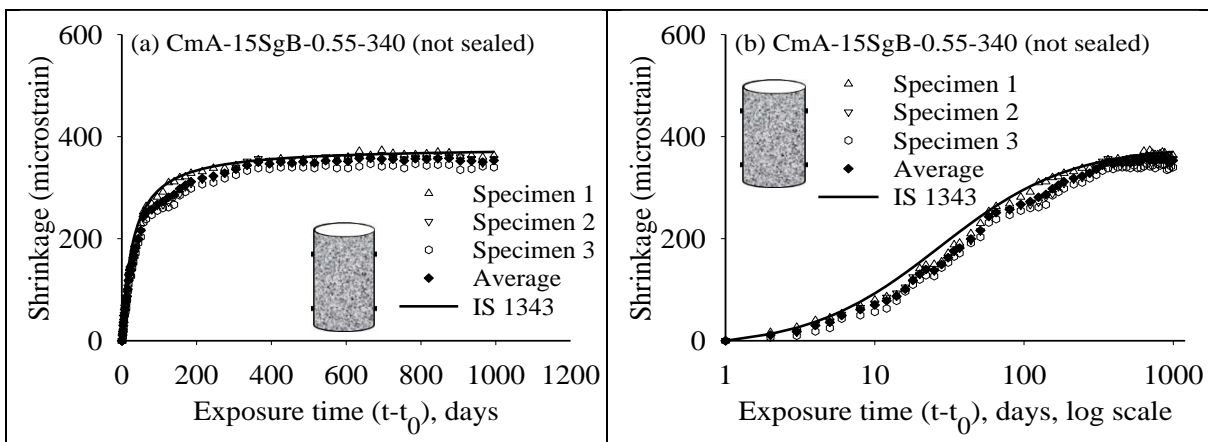


Figure 6.3 Comparison of experimental results and IS 1343 prediction for CmA-15SgB-0.55-340 concrete (unsealed): in (a) normal and (b) log scales

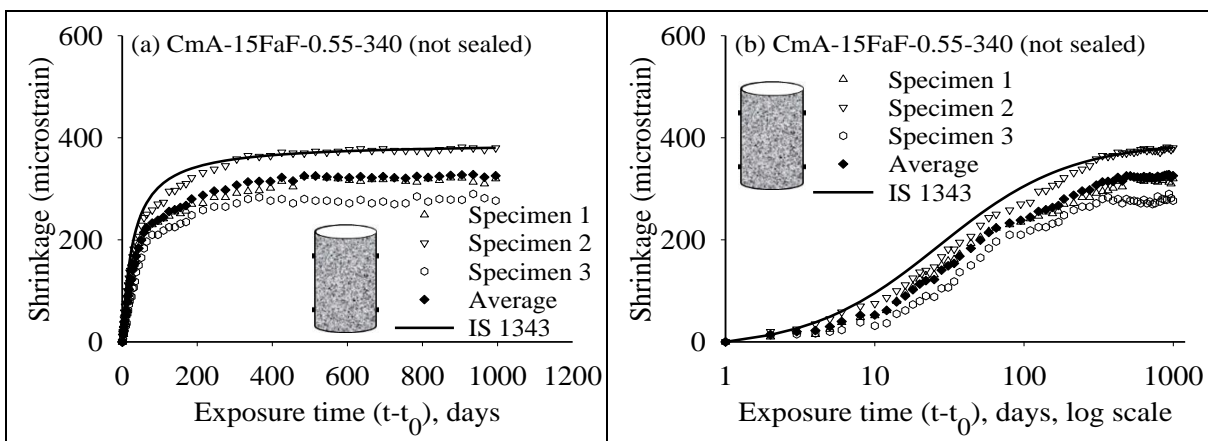


Figure 6.4 Comparison of experimental results and IS 1343 prediction for CmA-15FaF-0.55-340 concrete (unsealed): in (a) normal and (b) log scales

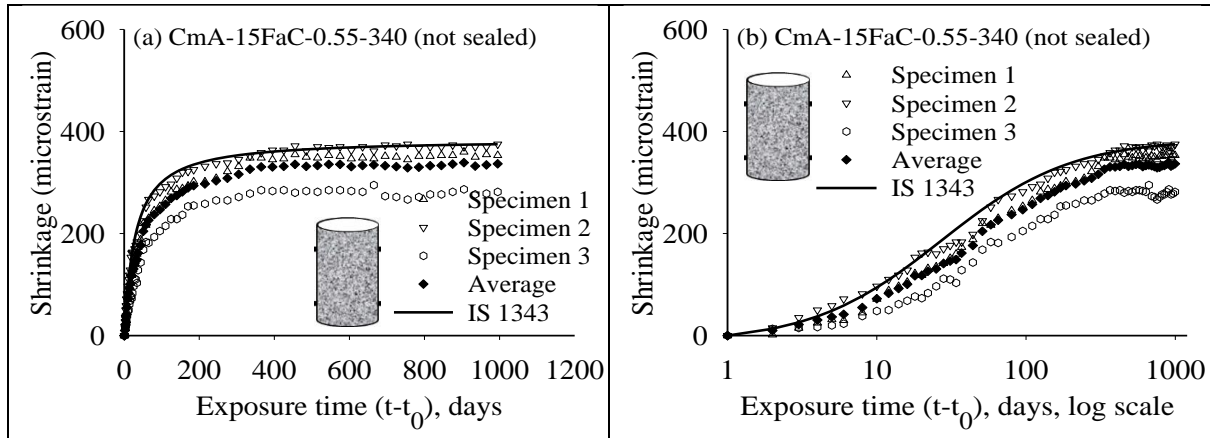


Figure 6.5 Comparison of experimental results and IS 1343 prediction for CmA-15FaC-0.55-340 concrete (unsealed): in (a) normal and (b) log scales

Table 6.3 shows that the difference between the experimental values and the predictions after the drying period of 90, 365, 730 and 1000 days is generally small, indicating reasonable predictions by this model, with the LC3 concretes being notable exceptions.

Table 6.3 Error in the prediction of total shrinkage by IS 1343 prediction model.

Sl. No.	Mix Nomenclature	Error (in microstrain) after different drying periods (days)			
		90	365	730	1000
1	CmP-NoSCM-0.65-280	131	55	-24	-31
2	CmP-30SgA-0.65-280	86	58	22	18
3	CmP-30SgB-0.65-280	101	72	28	30
4	CmP-30FaF-0.65-280	100	51	22	25
5	CmP-NoSCM-0.55-340	66	28	12	7
6	CmP-15SgA-0.55-340	79	4	-23	-25
7	CmP-15SgB-0.55-340	70	46	14	19
8	CmP-15FaF-0.55-340	59	-8	-61	-60
9	CmP-15FaC-0.55-340	76	-5	-56	-62
10	CmP-NoSCM-0.50-310	57	-11	-51	-59
11	CmP-15SgA-0.50-310	53	6	-55	-49
12	CmP-15SgB-0.50-310	42	3	-11	-8
13	CmP-15FaF-0.50-310	78	13	-31	-28
14	CmP-15FaC-0.50-310	62	15	-5	-6
15	CmP-30SgB-0.50-310	35	-28	-81	-81
16	CmP-30FaF-0.50-310	84	-1	-33	-35
17	CmP-30FaC-0.50-310	26	-36	-81	-73
18	CmP-50SgB-0.50-310	88	68	37	37
19	CmP-50FaF-0.50-310	91	67	61	70
20	CmP-20SgB-20FaF-0.50-310	117	84	61	61
21	CmP-20SgB-20FaC-0.50-310	89	67	29	33

Table 6.3 (continued) Error in the prediction of total shrinkage by IS 1343 prediction model

Sl. No.	Mix Nomenclature	Error (microstrain) after different drying periods (days)			
		90	365	730	1000
22	CmP-20FaF-20FaC-0.50-310	75	63	26	28
23	CmP-NoSCM-0.60-310	103	56	-8	-9
24	CmP-15SgA-0.60-310	55	-44	-70	-67
25	CmP-15SgB-0.60-310	57	-16	-73	-72
26	CmP-15FaF-0.60-310	116	101	60	68
27	CmP-15FaC-0.60-310	52	8	-31	-25
32	CmA-NoSCM-0.55-340	-21	-4	8	14
33	CmA-15SgA-0.55-340	36	46	72	75
34	CmA-15SgB-0.55-340	26	4	11	17
35	CmA-15FaF-0.55-340	63	49	55	55
36	CmA-15FaC-0.55-340	51	28	40	38
37	CmA-NoSCM-0.50-310	26	6	6	5
38	CmA-15SgA-0.50-310	40	10	8	4
39	CmA-15SgB-0.50-310	37	38	22	21
40	CmA-15FaF-0.50-310	28	1	-4	-1
41	CmA-15FaC-0.50-310	32	22	33	22
50	CmA-NoSCM-0.60-310	62	41	42	45
51	CmA-15SgA-0.60-310	16	42	53	60
52	CmA-15SgB-0.60-310	59	55	49	54
53	CmA-15FaF-0.60-310	45	23	27	28
54	CmA-15FaC-0.60-310	83	64	78	75
55	CmP-NoSCM-0.50-310x	17	-75	-111	-114
56	CmP-30FaF-0.45-310	34	-36	-122	N.A
57	LC3-NoSCM-0.50-310	9	-140	-177	
58	CmP-NoSCM-0.40-360	5	-82	-80	
59	CmP-30FaF-0.35-380	70	49	61	
60	LC3-NoSCM-0.40-340	-76	-250	-279	
61	CmP-NoSCM-0.45-360	13	-72	-68	
62	CmP-30FaF-0.45-360	22	43	38	
63	LC3-NoSCM-0.45-360	11	-34	-32	

6.2.2 *fib* Model Code 2010

The *fib* MC 2010 considers the 28-day mean compressive strength of cylinders in the prediction of shrinkage. For this, the mean cube compressive strength given in Table 4.1 has been converted to mean cylinder compressive strength by a factor of 1.21, which was taken from the average ratio of cylinder to cube mean compressive strengths obtained experimentally.

Figure 6.6 through Figure 6.10 show the experimental results along with the *fib* MC 2010 prediction model for different CmA concretes, where there is significant over-estimation, especially for the CmA concrete mixes with water binder ratio of 0.55 and total binder content of 340 kg/m^3 . It appears that the half-time shrinkage strain from experimental values is around 200 days, whereas the model seems to predict this as about 800 days. Appendix D2 provides the comparison of all the shrinkage data with the *fib* Model Code 2010 predictions.

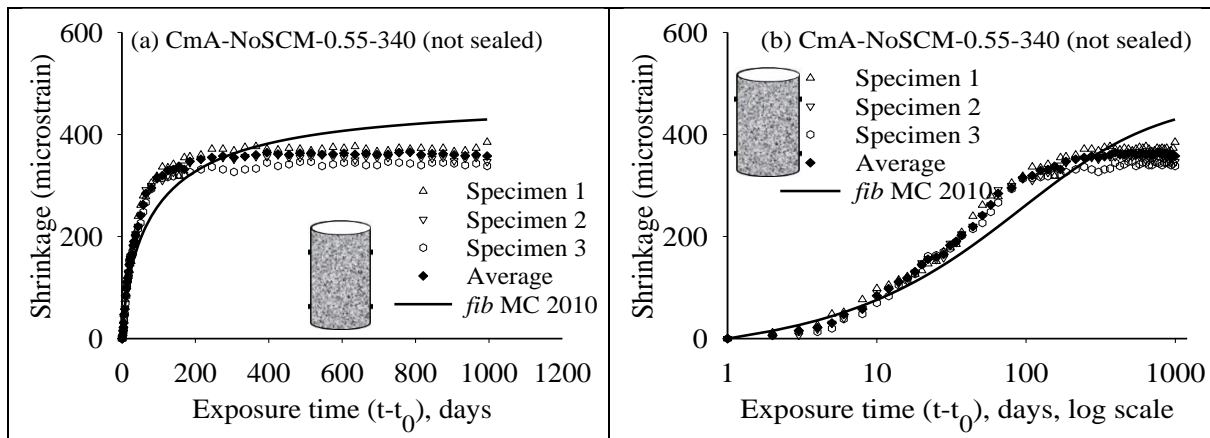


Figure 6.6 Comparison of experimental results and *fib* MC 2010 prediction for CmA-NoSCM-0.55-340 concrete: in (a) normal and (b) log scale

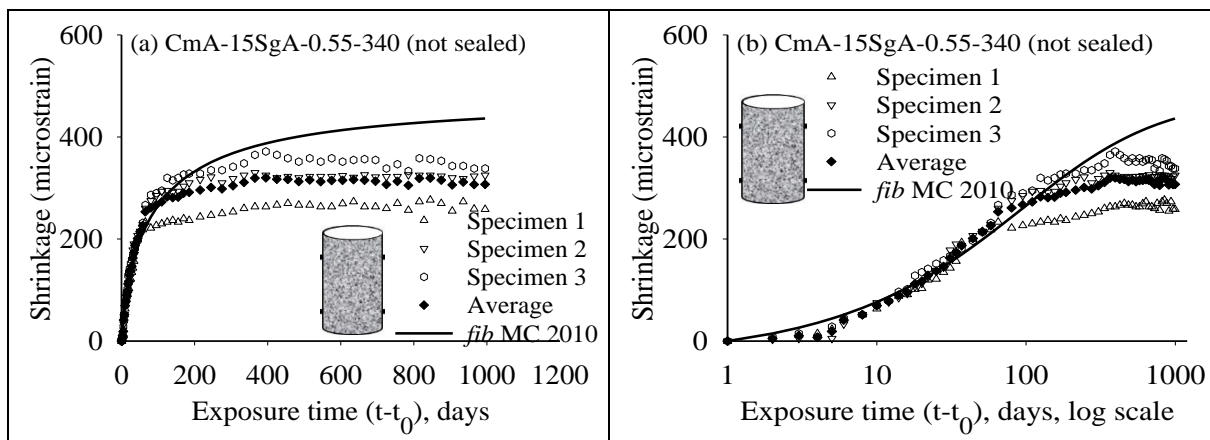


Figure 6.7 Comparison of experimental results and *fib* MC 2010 prediction for CmA-15SgA-0.55-340 concrete (unsealed): in (a) normal and (b) log scales

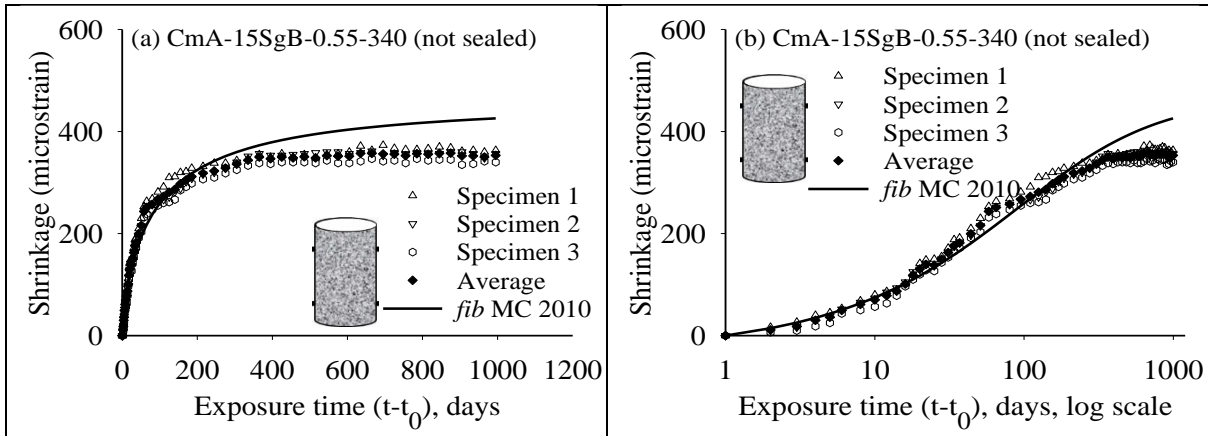


Figure 6.8 Comparison of experimental results and *fib* MC 2010 prediction for CmA-15SgB-0.55-340 concrete (unsealed): in (a) normal and (b) log scales

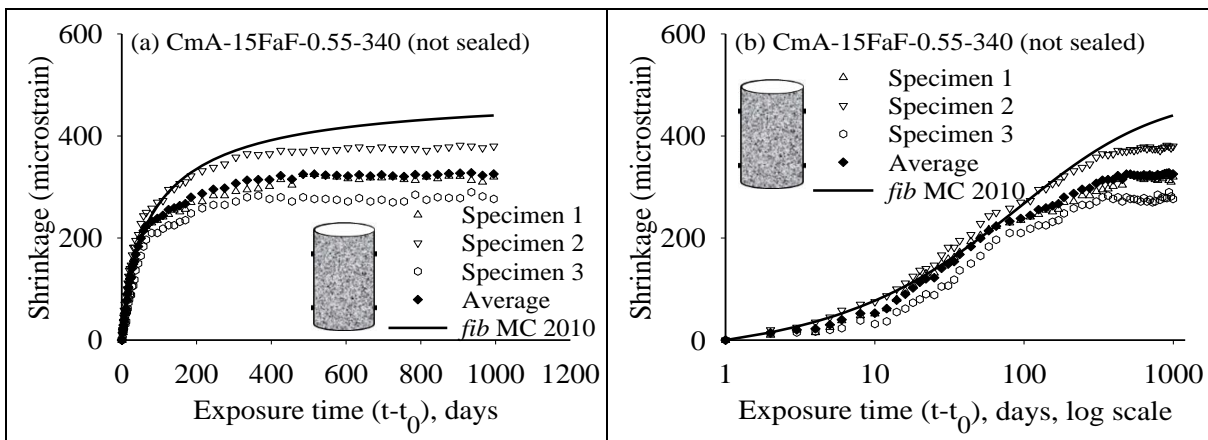


Figure 6.9 Comparison of experimental results and *fib* MC 2010 prediction for CmA-15FaF-0.55-340 concrete (unsealed): in (a) normal and (b) log scales

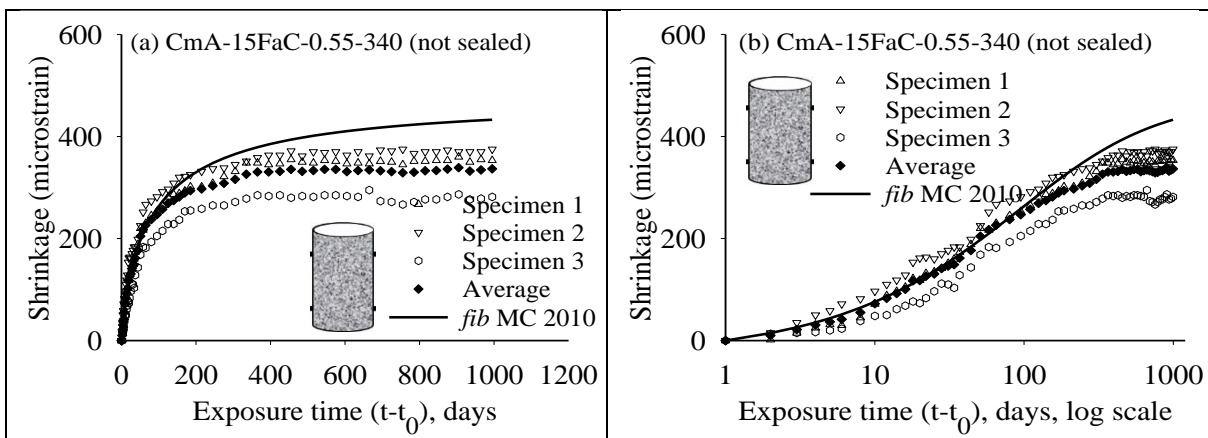


Figure 6.10 Comparison of experimental results and *fib* MC 2010 prediction for CmA-15FaC-0.55-340 concrete (unsealed): in (a) normal and (b) log scales

Table 6.4 provides the error in the *fib* Model Code 2010 predictions after 90,365, 730 and 1000 days of drying when compared to the experimental data obtained here. The values indicate that model, in general, over-estimates shrinkage strains by upto 50% at the end of 1000 days of exposure.

Table 6.4. Error in the predictions of total shrinkage by *fib* MC 2010 model.

Sl. No.	Mix Nomenclature	Error (microstrain) after different drying periods (days)			
		90	365	730	1000
1	CmP-NoSCM-0.65-280	86	82	36	41
2	CmP-30SgA-0.65-280	46	85	80	87
3	CmP-30SgB-0.65-280	58	100	88	101
4	CmP-30FaF-0.65-280	57	87	92	108
5	CmP-NoSCM-0.55-340	24	47	59	64
6	CmP-15SgA-0.55-340	38	30	32	41
7	CmP-15SgB-0.55-340	28	64	60	74
8	CmP-15FaF-0.55-340	15	12	-11	0
9	CmP-15FaC-0.55-340	33	13	-10	-6
10	CmP-NoSCM-0.50-310	16	8	-5	-3
11	CmP-15SgA-0.50-310	10	20	-15	-1
12	CmP-15SgB-0.50-310	1	18	30	43
13	CmP-15FaF-0.50-310	36	38	24	38
14	CmP-15FaC-0.50-310	21	39	47	57
15	CmP-30SgB-0.50-310	-4	-9	-35	-26
16	CmP-30FaF-0.50-310	35	21	19	27
17	CmP-30FaC-0.50-310	-17	-19	-37	-20
18	CmP-50SgB-0.50-310	43	86	83	94
19	CmP-50FaF-0.50-310	48	107	136	158
20	CmP-20SgB-20FaF-0.50-310	74	113	122	133
21	CmP-20SgB-20FaC-0.50-310	45	88	79	93
22	CmP-20FaF-20FaC-0.50-310	33	85	77	89
23	CmP-NoSCM-0.60-310	59	83	50	61
24	CmP-15SgA-0.60-310	10	-28	-26	-14
25	CmP-15SgB-0.60-310	15	13	-12	0
26	CmP-15FaF-0.60-310	71	128	118	137
27	CmP-15FaC-0.60-310	7	31	23	40
32	CmA-NoSCM-0.55-340	-59	16	55	72
33	CmA-15SgA-0.55-340	-7	62	116	129
34	CmA-15SgB-0.55-340	-13	23	57	73
35	CmA-15FaF-0.55-340	24	71	105	115
36	CmA-15FaC-0.55-340	12	48	88	96
37	CmA-NoSCM-0.50-310	-13	26	54	62
38	CmA-15SgA-0.50-310	2	29	55	61
39	CmA-15SgB-0.50-310	-1	56	66	74
40	CmA-15FaF-0.50-310	-14	13	34	46
41	CmA-15FaC-0.50-310	-11	36	73	72
50	CmA-NoSCM-0.60-310	21	65	96	110
51	CmA-15SgA-0.60-310	12	102	143	161

Table 6.4 (continued) Error in the predictions of total shrinkage by *fib* MC 2010 model

Sl. No.	Mix Nomenclature	Error (microstrain) after different drying periods (days)			
		90	365	730	1000
52	CmA-15SgB-0.60-310	20	78	100	115
53	CmA-15FaF-0.60-310	-3	40	73	84
54	CmA-15FaC-0.60-310	46	98	145	154
55	CmP-NoSCM-0.50-310x	-23	-56	-66	-59
56	CmP-30FaF-0.45-310	1	-8	-65	N.A
57	LC3-NoSCM-0.50-310	-29	-118	-128	
58	CmP-NoSCM-0.40-360	-32	-65	-40	
59	CmP-30FaF-0.35-380	34	67	103	
60	LC3-NoSCM-0.40-340	-114	-235	-240	
61	CmP-NoSCM-0.45-360	-28	-56	-26	
62	CmP-30FaF-0.45-360	-17	63	85	
63	LC3-NoSCM-0.45-360	-2	10	37	

6.2.3 RILEM B4s, 2014

The RILEM B4s model of Bažant considers the 28-day mean compressive strength of cylinders in the prediction of shrinkage. For this the conversion factor was taken as 1.21 as mentioned in Section 6.2.2. Also, the model accounts for the effect of aggregate in the shrinkage prediction. Since it is not evident how to obtain the relevant parameters for the aggregates used here, the default value of 1 have been taken for the aggregate dependent parameters $k_{\tau a}$ and k_{ca} . As seen from Figure 6.11 through Figure 6.15, the prediction for NoSCM and blended cement concrete with w/b = 0.55 and total binder content of 340 kg/m³ is slightly overestimated at later ages of drying (say, beyond 200 days), except in the case of SgB blended concrete. The plots comparing the shrinkage strain predictions using the B4s model with all the experimental data are given in Appendix D3.

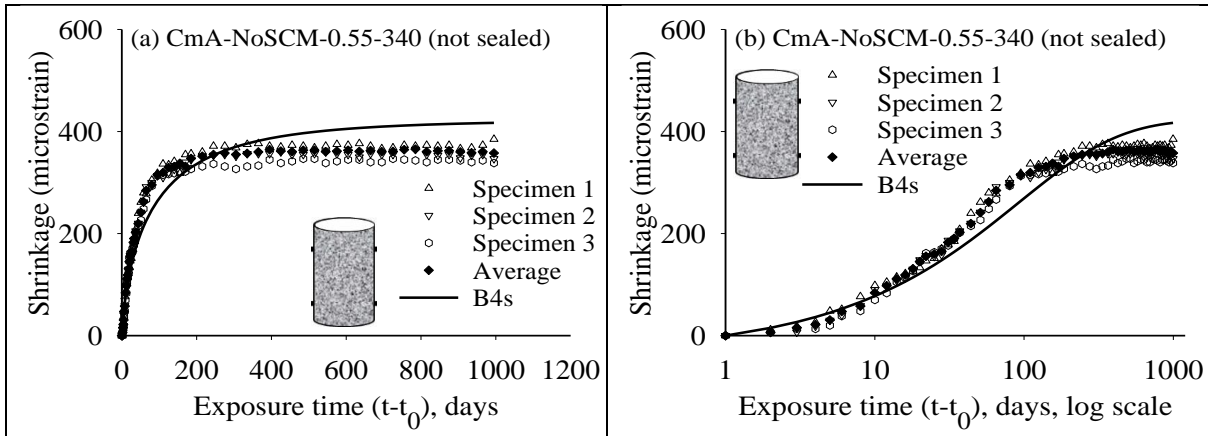


Figure 6.11 Comparison of experimental results and B4s predictions for CmA-NoSCM-0.55-340 concrete (unsealed): in (a) normal and (b) log scales

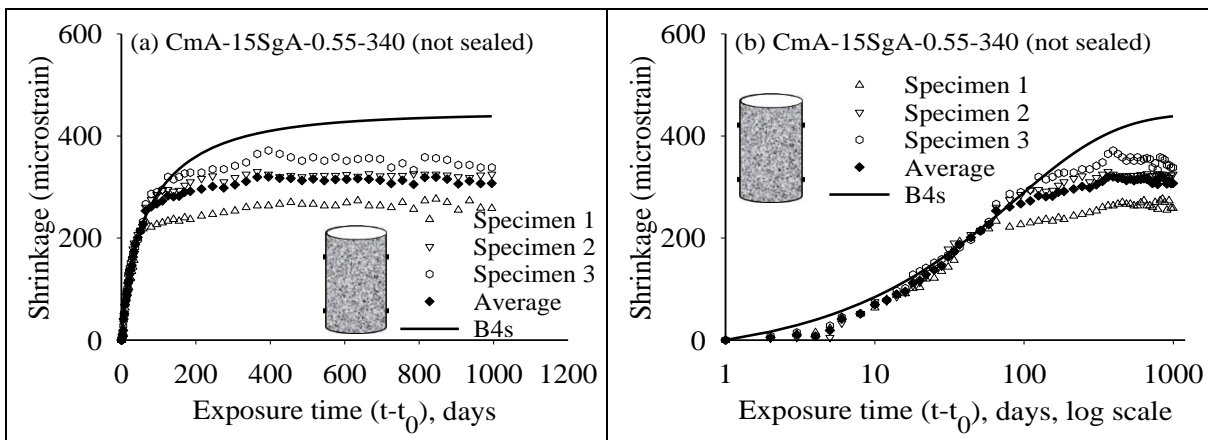


Figure 6.12 Comparison of experimental results and B4s predictions for CmA-15SgA-0.55-340 concrete (unsealed): in (a) normal and (b) log scales

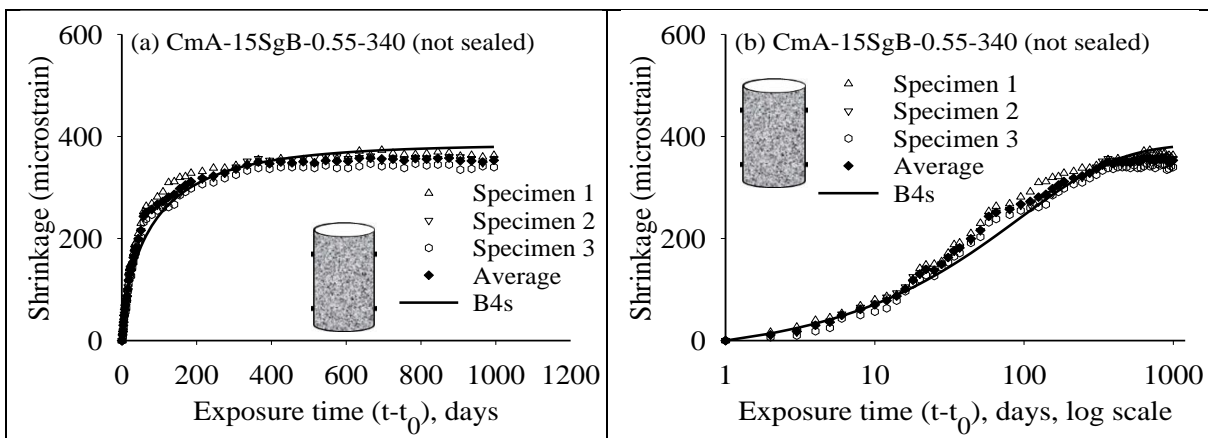


Figure 6.13 Comparison of experimental results and B4s prediction for CmA-15SgB-0.55-340 concrete (unsealed): in (a) normal and (b) log scales

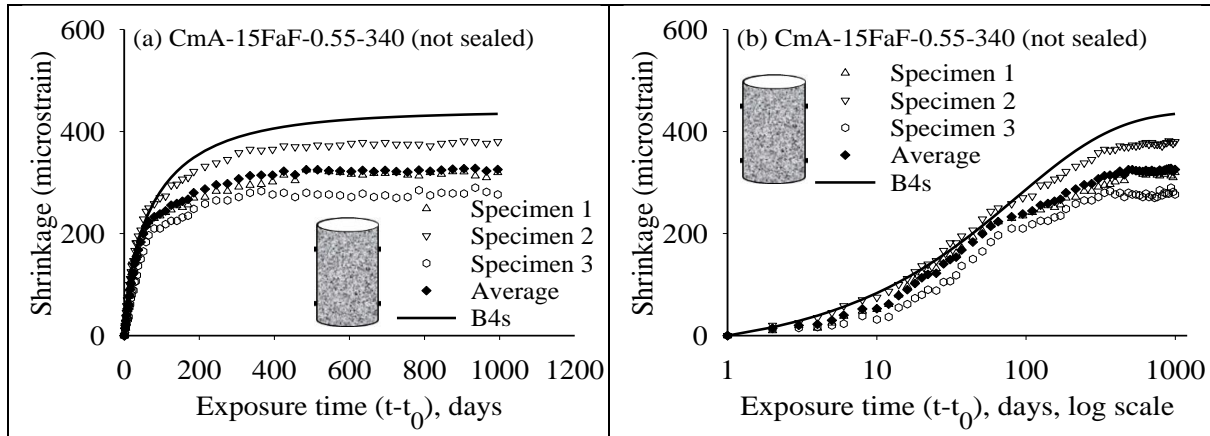


Figure 6.14 Comparison of experimental results and B4s prediction for CmA-15FaF-0.55-340 concrete (unsealed): in (a) normal and (b) log scales

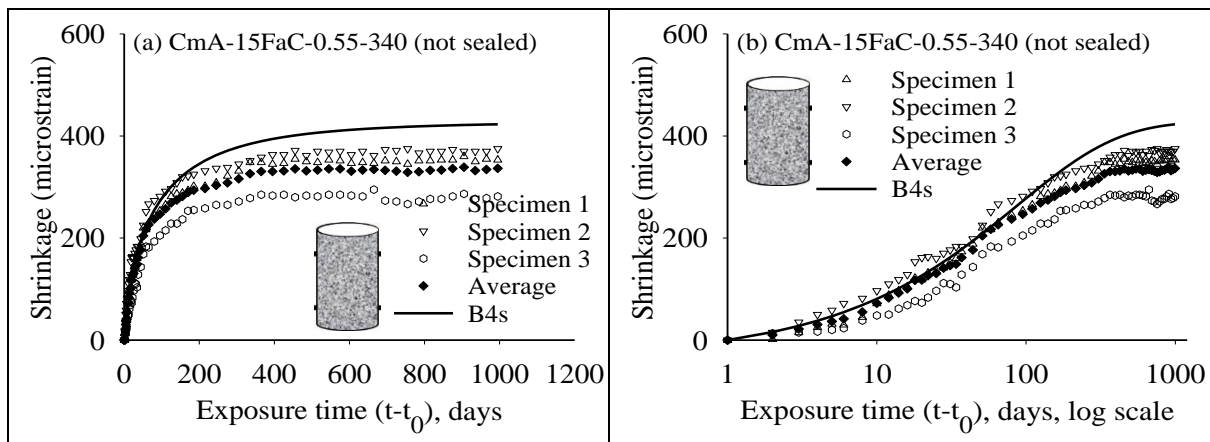


Figure 6.15 Comparison of experimental results and B4s prediction for CmA-15FaC-0.55-340 concrete (unsealed): in (a) normal and (b) log scales

Table 6.5 gives the difference between the experimental results and the B4s predictions at the end of 90, 365, 730 and 1000 days of drying. It shows that the error is generally acceptable limit, though in some cases the overestimation is by 100 to 260 μ strains. The predictions are unconservative for the LC3 concretes in general.

Table 6.5 Error in the prediction of total shrinkage by B4s model.

Sl. No	Mix Nomenclature	Error (microstrain) after different drying periods (days)			
		90	365	730	1000
1	CmP-NoSCM-0.65-280	124	128	68	64
2	CmP-30SgA-0.65-280	80	125	106	106
3	CmP-30SgB-0.65-280	89	137	111	116
4	CmP-30FaF-0.65-280	130	179	169	175
5	CmP-NoSCM-0.55-340	30	52	52	50
6	CmP-15SgA-0.55-340	53	46	36	37
7	CmP-15SgB-0.55-340	28	63	47	55

Table 6.5 (continued) Error in the prediction of total shrinkage by B4s model

Sl. No.	Mix Nomenclature	Error (microstrain) after different drying periods (days)			
		90	365	730	1000
8	CmP-15FaF-0.55-340	28	26	-10	-6
9	CmP-15FaC-0.55-340	39	18	-16	-19
10	CmP-NoSCM-0.50-310	21	11	-13	-17
11	CmP-15SgA-0.50-310	7	14	-32	-24
12	CmP-15SgB-0.50-310	-3	12	14	21
13	CmP-15FaF-0.50-310	55	81	79	81
14	CmP-15FaC-0.50-310	38	34	7	13
15	CmP-30SgB-0.50-310	-6	-13	-49	-47
16	CmP-30FaF-0.50-310	58	42	27	27
17	CmP-30FaC-0.50-310	-15	-18	-47	-37
18	CmP-50SgB-0.50-310	52	94	80	83
19	CmP-50FaF-0.50-310	133	215	230	241
20	CmP-20SgB-20FaF-0.50-310	107	152	148	150
21	CmP-20SgB-20FaC-0.50-310	58	103	82	88
22	CmP-20FaF-20FaC-0.50-310	42	94	74	79
23	CmP-NoSCM-0.60-310	91	121	75	77
24	CmP-15SgA-0.60-310	10	-24	-34	-28
25	CmP-15SgB-0.60-310	48	53	15	18
26	CmP-15FaF-0.60-310	105	168	145	156
27	CmP-15FaC-0.60-310	31	59	38	46
32	CmA-NoSCM-0.55-340	-52	22	50	59
33	CmA-15SgA-0.55-340	12	83	126	132
34	CmA-15SgB-0.55-340	-7	28	51	59
35	CmA-15FaF-0.55-340	38	84	107	109
36	CmA-15FaC-0.55-340	21	57	86	86
37	CmA-NoSCM-0.50-310	-4	33	50	51
38	CmA-15SgA-0.50-310	9	35	50	49
39	CmA-15SgB-0.50-310	0	55	55	57
40	CmA-15FaF-0.50-310	-7	21	31	38
41	CmA-15FaC-0.50-310	1	48	74	66
50	CmA-NoSCM-0.60-310	62	112	131	136
51	CmA-15SgA-0.60-310	10	106	134	144
52	CmA-15SgB-0.60-310	35	93	103	111
53	CmA-15FaF-0.60-310	30	73	94	98
54	CmA-15FaC-0.60-310	105	166	199	198
55	CmP-NoSCM-0.50-310x	-19	-53	-79	-75
56	CmP-30FaF-0.45-310	22	14	-52	N.A
57	LC3-NoSCM-0.50-310	-23	-109	-130	

Table 6.5 (continued) Error in the prediction of total shrinkage by B4s model

Sl. No	Mix Nomenclature	Error (microstrain) after different drying periods (days)			
		90	365	730	1000
58	CmP-NoSCM-0.40-360	-37	-64	-61	N.A
59	CmP-30FaF-0.35-380	30	61	85	
60	LC3-NoSCM-0.40-340	-120	-233	-259	
61	CmP-NoSCM-0.45-360	-26	-56	-40	
62	CmP-30FaF-0.45-360	-9	67	78	
63	LC3-NoSCM-0.45-360	-1	13	25	

6.3 COMPOSITION-BASED SHRINKAGE PREDICTION MODELS

The ACI 209 and B4 shrinkage prediction models are considered as composition-based models since their input parameters and the formulations include fresh concrete properties, such as slump and air content, and the composition of concrete, including cement content, aggregate type, water-binder ratio and admixtures (chemical and mineral).

6.3.1 ACI 209, 2008

This model considers parameters such as cement content, fine aggregate ratio, slump, air content, relative humidity and density of concrete to calculate the correction factors applied to the ultimate shrinkage strain. As seen from Figure 6.16 through Figure 6.20, with respect to CmA concrete with water to binder ratio of 0.55 and total binder content of 340 kg/m^3 , the shrinkage prediction by this model is comparable with the upper bound of the measured strain values. Appendix D5 gives the plots for all concrete mixtures comparing the measured shrinkage strains and the ACI 209 model predictions.

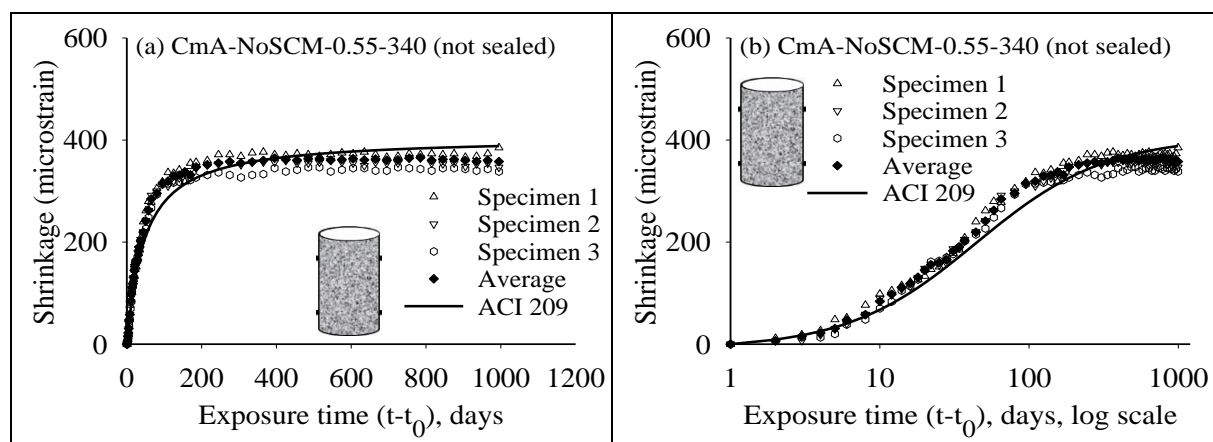


Figure 6.16 Comparison of experimental results and ACI 209 predictions for CmA-NoSCM-0.55-340 concrete (unsealed): in (a) normal and (b) log scales

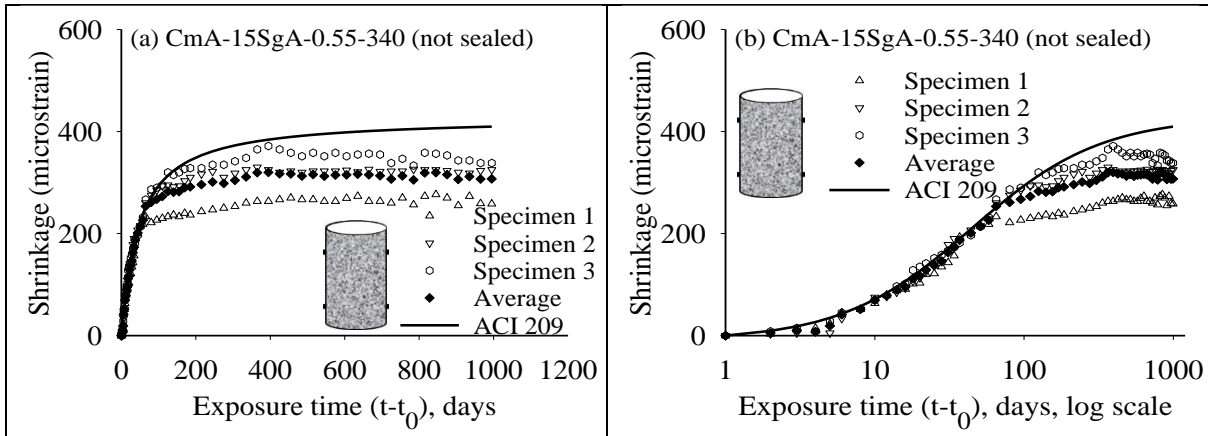


Figure 6.17 Comparison of experimental results and ACI 209 predictions for CmA-15SgA-0.55-340 concrete (unsealed): in (a) normal and (b) log scales

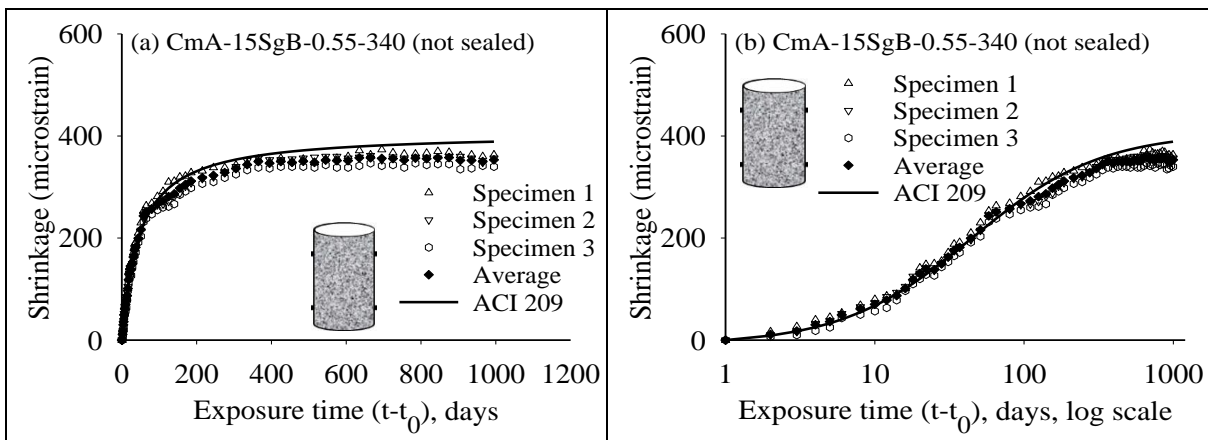


Figure 6.18 Comparison of experimental results and ACI 209 predictions for CmA-15SgB-0.55-340 concrete (unsealed): in (a) normal and (b) log scales

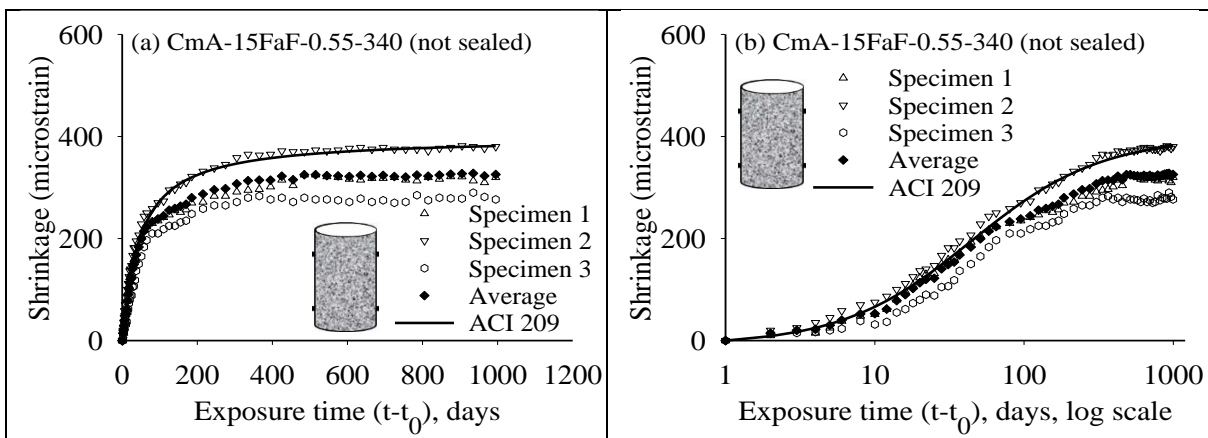


Figure 6.19 Comparison of experimental results and ACI 209 predictions for CmA-NoSCM-0.55-340 concrete (unsealed): in (a) normal and (b) log scales

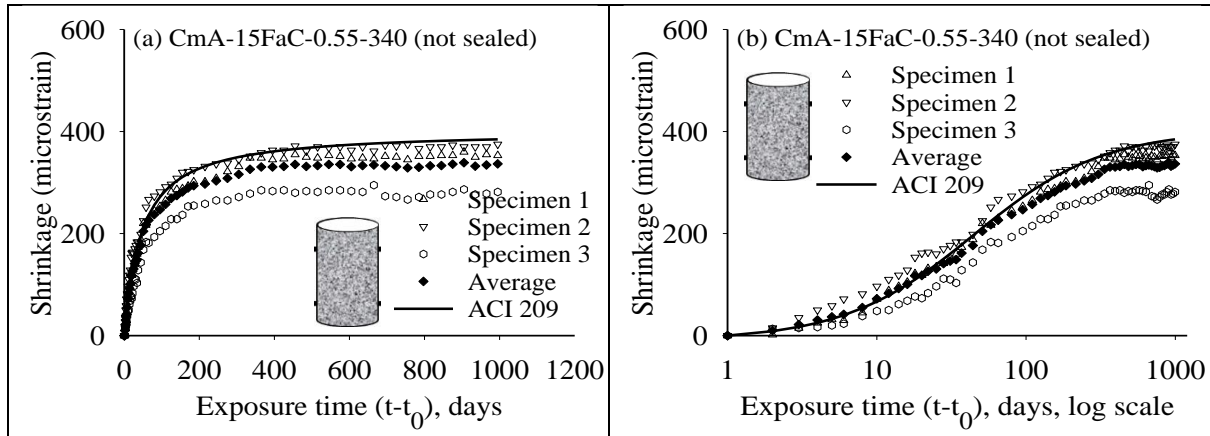


Figure 6.20 Comparison of experimental results and ACI 209 predictions for CmA-NoSCM-0.55-340 concrete (unsealed): in (a) normal and (b) log scales

Table 6.6 provides the errors in the predictions at the end of 90, 365, 730 and 1000 days of drying, and it can be seen that the error is generally low though slightly unconservative, at all the ages considered, with notable exceptions being the LC3 concretes.

Table 6.6 Error in the predictions of total shrinkage by ACI 209 model.

Sl. No.	Mix Nomenclature	Error (microstrain) after different drying periods (days)			
		90	365	730	1000
1	CmP-NoSCM-0.65-280	69	13	-59	-64
2	CmP-30SgA-0.65-280	48	43	15	14
3	CmP-30SgB-0.65-280	40	30	-7	-3
4	CmP-30FaF-0.65-280	25	-7	-30	-25
5	CmP-NoSCM-0.55-340	45	37	29	27
6	CmP-15SgA-0.55-340	58	16	-3	-2
7	CmP-15SgB-0.55-340	49	54	31	38
8	CmP-15FaF-0.55-340	24	-11	-55	-51
9	CmP-15FaC-0.55-340	51	-3	-45	-48
10	CmP-NoSCM-0.50-310	34	-7	-39	-44
11	CmP-15SgA-0.50-310	40	24	-28	-20
12	CmP-15SgB-0.50-310	44	41	37	44
13	CmP-15FaF-0.50-310	37	-4	-40	-35
14	CmP-15FaC-0.50-310	29	8	-4	-3
15	CmP-30SgB-0.50-310	6	-29	-74	-72
16	CmP-30FaF-0.50-310	44	-16	-40	-40
17	CmP-30FaC-0.50-310	-15	-47	-84	-74
18	CmP-50SgB-0.50-310	56	63	40	42
19	CmP-50FaF-0.50-310	17	13	13	23
20	CmP-20SgB-20FaF-0.50-310	65	54	39	41
21	CmP-20SgB-20FaC-0.50-310	46	48	17	23

Table 6.6 (continued) Error in the predictions of total shrinkage by ACI 209 model

Sl. No.	Mix Nomenclature	Error (microstrain) after different drying periods (days)			
		90	365	730	1000
22	CmP-20FaF-20FaC-0.50-310	46	62	33	37
23	CmP-NoSCM-0.60-310	38	12	-45	-43
24	CmP-15SgA-0.60-310	28	-43	-61	-56
25	CmP-15SgB-0.60-310	16	-31	-80	-76
26	CmP-15FaF-0.60-310	68	78	45	55
27	CmP-15FaC-0.60-310	-1	-24	-56	-48
32	CmA-NoSCM-0.55-340	-42	1	21	30
33	CmA-15SgA-0.55-340	22	61	96	102
34	CmA-15SgB-0.55-340	7	12	27	36
35	CmA-15FaF-0.55-340	31	40	54	56
36	CmA-15FaC-0.55-340	25	27	47	48
37	CmA-NoSCM-0.50-310	-6	-5	3	4
38	CmA-15SgA-0.50-310	8	-1	5	4
39	CmA-15SgB-0.50-310	25	54	47	49
40	CmA-15FaF-0.50-310	4	2	4	10
41	CmA-15FaC-0.50-310	2	16	34	26
50	CmA-NoSCM-0.60-310	20	22	31	36
51	CmA-15SgA-0.60-310	-25	24	42	52
52	CmA-15SgB-0.60-310	14	30	30	38
53	CmA-15FaF-0.60-310	0	0	11	14
54	CmA-15FaC-0.60-310	11	7	28	26
55	CmP-NoSCM-0.50-310x	-5	-71	-99	-99
56	CmP-30FaF-0.45-310	2	-48	-126	N.A
57	LC3-NoSCM-0.50-310	-21	-147	-177	
58	CmP-NoSCM-0.40-360	7	-49	-38	
59	CmP-30FaF-0.35-380	86	100	121	
60	LC3-NoSCM-0.40-340	-64	-204	-223	
61	CmP-NoSCM-0.45-360	0	-57	-45	
62	CmP-30FaF-0.45-360	17	-32	-68	
63	LC3-NoSCM-0.45-360	38	25	36	

6.3.2 RILEM B4, 2014

As specified in the description of the RILEM B4 model of Bažant in Chapter 2, the model captures the effects of the aggregate type. For comparison, the aggregate dependent parameters $k_{\tau a}$ and $k_{c a}$ were taken from Table 2.2 for granite. The factor for the SCMs were taken from Table 2.3 to calculate the shrinkage predictions. The model provides scaling factors only for fly ash and silica fume. Here, the scaling factor of fly ash has been considered also for slag.

Figure 6.21 through Figure 6.25 gives the comparison of the evolution of measured shrinkage and the B4 model predictions for the CmA concrete, with $w/b=0.55$ and total binder content of 340 kg/m^3 . As seen from the plots the model predictions are slightly over-conservative. Appendix D6 gives the comparison of the predictions and the experimental values for all the concretes.

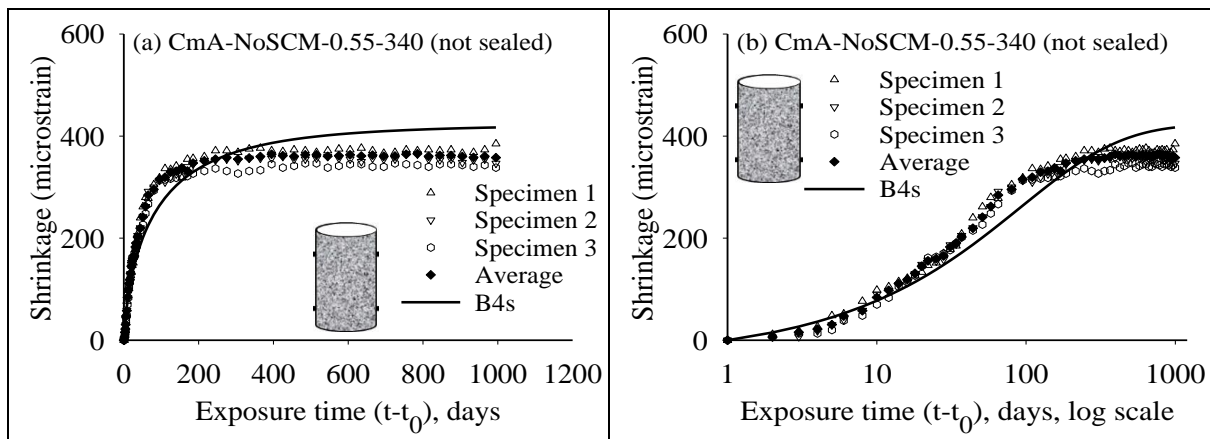


Figure 6.21 Comparison of experimental results and B4 predictions for CmA-NoSCM-0.55-340 concrete (unsealed): in (a) normal and (b) log scales

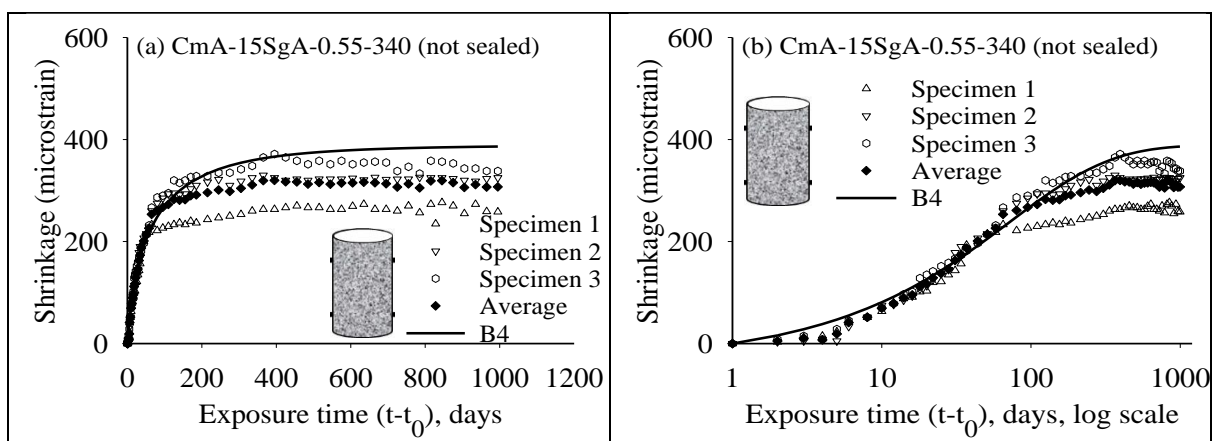


Figure 6.22 Comparison of experimental results and B4 predictions for CmA-15SgA-0.55-340 concrete (unsealed): in (a) normal and (b) log scales

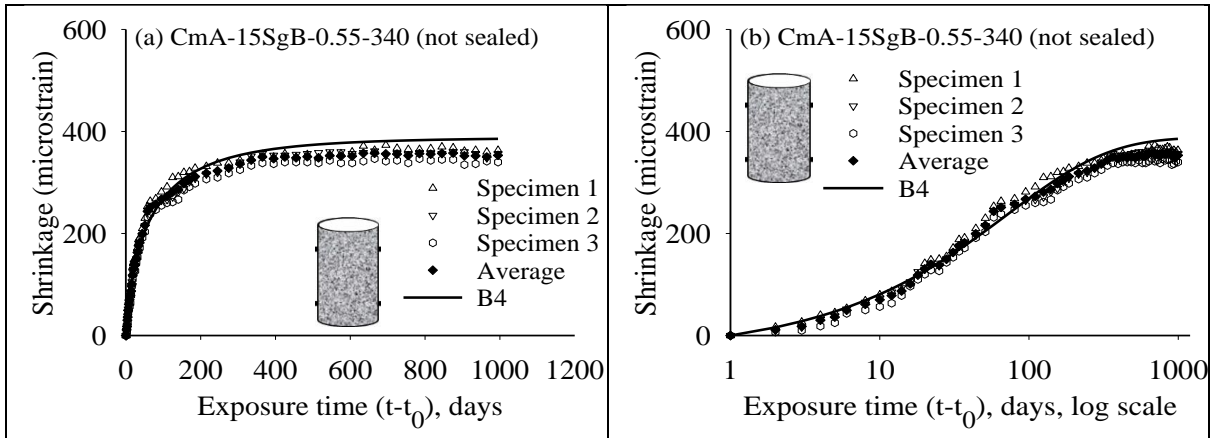


Figure 6.23 Comparison of experimental results and B4 predictions for CmA-15SgB-0.55-340 concrete (unsealed): in (a) normal and (b) log scales

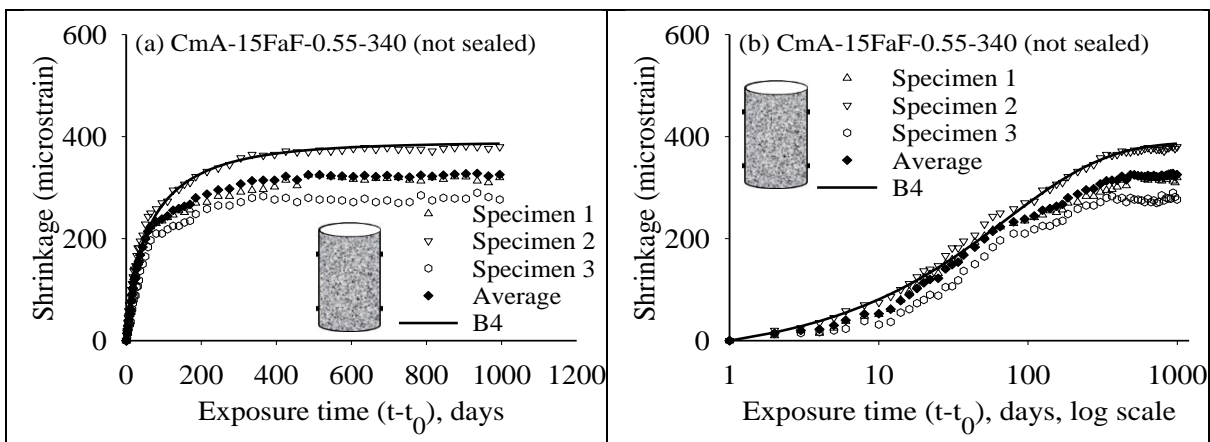


Figure 6.24 Comparison of experimental results and B4 predictions for CmA-15FaF-0.55-340 concrete (unsealed): in (a) normal and (b) log scales

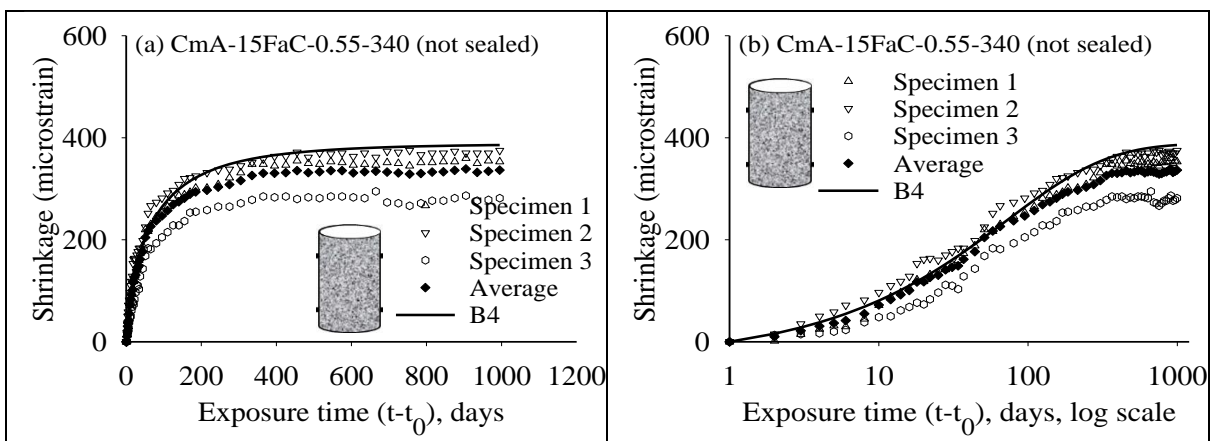


Figure 6.25 Comparison of experimental results and B4 prediction for CmA-15FaC-0.55-340 concrete (unsealed): in (a) normal and (b) log scales

Table 6.7 gives the error in the predictions of the B4 model at the end of 90, 365, 730 and 1000 days of drying, where it can be seen that the predictions are within the acceptable limit, with the LC3 concretes being the exceptions.

Table 6.7 Error in the prediction of total shrinkage by B4 model

Sl. No.	Mix Nomenclature	Error (microstrain) after different drying periods (days)			
		90	365	730	1000
1	CmP-NoSCM-0.65-280	-8	-23	-61	-54
2	CmP-30SgA-0.65-280	5	27	9	9
3	CmP-30SgB-0.65-280	19	45	20	26
4	CmP-30FaF-0.65-280	-2	0	-12	-5
5	CmP-NoSCM-0.55-340	-44	-14	15	26
6	CmP-15SgA-0.55-340	47	16	-3	-5
7	CmP-15SgB-0.55-340	51	74	51	56
8	CmP-15FaF-0.55-340	25	1	-44	-43
9	CmP-15FaC-0.55-340	50	14	-29	-35
10	CmP-NoSCM-0.50-310	-80	-105	-112	-107
11	CmP-15SgA-0.50-310	-5	-27	-84	-79
12	CmP-15SgB-0.50-310	-15	-30	-40	-37
13	CmP-15FaF-0.50-310	-16	-43	-60	-61
14	CmP-15FaC-0.50-310	-11	-58	-100	-98
15	CmP-30SgB-0.50-310	-50	-74	-111	-108
16	CmP-30FaF-0.50-310	-31	-81	-99	-98
17	CmP-30FaC-0.50-310	-69	-93	-122	-112
18	CmP-50SgB-0.50-310	-22	-1	-11	-5
19	CmP-50FaF-0.50-310	-58	-49	-35	-21
20	CmP-20SgB-20FaF-0.50-310	-10	-6	-8	-2
21	CmP-20SgB-20FaC-0.50-310	-25	-6	-23	-14
22	CmP-20FaF-20FaC-0.50-310	-31	-1	-17	-9
23	CmP-NoSCM-0.60-310	-30	-13	-34	-19
24	CmP-15SgA-0.60-310	31	-25	-44	-42
25	CmP-15SgB-0.60-310	11	-23	-74	-73
26	CmP-15FaF-0.60-310	67	91	56	63
27	CmP-15FaC-0.60-310	10	6	-26	-21
32	CmA-NoSCM-0.55-340	-135	-56	-3	19
33	CmA-15SgA-0.55-340	-3	44	76	79
34	CmA-15SgB-0.55-340	-3	12	26	32
35	CmA-15FaF-0.55-340	26	49	61	61
36	CmA-15FaC-0.55-340	17	32	51	49
37	CmA-NoSCM-0.50-310	-121	-102	-71	-62
38	CmA-15SgA-0.50-310	-39	-52	-51	-56
39	CmA-15SgB-0.50-310	-33	-13	-26	-28
40	CmA-15FaF-0.50-310	-46	-55	-58	-55
41	CmA-15FaC-0.50-310	-47	-39	-26	-38
50	CmA-NoSCM-0.60-310	-76	-38	3	19
51	CmA-15SgA-0.60-310	-34	25	40	48

Table 6.7 (continued) Error in the prediction of total shrinkage by B4 model

Sl. No.	Mix Nomenclature	Error (microstrain) after different drying periods (days)			
		90	365	730	1000
52	CmA-15SgB-0.60-310	22	53	52	57
53	CmA-15FaF-0.60-310	2	14	23	24
54	CmA-15FaC-0.60-310	21	32	51	48
55	CmP-NoSCM-0.50-310x	-121	-167	-177	-163
56	CmP-30FaF-0.45-310	-75	-113	-183	N.A
57	LC3-NoSCM-0.50-310	-131	-232	-236	
58	CmP-NoSCM-0.40-360	-119	-154	-134	
59	CmP-30FaF-0.35-380	-40	-33	-11	
60	LC3-NoSCM-0.40-340	-210	-339	-352	
61	CmP-NoSCM-0.45-360	-114	-148	-112	
62	CmP-30FaF-0.45-360	-73	-13	0	
63	LC3-NoSCM-0.45-360	-90	-79	-47	

6.4 ADJUSTMENT OF MODEL PARAMETERS FOR BETTER PREDICTION

Most proponents of the prediction models allow the adjustment or fine tuning of the parameters based on early shrinkage data to get better prediction at later ages. Accordingly, the B4s model parameters have been regressed by using the laboratory shrinkage data at one, two and three years. In the B4 model, the parameters have been modified considering the aggregate type as unknown and the effect of the performance enhancer in the OPC.

6.4.1 B4s-R

Binder type and the content are significant factors that affect the shrinkage response of concrete. The B4s model, being a strength-based model, is calibrated only for OPC cement that is used as binders in the concrete. In the present scenario, blended concrete has become very common and it is important that its effect be accounted for in the estimation of shrinkage strains. Therefore, in the B4s model, the variables $\mathcal{E}_{s, \text{cem}}$ and S_{ef} , which are dependent on the binder type, have been using regression analysis. The values obtained by regression for the different binder types are given in Table 6.8. Note that the parameters suggested in the model are $\mathcal{E}_{s, \text{cem}} = 590 \times 10^{-6}$ and $S_{\text{ef}} = -0.51$. Regression is done using the measured shrinkage strain data of one, two and three years, to study the effects of the test duration on the values obtained by regression. These regressed values are further substituted in the B4s model and the predictions of shrinkage strains at later ages are obtained. Figure 6.26 through Figure 6.30 give

the predictions based on the regression done with one-year data. Figure 6.31 through Figure 6.35 give the predictions based on two-year data, and Figure 6.36 through Figure 6.40 give the predictions using three-year data. It is generally seen that for concrete with only OPC, the regression based on one-year data is sufficient whereas for SCM concretes at least two-year data is required for good longer-term predictions.

Appendix D6 shows all the plots of the measured shrinkage strains along with the predicted shrinkage strains of the B4s and the B4s-R models. As mentioned earlier, it can be observed that, for almost all NoSCM and slag blended concrete, the regressed values of $\epsilon_{s,cm}$ and $S_{\epsilon f}$ from one year data give close estimation of the later measured shrinkage strains. However, for the fly ash blended concrete, the regressed values of $\epsilon_{s,cm}$ and $S_{\epsilon f}$ for two-year data give predictions that are comparable with the measured shrinkage strains. This could be due to the difference in the hydration of the binder and strength gain. Since, fly ash blended concrete has a lower rate of strength development, the shrinkage takes more time to stabilize. Therefore, it could be concluded that the use of SCM may necessitate testing up to two years to get good long-term predictions. Table 6.9 through Table 6.11 gives the errors in the prediction of the B4s regressed model at the end of 90, 365, 730 and 1000 days of drying, it can be seen that the predictions are slightly better but substantial in some cases.

Table 6.8 Regression of B4s prediction model parameters with experimental data of one, two and three years

Sl. No	Mix Nomenclature	regression with one-year data		regression with two-year data		regression with three-year data	
		$\epsilon_{s,cm} (\times 10^{-6})$	$S_{\epsilon f}$	$\epsilon_{s,cm} (\times 10^{-6})$	$S_{\epsilon f}$	$\epsilon_{s,cm} (\times 10^{-6})$	$S_{\epsilon f}$
1	CmP-NoSCM-0.65-280	512	-0.54	526	-0.53	530	-0.52
2	CmP-30SgA-0.65-280	514	-0.53	528	-0.53	529	-0.53
3	CmP-30SgB-0.65-280	515	-0.53	528	-0.52	529	-0.53
4	CmP-30FaF-0.65-280	513	-0.52	518	-0.54	527	-0.52
5	CmP-NoSCM-0.55-340	521	-0.52	532	-0.53	533	-0.55
6	CmP-15SgA-0.55-340	517	-0.54	531	-0.52	532	-0.54
7	CmP-15SgB-0.55-340	522	-0.53	534	-0.53	536	-0.55
8	CmP-15FaF-0.55-340	520	-0.52	530	-0.54	531	-0.54
9	CmP-15FaC-0.55-340	520	-0.55	532	-0.53	534	-0.54
10	CmP-NoSCM-0.50-310	522	-0.52	533	-0.53	535	-0.53
11	CmP-15SgA-0.50-310	525	-0.56	536	-0.54	538	-0.54
12	CmP-15SgB-0.50-310	525	-0.57	537	-0.56	538	-0.55
13	CmP-15FaF-0.50-310	516	-0.54	528	-0.53	530	-0.53
14	CmP-15FaC-0.50-310	520	-0.53	531	-0.53	532	-0.54
15	CmP-30SgB-0.50-310	524	-0.58	535	-0.55	537	-0.56
16	CmP-30FaF-0.50-310	516	-0.54	529	-0.53	531	-0.54
17	CmP30FaC-0.50-310	522	-0.52	533	-0.54	535	-0.54
18	CmP-50SgB-0.50-310	520	-0.53	531	-0.54	532	-0.55
19	CmP-50FaF-0.50-310	506	-0.54	517	-0.54	520	-0.54
20	CmP-20SgB-20FaF-0.50-310	515	-0.53	526	-0.53	528	-0.54
21	CmP-20SgB-20FaC-0.50-310	517	-0.54	531	-0.53	532	-0.53
22	CmP-20FaF-20FaC-0.50-310	521	-0.52	531	-0.53	533	-0.54
23	CmP-NoSCM-0.60-310	517	-0.52	529	-0.52	529	-0.53
24	CmP-15SgA-0.60-310	521	-0.53	532	-0.53	535	-0.53
25	CmP-15SgB-0.60-310	522	-0.53	528	-0.53	528	-0.53

Table 6.8 (continued) Regression of B4s prediction model parameters with experimental data of one, two and three years

Sl. No	Mix Nomenclature	regression with one-year data		regression with two-year data		regression with three-year data	
		$\epsilon_{s, cem} (\times 10^{-6})$	$S_{\epsilon f}$	$\epsilon_{s, cem} (\times 10^{-6})$	$S_{\epsilon f}$	$\epsilon_{s, cem} (\times 10^{-6})$	$S_{\epsilon f}$
26	CmP-15FaF-0.60-310	515	-0.53	528	-0.52	529	-0.53
27	CmP-15FaC-0.60-310	517	-0.53	528	-0.53	530	-0.53
32	CmA-NoSCM-0.55-340	514	-0.52	527	-0.53	531	-0.54
33	CmA-15SgA-0.55-340	510	-0.54	524	-0.54	530	-0.53
34	CmA-15SgB-0.55-340	514	-0.52	528	-0.52	531	-0.54
35	CmA-15FaF-0.55-340	510	-0.54	524	-0.54	530	-0.53
36	CmA-15FaC-0.55-340	513	-0.53	526	-0.54	531	-0.53
37	CmA-NoSCM-0.50-310	514	-0.54	527	-0.54	531	-0.54
38	CmA-15SgA-0.50-310	515	-0.52	527	-0.54	532	-0.54
39	CmA-15SgB-0.50-310	516	-0.57	530	-0.57	534	-0.54
40	CmA-15FaF-0.50-310	515	-0.54	529	-0.52	533	-0.54
41	CmA-15FaC-0.50-310	513	-0.53	527	-0.52	531	-0.54
50	CmA-NoSCM-0.60-310	507	-0.53	522	-0.53	523	-0.54
51	CmA-15SgA-0.60-310	508	-0.53	522	-0.53	528	-0.52
52	CmA-15SgB-0.60-310	511	-0.54	524	-0.54	529	-0.53
53	CmA-15FaF-0.60-310	512	-0.52	526	-0.51	528	-0.53
54	CmA-15FaC-0.60-310	506	-0.53	512	-0.55	520	-0.54

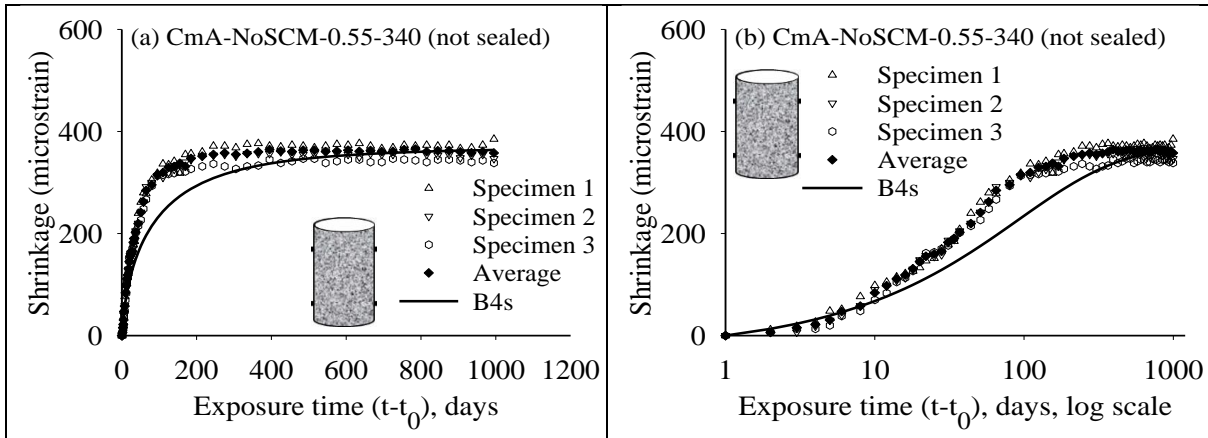


Figure 6.26 Comparison of experimental results and prediction with regressed B4s with one year data for CmA-NoSCM-0.55-340 concrete (unsealed): in (a) normal and (b) log scales

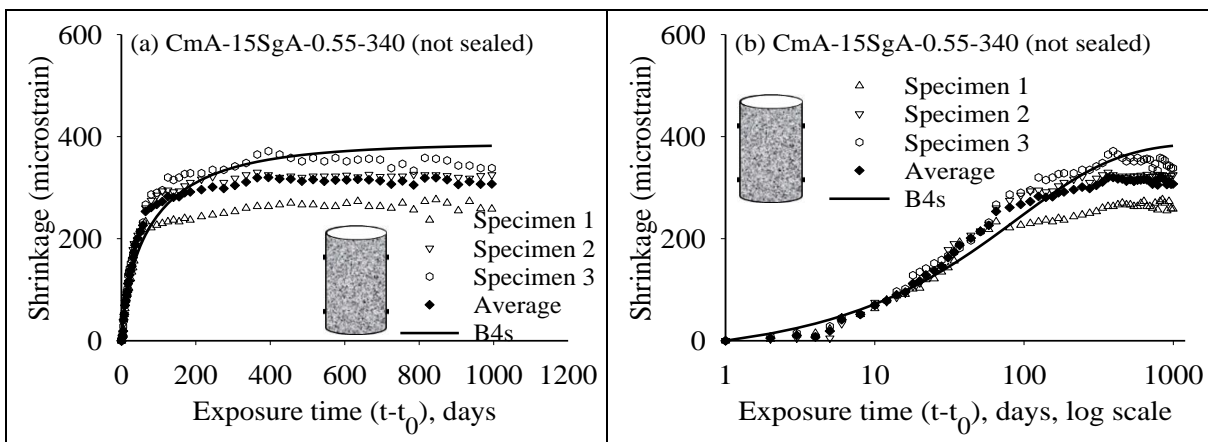


Figure 6.27 Comparison of experimental results and prediction with regressed B4s with one year data for CmA-15SgA-0.55-340 concrete (unsealed): in (a) normal and (b) log scales

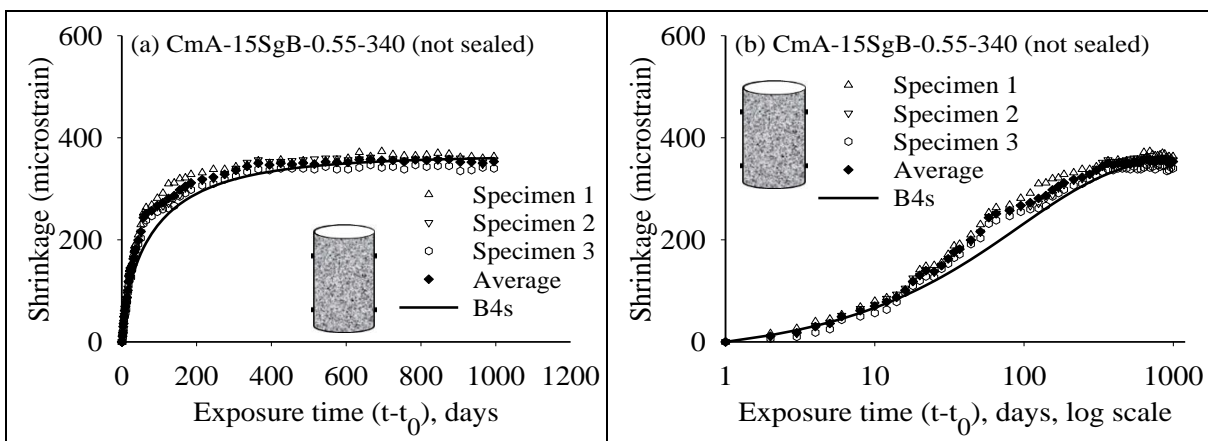


Figure 6.28 Comparison of experimental results and prediction with regressed B4s with one year data for CmA-15SgB-0.55-340 concrete (unsealed): in (a) normal and (b) log scales

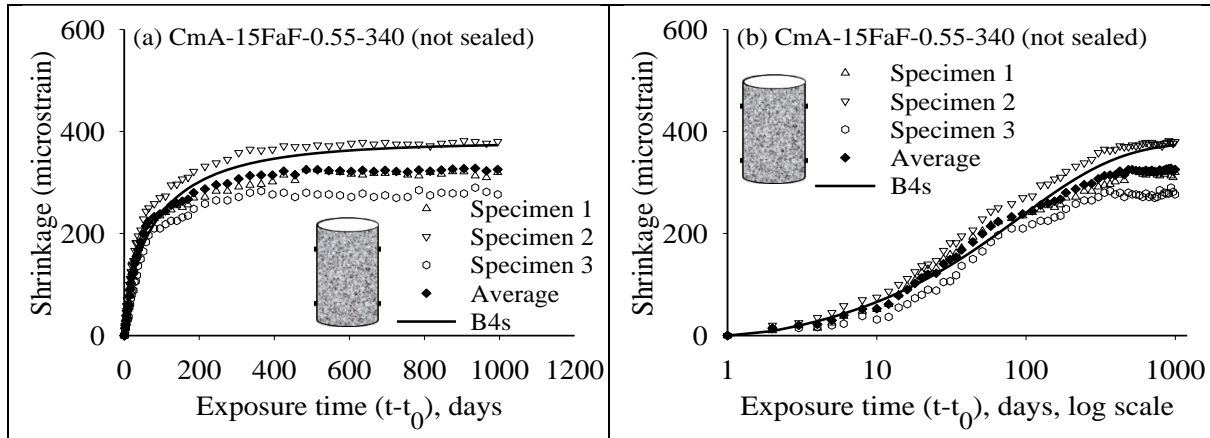


Figure 6.29 Comparison of experimental results and prediction with regressed B4s with one year data for CmA-15FaF-0.55-340 concrete (unsealed): in (a) normal and (b) log scales

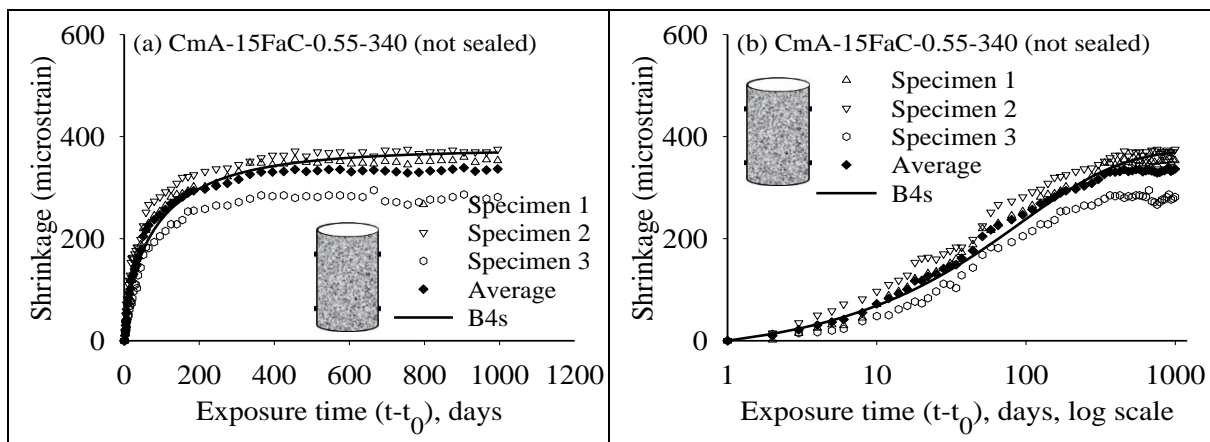


Figure 6.30 Comparison of experimental results and prediction with regressed B4s with one year data for CmA-15FaC-0.55-340 concrete (unsealed): in (a) normal and (b) log scales

Table 6.9 Errors in the prediction of total shrinkage by B4s model with the parameters regressed using one-year data.

Sl. No.	Mix Nomenclature	Error (microstrain) after different drying periods (days)			
		90	365	730	1000
1	CmP-NoSCM-0.65-280	88	73	9	4
2	CmP-30SgA-0.65-280	44	70	48	46
3	CmP-30SgB-0.65-280	54	84	54	58
4	CmP-30FaF-0.65-280	87	114	101	105
5	CmP-NoSCM-0.55-340	1	8	5	3
6	CmP-15SgA-0.55-340	23	-1	-15	-14
7	CmP-15SgB-0.55-340	2	21	3	9
8	CmP-15FaF-0.55-340	-1	-19	-58	-55
9	CmP-15FaC-0.55-340	11	-25	-63	-67
10	CmP-NoSCM-0.50-310	-7	-32	-59	-64
11	CmP-15SgA-0.50-310	-18	-25	-74	-66
12	CmP-15SgB-0.50-310	-27	-27	-28	-22

Table 6.9 (continued) Errors in the prediction of total shrinkage by B4s model with the parameters regressed using one-year data

Sl. No	Mix Nomenclature	Error (microstrain) after different drying periods (days)			
		90	365	730	1000
13	CmP-15FaF-0.50-310	22	31	25	26
14	CmP-15FaC-0.50-310	8	-11	-42	-37
15	CmP-30SgB-0.50-310	-31	-53	-92	-91
16	CmP-30FaF-0.50-310	26	-7	-25	-26
17	CmP-30FaC-0.50-310	-42	-60	-92	-83
18	CmP-50SgB-0.50-310	23	49	32	34
19	CmP-50FaF-0.50-310	88	146	157	167
20	CmP-20SgB-20FaF-0.50-310	72	98	90	92
21	CmP-20SgB-20FaC-0.50-310	28	56	31	37
22	CmP-20FaF-20FaC-0.50-310	13	49	26	30
23	CmP-NoSCM-0.60-310	57	68	18	20
24	CmP-15SgA-0.60-310	-17	-67	-80	-76
25	CmP-15SgB-0.60-310	47	52	14	17
26	CmP-15FaF-0.60-310	70	114	88	97
27	CmP-15FaC-0.60-310	-2	8	-17	-9
32	CmA-NoSCM-0.55-340	-85	-27	-3	6
33	CmA-15SgA-0.55-340	-24	31	70	75
34	CmA-15SgB-0.55-340	-40	-21	-1	7
35	CmA-15FaF-0.55-340	-3	28	46	48
36	CmA-15FaC-0.55-340	-13	8	32	32
37	CmA-NoSCM-0.50-310	-37	-15	-2	-2
38	CmA-15SgA-0.50-310	-24	-13	-1	-3
39	CmA-15SgB-0.50-310	-31	10	6	7
40	CmA-15FaF-0.50-310	-39	-26	-19	-13
41	CmA-15FaC-0.50-310	-33	-1	22	13
50	CmA-NoSCM-0.60-310	20	53	67	72
51	CmA-15SgA-0.60-310	-30	48	72	81
52	CmA-15SgB-0.60-310	-1	41	47	54
53	CmA-15FaF-0.60-310	-8	19	36	38
54	CmA-15FaC-0.60-310	59	100	129	127

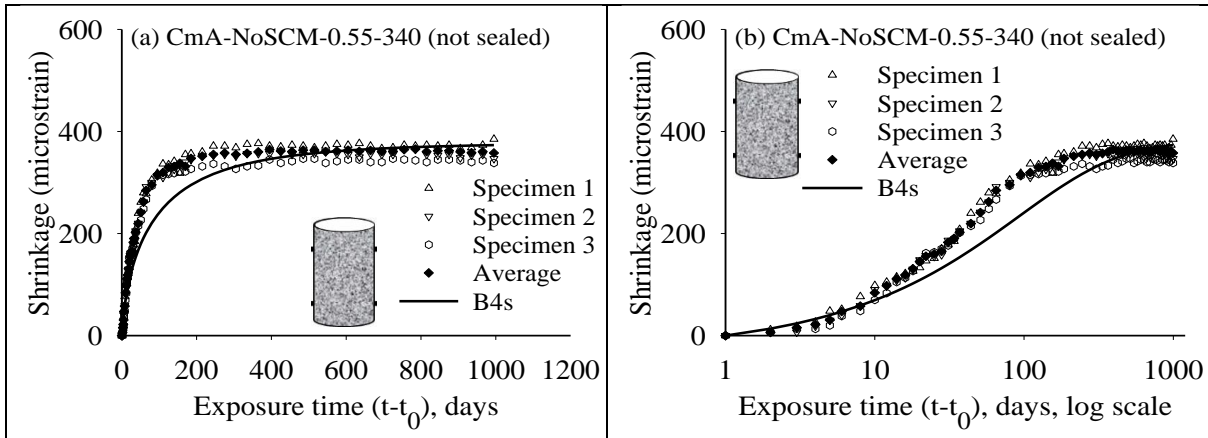


Figure 6.31 Comparison of experimental results and prediction with regressed B4s with two year data for CmA-NoSCM-0.55-340 concrete (unsealed): in (a) normal and (b) log scales

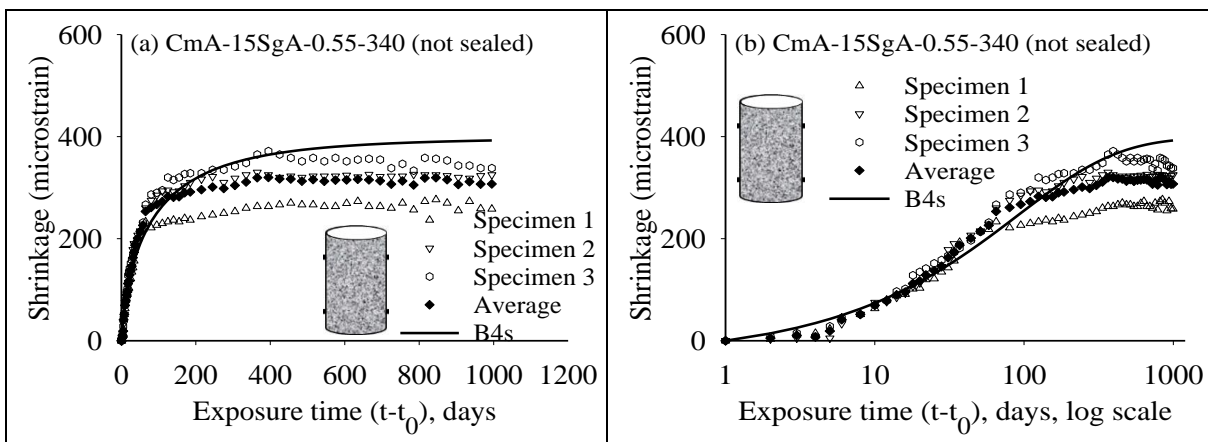


Figure 6.32 Comparison of experimental results and prediction with regressed B4s with two year data for CmA-15SgA-0.55-340 concrete (unsealed): in (a) normal and (b) log scales

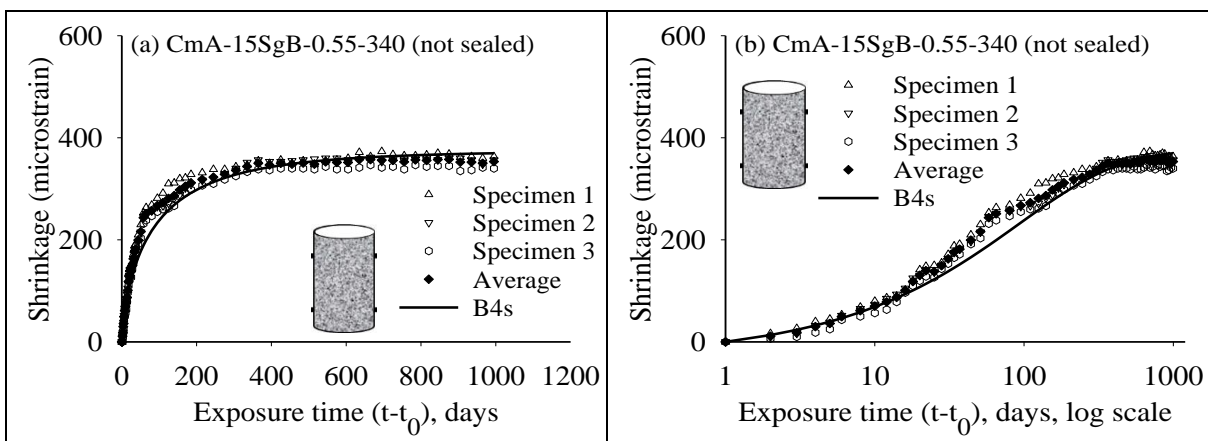


Figure 6.33 Comparison of experimental results and prediction with regressed B4s with two year data for CmA-15SgB-0.55-340 concrete (unsealed): in (a) normal and (b) log scales

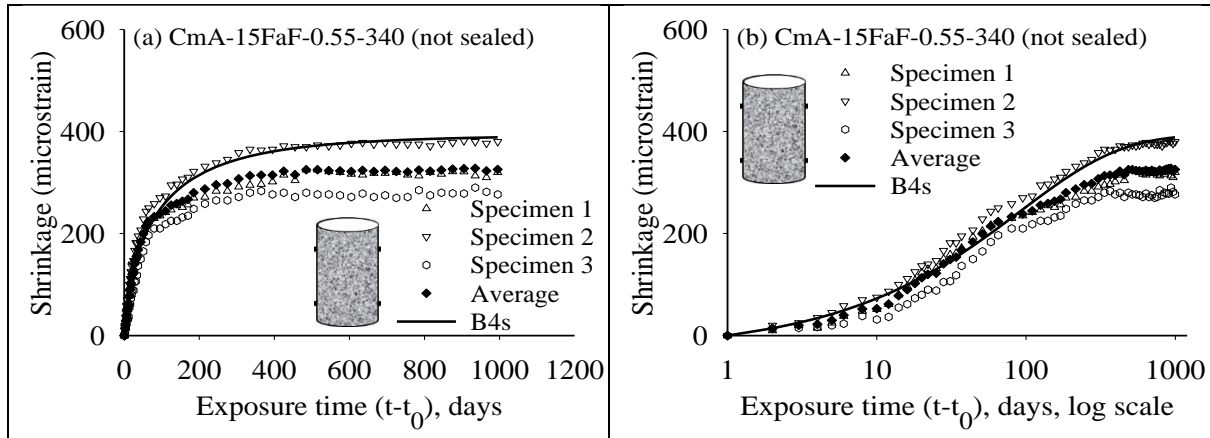


Figure 6.34 Comparison of experimental results and prediction with regressed B4s with two year data for CmA-15FaF-0.55-340 concrete (unsealed):, in (a) normal and (b) log scales

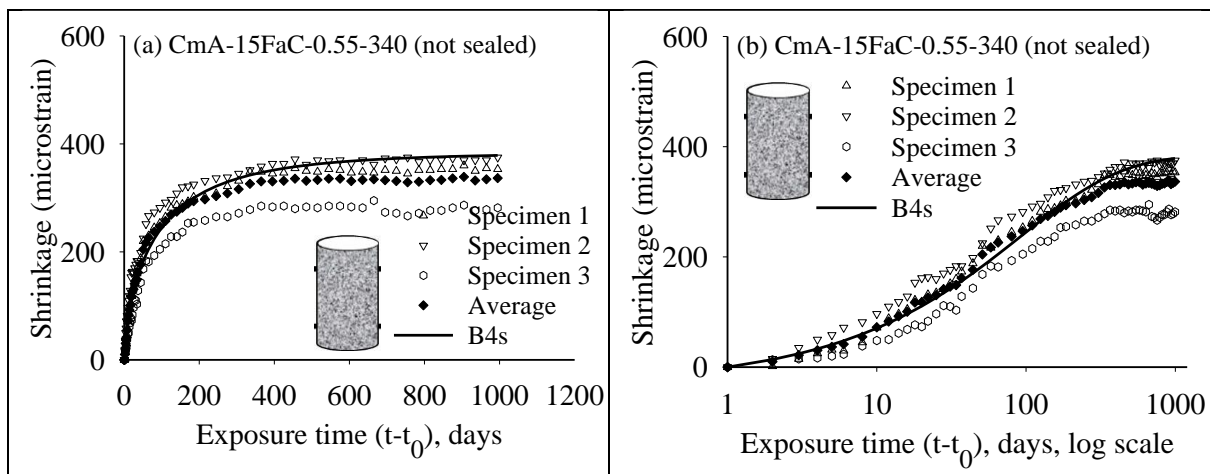


Figure 6.35 Comparison of experimental results and prediction with regressed B4s with two year data for CmA-15FaC-0.55-340 concrete (unsealed): in (a) normal and (b) log scales

Table 6.10 Errors in the prediction of total shrinkage by B4s model using parameters regressed using two-year data.

Sl. No	Mix Nomenclature	Error (microstrain) after different drying periods (days)			
		90	365	730	1000
1	CmP-NoSCM-0.65-280	94	82	18	14
2	CmP-30SgA-0.65-280	51	80	59	57
3	CmP-30SgB-0.65-280	60	93	64	68
4	CmP-30FaF-0.65-280	94	124	111	116
5	CmP-NoSCM-0.55-340	6	16	13	11
6	CmP-15SgA-0.55-340	28	7	-6	-5
7	CmP-15SgB-0.55-340	7	29	11	17
8	CmP-15FaF-0.55-340	3	-13	-51	-49
9	CmP-15FaC-0.55-340	16	-18	-55	-59
10	CmP-NoSCM-0.50-310	-3	-25	-51	-56

Table 6.10 (continued) Errors in the prediction of total shrinkage by B4s model using parameters regressed using two-year data.

Sl. No	Mix Nomenclature	Error (microstrain) after different drying periods (days)			
		90	365	730	1000
11	CmP-15SgA-0.50-310	-14	-18	-66	-59
12	CmP-15SgB-0.50-310	-23	-20	-20	-15
13	CmP-15FaF-0.50-310	24	36	31	33
14	CmP-15FaC-0.50-310	13	-4	-34	-29
15	CmP-30SgB-0.50-310	-27	-46	-85	-84
16	CmP-30FaF-0.50-310	32	2	-17	-17
17	CmP-30FaC-0.50-310	-37	-53	-84	-75
18	CmP-50SgB-0.50-310	28	57	40	42
19	CmP-50FaF-0.50-310	96	158	169	180
20	CmP-20SgB-20FaF-0.50-310	78	107	100	102
21	CmP-20SgB-20FaC-0.50-310	33	64	40	46
22	CmP-20FaF-20FaC-0.50-310	18	57	33	38
23	CmP-NoSCM-0.60-310	62	77	28	29
24	CmP-15SgA-0.60-310	-13	-60	-73	-68
25	CmP-15SgB-0.60-310	19	8	-33	-30
26	CmP-15FaF-0.60-310	76	123	97	107
27	CmP-15FaC-0.60-310	3	16	-8	0
32	CmA-NoSCM-0.55-340	-79	-18	7	15
33	CmA-15SgA-0.55-340	-17	41	80	85
34	CmA-15SgB-0.55-340	-34	-12	8	16
35	CmA-15FaF-0.55-340	9	42	61	63
36	CmA-15FaC-0.55-340	-7	16	42	42
37	CmA-NoSCM-0.50-310	-31	-6	7	8
38	CmA-15SgA-0.50-310	-18	-4	8	6
39	CmA-15SgB-0.50-310	-25	19	16	17
40	CmA-15FaF-0.50-310	-33	-17	-9	-4
41	CmA-15FaC-0.50-310	-27	8	31	22
50	CmA-NoSCM-0.60-310	28	63	79	83
51	CmA-15SgA-0.60-310	-23	58	83	92
52	CmA-15SgB-0.60-310	6	51	57	65
53	CmA-15FaF-0.60-310	-2	28	45	48
54	CmA-15FaC-0.60-310	66	110	140	139

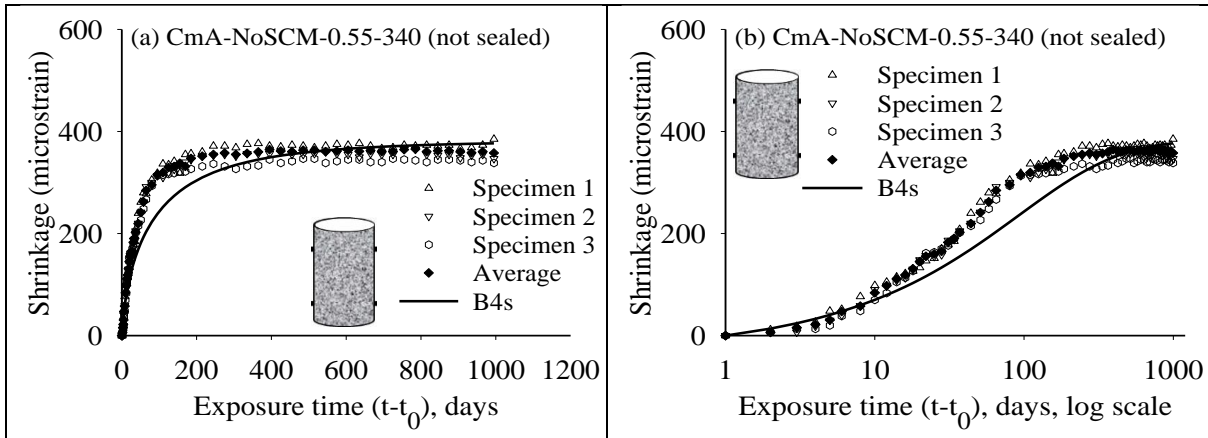


Figure 6.36 Comparison of experimental results and prediction with regressed B4s with three year data for CmA-NoSCM-0.55-340 concrete (unsealed): in (a) normal and (b) log scales

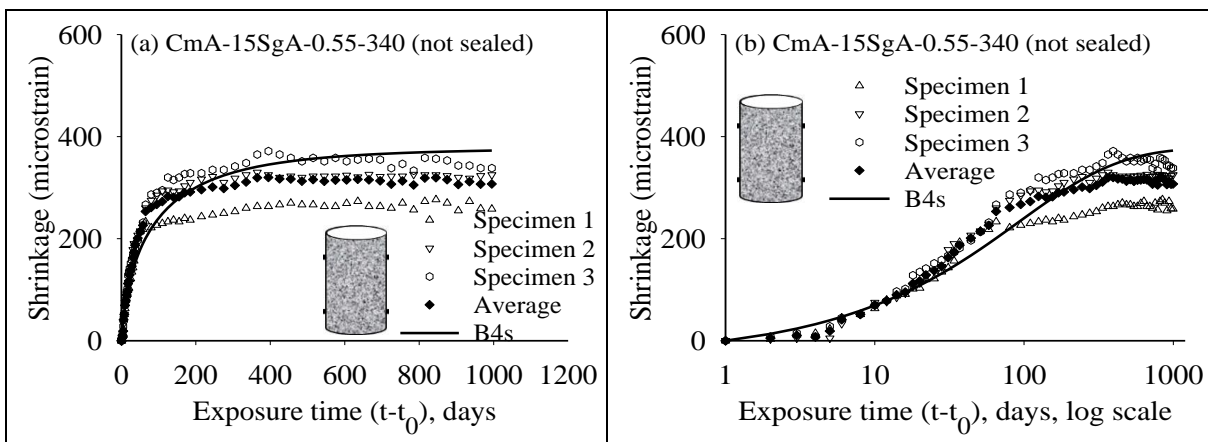


Figure 6.37 Comparison of experimental results and prediction with regressed B4s with three year data for CmA-15SgA-0.55-340 concrete (unsealed), in (a) normal and (b) log scales

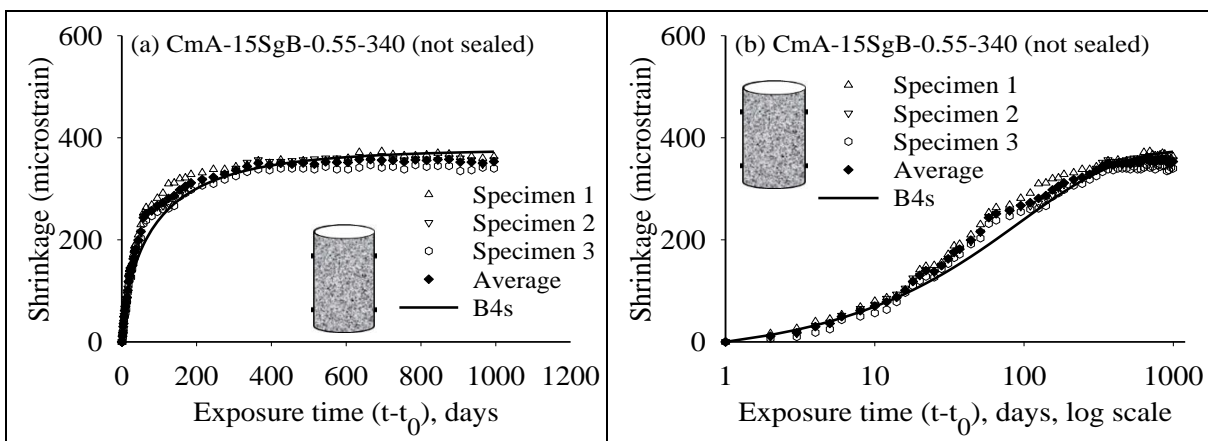


Figure 6.38 Comparison of experimental results and prediction with regressed B4s with three year data for CmA-15SgB-0.55-340 concrete (unsealed), in (a) normal and (b) log scales

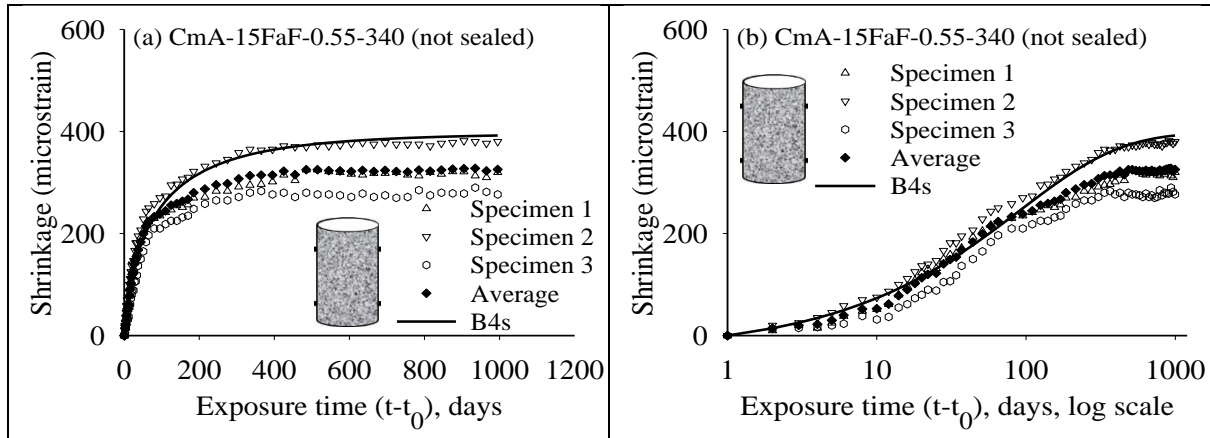


Figure 6.39 Comparison of experimental results and prediction with regressed B4s with three year data for CmA-15FaF-0.55-340 concrete (unsealed), in (a) normal and (b) log scales

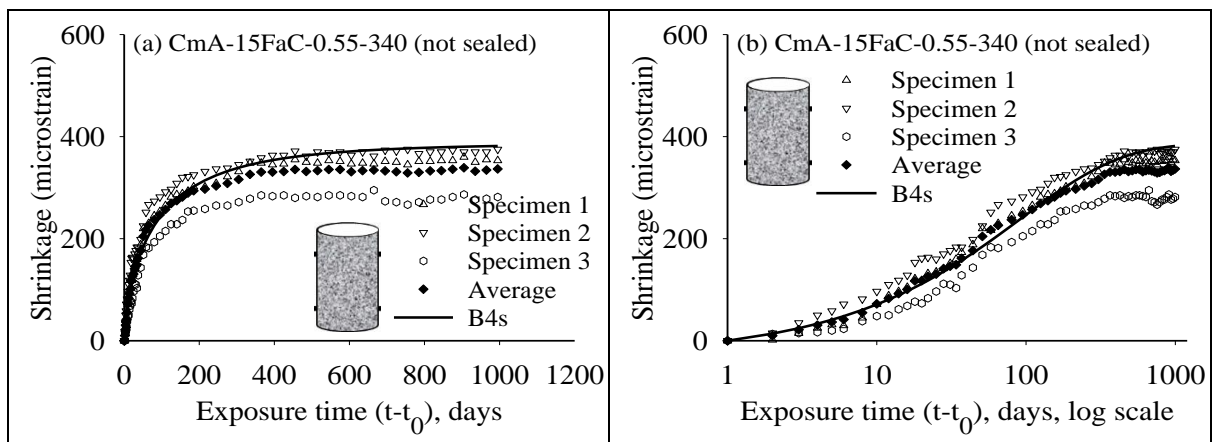


Figure 6.40 Comparison of experimental results and prediction with regressed B4s with three year data for CmA-15FaC-0.55-340 concrete (unsealed), in (a) normal and (b) log scales

Table 6.11 Errors in the predictions of total shrinkage by B4s model with parameters regressed with three-year data.

Sl. No	Mix Nomenclature	Errors (microstrain) after different drying periods (days)			
		90	365	730	1000
1	CmP-NoSCM-0.65-280	95	84	21	16
2	CmP-30SgA-0.65-280	52	82	60	59
3	CmP-30SgB-0.65-280	61	94	66	70
4	CmP-30FaF-0.65-280	95	126	114	118
5	CmP-NoSCM-0.55-340	7	17	15	12
6	CmP-15SgA-0.55-340	29	9	-4	-4
7	CmP-15SgB-0.55-340	7	30	12	19
8	CmP-15FaF-0.55-340	4	-11	-50	-47
9	CmP-15FaC-0.55-340	17	-17	-54	-57
10	CmP-NoSCM-0.50-310	-2	-23	-50	-54
11	CmP-15SgA-0.50-310	-13	-17	-65	-58

Table 6.11 (continued) Errors in the predictions of total shrinkage by B4s model with parameters regressed with three-year data.

Sl. No	Mix Nomenclature	Errors (microstrain) after different drying periods (days)			
		90	365	730	1000
12	CmP-15SgB-0.50-310	-22	-19	-20	-14
13	CmP-15FaF-0.50-310	28	41	36	37
14	CmP-15FaC-0.50-310	14	-2	-32	-28
15	CmP-30SgB-0.50-310	-26	-45	-84	-82
16	CmP-30FaF-0.50-310	33	3	-15	-15
17	CmP-30FaC-0.50-310	-36	-52	-83	-74
18	CmP-50SgB-0.50-310	29	58	41	43
19	CmP-50FaF-0.50-310	97	160	171	182
20	CmP-20SgB-20FaF-0.50-310	79	109	102	104
21	CmP-20SgB-20FaC-0.50-310	34	66	42	47
22	CmP-20FaF-20FaC-0.50-310	19	58	35	39
23	CmP-NoSCM-0.60-310	63	78	29	30
24	CmP-15SgA-0.60-310	-12	-59	-71	-66
25	CmP-15SgB-0.60-310	20	9	-32	-29
26	CmP-15FaF-0.60-310	77	125	99	109
27	CmP-15FaC-0.60-310	5	18	-6	2
32	CmA-NoSCM-0.55-340	-77	-15	10	19
33	CmA-15SgA-0.55-340	-15	44	83	89
34	CmA-15SgB-0.55-340	-32	-9	11	19
35	CmA-15FaF-0.55-340	11	45	65	67
36	CmA-15FaC-0.55-340	-5	19	45	45
37	CmA-NoSCM-0.50-310	-29	-4	10	11
38	CmA-15SgA-0.50-310	-16	-1	11	9
39	CmA-15SgB-0.50-310	-23	21	18	19
40	CmA-15FaF-0.50-310	-31	-14	-6	-1
41	CmA-15FaC-0.50-310	-25	11	35	26
50	CmA-NoSCM-0.60-310	30	66	82	87
51	CmA-15SgA-0.60-310	-20	61	87	96
52	CmA-15SgB-0.60-310	8	53	60	68
53	CmA-15FaF-0.60-310	0	31	49	52
54	CmA-15FaC-0.60-310	69	114	144	143

6.4.2 Effect of aggregate type in the B4 prediction model

As detailed in the study of the B4 model, the influence of the aggregate type used in the concrete is explicitly considered; it is suggested that a value of 1 be taken when information on aggregate type is unknown. Therefore, the aggregate dependent parameter scaling factors k_{ta} and k_{ca} were taken as 1 in the calculation, and the evolution of the shrinkage strain was compared with the laboratory test data. Note that in Section 6.3.2 the model prediction was made taking the aggregate parameters as that of granite. It can be seen in Figure 6.41 through Figure 6.45 that the change in aggregate parameters causes over-estimation of early shrinkage in some cases. Appendix D7 gives the predictions for all concretes and the comparisons with experimental data.

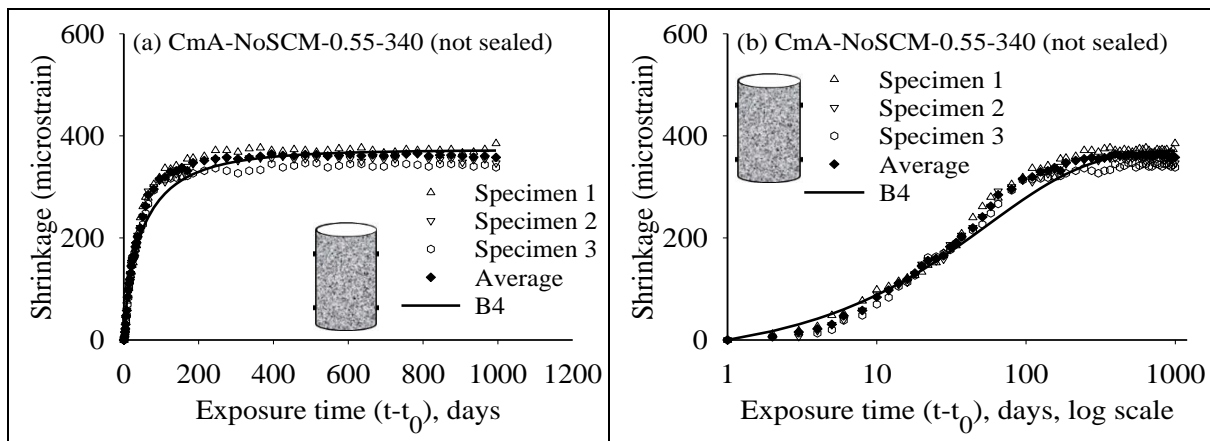


Figure 6.41 Comparison of experimental data and B4 predictions by considering aggregates as unknown for CmA-NoSCM-0.55-340 concrete (unsealed): in (a) normal and (b) log scales

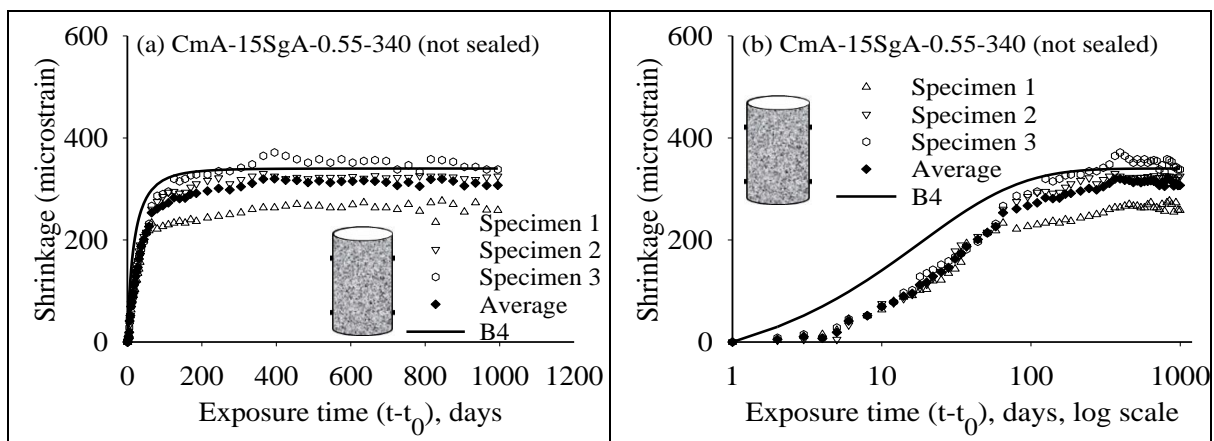


Figure 6.42 Comparison of experimental data and B4 predictions by considering aggregates as unknown for CmA-15SgA-0.55-340 concrete (unsealed): in (a) normal and (b) log scales

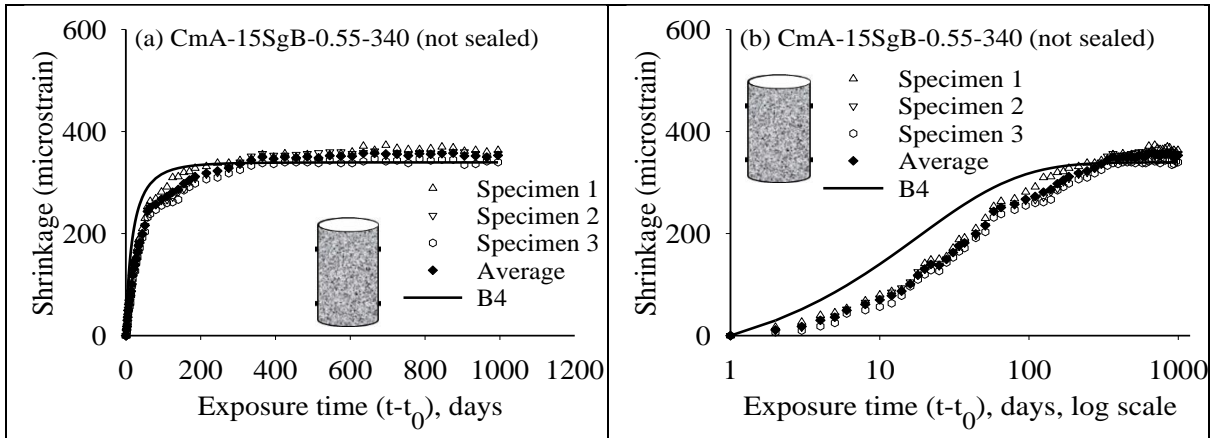


Figure 6.43 Comparison of experimental data and B4 predictions by considering aggregates as unknown for CmA-15SgB-0.55-340 concrete (unsealed): in (a) normal and (b) log scales

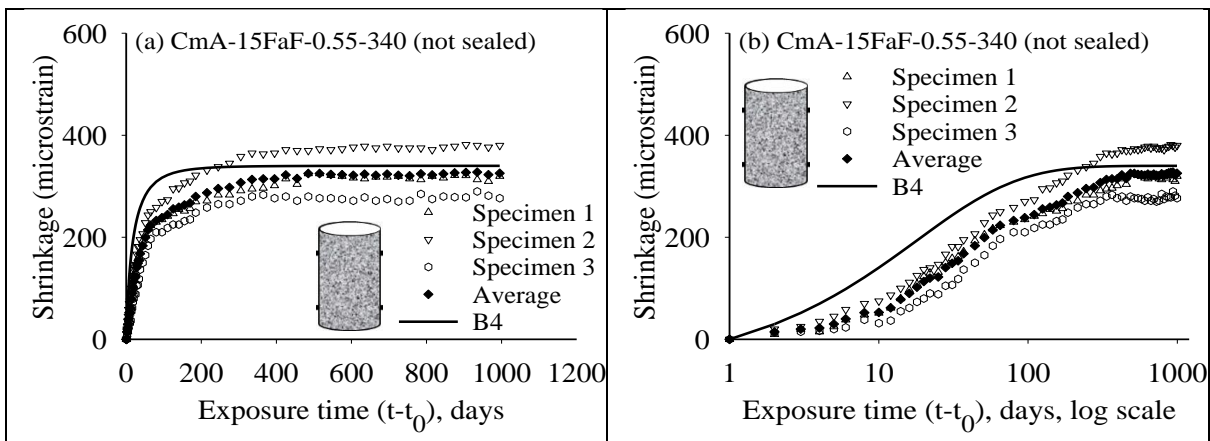


Figure 6.44 Comparison of experimental data and B4 predictions by considering aggregates as unknown for CmA-15FaF-0.55-340 concrete (unsealed): in (a) normal and (b) log scales

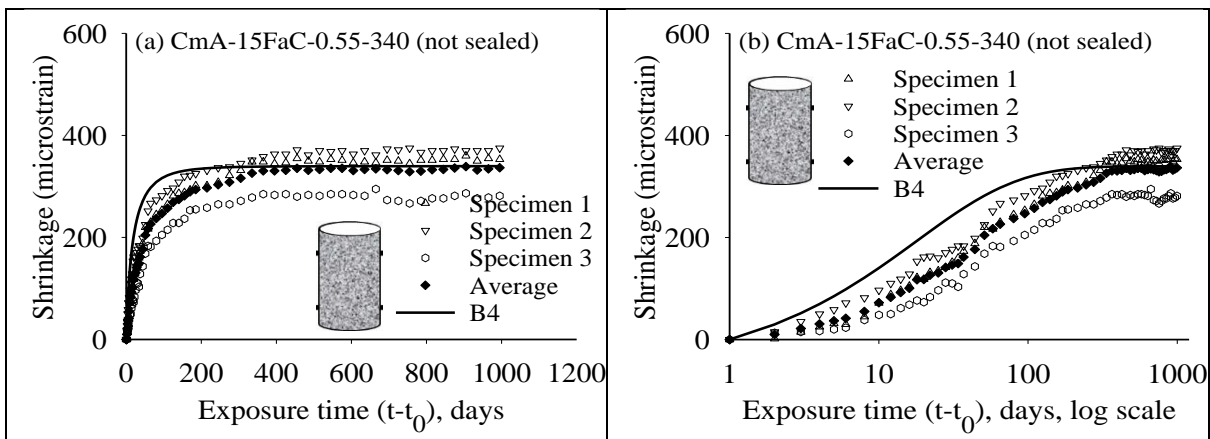


Figure 6.45 Comparison of experimental data and B4 predictions by considering aggregates as unknown for CmA-15FaC-0.55-340 concrete (unsealed): in (a) normal and (b) log scales

Table 6.12 shows that the modified parameters lead to overall under-prediction of the long-term data, which suggest that more calibration for the aggregate type may be needed.

Table 6.12. Errors in the prediction of total shrinkage by B4 prediction model by considering aggregate type as unknown.

Sl. No.	Mix Nomenclature	Errors (microstrain) at different drying periods (days)			
		90	365	730	1000
1	CmP-NoSCM-0.65-280	87	27	-54	-63
2	CmP-30SgA-0.65-280	85	27	-20	-28
3	CmP-30SgB-0.65-280	101	46	-9	-11
4	CmP-30FaF-0.65-280	80	1	-41	-42
5	CmP-NoSCM-0.55-340	52	41	26	20
6	CmP-15SgA-0.55-340	111	-7	-47	-52
7	CmP-15SgB-0.55-340	115	51	7	8
8	CmP-15FaF-0.55-340	86	-23	-87	-91
9	CmP-15FaC-0.55-340	112	-10	-73	-82
10	CmP-NoSCM-0.50-310	-2	-63	-105	-114
11	CmP-15SgA-0.50-310	45	-47	-120	-118
12	CmP-15SgB-0.50-310	35	-50	-76	-76
13	CmP-15FaF-0.50-310	32	-63	-95	-100
14	CmP-15FaC-0.50-310	37	-79	-135	-137
15	CmP-30SgB-0.50-310	18	-71	-133	-138
16	CmP-30FaF-0.50-310	37	-78	-121	-127
17	CmP-30FaC-0.50-310	0	-89	-145	-141
18	CmP-50SgB-0.50-310	52	15	-24	-28
19	CmP-50FaF-0.50-310	17	-32	-49	-44
20	CmP-20SgB-20FaF-0.50-310	64	11	-22	-25
21	CmP-20SgB-20FaC-0.50-310	49	10	-37	-37
22	CmP-20FaF-20FaC-0.50-310	43	15	-31	-32
23	CmP-NoSCM-0.60-310	67	40	-25	-27
24	CmP-15SgA-0.60-310	90	-50	-89	-90
25	CmP-15SgB-0.60-310	73	-49	-118	-122
26	CmP-15FaF-0.60-310	129	66	12	15
27	CmP-15FaC-0.60-310	72	-19	-71	-69
32	CmA-NoSCM-0.55-340	-41	-4	8	13
33	CmA-15SgA-0.55-340	49	20	33	33
34	CmA-15SgB-0.55-340	49	-11	-16	-14
35	CmA-15FaF-0.55-340	78	25	18	15
36	CmA-15FaC-0.55-340	70	8	9	3
37	CmA-NoSCM-0.50-310	-45	-61	-64	-67
38	CmA-15SgA-0.50-310	2	-73	-86	-94

Table 6.12 (continued) Errors in the prediction of total shrinkage by B4 prediction model by considering aggregate type as unknown

Sl. No.	Mix Nomenclature	Errors (microstrain) at different drying periods (days)			
		90	365	730	1000
39	CmA-15SgB-0.50-310	7	-34	-61	-66
40	CmA-15FaF-0.50-310	-6	-75	-93	-93
41	CmA-15FaC-0.50-310	-6	-60	-61	-76
50	CmA-NoSCM-0.60-310	18	12	11	12
51	CmA-15SgA-0.60-310	16	-1	-3	1
52	CmA-15SgB-0.60-310	72	27	8	10
53	CmA-15FaF-0.60-310	52	-12	-20	-23
54	CmA-15FaC-0.60-310	71	7	8	1
55	CmP-NoSCM-0.50-310x	-53	-121	-161	-160
56	CmP-30FaF-0.45-310	-80	-113	-176	Data N.A
57	LC3-NoSCM-0.50-310	-63	-186	-220	
58	CmP-NoSCM-0.40-360	-65	-120	-129	
59	CmP-30FaF-0.35-380	-48	-37	-10	
60	LC3-NoSCM-0.40-340	-161	-310	-348	
61	CmP-NoSCM-0.45-360	-47	-102	-97	
62	CmP-30FaF-0.45-360	-79	-13	6	
63	LC3-NoSCM-0.45-360	-22	-34	-32	

6.4.3 Effect of binder composition on the B4 standard prediction model

Instead of OPC, an attempt was considered that blended cement was used in the prediction with the B4 model in line with the practice in India to use 5% performance enhancer. Therefore, instead of using 100% OPC in the model, a blended cement with 95% OPC and 5% SCM (in this case, fly ash or slag) was tried. Consequently, the scaling factors for the SCMs (mineral admixtures as mention in the model) corresponds to $\leq 15\%$ replacement level. The scaling factor will change according to the SCM content in the mix as mentioned in Table 2.4. For example, the binder of 15% fly ash replacement is now considered as 20% fly ash replacement. Figure 6.46 through Figure 6.50 show the prediction with the modified cases along with the experimental data. In general, the overall prediction seems better but the final value is over-estimated. This again may be need further study. Appendix D8 gives the comparison of the predictions with the modified parameters and the experimental data for all concretes.

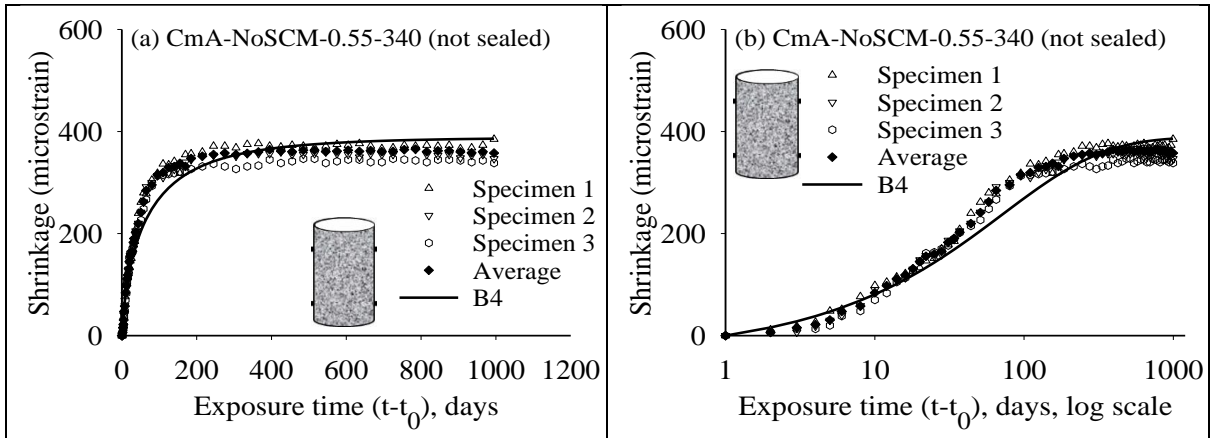


Figure 6.46 Comparison of experimental results and B4 prediction by considering the effect of binder composition and aggregate as granite for CmA-NoSCM-0.55-340 concrete (unsealed): in (a) normal and (b) log scales

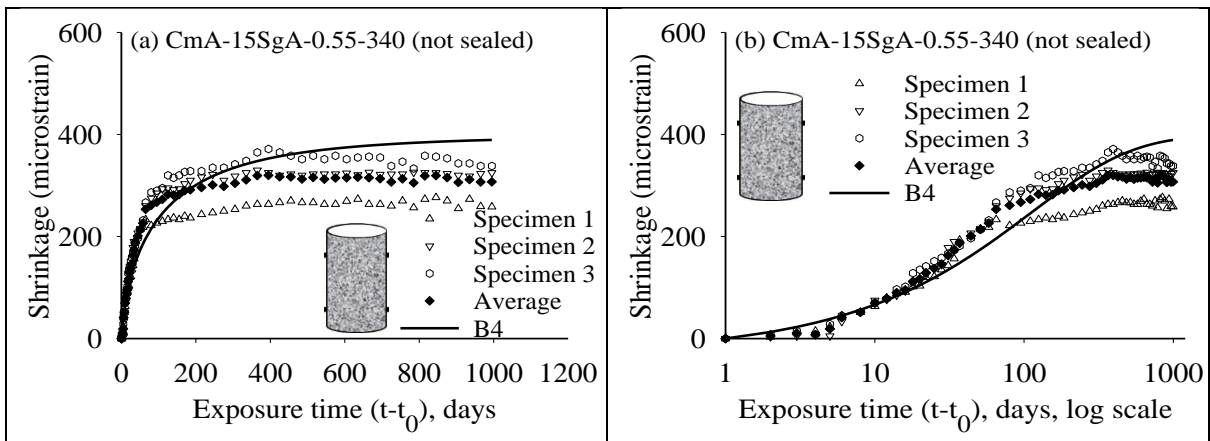


Figure 6.47 Comparison of experimental results and B4 prediction by considering the effect of binder composition and aggregate as granite for CmA-15SgA-0.55-340 concrete (unsealed): in (a) normal and (b) log scales

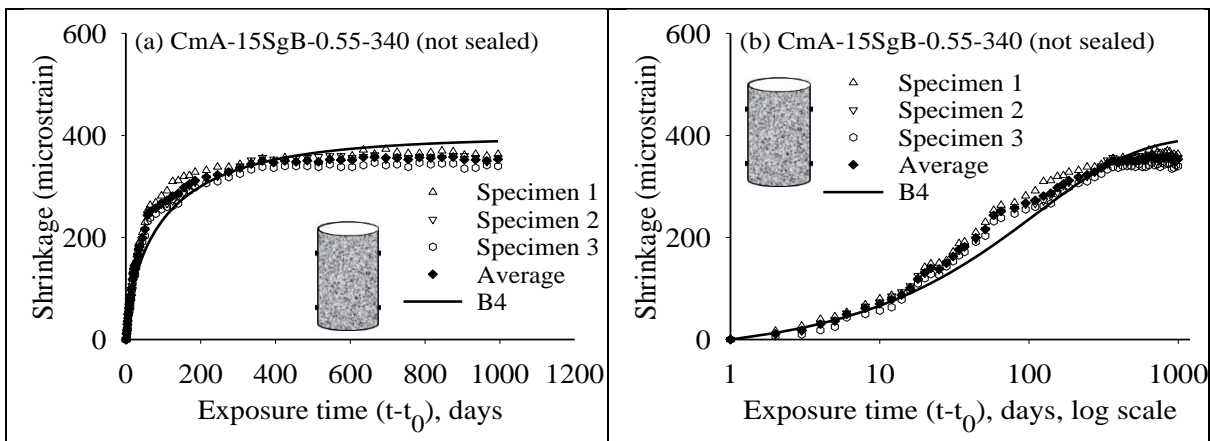


Figure 6.48 Comparison of experimental results and B4 prediction by considering the effect of binder composition and aggregate as granite for CmA-15SgB-0.55-340 concrete (unsealed): in (a) normal and (b) log scales

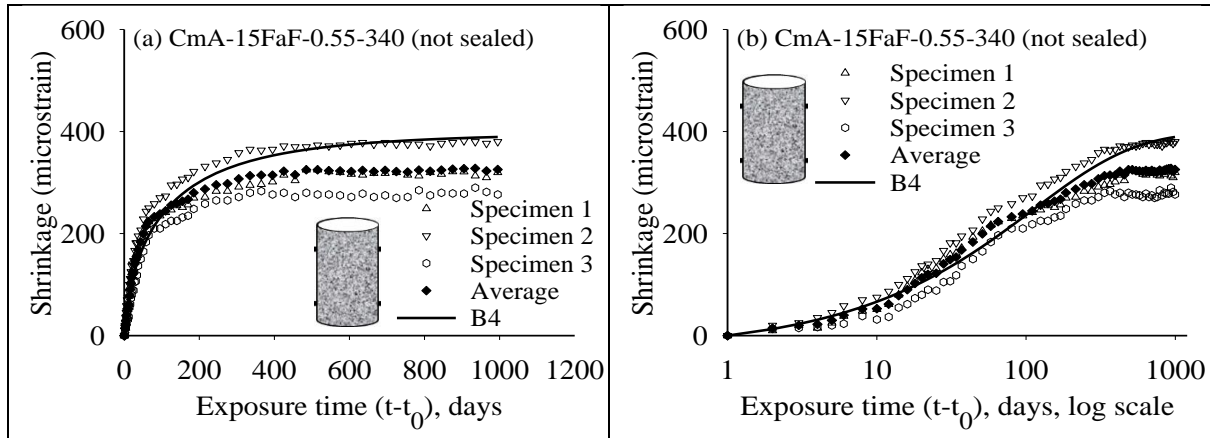


Figure 6.49 Comparison of experimental results and B4 prediction by considering the effect of binder composition and aggregate as granite for CmA-15FaF-0.55-340 concrete (unsealed): in (a) normal and (b) log scales

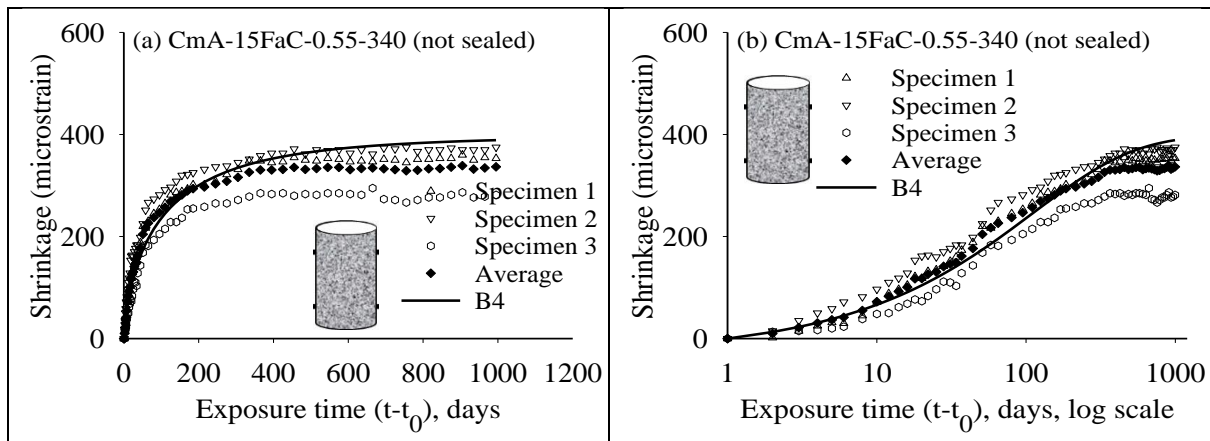


Figure 6.50 Comparison of experimental results and B4 prediction by considering the effect of binder composition and aggregate as granite for CmA-15FaC-0.55-340 concrete (unsealed): in (a) normal and (b) log scales

In Table 6.13, it can be seen that the errors in the prediction with the modified parameters for the cement indicate that the overall prediction is satisfactory. However, there are cases such as LC3 concrete where the predictions are worse than before.

Table 6.13 Errors in the prediction of total shrinkage by B4 prediction model by considering the effect of cement composition and aggregate as granite.

Sl. No	Mix Nomenclature	Errors (microstrain) at different drying periods (days)			
		90	365	730	1000
1	CmP-NoSCM-0.65-280	78	37	-37	-45
2	CmP-30SgA-0.65-280	2	31	20	24
3	CmP-30SgB-0.65-280	16	49	31	40
4	CmP-30FaF-0.65-280	-5	4	0	10
5	CmP-NoSCM-0.55-340	41	48	40	35
6	CmP-15SgA-0.55-340	12	0	-5	-2

Table 6.13 (continued) Errors in the prediction of total shrinkage by B4 prediction model by considering the effect of cement composition and aggregate as granite

Sl. No	Mix Nomenclature	Error (microstrain) at different drying periods (days)			
		90	365	730	1000
7	CmP-15SgB-0.55-340	16	58	49	59
8	CmP-15FaF-0.55-340	-9	-15	-45	-40
9	CmP-15FaC-0.55-340	16	-3	-31	-31
10	CmP-NoSCM-0.50-310	-13	-60	-96	-104
11	CmP-15SgA-0.50-310	-32	-39	-84	-76
12	CmP-15SgB-0.50-310	-42	-42	-40	-33
13	CmP-15FaF-0.50-310	-43	-54	-60	-57
14	CmP-15FaC-0.50-310	-38	-70	-100	-94
15	CmP-30SgB-0.50-310	-55	-74	-104	-99
16	CmP-30FaF-0.50-310	-36	-81	-92	-88
17	CmP-30FaC-0.50-310	-74	-92	-115	-102
18	CmP-50SgB-0.50-310	-22	-1	-11	-5
19	CmP-50FaF-0.50-310	-58	-49	-35	-21
20	CmP-20SgB-20FaF-0.50-310	-10	-6	-8	-2
21	CmP-20SgB-20FaC-0.50-310	-25	-6	-23	-14
22	CmP-20FaF-20FaC-0.50-310	-31	-1	-17	-9
23	CmP-NoSCM-0.60-310	56	49	-9	-10
24	CmP-15SgA-0.60-310	-4	-41	-46	-39
25	CmP-15SgB-0.60-310	-24	-40	-75	-70
26	CmP-15FaF-0.60-310	32	75	55	66
27	CmP-15FaC-0.60-310	-24	-10	-28	-17
32	CmA-NoSCM-0.55-340	-51	3	21	28
33	CmA-15SgA-0.55-340	-36	28	74	82
34	CmA-15SgB-0.55-340	-36	-3	25	35
35	CmA-15FaF-0.55-340	-7	33	60	64
36	CmA-15FaC-0.55-340	-16	17	50	52
37	CmA-NoSCM-0.50-310	-55	-58	-55	-58
38	CmA-15SgA-0.50-310	-65	-63	-51	-52
39	CmA-15SgB-0.50-310	-59	-24	-26	-24
40	CmA-15FaF-0.50-310	-72	-66	-58	-51
41	CmA-15FaC-0.50-310	-59	-51	-24	-19
50	CmA-NoSCM-0.60-310	19	30	30	33
51	CmA-15SgA-0.60-310	-68	10	39	51
52	CmA-15SgB-0.60-310	-12	38	50	60
53	CmA-15FaF-0.60-310	-32	-1	22	27
54	CmA-15FaC-0.60-310	-13	17	50	51

Table 6.13 (continued) Error in the prediction of total shrinkage by B4 prediction model by considering the effect of cement composition and aggregate as granite

Sl. No	Mix Nomenclature	Errors (microstrain) at different drying periods (days)			
		90	365	730	1000
55	CmP-NoSCM-0.50-310x	-10	-141	-196	-199
56	CmP-30FaF-0.45-310	-10	-97	-190	Data N.A
57	LC3-NoSCM-0.50-310	-20	-206	-255	
58	CmP-NoSCM-0.40-360	-21	-136	-160	
59	CmP-30FaF-0.35-380	13	-20	-19	
60	LC3-NoSCM-0.40-340	-122	-325	-378	
61	CmP-NoSCM-0.45-360	1	-121	-133	
62	CmP-30FaF-0.45-360	-4	6	-7	
63	LC3-NoSCM-0.45-360	24	-52	-68	

7. CONCLUSIONS AND SCOPE FOR FUTURE WORK

7.1 GENERAL CONCLUSIONS

The use of supplementary cementitious materials (SCMs) is one way to reduce the carbon footprint of cement/concrete industry. Because of this and due to the benefits of SCMs in enhancing the strength and durability of concrete systems, the use of many SCMs has seen remarkable growth in the last few decades. For example, the last few decades have witnessed remarkable growth in the use of fly ash and slag in concrete. Also, the use of limestone calcined in concrete has also increased recently. For any concrete structure, understanding the compressive strength, elastic modulus, and shrinkage behaviour of concrete is important to ensure crack resistance and desired long-term structural and durability performance. Significant information on shrinkage characteristics of concretes used abroad (with fly ash and slag) has been reported. However, such information on concretes made with fly ash and slag sourced from India is very limited. Moreover, very limited information is available on the shrinkage characteristics of concretes made with limestone calcined clay systems.

This thesis performed an extensive 3-year laboratory exposure study and determined the effect of fly ash, slag, and limestone calcined clay systems on the compressive strength, elastic modulus and shrinkage of concrete. From the present research work, it can be concluded that the incorporation of SCMs increases the compressive strength of concrete at later ages. However, slag and fly ash lead to slower early age strength evolution due to their slow pozzolanic reactivity and lower surface area. Additionally, the investigation provides broad information on the shrinkage response of SCM blended concrete in the Indian context. Shrinkage of concrete is dependent on the type and composition of cementitious materials, mixture proportion of such materials in concrete, type of aggregates in concrete, etc. The parameters investigated in this study were water-to-binder ratio, total binder content, and type and dosage of the SCM. In general, it can be concluded that the partial replacement of Ordinary Portland cement with SCMs do not significantly change the shrinkage properties of concrete. This thesis also evaluated the various shrinkage prediction models and their applicability to the concretes made with fly ash, slag, limestone calcined clay systems available in India.

7.2 SPECIFIC CONCLUSIONS

On the basis of the results obtained from the laboratory experimental programme, analysis of the results and the assessment of the shrinkage prediction models, the following specific conclusions have been drawn.

7.2.1 Effect of slag and fly ash on compressive strength development and elastic modulus of concrete

- The fly ash blended concrete shows a significant increase in the compressive strength beyond 28 days of curing, However, the same trend was not observed in the case of slag blended concrete systems
- Incorporation of Class C fly ash, up to 30% by the weight of the binder increases the compressive strength by 5 to 10 MPa. This is also true in the case of Class F fly ash except during the early ages of testing.
- The compressive strength development of high volume (at 50% replacement of cement) slag and fly ash blended concrete is initially slower than that of control concrete; however, at age of 90 days and beyond, the two concretes attained similar strength level. The ternary blended concrete shows a marginal increase in the compressive strength of about 5 to 8 % than the binary blended systems at a prolonged curing time.
- LC3 concrete showed higher gain in compressive strength, by about 8 to 10% more than OPC and fly ash blended concrete with prolonged curing. Additionally, the total binder content required to make high strength concrete (say, M50) was lower in the case of LC3 compared to that of the other binders. In the case of concrete made with $w/b = 0.45$ and total binder content 340 kg/m^3 , the LC3 system yields higher compressive strength (say, 10% higher) at all ages of testing.
- The time dependent strength development, as given in ACI 209, seems to estimate better beyond 28 days, while the estimates at 2 and 7 days seems to be conservative. The FaF concrete behaves differently than the prediction with a higher rate of increase in strength from 90 to 365 days when compared to the OPC mixes.
- The static elastic modulus of concrete increased with an increase in the compressive strength, and the relation between the compressive strength and the elastic modulus was similar for both blended and non-blended concrete systems. In the case of LC3 concrete,

the elastic modulus was comparable with the conventional OPC concrete. It is clear from this study, that the ACI 209 and ACI 318 model predictions for the elastic modulus of concrete are more conservative than the recommendations of IS 456 and *fib* MC 2010.

7.2.2 Effect of slag and fly ash on shrinkage response of concrete

- It can be concluded that the influence of SCMs on shrinkage response is highly variable and cannot be generalized, though no significant difference was observed in the shrinkage strains within the group of concretes studied here. The shrinkage of high-volume slag and fly ash blended concrete was lower than the OPC concrete.
- The source of slag was insignificant on the shrinkage evolution and the two fly ashes (FaF and FaC) is either higher than or equal to that of the OPC concrete.
- At 800 days of exposure, the total shrinkage of LC3 concrete in the case of M30 grade concrete is about 6% higher than the OPC and FAF concrete. Also, it is marginally higher (say, 70%) than in fly ash blended concrete systems for M50 concrete. This could be attributed to higher water to binder ratio adopted for the LC3 concrete systems. However, there was no clear difference in the evolution of the shrinkage strain between the concretes
- Concrete with water-binder ratio less than 0.40 yields higher additional autogenous shrinkage of about 100 microstrain in comparison with high water to binder ratio (say, ≥ 0.50), even after the curing period. Also, increasing the amount of binder content with lower w/b increases the autogenous shrinkage of concrete around of 70 to 120 microstrain.

7.2.3 Application of shrinkage prediction models for blended cement concrete

- All the shrinkage prediction models are satisfactory, except *fib* Model Code 2010 equation seems to overpredict the shrinkage.
- The error in the prediction of total shrinkage by IS 1343 model at the age of 90 and 1000 days of drying was 130 and 75 microstrain, respectively. However, the *fib* Model Code 2010 over-estimates the strain by about 50% at the end of 1000 days. In the case

of the B4s prediction model, the error is in the higher range of -10 to 240 microstrain at the end of 1000 days of exposure.

- The B4s model parameters have been calibrated using the measurements by regression analysis (B4s-R) to capture the later age shrinkage of concrete, and the numerical predictions have been found to be in agreement with the experimental results at the end of 90, 365, 730 and 1000 days of drying, with an error of about 10 to 15% at the specified days in comparison with the B4s model.

7.3 RECOMMENDATIONS FOR FUTURE WORK

The research work presented in this thesis has focussed on the influence of SCMs on the short and long-term performance of concrete. However, further investigations are still required. The following are the recommendations for possible future studies related to this research work.

- Detailed investigations on the effect of slag and fly ash on the long-term creep response of concrete is required.
- Future research may include the effect of other SCMs, such as silica fume and metakaolin, on the long-term mechanical performance of concretes.
- The present study focused on the shrinkage response of normal strength concrete. Hence, further studies are needed on the behaviour of high strength/performance concrete. Also, an extended research work is required to study the early age shrinkage response of blended cement concrete.
- Further research could include the influence of curing condition and period, and the effect of the type of coarse aggregates on the long-term creep and shrinkage response of concrete.

8. REFERENCES

- ACI 209.2R** (2008). Guide for Modelling and Calculating Shrinkage and Creep in Hardened Concrete, *American Concrete Institute, USA*.
- ACI 232.2R-96** (2002). Use of Fly Ash in Concrete. *American Concrete Institute, USA*.
- ACI 233R-95** (2000). Ground granulated blast furnace slag as cementitious constituents in concrete. *American Concrete Institute, USA*
- ACI 318** (2014) Building Code Requirements for Structural Concrete, *American Concrete Institute, USA*.
- Akkaya, Y., and Konsta, M.** (2004). The pore structure and autogenous shrinkage of high-performance concrete with ternary binders
- Akkaya, Y., Ouyang, C., and Shah, S. P.** (2007). Effect of supplementary cementitious materials on shrinkage and crack development in concrete. *Cement and Concrete Composites*, pp.117-123.
- Almudaiheem, J., and Hansen, W.** (1987). Effect of specimen size and shape on drying shrinkage of concrete, *ACI Materials Journal*, pp.130-135.
- Alsayed, S. H.** (1998). Influence of superplasticizers, plasticizers, and silica fume on the drying shrinkage of high strength concrete subjected to hot dry field conditions, *Cement and Concrete Research*, pp.1405-1415.
- Al-Sugair, F. H.** (1995). Analysis of time dependent volume reduction of concrete containing silica fume. *Magazine of Concrete Research*, pp. 77-81.
- Antoni, M., Rossen, J., Martirena, F., and Scrivener, K. L. (2012).** Cement substitution by a combination of metakaolin and limestone. *Cement and Concrete Research*, pp. 1579-1589.
- ASTM C1064** (2012). Standard Test Method for Temperature of Freshly Mixed Hydraulic-Cement Concrete, *American Society of Testing and Materials, USA*.
- ASTM C143** (2000) Standard test method for slump of hydraulic-cement concrete, *Annual book of ASTM standards, USA*.
- ASTM C157** (2008). Standard Test Method for Length Change of Hardened Hydraulic-Cement Mortar and Concrete, *American Society of Testing and Materials, USA*.
- ASTM C204** (2011) Standard test methods for fineness of hydraulic cement by air permeability apparatus, *American Society for Testing and Materials, USA*.
- ASTM C231** (1997). Standard test method for air content of freshly mixed concrete by pressure method, *Annual book of ASTM standards, West Conshohocken, PA, USA*.
- ASTM C469** (2010). Standard Test Method for Static Modulus of Elasticity and Poisson's Ratio of Concrete in Compression, *American Society of Testing and Materials, USA*.
- ASTM: C138** (2001) Standard test method for density (unit weight), yield, and air content (gravimetric) of concrete, *Annual book of ASTM standards, USA*.

- Atis, C. D.** (2003). High-volume fly ash concrete with high strength and low drying shrinkage. *Journal of Materials in Civil Engineering*, pp.153-156.
- Atis, C. D., Bilim, C., Celik, O., and Karahan, O.** (2009). Influence of activator on the strength and drying shrinkage of alkali-activated slag mortar. *Construction and Building Materials*, pp. 548-555.
- Atis, C. D., Kilic, A., and Sevim U. K.** (2004). Strength and shrinkage properties of mortar containing a nonstandard high calcium fly ash. *Cement and Concrete Research*, pp.99-102.
- Atis, C.D., and Bilim, C.** (2007). Wet and dry cured compressive strength of concrete containing ground granulated blast-furnace slag. *Building and Environment*, pp. 3060-3065
- Bissonnette, B., Pierre, P., and Pigeon, M.** (1999). Influence of key parameters on drying shrinkage of cementitious materials. *Cement and Concrete Research*, pp.1655-1662.
- Bleszynski, R., Hooton, R. D., Thomas, M. D. A., and Rogers, C. A.** (2002). Durability of ternary blend concrete with silica fume and blast-furnace slag: Laboratory and outdoor exposure site studies. *ACI Materials Journals*, pp. 499-508.
- Bloom, R. and Bentur, A.** (1995). Free and restrained shrinkage of normal and high strength concretes, *ACI Materials Journal*, pp. 211-217.
- Borsoi, A., Colleparidi, M., Colleparidi, S., and Troli R.** (2009). Influence of fly ashes on the drying shrinkage of superplasticized concretes in the presence of SRA, *International Concrete Abstracts Portal, Special Publication-262-21, American Concrete Institute, USA*. pp. 297-296.
- Brooks, J. J.** (1992). Influence of slag type and replacement level on strength, elasticity, shrinkage, and creep of concrete. *ACI Proceedings Fourth International Conference: Fly Ash, Silica Fume, Slag, and Natural Pozzolans in Concrete*, Istanbul, Turkey. pp. 1325-1341.
- Brooks, J. J., and Neville, A. M.** (1992). Creep and shrinkage of concrete as affected by admixtures and cement replacement materials, *Creep and Shrinkage of Concrete: Effect of Materials and Environment, ACI SP-135*, pp.19-36
- Chan, Y. W., Liu, C. Y., and Lu, Y.S.** (1998). Effect of slag and fly ash on the autogenous shrinkage of high-performance concrete. *Proceedings of the International Workshop on Autogenous Shrinkage of Concrete*, Japan Concrete Institute, Japan, pp. 221-228.
- Chen J. C., and Chan, Y.W.** (1989). “Deformations of concretes made with blast-furnace slag cement and ordinary portland cement. *ACI Materials Journal*, pp.372-382.
- Chindaprasirt, P., Homwuttiwong, S., Sirivivatnanon, V.** (2004). Influence of fly ash fineness on strength, drying shrinkage and sulfate resistance of blended cement mortar. *Cement and Concrete Research*, pp. 1087-1092.
- Chowdhury, S., and Basu, P. C.** (2010). Strength-cementitious material-water relationship for proportioning of fly ash-based concrete. *ACI Materials Journal*, pp. 340–348.
- Collins, F., Sanjayan, J. G.** (2000). Cracking tendency of alkali-activated slag concrete subjected to restrained shrinkage. *Cement and Concrete Research*, pp. 791-798

- Cripwell, J. B., Brooks, J. J., and Wainwright, P. J.** (1984). Time dependent properties of concrete containing pulverized fuel ash and a superplasticiser. *Proc., 2nd Int. Conf. on Ash Technology and Marketing*, Central Electricity Generating Board, London, pp. 115-120.
- Davis, D. A.** (2012). Effects of high-volume fly ash and powder activators on plastic and hardened concrete properties. *MS Thesis. Missouri: Missouri Institution of Science and Technology* (Online). Available at: <http://www.scholarsmine.mst.edu>
- Deshpande, S., Darwin, D., and Browning, J.** (2007). Evaluating free shrinkage of concrete or control of cracking in bridge decks. *Structural Engineering and Engineering Materials SM Report No. 89 290*, University of Kansas Center for Research, USA.
- Dunstan, E.,** (1984). Fly ash and fly ash concrete. *Engineering and Research Center Report No. REC-ERC-82-1, Bureau of Reclamation U. S. Department of the Interior*, USA.
- Erdogan, T. Y.** (1997). Admixtures for concrete. *Middle East Technical University Press*, Ankara, Turkey
- fib Mode Code for Concrete Structures 2010*, (2013). Earnest and Soln, Germany.
- Fraay, A. L. A., Bijen, J. M., and de Haan, Y. M.** (1989). The reaction of fly ash in concrete: a critical examination. *Cement and Concrete Research*, pp. 235-246.
- Garci Juenger, M. C., and Jennings, H. M.** (2002). Examining the relationship between the microstructure of calcium silicate hydrate and drying shrinkage of cement pastes. *Cement and Concrete Research*, pp.289-296.
- Gesoğlu, M., Güneysi, E., and Özbay, E.** (2009). Properties of self-compacting concretes made with binary, ternary, and quaternary cementitious blends of fly ash, blast furnace slag, and silica fume, *Construction and Building Materials*, pp. 1847-1854.
- Ghosh, R. S., and Timusk, J.** (1981). Creep of Fly Ash Concrete, *ACI Materials Journal*, pp 78-30.
- Githachuri, K., Alexander, M. G.** (2013). Durability performance potential and strength of blended Portland limestone cement concrete. *Cement and Concrete Composites*, pp. 115-121.
- Guneyisi, E., Gesoğlu, M., Ozbay, E.** (2010). Strength and drying shrinkage properties of self- compacting concretes incorporating multi-system blended mineral admixtures. *Construction and Building Materials*, pp. 1878-1887.
- Hamling, J.W., and Kriner, R. W.** (1992). Evaluation of granulated blast furnace slag as a cementitious admixture-a case study. *Cement, Concrete, and Aggregates*, pp 13-20.
- Holt, E. E. (2001).** Early-Age Autogenous Shrinkage of Concrete. Technical Research Centre of Finland, VTT Publications, No. 446.
- Holt, E.,** (2005) Contribution of mixture design to chemical and autogenous shrinkage of concrete at early ages. *Cement and Concrete Research*, pp. 464-472.
- Hooton, R. D.** (2000). Canadian use of ground granulated blast-furnace slag as a supplementary cementing material for enhanced performance of concrete. *Canadian Journal of Civil Engineering*, pp. 754 -760.

- Hooton, R. D., Stanish, K., and Prusinski, K.** (2009). The effect of ground granulated blast furnace slag (slag cement) on the drying shrinkage of concrete—a critical review of the literature, *Heat & Mass Transfer*, pp.429-436.
- Hui-sheng, S., Bi-wan, X., Xiao-chen, Z.** (2009). Influence of mineral admixtures on compressive strength, gas permeability and carbonation of high performance concrete. *Construction and Building Materials*, pp. 1980-1985
- Huo, S., Al-omaishi, N., and Tadros, M. K.,** (2001). Creep, shrinkage, and modulus of elasticity of high- performance concrete. *ACI Materials Journal*, pp. 440-449.
- IS 2386 (Part III)** (1963). Indian Standard methods of test for Aggregates for Concrete, *Bureau of Indian Standards*, New Delhi, India.
- IS 10262** (2009). Indian Standard methods for Concrete Mix Proportioning – Guidelines, *Bureau of Indian Standards*, New Delhi. India.
- IS 1727** (2004). Indian Standard methods of test for pozzolanic materials, *Bureau of Indian Standards*, New Delhi, India.
- IS 2386 – Part 1** (2007). Indian Standard methods of test for Aggregates for Concrete Part I Particle Size and Shape, *Bureau of Indian Standards*, New Delhi, India.
- IS 383** (2007). Indian Standard methods of test for Specification for Coarse and Fine Aggregates from Natural Sources for Concrete, *Bureau of Indian Standards*, New Delhi, India.
- IS 456** (2000) Plain and reinforced concrete code of practice, *Bureau of Indian Standards*, New Delhi, India
- IS 516** (2004) Indian standard methods of tests for strength of concrete, *Bureau of Indian Standards*, New Delhi, India.
- Isaia, G. C., Gastaldini, A. L. G., and Moraes, R.** (2003). Physical and pozzolanic action of mineral additions on the mechanical strength of high-performance concrete. *Cement and Concrete Composites*, pp. 69-76.
- Jianyong, L., and Yan, Y. A.** (2001). Study on creep and drying shrinkage of high-performance concrete. *Cement and Concrete Research*, pp. 1203-1206.
- Jin, X., Li, Z.** (2003). Effects of mineral admixture on properties of young concrete. *ASCE Journal of Materials in Civil Engineering*, pp. 435-442.
- Johari, M. A. M., Brooks, J. J., Kabir, S., and Rivard, P.** (2011). Influence of supplementary cementitious materials on engineering properties of high strength concrete. *Construction and Building Materials*, pp. 2639-2648.
- Khan, M. I., Lynsdale, C. J., and Waldron, P.** (2000). Porosity and strength of PFA/SF/OPC ternary blended paste. *Cement and Concrete Research*, pp. 1225-1229.
- Khatib, J. M., and Hibbert, J. J.** (2005). Selected engineering properties of concrete incorporating slag and metakaolin *Construction and Building Materials*, pp.460-472
- Khatib, J., M.** (2008). Performance of self-compacting concrete containing fly ash. *Construction and Building Materials*, pp. 1963-1971

- Khatri, R. P., Sirivivatnanon, V., and Gross, W.** (1995). Effect of different supplementary cementitious materials on mechanical properties of high-performance concrete. *Cement and Concrete Research*, pp. 209-220
- Khayat, K. H., and Mitchell D.** (2009). Self-consolidating concrete for precast, prestressed concrete bridge elements. *National cooperative highway research program. national research council (U.S.). Transportation research board.* American association of state highway and transportation officials, USA.
- Kuder, K., Lehman, D., Berman, J., Hannesson, G., and Shogren, R.** (2012). Mechanical properties of self-consolidating concrete blended with high volumes of fly ash and slag. *Construction and Building Materials*, pp.285-295
- Lane, R. O., and Best, J. F.** (1982). Properties and use of fly ash in portland cement concrete. *Concrete International: Design & Construction*, pp. 81-92.
- Lee, K. M., Lee, H. K., Lee, S. H., and Kim, G. Y.** (2006). Autogenous shrinkage of concrete containing granulated blast-furnace slag, *Cement and Concrete Research*, pp. 1279-1285
- Li, G., Zhao, X.** (2003). Properties of concrete incorporating fly ash and ground granulated blast-furnace slag. *Cement and Concrete Composites*, pp. 293-299
- Lim, S. N., and Wee, T. H.** (2000). Autogenous shrinkage of ground-granulated blast-furnace slag concrete. *Materials Journal*, pp. 587-593.
- Liu, J., Yao, Y.** (2001). A study on creep and drying shrinkage of high-performance concrete. *Cement and Concrete Research*, pp. 1203-1206.
- Lothenbach, B., Scrivener, K., and Hooton, R. D.** (2011). Supplementary cementitious materials. *Cement and Concrete Research*, pp.1244-1256.
- Lübeck, A., Gastaldini, A. L. G., Barin, D. S., and Siqueira, H. C.** (2012). Compressive strength and electrical properties of concrete with white portland cement and blast-furnace slag. *Cement and Concrete Composites*, pp. 392-399.
- Lura P., Jensen O. M., and Van B. K.** (2003) Autogenous shrinkage in high-shrinkage cement paste: An evaluation of basic mechanisms. *Cement and Concrete Research*, pp 223- 232.
- Mehta, P. K.** (1983). Pozzolanic and cementitious by-products as mineral admixture for concrete - A critical review. *First International Conference on the Use of Fly Ash, Silica Fume, Slag and Other Mineral by- Products in Concrete*, pp. 1-46
- Mehta, P. K.** (1989). Pozzolanic and cementitious by-products in concrete: another look. *In: Proceedings of the 3rd CANMET/ACI international conference on fly ash, silica fume, slag and natural pozzolans in concrete*, Trondheim, Norway, pp. 1–43.
- Mehta, P. K., and Gjörv, O. E.** (1982). Properties of portland cement concrete containing fly ash and condensed silica fume. *Cement and Concrete Research*, pp. 587-595.
- Mehta, P. K., and Monteiro, P. J. M.** (2006). *Concrete Structure, Properties, and Materials*, 2nd Edition. Prentice Hall, Englewood Cliffs, NJ.

- Mokhtarzadeh, A., and French, C.** (2000). Time-dependent properties of high-strength concrete with consideration for precast applications. *ACI Materials Journal*, pp. 263-271.
- Mostafa, N.Y., El-Hemaly, S. A. S., Al-Wakeel, E. I., El-Korashy, S. A., and Brown, P. W.** (2001). Hydraulic activity of water-cooled slag and air-cooled slag at different temperatures, *Cement and Concrete Research*, pp. 475-484.
- Mostafa, N.Y., El-Hemaly, S. A., Al-Wakeel, E. I., El-Korashy, S.A., and Brown, P.W.** (2001). Hydraulic activity of water-cooled slag and air-cooled slag at different temperatures. *Cement and Concrete Research*, pp. 475-484.
- Munday, J. G. L., Ong, L. T., Wong, L. B., and Dhir, R. K.** (1982). Load independent movements in OPC/PFA concrete. *Proc., Int. Symp. on the Use of PFA in Concrete*, Leeds, U.K., pp. 243-253.
- Naik, T. R., Singh, S., and Ramme, B.** (1998). Mechanical properties and durability of concrete made with blended fly ash. *ACI Materials Journal*, pp 454-560
- Naik, T. R., Chun, Y.M., and Kraus, R. N.** (2007). Shrinkage of concrete with and without fly ash. *Ninth CANMET/ACI International Conference on Fly Ash, Silica Fume, Slag, and Natural Pozzolans in Concrete*, Warsaw. Poland.
- Nail, T., Ramme, B., Kraus, R., and Siddique, R.** (2003). Long-term performance of high-volume fly ash concrete pavements. *ACI Materials Journal*, pp. 150-155.
- Nassif, H. N., Husam, N., and Suksawang, N.** (2005). Effective of pozzolanic materials and curing methods on elastic modulus of high-performance concrete, *Cement and Concrete Composites*, pp. 661-670.
- Nelson, P., Srivivatnanon, V., and Khatri, R.** (1992). Development of high-volume fly ash concrete for pavements. *Proc., 16th ARRB Conference*. pp. 37-47.
- Neville, A. M.** (2006). *Properties of Concrete: Fourth and Final Edition*. Addison Wesley Longman Limited, London
- Neville, A.M.,** (2006). *Properties of Concrete, 4th Edition*, Pearson Education Asia Pvt. Ltd.
- Nishiyama, M.** (2009). Mechanical properties of concrete and reinforcement-state-of-the-art report on HSC and HSS in Japan. *Journal of Advanced Concrete Technology*, pp. 157-182.
- Nithya Nair,** (2018). Experimental study of the flow behaviour of superplasticized pastes and concretes with limestone calcined clay cement (LC3). *M.S., thesis submitted to Department of Civil Engineering, Indian Institute of Technology Madras, India.*
- Omar, W., Makhtar, A. M., Lai, T. P., Omar, R., and Kwong, N. M.** (2008). Creep, shrinkage and elastic modulus of Malaysian concrete. *Final Report-Project, No: LPIPM/CREAMiUPP 02-02-06-09-23.*
- Oner, A., Akyuz, S.** (2007). An experimental study on optimum usage of GGBS for the compressive strength of concrete. *Cement and Concrete Composite*, pp. 504-545.

- Oner, A., Akyuz, S., and Yildiz, R.** (2005). An experimental study on strength development of concrete containing fly ash and optimum usage of fly ash in concrete. *Cement and Concrete Research*, pp. 1165-1171.
- Ortega, J. M., Pastor, J. L., Albaladejo, A., Sánchez, I., and Climent, M. A.,** (2014). Durability and compressive strength of blast furnace slag-based cement grout for special geotechnical applications. *Materials and Constructions*. <http://dx.doi.org/10.3989/mc.2014.04912>
- Ozyildirim, C., and Halstead, W. J.** (1994). Improved concrete quality with combinations of fly ash and silica fume. *ACI Materials Journal*, pp. 587-594
- Papadakis, V. G.** (2000). Effect of fly ash on Portland cement systems. part II. high-calcium fly ash. *Cement and Concrete Research*, pp.1647-1654.
- Poon, C. S., Lam, L., and Wong, Y. L.** (2000). A Study on high-strength concrete prepared with large volumes of low calcium fly ash, *Cement and Concrete Research*, pp. 447-455.
- Ravindrarajah, S. R., and Tam C. T.** (1989). Properties of concrete containing low calcium fly ash under hot and humid climate. In: *Proceedings of the 3th CANMET/ACI international conference on fly ash, silica fume, slag and natural pozzolans in concrete*, Trondheim, Norway. pp. 139-155.
- Rezansoff, T., and Stott, D.** (1990). Durability of concrete containing chloride based accelerating admixtures. *Canadian Journal of Civil Engineering*, pp.102-111.
- RILEM TC 107-CSP:** (1998). Creep and Shrinkage Prediction Models: Principles of their Formation, *Materials and Structures*, pp. 507-512.
- Rivest, M., Bouzoubaa, N., and Malhotra, V.** (2004). Strength development and temperature rise in high-volume fly ash and slag concretes in large experimental monoliths. *Eighth CANMET/ACI International Conference on Fly Ash, Silica Fume, Slag, and Natural Pozzolans in Concrete*, pp. 859-878.
- Rupnow, T. D.,** (2012). Evaluation of ternary cementitious combinations. *Report No.: FHWA/LA.11/486*, Federal Highway Administration, USA.
- Saha, A.K., and Sarker, P. K.** (2017). Sustainable use of ferronickel slag fine aggregate and fly ash in structural concrete: mechanical properties and leaching study. *Journal of Cleaner Production*, pp. 438-448.
- Sakai, K. W.** (1992). Properties of granulated blast-furnace slag cement concrete. *ACI Proceedings Fourth International Conference: Fly Ash, Silica Fume, Slag, and Natural Pozzolans in Concrete*, Vol. 2, Istanbul, Turkey. pp. 1367-1383.
- Saric-Coric, M., and Pierre-Claude Aïtcin** (2003). Influence of curing conditions on shrinkage of blended cements containing various amounts of slag. *ACI Materials Journal*, pp. 477-484.
- Sata, V., Jaturapitakkul, C., and Kiattikomol, K.** (2007). Influence of pozzolan from various by-product materials on mechanical properties of high-strength concrete, *Construction and Building Materials*. pp. 1589-1598

- Schlorholtz, S.** (2004). Development of performance of ternary mixes: Scoping study. *Rep. No. DTFH61-01-X-00042 (Project 13), Centre for Portland Cement Concrete Pavement Technology*, Iowa State University, Ames, IA.
- Scrivener, K. L.** (2014) Options for the future of cement. *The Indian Concrete Journal*, pp.11- 21
- Scrivener, K. L.** (2014). Future Cements Options for the future of cement, *The Indian Concrete Journal*, pp. 11–21.
- Sennour M. L., and Carrasquillo R. L.** (1989). Creep and shrinkage properties in concrete containing fly ash, *Research report number 481/6*, The centre for Transportation Research, Bureau of Engineering Research, The University of Texas at Austin.
- Shariq, M., Prasad, J., and Masood, A.** (2010). Effect of GGBFS on time dependent compressive strength of concrete. *Construction and Building Materials*, pp. 1469-1478.
- Siddique, R.** (2004). Performance characteristics of high-volume Class F fly ash concrete. *Cement and Concrete Research*, pp.487-493.
- Sivasundaram, V., and Malhotra, V. M.** (1992). Properties of concrete incorporating low quantity of cement and high volumes of ground granulated slag, *ACI Materials Journal*, pp. 554-563.
- Swamy, R. N., and Bouikni, A.** (1990). Some engineering properties of slag concrete as influence by mix proportioning and curing. *ACI Materials Journal*, pp. 210-220.
- Symons, M. G., and Fleming, K. H.** (1980). Effect of post Augusta fly Ash on concrete shrinkage. *Civil Engineering Transactions*, pp. 181-185.
- Tan, K., and Pu, X.** (1998). Strengthening effects of finely ground fly ash, granulated blast furnace slag, and their combination. *Cement and Concrete Research*, pp.1819-1825.
- Tangtermsirikul, S.** (1998). Effect of chemical composition and particle size of fly ash on autogenous shrinkage of paste. Proceedings of the International Workshop on Autogenous Shrinkage of Concrete, Japan Concrete Institute, Japan, pp. 175-186
- Tazawa, E., and Miyazawa, S.** (1995). Influence of cement and admixture on autogenous shrinkage of cement paste, *Cement and Concrete Research*, pp. 281-287.
- Tazawa, E., and Miyazawa, S.** (1997). Study on the prediction of autogenous shrinkage. *Proceedings of Japan Society of Civil Engineers*, pp. 211-219.
- Tazawa, E., Yonekura, A., and Tanaka, S.** (1989). Drying shrinkage and creep of concrete containing granulated blast furnace slag in *Proceedings of the Fly Ash, Silica Fume, Slag, and Natural Pozzolans in Concrete: Proceedings of Third International Conference*, American Concrete Institute, Trondheim, Norway. pp. 1325-1343.
- Termkhajornkit, P., Nawa, T., Nakai, M., and Saito, T.** (2005) Effect of fly ash on autogenous shrinkage, *Cement and Concrete Research*, pp. 473-482
- Thomas, M., D., A., Scott, A., Bremner, T., Bilodeau, A., and Day D.** (2008). Performance of slag concrete in marine environment. *ACI Materials Journal*, pp. 628-634

- Tia, M., Liu, Y., and Brown, D.,** (2005). Modulus of elasticity, creep and shrinkage of concrete. *U.F. Project No. 49104504973-12*, Department of Civil and Coastal Engineering, College of Engineering, University of Florida Gainesville, Florida.
- Tia, M., Subramanian, R., Brown, D. and Broward, C.** (2005). Evaluation of shrinkage cracking potential of concrete used in bridge decks in Florida. *Technical Report*. Florida: University of Florida.
- Tikal'sky, P. J., and Carrasquillo, R. L.** (1992) Influence of fly ash on the sulphate resistance of concrete, *ACI Materials Journal*, pp. 69-75.
- Tironi, A., Trezza, M. A., Scian, A. N., and Irassar, E. F.** (2013). Assessment of pozzolanic activity of different calcined clays, *Cement and Concrete Composites*, pp. 319 -327
- Vandewalle, .L.** (2000). Concrete creep and shrinkage at cyclic ambient conditions *Cement and Concrete Composites*, pp: 201-208.
- Wainwright, P. J., and Rey, N.** (2000). The influence of ground granulated blast furnace slag (GGBS) additions and time delay on the bleeding of concrete. *Cement and Concrete Composites*, pp.253-257
- Wedding, P., Hogan, F., and Meusel, J.** (1981). Evaluation for durability and strength development of a ground granulated blast furnace slag. *Cement, Concrete and Aggregates*, pp. 40-52.
- Whiting, D.A., Detwiler, R.J., and Lagergren, E. S.** (2000). Cracking tendency and drying shrinkage of silica fume concrete for bridge deck applications. *ACI Materials Journal*, pp. 96- 100.
- Wiegrink, K., Marikunte, S., and Shah, S. P.** (1996). Shrinkage cracking of high strength concrete. *ACI Materials Journal*, pp. 409-415.
- Wu, Z., and Naik, T. R.** (2003). Chemically Activated Blended Cements, *ACI Materials Journal*, pp. 434-440.
- Yang E. H., Yang, Y., and Li, V. C.** (2007). Use of high volumes of fly ash to improve ECC mechanical properties and material greenness. *ACI Materials Journal*, pp.620-628.
- Yang, E. H., Yang, Y. Z., and Li, V. C.** (2007). Use of high volume of fly ash to improve ECC mechanical properties and material greenness. *ACI Materials Journal*, pp. 303-311
- Yildirim, H. A.** (2011). Modulus of elasticity of substandard and normal concretes. *Construction and Building Materials*, pp 1645-1652.
- Yildirim, H., Sümer, M., Akyüncü, V., and Gürbüz, E.** (2011). Comparison on efficiency factors of F and C types of fly ashes. *Construction and Building Materials*, pp. 2939-2947.
- Yuan, J., Lindquist, W., Darwin, D., and Browning, J.** (2015). Effect of slag cement on drying shrinkage of concrete. *ACI Materials Journal*, pp.267-276.
- Yurdakul, E., Taylor, P. C., Ceylan, H., and Bektas, F.** (2014). Effect of water-to-binder ratio, air content, and type of cementitious materials on fresh and hardened properties of binary and ternary blended concrete. *Journal of Materials in Civil Engineering*, pp. 401-411.

LIST OF PUBLICATIONS BASED ON THIS THESIS

a) REFEREED JOURNALS

1. Yuvaraj Dhandapani, **T. Sakthivel**, Manu Santhanam, Ravindra Gettu, and Radhakrishna G. Pillai (2018) “Mechanical properties and durability performance of concrete with limestone calcined clay cement (LC3)” *Cement and Concrete Research*, 107, pp.136-151.
2. **Sakthivel, T.**, Gettu, R. and Pillai, R.G. (2019) “Compressive Strength and Elastic Modulus of Concretes with Fly Ash and Slag” *Journal of Institution of Engineers (India): Series A*. <https://doi.org/10.1007/s40030-019-00376-w>

b) CONFERENCE PAPERS

1. **T. Sakthivel**, Ravindra Gettu, and Radhakrishna G. Pillai “Influence of incorporation of fly ash and slag on the shrinkage response of common concretes” *International conference on advances in construction materials and systems, 71st RILEM Week and ICACMS, Chennai, India, September 3-8, 2017*. (Poster Presentation)
2. **T. Sakthivel**, Ravindra Gettu and Radhakrishna G. Pillai “Influence of supplementary cementitious materials on the mechanical performance of concrete” *Concrete Research in India, Research Scholar Symposium, Mumbai, India, December 14, 2018*. (Poster Presentation)
3. **T. Sakthivel**, Swathi Shantharaju, Ravindra Gettu and Radhakrishna G. Pillai “Assessment of shrinkage prediction models for fly ash concrete” *International Conference on Advances in Construction Materials and Systems, 3rd R. N. Raikar Memorial International Conference and Gettu Kodur International Symposium, Mumbai, India, December 14-15, 2018*. (Oral Presentation)
4. Ravindra Gettu, Manu Santhanam, Radhakrishna G. Pillai, Yuvaraj Dhandapani, **Sakthivel T.**, Sripriya Rengaraju, Fathima Suma M., Sanoop Prakasan, Sundar Rathnarajan, and Anusha S. Basavaraj “Recent research on limestone calcined clay cement (LC3) at IIT madras” Conference in Honour of Centennial of Laboratory of Construction Materials and

60th Birthday of Prof. Karen Scrivener (Lausanne, Switzerland), At Ecole Polytechnique Federale de Lausanne, Lausanne, Switzerland, 22 Aug 2018, Volume: pp. 76-79

5. Ravindra Gettu, Manu Santhanam, Radhakrishna G. Pillai, Yuvaraj Dhandapani, **Sakthivel T.**, Sripriya Rengaraju, Sundar Rathnarajan, Fathima Suma M., Anusha S. Basavaraj and Sanoop Prakasan, “Summary of 4-years of research at IIT Madras on concrete with lime stone calcined clay cement (LC3)” *International Conference on Sustainable Materials, Systems and Structures 2019, Rovinj, Croatia*

DOCTORAL COMMITTEE

CHAIRPERSON

Prof. K. Ramamurthy
Professor and Head
Department of Civil Engineering

GUIDE

Prof. Ravindra Gettu
Professor
Department of Civil Engineering

CO-GUIDE

Dr. Radhakrishna G. Pillai
Associate Professor
Department of Civil Engineering

MEMBERS

Prof. Manu Santhanam
Professor
Department of Civil Engineering

Prof. Devdas Menon
Professor
Department of Civil Engineering

Prof. S. Nallayarasu
Professor
Department of Ocean Engineering

Prof. M. S. Sivakumar
Professor
Department of Applied Mechanics

CURRICULUM VITAE

Name : **T. SAKTHIVEL**

Date of birth : April 01, 1984

Educational qualifications

2007

Specialization

Institution

Bachelor of Engineering (B.E.)

Civil Engineering

Kongu Engineering College, Erode

Affiliated to Anna University, Chennai

INDIA

2009

Specialization

Institution

Master of Engineering (M.E.)

Structural Engineering

Faculty of Engineering and Technology (FEAT)

Annamalai University, Annamalai Nagar

INDIA

2018

Specialization

Institution

Doctor of Philosophy (Ph.D.)

Long-term Performance of Concrete Systems

Indian Institute of Technology Madras, Chennai

INDIA

